OPEN ACCESS

University of BRISTOL

This electronic thesis or dissertation has been downloaded from Explore Bristol Research, http://research-information.bristol.ac.uk

Author:
Price, David A

Title:
An integrated approach to modelling floodplain hydraulics, hydrology and nitrate chemistry

General rights
The copyright of this thesis rests with the author, unless otherwise identified in the body of the thesis, and no quotation from it or information derived from it may be published without proper acknowledgement. It is permitted to use and duplicate this work only for personal and non-commercial research, study or criticism/review. You must obtain prior written consent from the author for any other use. It is not permitted to supply the whole or part of this thesis to any other person or to post the same on any website or other online location without the prior written consent of the author.

Take down policy
Some pages of this thesis may have been removed for copyright restrictions prior to it having been deposited in Explore Bristol Research. However, if you have discovered material within the thesis that you believe is unlawful e.g. breaches copyright, (either yours or that of a third party) or any other law, including but not limited to those relating to patent, trademark, confidentiality, data protection, obscenity, defamation, libel, then please contact: open-access@bristol.ac.uk and include the following information in your message:

• Your contact details
• Bibliographic details for the item, including a URL
• An outline of the nature of the complaint

On receipt of your message the Open Access team will immediately investigate your claim, make an initial judgement of the validity of the claim, and withdraw the item in question from public view.

An integrated approach to modelling floodplain hydraulics, hydrology and nitrate chemistry

David A. Price

A thesis submitted to the University of Bristol in accordance with the requirements of the degree of Ph.D. in the Faculty of Science

Department of Geography

February 1997

Abstract

As part of the effort to satisfy the ever increasing demand for a greater understanding of fluvial, hydrological, chemical, sedimentological and geomorphological processes operating on the floodplain, mathematical simulation models have come to play a significant role in the understanding, prediction and management of the floodplain environment.

Underlying the accurate numerical representation of hydraulically driven processes is the provision of a suitable floodplain hydrology model which accounts for the interaction between surface hydraulics and subsurface hydrology. Such a numerical representation is currently not available at the spatial and temporal resolution required. It is the aim of this thesis to develop a novel conceptual approach to modelling floodplain hydrology in which the fundamental need to consider the interaction between surface and subsurface flow is the floodplain environment is addressed.

This is achieved through the interactive coupling of a one-dimensional finite difference infiltration model with the state-of-the-art two-dimensional physically based finite element hydraulic model, TELEMAC2D. The coupled model provides an unparalleled spatial and temporal representation of surface and subsurface flow processes within the floodplain environment.

The utility of this integrated approach is explored through an application of the model to two areas of contemporary floodplain research. In the first of these the model is run to assess the impact of infiltration on flood flow prediction for an 11km reach of the River Culm, UK, over a range of flood and soil conditions. In the second the model is run to investigate the nitrate buffering potential of floodplain riparian soils during flooding. For this investigation a model accounting for nitrate transport and denitrification is developed within the existing integrated hydraulic-infiltration model structure.

An evaluation of the results from both of these investigations supports the need for a new approach to modelling fluvially driven floodplain processes which accounts for the spatially interactive nature of floodplain hydrology.

Acknowledgements

I would like express my gratitude to all those who have assisted in the completion of this thesis. I would like to begin by thanking both Malcolm Anderson and Tim Burt for their supervision and encouragement throughout. I am also indebted to NERC for their financial support for the research.

I would especially like to thank Paul Bates for his guidance with the TELEMAC2D model, Ed Thomas for his help with FORTRAN and for his tremendous efforts in keeping gma up and running, Chris Smith for his conceptual insight and those at EDF, especially Stephane and Martine, who made my trips to Paris all the more enjoyable. I would also like to thank the many members, past and present, of room 1.6N all of whom have helped in many ways. I am very grateful to those who have helped in the later stages of completion, including Simon Godden for his graphical expertise and numerous others who have offered their help and encouragement - in this respect my thanks must go to the whole department!

I would especially like to thank Dave Thurston and Simon Meadows for enduring my student tendencies over the past years and Nichola Tooke for keeping me happily sane over the past months. Finally, I would like to thank my parents for their support and encouragement in all that I have chosen to do.

Declaration

This thesis is the original work of the candidate except where acknowledgement is given and has not been submitted previously for a higher degree in this or any other University.

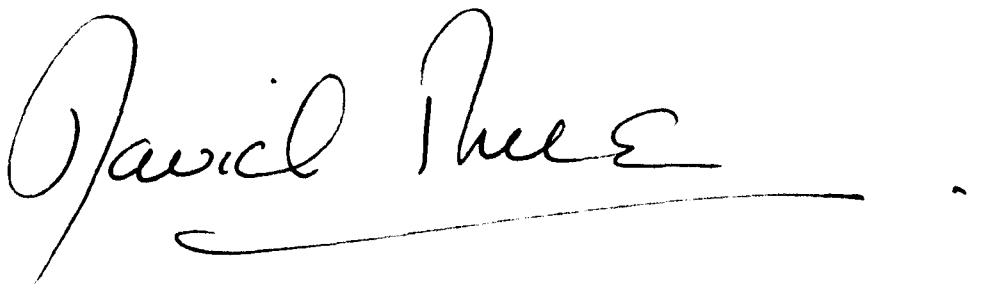

David A. Price
February, 1997.

Summary of Contents

Chapter one Introduction

Chapter two Development of a research design

Chapter three Development of an integrated floodplain hydraulic-infiltration model

Chapter four Modelling nitrate dynamics in the floodplain

Chapter five Selection and Parameterisation of a reach application

Chapter six Hydraulic model response to infiltration

Chapter seven An investigation into the nitrate loading and buffering capacity of flood flow in the floodplain environment

Chapter eight Conclusions and Recommendations

list of figures

List of tables

Over the high coast mountains and over the valleys the grey clouds marched in from the ocean. The wind blew fiercely and silently, high in the air, and it swished in the brush, and it roared in the forests. The clouds came in brokenly, in puffs, in folds, in grey crags; and they piled in together and settled low over the west. And then the wind stopped and left the clouds deep and solid. The rain began with gusty showers, pauses and downpours; and then gradually it settled to a single tempo, small drops and a steady beat, rain that was grey to see through, rain that cut midday light to evening. And at first the dry earth sucked the moisture down and blackened. For two days the earth drank the rain, until the earth was full. Then puddles formed, and in the low places little lakes formed in the fields. The muddy lakes rose higher, and the steady rain whipped the shining water. At last the mountains were full, and the hillsides spilled into the streams, built them to freshets, and sent them roaring down the canyons into the valleys. The rain beat on steadily. And the streams and the little rivers edged up to the bank sides and worked at willows and tree roots, bent the willows deep in the current, cut out the roots of cottonwoods and brought down the trees. The muddy water whirled along the bank sides and crept up the banks until at last it spilled over, into the fields, into the orchards, into the cotton patches where the black stems stood. Level fields became lakes, broad and grey, and the rain whipped up the surfaces. Then the water poured over the highways, and cars moved slowly, cutting the water ahead and leaving a boiling muddy wake behind. The earth whispered under the beat of the rain, and the streams thundered under the churning freshets.

..... And the rain pattered relentlessly down, and the streams broke their banks and spread out over the country.

(John Steinbeck)

Introduction

1.1 Establishing a context for the research

Human activity often comes into direct conflict with the natural hydraulic, hydrological and chemical functions of floodplains. As human activity on the floodplain has increased so has the demand for a greater understanding of fluvial, hydrological, chemical, sedimentological and geomorphological processes operating on the floodplain. As part of the increasing effort to satisfy these demands, mathematical simulation models have come to play a significant role in the understanding, prediction and management of the floodplain environment.

Research in the floodplain considers processes which are spatially interactive; for example, the interaction between surface and subsurface hydrology (Abbott *et al.*, 1986; Phillips, 1989b; Maltby *et al.*, 1991), the hydrology of the hillslope-floodplain-channel continuum (Kirkby, 1969; Anderson and Burt, 1978; Haycock and Burt, 1993; Burt and Haycock, 1996) and surface and subsurface floodplain chemistry (Brunet *et al.*, 1994; Burt and Haycock, 1996; Maltby *et al.*, 1996). Thus, the need for a spatially integrated approach is evident. However, in many areas of contemporary investigation in the floodplain such an approach is lacking. Significantly, hydraulically driven processes which rely on the accurate prediction of compound channel flow at both a high spatial and temporal resolution currently depend upon a generation of physically-based two-dimensional (2D) hydraulic models which fail to account for floodplain hydrology through the assumption of zero flux boundaries at the hillslope-floodplain and surface-subsurface interfaces. This has potentially far reaching implications for the prediction of floodplain flows and the processes reliant upon these. It is this current inability to model the spatially interactive nature of floodplain hydrology through a failure to account for the interaction between surface hydraulics and subsurface hydrology at an appropriate spatial resolution which provides the focus of the research presented in this thesis.

Underlying the accurate representation of floodplain fluvial, hydrological, chemical, sedimentological and geomorphological processes is the provision of a suitable floodplain

hydrology model which represents the interaction between surface hydraulics and subsurface hydrology at a spatial and temporal resolution able to capture the highly distributed nature of floodplain flow processes. Such numerical representation of the floodplain is not currently available. However, the latest generation of 2D finite element hydraulic models offer the potential for the development of such a research platform where the there is a need for compound channel flow to be described at a high spatial and temporal resolution[1].

This thesis is concerned with the development of a novel conceptual approach to modelling floodplain hydrology which addresses the fundamental need to consider the interaction between surface and subsurface flow in the floodplain environment. This is achieved through the relaxation of the surface boundary of a state-of-the-art distributed 2D finite element hydraulic model by explicitly accounting for infiltration. The integrated floodplain hydrology model is then applied to assess the implications of such an approach on the following two areas of contemporary floodplain research;

- the impact of infiltration on flood flow prediction using 2D finite element hydraulic models
- the impact of flood events on surface and subsurface nitrate (NO_3-N) dynamics in the floodplain

The remainder of this chapter establishes the requirement for the prediction of floodplain surface flow and NO_3-N dynamics in the floodplain environment.

1.2 The need for prediction in floodplain environments

The ability to predict the pattern and nature of flood inundation and NO_3-N interactions within the floodplain environment is of considerable importance for reasons including the protection of life and property and the protection of surface and groundwater quality.

1.2.1 Flood prediction

Predicting the behaviour of floodplain hydraulics is important in a number of respects, not least for the ability to predict flood events. Models have been used to extend flood records where these are limited, to predict the magnitude of large return period floods, to allow engineers to determine required construction specifications and, to allow prediction of the impact of physical changes within the catchment prior to those changes actually occurring.

[1] For example see Charlton (1995) and Bates *et al.* (1996) for research into the effects of hillslope hydrology on 2D finite element model prediction.

In any catchment liable to flooding an appreciation of the interaction between the various catchment parameters and flood magnitude is central to flood warning schemes and the implementation of flood prevention measures. For most catchments few empirical data exist regarding flood events and existing knowledge can be extended with the aid of numerical models and computer simulations (Kuehuet and Fach, 1983; Kachroo, 1991). In planning the design of flood control measures engineers must first be able to determine the remedial measures required and secondly, be able to determine design specification requirements. By using models of floodplain flows over a range of flood magnitudes, some of which may have been extrapolated from existing data, the engineer is able to determine both the required control measures and design specification. Indeed, the greater the accuracy with which flood waves in the river can be predicted, the better the corresponding control measures that can be planned and implemented (Kuehuet and Fach, 1983).

Just as models may be applied to predicting the outcome of engineering works and flood alleviation constructions, they can also be applied to predict the effects resulting from other physical changes within the floodplain (Nash and Sutcliffe, 1970). For example, models of floodplain flows can be instrumental in predicting the possible outcome of changing land use on a floodplain. This may include deforestation of a floodplain area leading to reduced friction effects and associated changes in flood hydraulics. It may also include the proposed development of a floodplain site for industry or housing (Havno *et al.*, 1995), which again will generate altered flow characteristics and the possibility of additional flow inputs through increased surface drainage.

Accurate simulation of floodplain flows is also essential for research into other hydraulically driven floodplain processes including floodplain geomorphology, sedimentology (Walling *et al.*, 1986; Walling *et al.*, 1992; Marron, 1989; Marriot, 1996) and the transfer of pollutants in surface water (Brunet *et al.*, 1994; Stewart *et al.* (*in press*)). For example, whilst it is known that the floodplains of lowland rivers commonly experience sediment deposition during flood events, little is known about the rates and spatial patterns of contemporary sediment deposition and the significance of the floodplain as a sediment sink (Walling *et al.*, 1992). Modelling the spatially distributed depth and velocity characteristics of floodplain flow represents an important advance in the interpretation of floodplain sediment patterns and is critical in the construction of numerical models describing sedimentation processes.

There exists, therefore, the need for accurate prediction of floodplain flows at a spatial and temporal resolution commensurate with the needs of floodplain hydraulic, geomorphological, sedimentological and chemical research at the reach scale.

1.2.2 Modelling the behaviour of nitrate in the floodplain

Evidence of the nutrient buffering capacity of floodplains began appearing in the late 1970s and early 1980s (eg McColl, 1978; Schlosser and Karr, 1981). Over the intervening years the capacity of the floodplain to provide a sink for both sediment-borne (Marron, 1989, 1992; Brunet *et al.*, 1994) and dissolved contaminants (Haycock and Pinay, 1993; Haycock and Burt, 1993; Groffman *et al.*, 1991, Chesheir *et al.*, 1987; Jordan *et al.*, 1993; Lowrance, 1992; Maltby *et al.*, 1991; Maltby *et al.*, 1996) has been widely demonstrated. A considerable literature now exists regarding the nutrient buffering potential of so called floodplain riparian or buffer zones adjacent to river and stream channels which have been shown to reduce agricultural non-point source pollution, primarily NO_3-*N* and sediment, reaching and subsequently contaminating surface waters. The majority of the studies have concentrated on shallow groundwater passing laterally from hillslopes to the water courses which interacts with the microbially active upper floodplain soil layers on route. Although much literature now exists to testify to the filtering potential of riparian zones, these data are often site-specific and only a few attempts have been made to model the internal processes of buffer zones for studying combinations of conditions or aiding the development of management models. A few notable exceptions exist including the models of Chesheir *et al.* (1987) and Phillips (1989a, b).

While the role of riparian zones in influencing the quality of groundwater has received considerable attention, little research has been directed at quantitatively assessing the fate of nitrogen during flood events or the impact of flood water on the hydrology and chemical function of floodplain buffer zones. Where research has considered these aspects the floodplain has been shown to provide a potentially significant sink for both particulate nitrogen (N) (Brunet *et al.*, 1994) and dissolved NO_3-*N* (Maltby *et al.*, 1991; Maltby *et al.*, 1996; Phillips, 1989b). For example, Brunet *et al.* (1994) calculated that up to 2% of the total N budget for a catchment can be lost through the combined effects of the storage of organic forms of N, the adsorption of ammonium and the denitrification of NO_3-*N* in shallow standing water. However, despite this and other such work in this area there remains a significant lack of quantitative data regarding the fate of riverine and soil N during river flood events due to the inherent difficulties associated with scaling field data to reach or catchment scales. The availability of such data would be of considerable value for the management of floodplains where the interaction of flood water and riparian soils can have a potentially profound effect upon stream water N budgets. Where floods form a significant part of the hydrological cycle, such as in the case of many lowland floodplains and wetlands, they represent an important area of investigation in terms of their nutrient loading capacity and their impact upon the buffering function of floodplain soils.

There exists, therefore, the need for quantitatively assessing the NO_3-N loading and NO_3-N buffering capacity of flood events in floodplain riparian zones at the reach scale.

1.3 Conclusions

In *Chapter 1* the need for a novel conceptual approach to modelling floodplain hydrology which addresses the fundamental need to account for the interaction between surface and subsurface flow in floodplain hydraulic models is established. It is suggested that this can be achieved through the relaxation of the surface boundary of a state-of-the-art physically based 2D finite element hydraulic model by explicitly accounting for infiltration. Two areas of contemporary research in which such a modelling approach has potential significance are then identified and the following requirements established:

- the need for the accurate prediction of floodplain flows at a spatial and temporal resolution commensurate with the needs of floodplain hydraulic, geomorphological, sedimentological and chemical research at the reach scale

- the need for quantitative assessment of the NO_3-N loading and NO_3-N buffering capacity of flood events in floodplain riparian zones at the reach scale

Chapter 2 now considers both of these areas of contemporary research in the context of the need for a spatially and temporally integrated approach to modelling hydraulic, hydrological and chemical processes in the floodplain.

Development of a research design

2.1 Introduction and Chapter Objectives

In *Chapter 1* the need for a novel conceptual approach to modelling floodplain hydrology is identified as a prerequisite to the accurate representation of fluvial, hydrological, chemical, sedimentological and geomorphological processes operating on the floodplain. The need for this modelling approach is explored further in *Chapter 2* with reference to the two areas of contemporary floodplain research identified in *Chapter 1*, namely modelling floodplain surface flow and flood mediated NO_3-N dynamics.

The Chapter begins by providing a summary of the physical basis of compound channel flow, the numerical simulation of which provides the basis of the research presented in this thesis.

The chapter then develops the arguments for investigating the floodplain as a hydrologically integrated system through the examples of floodplain flow prediction using numerical models and flood nutrient loading and buffering with reference to the NO_3-N ion. Based on the discussion presented, the chapter concludes with the development of a research strategy which is then pursued in the remaining chapters of the thesis.

2.2 Numerical representation of floodplain flow

The following section considers the ways in which floodplain flows are treated numerically and reviews these in terms of the need to account for both surface and subsurface flow components. This section begins with a short discussion of the physical basis of compound channel flow.

2.2.1 The physical basis of compound channel flow

An appreciation of the potential and failings of numerical models of floodplain flow lies in an understanding of the physical components of compound channel flow. Although rivers are most

often confined to easily identifiable channels in which the flow may be treated predominantly as one-dimensional (1D) in the downstream direction, during periods of overbank flow channel hydraulic conditions alter considerably (Sellin, 1964; Knight and Shiono, 1996). During over-bank flow a number of 3D processes deriving from the interaction between channel and floodplain flows become significant in determining the pattern and behaviour of what is now compound channel flow.

The dominant hydraulic processes associated with overbank flow are summarised by Shiono and Knight (1991) in Figure 2.1 for which detailed explanation is also given by Imamato and Ishigaki (1987), Shiono and Knight (1991) and Knight and Shiono (1996) and only a summary covering the salient aspects is presented here.

In all channels turbulence introduces a random chaotic element into the flow and increases viscous resistance effects. In addition, overbank flow generates two significant 3D processes with important implications for compound channel flow. Firstly, at the interface between the faster moving channel flow and the slower moving floodplain flow the development of a shear layer is observed (Selin, 1964). This shear layer is responsible for the development of interface vortices, illustrated in Figure 2.1, with vertical axes aligned along the channel/floodplain interface. Secondly, spillage of water onto the floodplain delivered by the channel and its subsequent return has been identified as having a significant impact on flow behaviour. Indeed, these mechanisms are responsible for a potentially significant transfer of momentum between the channel and the floodplain. Thus, the physical complexity of channel flow dramatically increases during periods of out-of-bank flow when a number of 3D flow structures develop to play a potentially significant role in floodplain hydraulics. The next section considers the numerical methods currently available for simulating river and flood hydraulics in light of the physical basis of such flows.

2.2.2 Numerical models of flood prediction

It was stated in *Chapter 1* that the current generation of 2D finite element hydraulic models currently provide the best hydraulic representation in the floodplain environment. This is also supported, in part, by the discussion of the physical basis of compound channel flow presented above where it is evident that such flows comprise considerable lateral processes. In the following section a number of widely used methods for modelling floodplain flows are critically reviewed.

Progress in hydrology and river hydraulics together with advances in computer technology have now made it feasible to perform flood prediction through the use of advanced and comprehensive

mathematical models which solve the partial differential equations of flow and transport, derived ultimately from the Navier-Stokes equations, in either 1-, 2-, or 3-dimensions.

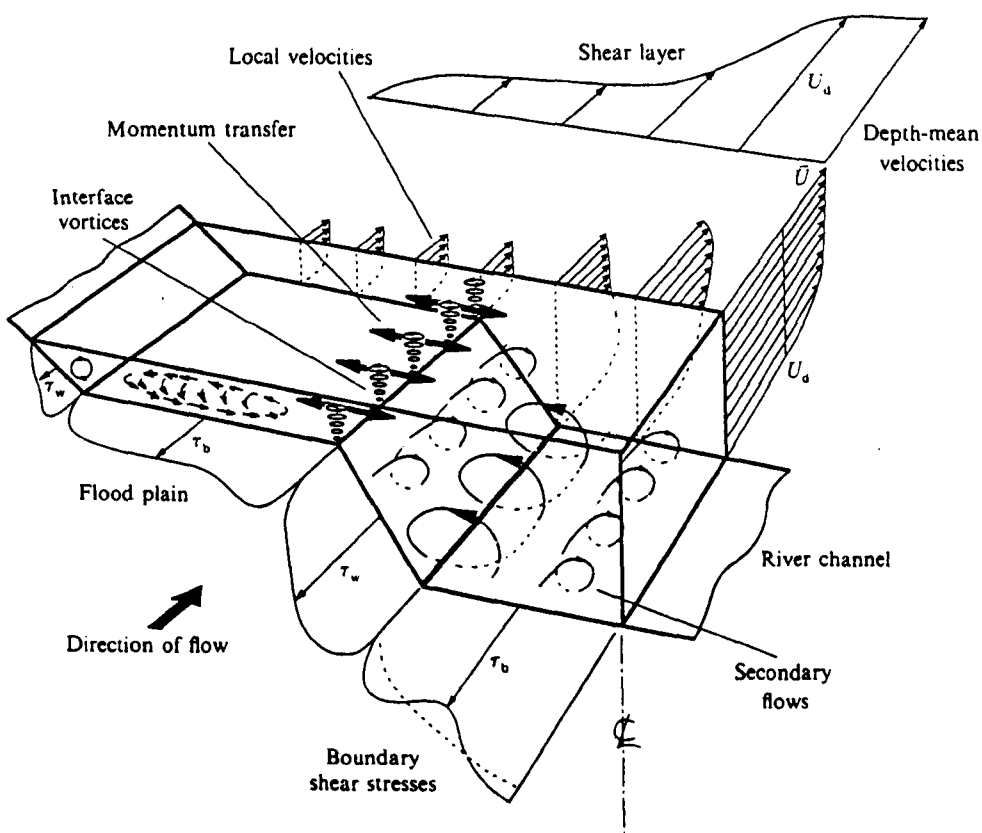

Figure 2.1 A summary of the dominant processes associated with overbank flow (after Shiono and Knight, 1991).

Channel and flood flow is represented in varying degrees of complexity in both *hydraulic* and *catchment hydrology* models. While hydraulic models are generally applied to lowland reaches catchment hydrology models are formulated to determine catchment response to rainfall events and are generally applied to upland areas. In catchment hydrology models the channel is represented as an integral part of the catchment which receives surface and subsurface flows from adjacent hillslopes such that channel flow originates from simulated hillslope runoff processes. This contrasts with hydraulic flood models in which the computational domain is usually represented solely by the channel and for which flows are not generated from internal model processes but are input through an observed flood hydrograph. The following section reviews the ways in which these models spatially represent channel and floodplain flows and considers their suitability to the proposed research which requires a high spatial and temporal representation of compound channel flow.

One-dimensional representation of channel flow: The majority of numerical models, both hydraulic and catchment hydrology, represent channel flow in 1D.

1D hydraulic models which solve the 1D form of the 3D Navier-Stokes equations represent the standard technique in flood prediction (Kuehnet and Faeh, 1983; Refsgaard and Havnoe, 1983). Although varied in nature, 1D hydraulic models conform to a general structure in which the 1D flow equations are solved for the entire reach while data on the lateral extent of surface water is provided at specified cross-sections throughout the reach.

Kuehnet and Faeh (1983) report on a 1D mathematical model (FLORIS) based on the Saint-Venant equations which they apply to a study of the River Thur, N.E. Switzerland. The equations are solved to give the unknowns (discharge and water elevation) at given discrete points in time at chosen locations on the river. Each branch in the model (a branch represents that section of the modelled river between junction nodes which define the intersection between two branches) is subdivided into a number of intervals at which the corresponding cross-section profile is specified. At each cross-section the model equations (continuity and momentum) are solved for different values of parameters which are functions of the water level and which include area of flow, storage width and conveyance. Thus, at each cross section the flow across the entire floodplain profile is determined. In this particular application to the River Thur 170 cross-sections were defined along a 23 km reach.

The problems associated with this class of hydraulic model derive mainly from the simplifying assumptions necessary and the inability to represent topographic and other floodplain features spatially. The construction of cross-sections at which the full floodplain flow characteristics can be

determined are laterally aligned in the downstream direction which precludes the full representation of floodplain topography, additional floodplain features and channel morphology, for much of the floodplain (those areas between cross-sections). Significantly, no differentiation is made between the channel and the floodplain thus no account is taken of the complex flow interactions at this interface (ie momentum exchange between channel and floodplain water). Finally, as flow is described in 1D, all flow paths must be fixed *a priori*. Thus, where a high spatial representation of complex floodplain flow processes is required (for example, the spatial distribution of inundation, flow depth and velocities over the entire floodplain surface) the application of 1D models is limited. Despite this, 1D hydraulic models remain the standard technique for many engineering problems.

1D channel flow is also incorporated within a number of advanced catchment hydrology models which typically account for the interaction between surface flows and catchment hydrology in varying degrees of complexity. However, as is the case with 1D hydraulic models, they are similarly limited in their representation of compound channel flow. Perhaps the most advanced catchment hydrology models currently available derive from the grid-based SHE model (Abbott *et al.*, 1986). The SHE model itself solves the Saint-Venant equation for surface flow and the Richard's equation for saturated subsurface flow over 2D square or rectangular grids using finite difference schemes. The structure of the model is illustrated in Figure 2.2. These two grids are linked by a 1D infiltration model, representing vertical unsaturated flow, which lies beneath each grid point. Fluvial processes, however, are represented by a 1D finite difference approximation of the Saint-Venant equation and channel flow is restricted to the boundaries between grid squares which results in a very simplified expression of the channel network pattern. An example of the simplified channel network is provided by an application of the SHE model to the Wye catchment by Bathurst (1986) which is represented in Figure 2.3. The model does, however, account for seepage losses and groundwater inputs between channel and aquifer (Figure 2.2b). Problems in representing catchment and floodplain topography arise from the inflexible nature of the SHE's square and rectangular finite difference grids. The ridged grid structure prevents an accurate representation of catchment topography, with topographic features having to be approximated in order to fit in with the model structure if they fail to coincide spatially with the point of a grid node. The finite difference procedure does not facilitate a flexibility in element shape which can be used to 'mould' elements to the topography as is the case with finite element techniques. The problem is partially overcome by employing smaller elements in regions where rapid changes in slope occur and at the hillslope-channel interface where topography is a sensitive control on the formation of saturated wedges and variable source areas. However, the problem is perhaps most acute on the river floodplain itself where the SHE fails to provide an accurate representation of the form of the river network or of the

floodplain topography. The result is a schematic representation of river form (Bathurst, 1986; Jain *et al.*, 1992) and an inability to predict the true extent of river flooding.

(a)

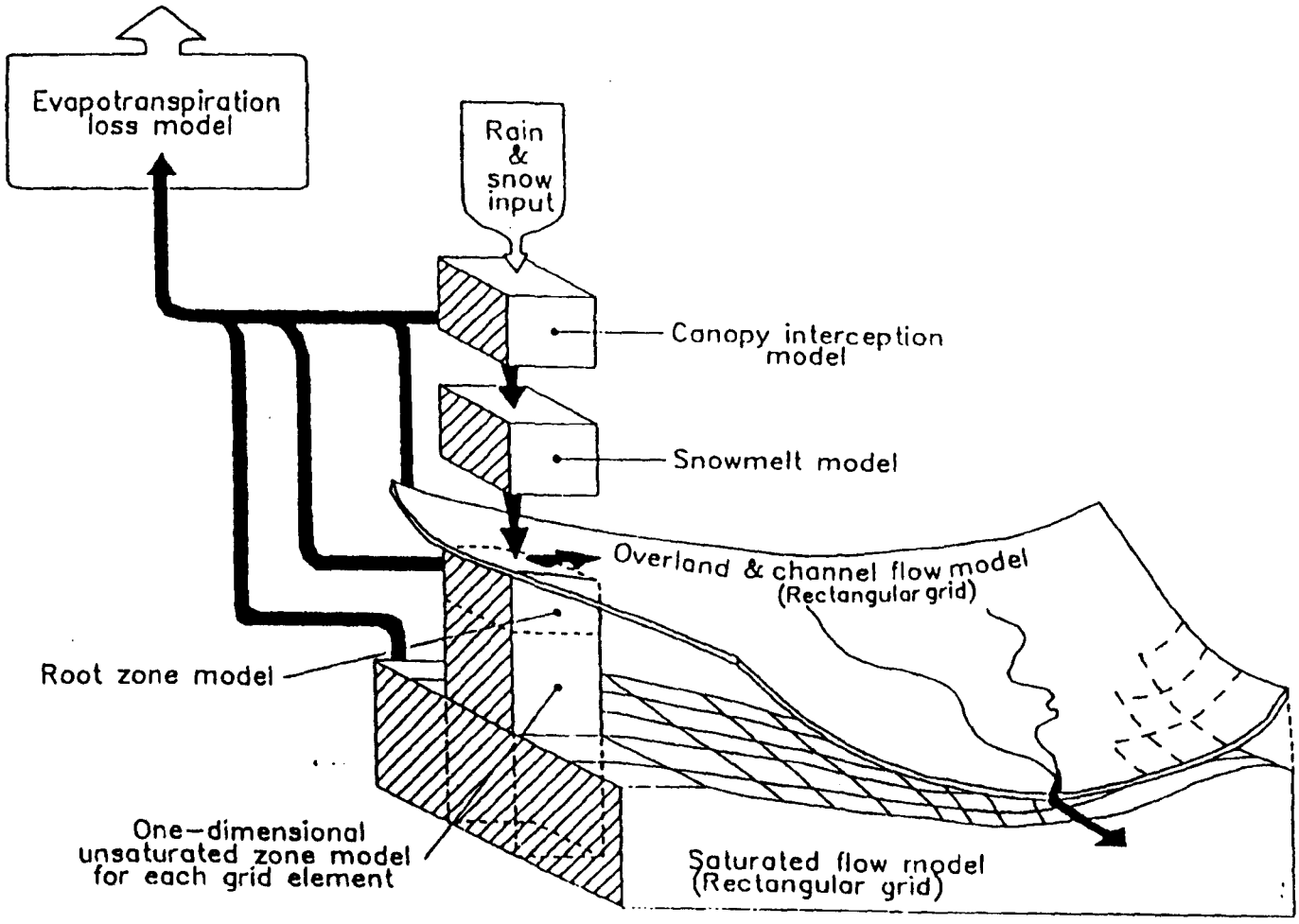

Figure 2.2 The SHE model. (a) Schematic representation of the model structure (After Abbot *et al.* 1986) (b) schematic representation of the processes modelled in the overland and channel flow component of the SHE model (After Abbott *et al.* 1986).

(b)

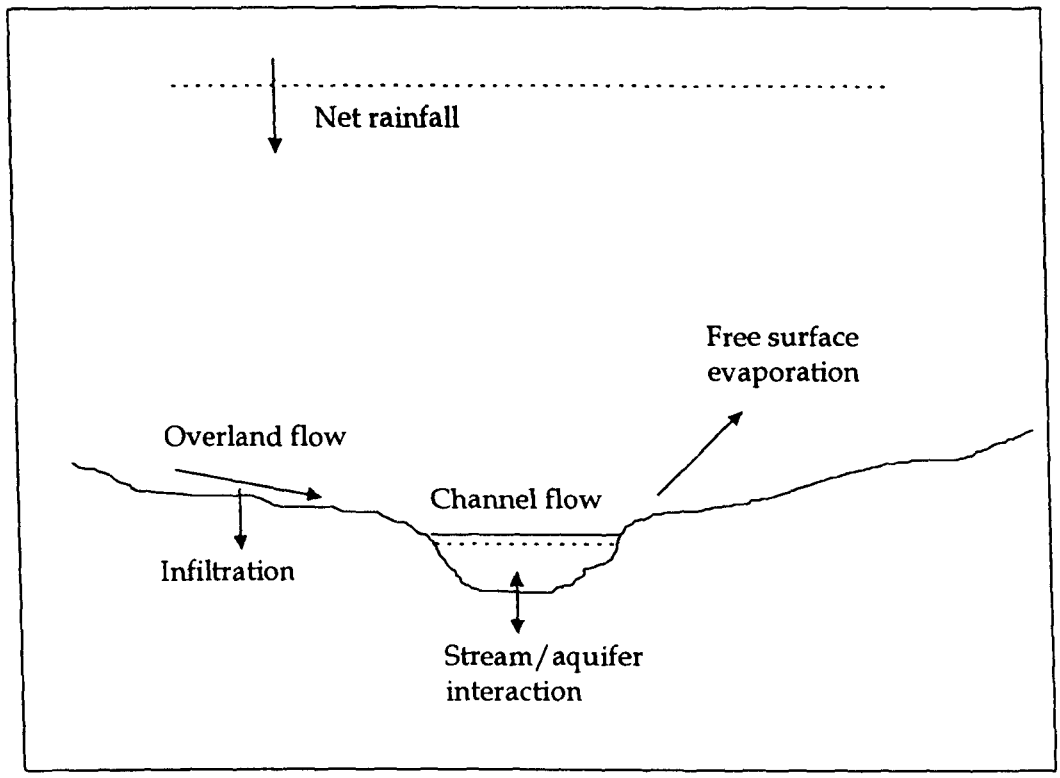

Figure 2.2 (continued).

(a) (b)

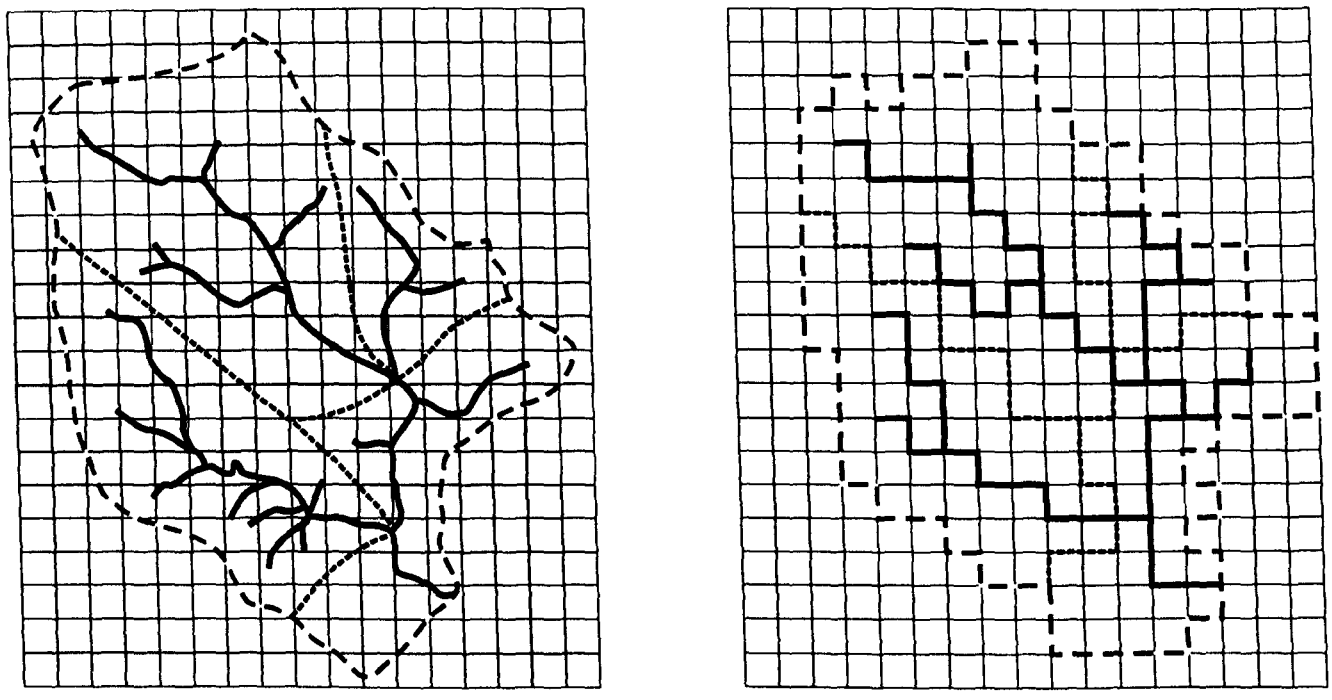

Figure 2.3 (a) Illustration of the Wye catchment and channel system superimposed on the grid network adopted for modelling the catchment (b) representation of the catchment and river system used in the SHE model simulations. Each square represents an area of 250 x 250m^2 (after Bathurst, 1986).

Continued development of the SHE model at the Danish Hydraulic Institute has resulted in significant improvements over the original SHE model in representing channel and floodplain flows through the development of the MIKE-SHE (Refsgaard and Storm; 1995) and MIKE-11 (Havno *et al.*, 1995) models. Specifically, MIKE-11 provides an enhanced representation of channel and floodplain hydraulics providing a flood simulation potential similar to that of 1D hydraulic models such as FLORIS discussed above. Where the two models (MIKE-SHE and MIKE-11) are coupled they provide a unique system combining an integrated hydrological modelling system (MIKE-SHE) with an advanced river modelling system (MIKE-11). Run simultaneously, the two models follow five basis steps:

- MIKE-11 calculates flow and stage at predetermined cross-sections.

- calculated stage is transferred to MIKE-SHE.

- MIKE-SHE maps the areal extent of flooding through a comparison of stage calculated in MIKE-11 with topographic information stored in MIKE-SHE.

- MIKE-SHE calculates the water flows in the remaining part of the hydrological cycle where the following processes can result in the exchange of water with MIKE-11:

    - evaporation from surface water
    - infiltration
    - overland flow
    - river/aquifer exchange

- Based on the exchanges resulting from step (iv) water is transferred between MIKE-11 and MIKE-SHE using source/sink terms.

In principle the MIKE-SHE - MIKE-11 coupling is simply a bookkeeping procedure ensuring the conservation of mass combined with a GIS component which maps the water depth as well as areal extent of floodplain by linking calculated water levels from MIKE-11 cross-sections to the computational grid network of MIKE-SHE. The MIKE SHE - MIKE 11 coupling offers potential advantages over 1D hydraulic models as catchment and floodplain hydrology is explicitly accounted for. Nevertheless, in terms of floodplain flow representation, this model is similarly limited in terms of its representation of compound channel flow.

Channel hydraulics are also approximated by a 1D representation of the Navier-Stockes equations in segment-based distributed models such as the IHDM (Institute of Hydrology Distributed Model) (Calver and Wood, 1985). The IHDM was originally formulated for application to steep upland catchments for which the downslope flow component of partially saturated near surface soils was considered to be important in generating the storm hydrograph. In the IHDM the catchment is divided into hillslope areas and channel lengths which are represented in the model by rectangular sloping planes termed hillslope elements and straight channels of constant cross section termed channel elements. Simplifying the catchment geometry allows for simple boundary conditions for the flow equations used. An effect of the large scale at which the model is applied precludes the representation of the fine detail of the flow network in the catchment which is essentially lumped at the scale of the hillslope element. Subsurface unsaturated and saturated flow are represented in 2D vertical slices while surface and channel flow is considered in only 1D. The segment based structure of the IHDM is very different to that of the grid based SHE model. The structure provides a more accurate representation of sub-surface flow process in cross-section than the SHE model, but provides a poorer horizontal representation of the catchment with less spatial discretization and with overland flow represented in only 1D and the lack of detail at the river/slope interface precludes any detailed representation of overbank flow and river flooding.

Thus, while both hydraulic and catchment based hydrology models are able to represent channel flow in 1D where the lateral extent of inundation is extrapolated at pre-determined cross-sections along the channel, 1D representation of the Navier-Stokes equations effectively constrains the ability of these models to represent the physical processes of overbank flow. Indeed, 1D flow representation precludes the representation of lateral momentum transfer between the channel and floodplain and an accurate representation of topography while a description of the lateral extent of inundation is restricted to discrete cross-sections all of which must be defined *a priori*. 1D representation of channel flow typically takes no account of the effects of turbulence. These deficiencies in 1D flow representation limit the application of models employing 1D representation where the requirement is for a detailed spatially distributed description of inundation characteristics.

Two-dimensional channel representation: Currently two-dimensional (2D) approximations of channel flow are restricted to a small number of hydraulic models. Examples of which include RMA-2 (King and Roig, 1988), TELEMAC2D (Hervouet and Van Haren, 1996) and a model developed by Defina *et al.* (1994).

2D hydraulic models employ the 2D depth averaged shallow water equations for surface flow (otherwise known as the Saint-Venant equations) which are ultimately derived from the full 3D

Navier-Stokes equations. These equations, which have a lateral component (being 2D in plan) allow a full 2D spatial representation of channel geometry, floodplain topography and the resulting floodplain flow (a representation of momentum exchange is usually included in two-dimensional models). Indeed, 2D hydraulic models can potentially provide a solution to the four specific problems identified with 1D representation where lateral velocity components and an explicit description of turbulence are integral to the mathematical description and the 2D spatial discretization allows complex topography and channel form to be more accurately represented. Consequently, there is no need to assume aspects of the flow field prior to the simulation.

The general approach adopted for solving the equations of flow over a 2D surface is one in which the domain of interest is discretised spatially into a finite number of discrete cells, usually termed elements, thereby forming a mesh of points over which the equations are solved to obtain pointwise approximations of the internal state of the system. To this end, 2D hydraulic flow models usually employ a finite difference or a finite element numerical solution technique. The finite difference method (FDM) involves discretising the domain into a mesh of nodes which define the corners of regularly shaped rectangles while the finite element method (FEM) allows for a more flexible element geometry where it is possible to define elements with arbitrary shapes which may be may be linear triangles, distorted rectangles or even shapes defined with curved boundaries. Thus, by using the FEM the geometry of the mesh is much more flexible. The increased flexibility with which elements can be defined by the FEM increases considerably their ability to represent domain topography. By using a FEM the positioning of nodes is not restricted to the regular pattern demanded by FDM and a mesh can be created which faithfully represents topographic features. Both methods require the definition of shape functions which are used to interpolate nodal values throughout the mesh (Pinder and Grey, 1977). In the FDM these functions are exclusively linear while in the FEM, although linear functions can be used, it is possible to define more complex interpolators, including cubic and quadratic.

For linear 1D applications the FEM offers no advantages over the FDM and will result in identical results but by way of a more complex procedure. The FEM comes into its own for applications which are multi-dimensional where the mesh can be refined to represent complex topography and associated flow patterns. 2D domain discretisation using a standard finite difference method and a finite element method are presented in Figure 2.4 while in Figure 2.5 two examples of the nature of the finite element mesh developed for the TELEMAC2D finite element model (Hervouet and Van Haren, 1996) are given. The first represents the discretisation for a 40 km reach of the River Severn (Bates *et al.*, 1996) while the second illustrates the 20000 element discretisation resulting from an application of the model to a dam break study (Hervouet and Van Haren, 1996).

While these models provide good representation of floodplain processes in a hydraulic context, currently their predictive power is compromised through the failure to account for floodplain hydrology. The model structure assumes zero flux boundaries at all points on the reach except for the upstream inflow and downstream outflow boundaries and at the interface between the channel and tributaries. Typically the floodplain is assumed to receive zero inputs from adjacent hillslopes (Charlton, 1995; Bates *et al.*, 1996) and to experience zero flux through the floodplain surface which is assumed to be impermeable. The hydrology of the floodplain and its potential contribution to flood flows is thus ignored.

(a)

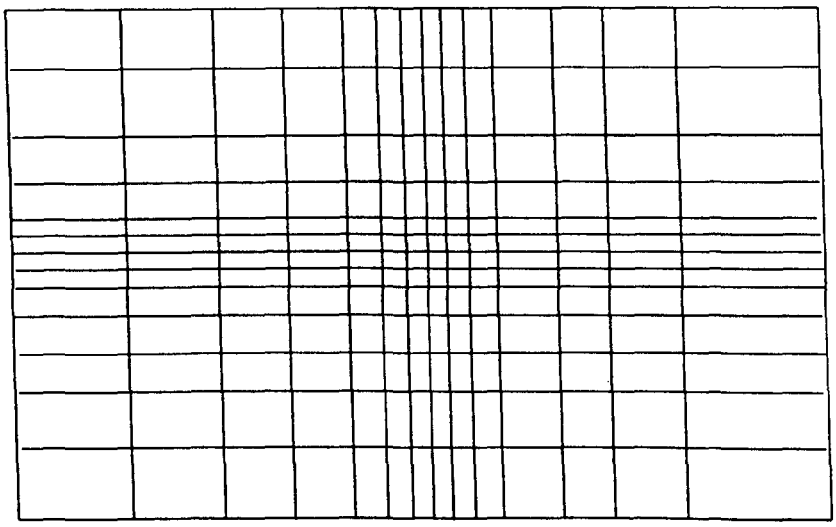

(b)

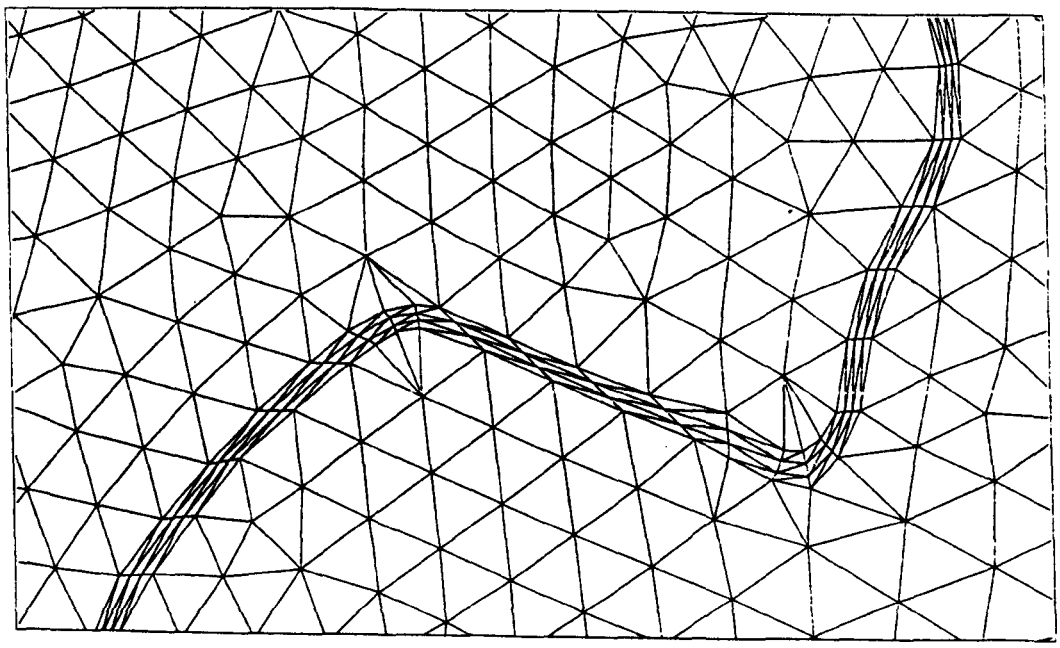

Figure 2.4 Illustration of 2D domain discretisation using (a) a standard finite difference method and (b) a finite element method.

(a)

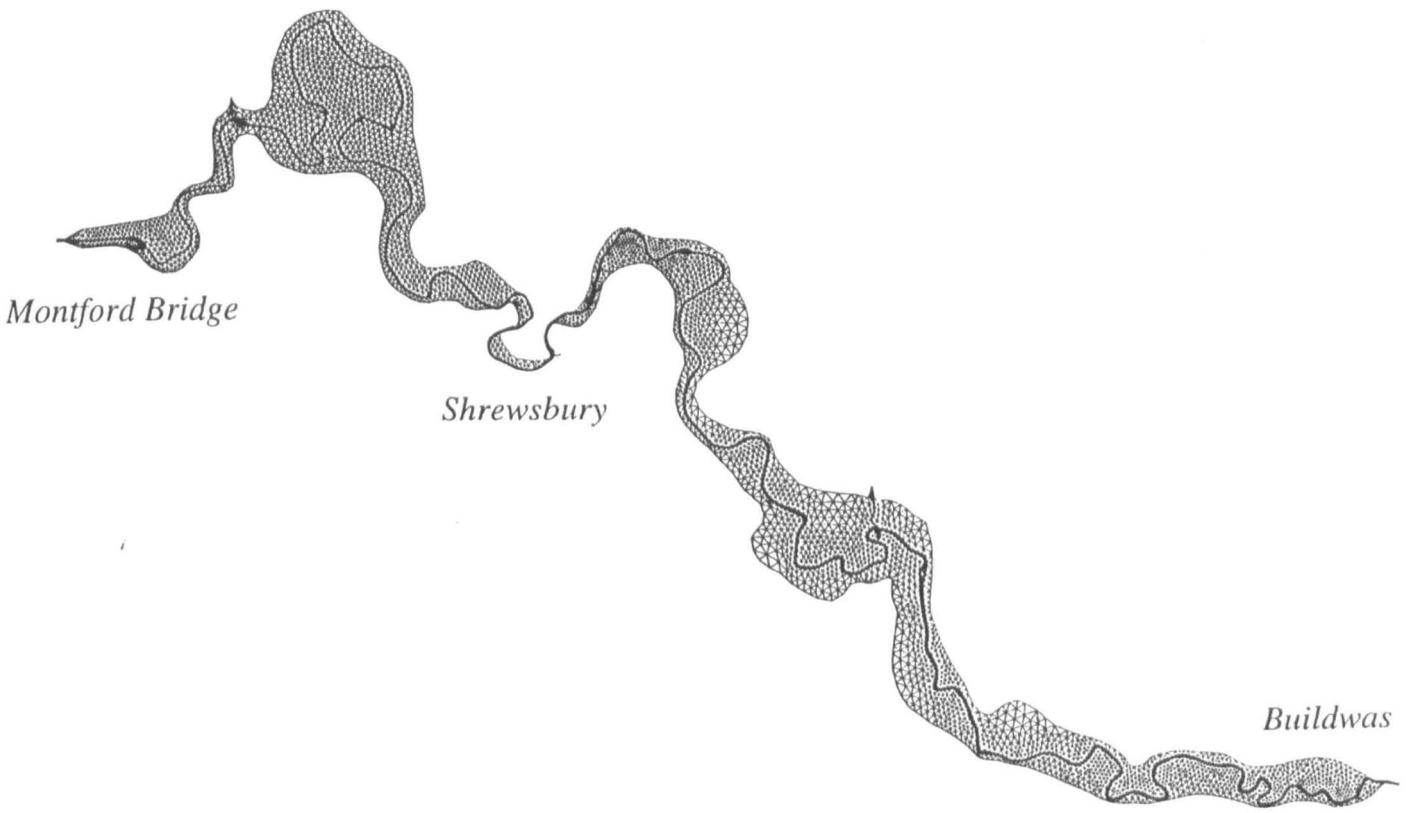

(b)

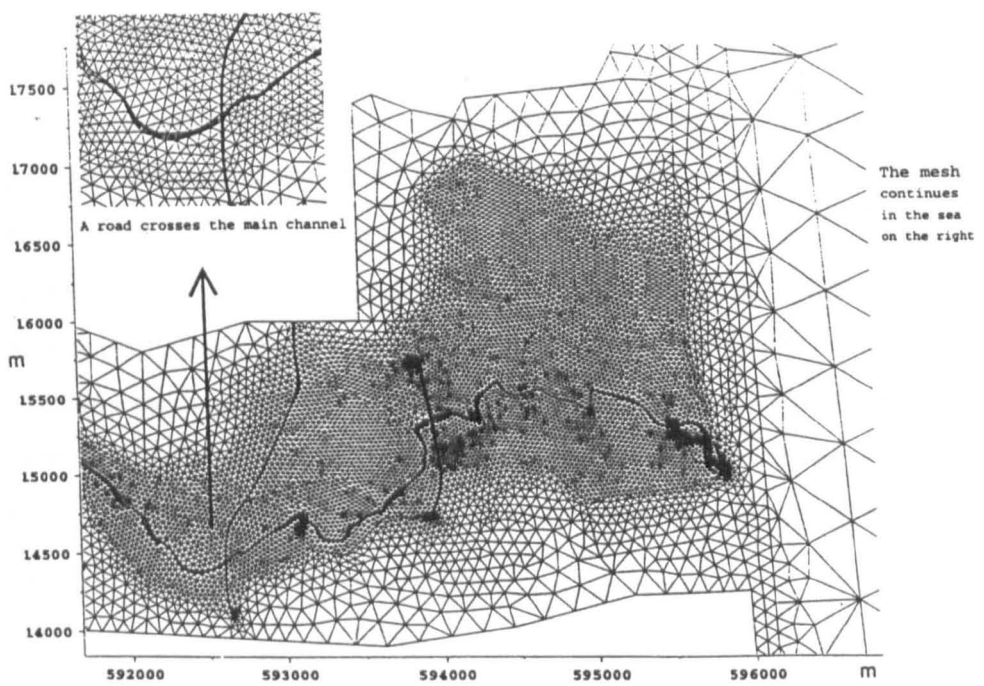

Figure 2.5 Examples of 2D finite element mesh discretisations developed for floodplain flow applications. (a) A 2D finite element discretisation for a 40 km reach of the River Severn, UK (after Bates *et al.*, 1996) and (b) a 2D mesh comprising 20000 elements developed by Hervourt and Van Haren (1996) for a dam break simulation.

Three-dimensional channel representation: 3D models have been developed for fluid flow but due to their complexity and computing requirements their application is generally limited to small and generally specialist cases. Although they offer increased physical representation, being able to simulate secondary flow cells, vertical flows, and the structure of the shear layer, they require a large number of empirical constants, are extremely computer intensive and, as yet, have not found general application in engineering design or river reach studies, although a number of research applications have been attempted. Hervouet and Van Haren (1996) describe the application of the TELEMAC system to 3D free surface flows. Infact, the model solves the 3D version of the 2D shallow water equations and assumes hydrostatic pressure. The model was applied to an 80km reach of the River Loire, France, which required a 3D mesh, obtained by superimposing 2D meshes through the water depth, comprising 60,000 prisms. Such applications remain at the limit of present computing capabilities while the advantage gained through a 3D over a 2D representation has yet to be assessed for flood prediction. Indeed, it is possible that any advantage derived is small and Knight and Shiono (1996) have suggested that the variability (in hydraulic behaviour) imposed by the hydrology of the floodplain may be of greater practical significance than a more detailed understanding of the 3D hydrodynamics of overbank flow.

Table 2.1 presents a summary of the models discussed in the preceding section.

2.2.3 Incorporating the effects of infiltration in 2D floodplain flow representation

In *Chapter 1* it was stated that 2D finite element hydraulic models currently provide the best practically achievable representation of floodplain hydraulics. This is supported by the preceding discussion where the deficiencies identified in 1D representation are overcome in 2D representation and the restriction in element flexibility in 2D finite difference formulations is overcome by the flexibility in elemental shape inherent in the finite element technique as illustrated in Figure 2.5. 3D hydraulic representation, on the other hand, presents a solution which more accurately considers the 3D structure of compound channel flow as illustrated by Shiono and Knight in figure 2.1 yet the solutions are excessively computer intensive and any advantage they infer over 2D flow representation has yet to be established.

2D finite element hydraulic models thus represent the state-of-the art in floodplain flow modelling. However, although they have the necessary resolution to represent complex topography and surface flow in the floodplain their predictive power in some environments is potentially compromised through their inability to represent the interaction between surface and subsurface flow. In contrast, physically based distributed models of catchment hydrology account for a greater number of

interacting flow processes at the catchment scale but do not represent floodplain morphology and flow at sufficient spatial resolution. Thus, although adequate for the flow routing necessary in catchment hydrology simulations these models cannot fully describe the complexities of overland flow as this is represented in 1D. In addition, typical cell sizes of 50 to 500m do not allow an accurate discretisation of the channel - floodplain topography to be made which results in a poor representation of spatially complex flood flows.

Model	Type	Spatial representation of channel and floodplain flow
FLORIS (Kuehnet and Faeh, 1983)	Distributed hydraulic model	1D finite difference (lateral extent of flood water calculated at specified sections along the reach)
SHE (Abbott *et al.*, 1986)	Grid-based distributed catchment hydrology model	1D finite difference (no account taken of lateral extent of floodwater flow)
MIKE-SHE (Refsgaard and Storm, 1995)	Grid-based distributed catchment hydrology model	1D finite difference (no account taken of lateral extent of floodwater flow)
MIKE-11 (Havno *et al.*, 1995)		1D (lateral extent of flood water calculated at specified sections along the reach in combination with the MIKE SHE model)
IHDM (Calvar and Wood, 1985)	Segment-based distributed hydrological model	1D finite difference
RMA-2 (King and Roig, 1988)	Distributed hydraulic model	2D finite element representation
TELEMAC2D (Hervouet and Van Haren, 1996)	Distributed hydraulic model	2D finite element representation
TELEMAC3D (Hervouet and Van Haren, 1996)	Distributed hydraulic model	3D representation of the 2D Saint-Venant Equations of surface flow.

Table 2.1 Spatial representation of channel and flood flow for selected numerical models.

Thus, although catchment hydrology models such as the MIKE-SHE (Refsgaard and Storm, 1995) can simulate hillslope and floodplain surface and subsurface flow pathways (for example see Figure 2.2), their representation of channel and near channel areas is inadequate to represent the spatially dynamic nature of flood events. 2D hydraulic models have been developed to a resolution appropriate to floodplain flow simulation in a hydraulic sense yet their predictive power in some

environments is potentially compromised through their inability to account for floodplain hydrology, specifically infiltration.

Their is an obvious requirement therefore for the inclusion of subsurface flow processes in 2D hydraulic models.

2.3 Predicting the behaviour of NO_3-N in the floodplain

Concerns about losses of NO_3-N to surface and ground waters are not new. Concern was initially expressed by agronomists after the economic consequences of lost NO_3-N to farmers was realised. This concern has now extended to include the detrimental environmental and health problems associated with excess NO_3-N in receiving waters. Although it is now widely accepted that the concentration of NO_3-N in surface waters has increased over recent decades it has been difficult to clearly isolate the assumed link between land use, fertilisers and surface water quality predominantly as the source of NO_3-N is generally diffuse. However, it is generally accepted that in rural catchments agricultural sources represent the most significant contribution to the NO_3-N load of receiving waters and that this arrives largely from non-point or diffuse sources. In heavily urbanised catchments wastewater from domestic and industrial sources can also result in large NO_3-N loads in receiving waters (Hanson *et al.*, 1994).

The floodplain occupies a unique position in the catchment between the terrestrial and aquatic ecosystems and has been shown to be instrumental in controlling the flux of energy and material between the two. It is the capacity of the floodplain to function as a regulator of nutrient fluxes primarily between farmed (Haycock and Burt, 1993; Jordan *et al.*, 1993; Lowrance, 1992) and urbanised (Hanson *et al.*, 1994) terrestrial ecosystems and the aquatic ecosystem within the catchment which has generated a considerable literature dedicated to investigating the potential of floodplains to buffer nutrient rich runoff from land adjoining water courses. Much of this work has concentrated on the zone immediately adjacent to the stream or river channel, the so called 'buffer zone', which has been shown, under certain circumstances, to enhance nutrient retention and cycling and which may include part or all of the floodplain. Although buffer zones have a range of possible functions including habitat conservation, maintenance of biological diversity and recreation to name a few, perhaps their greatest potential lies in their implementation for use in reducing diffuse pollution reaching surface waters and, ultimately, drinking water (Phillips, 1989a). It is as mediators of nutrient and sediment fluxes within the catchment that buffer zones attract most research interest.

The NO_3-N removal potential of buffer zones has been investigated in a number of floodplain buffer systems of varying hydrology, geology, soil type, vegetation cover and size. Forested riparian

systems developed on floodplains have been acknowledged as effective filters against diffuse NO_3-N inputs from agricultural land by numerous authors (Simmons *et al.*, 1992; Groffman *et al.*, 1992; Jordan *et al.*, 1993; Jacobs and Gilliam, 1985; Lowrance, 1992; Haycock and Pinay, 1993). Simmons *et al.* (1992) report removal of groundwater NO_3-N in a forested wetland location to be generally in excess of 80% during both the growing and dormant seasons while in the zone immediately upslope of the wetland location, NO_3-N losses were reported to be less than 36% during the growing season and from 50 to 78% during the dormant season. The authors observe that NO_3-N attenuation in the transition zone consisting of 'somewhat poorly' and 'moderately well drained' soils was positively correlated to water table elevation and suggest that the higher NO_3-N attenuation in these soils during the dormant season resulted from the interaction of the contaminant plume with the upper soil layers which exhibited high organic contents and high denitrification potentials. Jordan *et al.* (1993) found that the NO_3-N concentration measured in groundwater decreased from about $8mgl^{-1}$ at the edge of an agricultural field (corn field) to less than $0.4mgl^{-1}$ between 25 and 35m from the corn field, half way through the riparian forest. Most of the reduction in NO_3-N concentration was observed to occur at the edge of a floodplain within the forest where the water table was closest to the soil surface and the soil conditions were highly reducing (-90mV). Loss of NO_3-N was not accompanied by an increase in NH_4-N confirming that nitrate assimilation (the microbial reduction of NO_3-N to NH_4-N) was not responsible for the observed decrease in NO_3-N. Lowrance (1992) conducted denitrification enzyme assays (DEA) to determine the spatial and temporal distribution of denitrification potential relative to changes in NO_3-N concentrations in a Georgia coastal plain, USA. Denitrification activity was found to be concentrated in the top 10 cm of soil and to be minimal at the top of the water table. The results show that in this case denitrification potential in the shallow aquifer does not coincide with the rapid disappearance of NO_3-N observed in the first 10m of the riparian forest which led the author to suggest vegetative uptake as the primary NO_3-N removal mechanism for this riparian system during winter. Carbon availability at depth is generally thought to be an influential determinant of denitrification rates and several studies have shown that the potential for denitrification in the subsurface is low due to low levels of available carbon (Obenhuber and Lowrance, 1991; Parkin and Meisinger, 1989).

Effective NO_3-N filtering has also been reported for floodplains under grass (Haycock and Burt, 1993; Haycock and Pinay, 1993). Haycock and Burt (1993) found reductions in the mean winter concentration of groundwater NO_3-N of 82% as flow passed from the hillslope to the floodplain. Haycock and Pinay (1993) compared the effectiveness of grass and poplar vegetated buffer strips during the winter for the River Leach catchment, England, and found that for comparable groundwater transit times the grass riparian site, which was able to retain 84% of the NO_3-N load, was marginally less effective than the poplar site which retained almost all NO_3-N. This authors

suggest that the observed difference in buffering capacities may be due to carbon limited bacterial activity in the grass site, suggesting the importance of vegetation in sustaining the viability of a soil microbial population able to undertake denitrification.

Most authors use expressions such as 'retained' (Haycock and Pinay, 1993; Jordan *et al.*, 1993), 'absorbed' or 'attenuated' (Simmons *et al.*, 1992) to describe the fate of NO_3-*N* within riparian soils as the mechanisms of NO_3-*N* removal from groundwater in riparian systems are poorly understood (Burt and Haycock, 1996). It is probable that the relative contribution of the different attenuation mechanisms described above varies both spatially and temporally during the year. During the growing season plant uptake, microbial immobilisation and denitrification are all likely to contribute to the attenuation of NO_3-*N* while during the dormant season it is probable that only microbial activity (denitrification and immobilisation) is responsible for the observed reduction in measured NO_3-*N* (Groffman *et al.*, 1992). During the dormant winter period there is much evidence to suggest that NO_3-*N* attenuation is indeed the result of denitrification where observed losses coincide with elevated soil moisture contents, reduced redox potentials (Jacobs and Gilliam, 1985) and high levels of organic matter and available carbon (usually in the upper soil layers) especially when temperatures remain above freezing. Microbial immobilisation is also implicated as a possible mechanism in the observed winter losses of NO_3-*N* (Simmons *et al.*, 1992). This leads most authors to conclude that both denitrification and microbial immobilisation are the primary mechanisms for the observed reduction in NO_3-*N* concentrations during the dormant vegetative phase and that these processes will only occur if the local hydrology results in flow patterns that transport NO_3-*N* loaded water through the upper soil layers of the riparian zone which consistently exhibit elevated levels of available carbon and denitrification rates (Simmons *et al.*, 1992; Jordan *et al.*, 1993; Lowrance *at al*, 1992; Hanson *et al.*, 1994).

While considerable functional differences both between and within buffer zones implies the need for continued research to determine the environmental conditions required to achieve nutrient removal and indeed, how often these are met, the dominant driving force behind buffer zone function is their hydrology (Burt and Haycock, 1996). It is recognised that the efficiency of a buffer system, measured in terms of NO_3-*N* attenuation, is intimately associated with the hydrology of the hillslope-floodplain continuum, the major flow paths of which are summarised in Figure 2.6. Denitrification is generally considered to be low both in oxygenated surface runoff (Hill, 1990a; b) and in groundwater which passes beneath surface floodplain soils supporting high denitrification potentials (DNP). In the latter, which may result from either a low water table or less permeable surface sediments, the only interaction with the buffer system occurs briefly at the water sediment interface of the channel bed. At this point it is worth noting that reduced NO_3-*N* concentrations have

also been observed in circumstances where NO_3-N rich groundwater has little opportunity to interact with zones of high DNP, notably when groundwater flows at depth, and where vegetative uptake is not implied, alternative explanations are being sought (Burt and Haycock, 1996). The greatest reported losses through denitrification have been associated with subsurface flow which passes through the upper floodplain soil layers which maximises the opportunity for interaction with the processes of NO_3-N attenuation in the buffer system.

During flood events floodplain buffers have also been shown to be effective in removing organic N from surface flow as sediment (Brunet *et al.*, 1994) while floodplain soils have been shown to support higher rates of denitrification through the combined effects of NO_3-N additions in infiltrating floodwater and an increase in soil moisture content (Maltby *et al.*, 1991; Maltby *et al.*, 1996). It is to the potential of floodplain soils as mediators of floodplain NO_3-N concentrations during flood events that the discussion now turns.

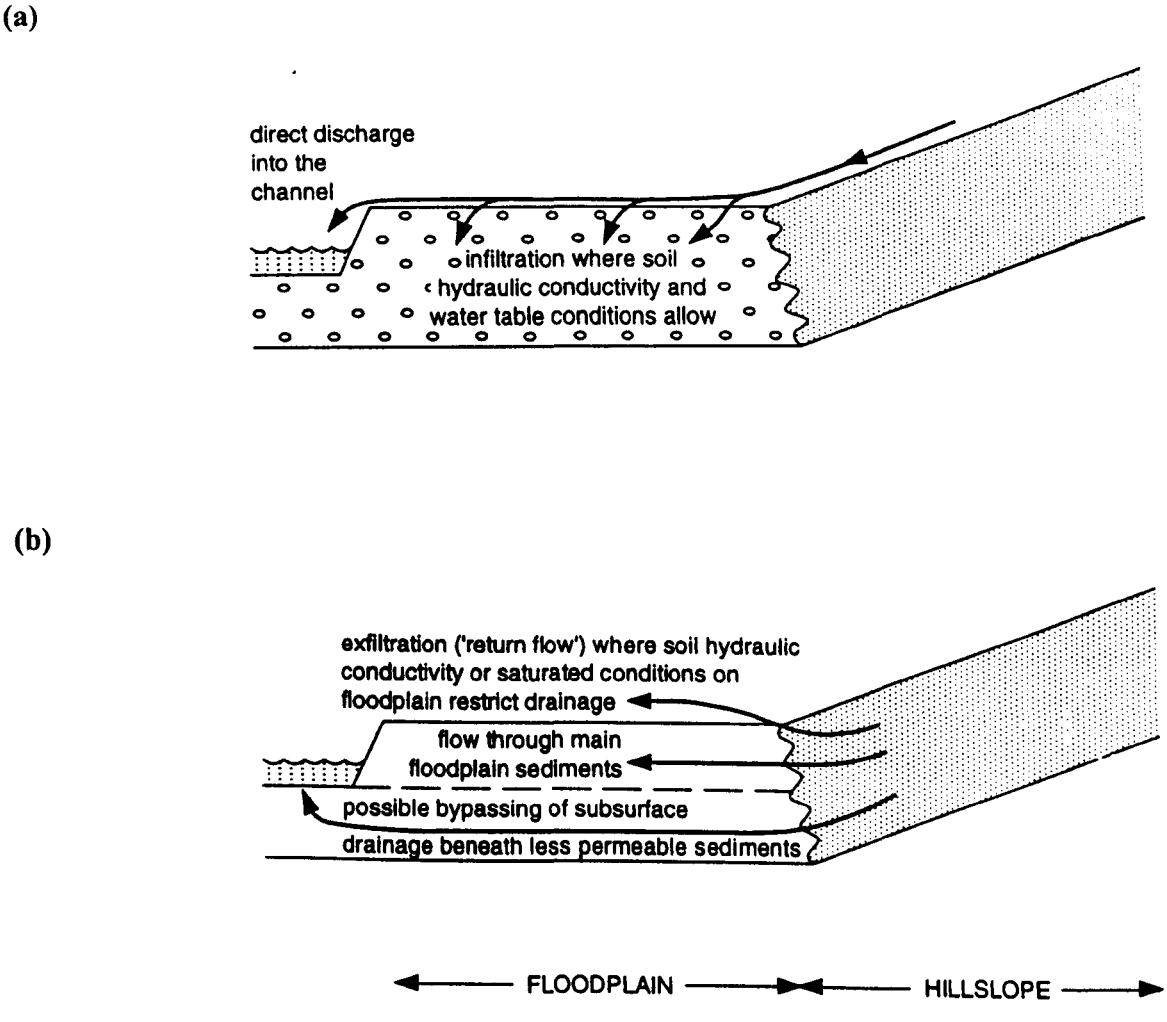

Figure 2.6 Summary of the main flow paths by which hillslope discharge moves through a floodplain to reach the stream channel (a) overland flow (b) subsurface flow (from Burt and Haycock, 1996).

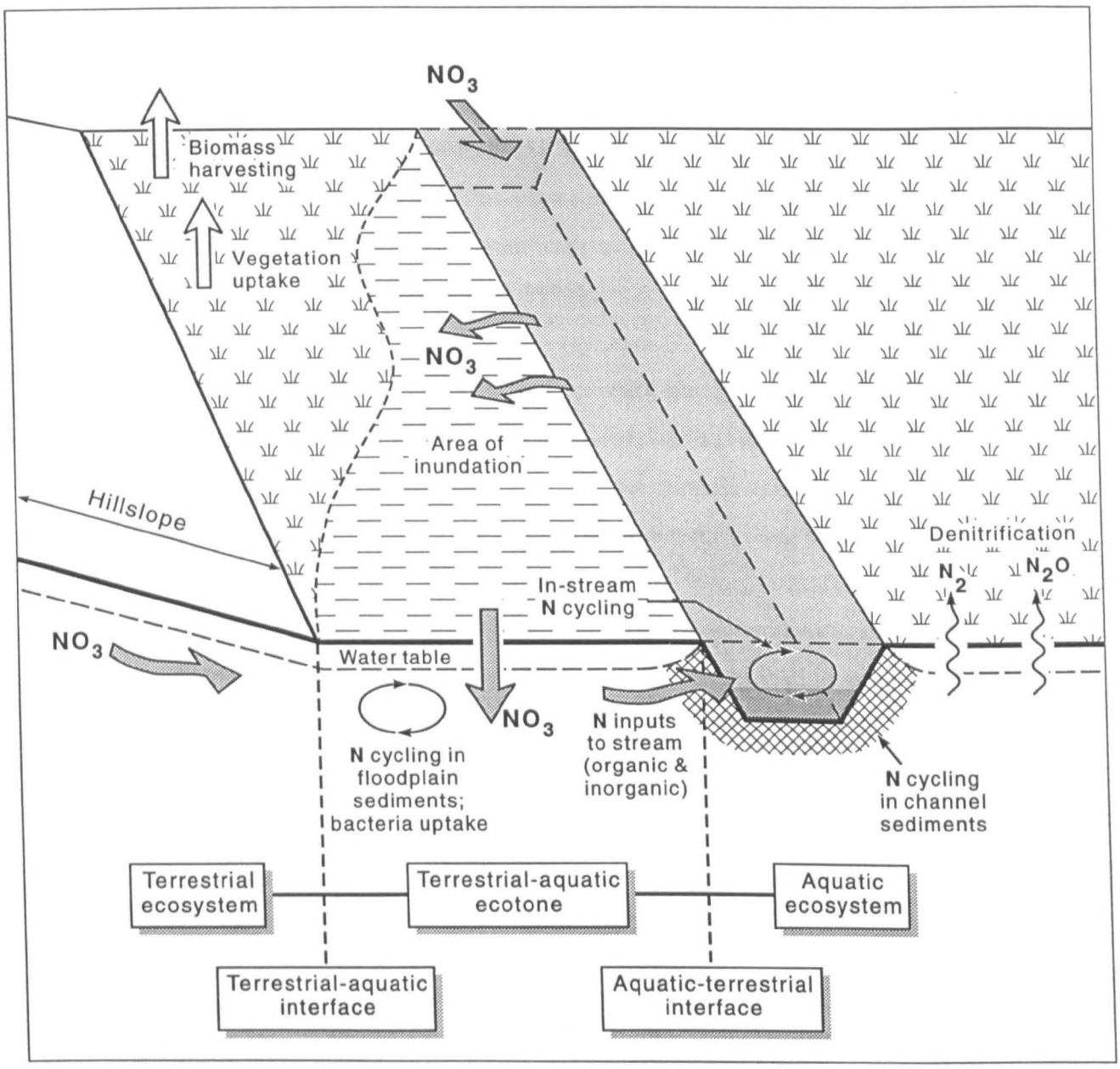

Figure 2.7 An idealised representation of the function of a floodplain buffer zone.

The majority of research undertaken in floodplain systems has been concerned with nutrient retention, most often NO_3-N, from hydrologically driven flow moving laterally towards the channel. The role of the floodplain in influencing the quality of riverine water once this has left the channel and indeed the role of floodwater in creating conditions suitable for denitrification in floodplain soils is an area of research which has received little attention, although its potential importance in floodplain buffer function has been considered both numerically (Phillips, 1989b; Chesheir *et al.*, 1987) and in the field (Maltby *et al.*, 1991; 1996). Infiltrating floodwater can both supply substrate (NO_3-N , C) and create or enhance the saturated, anaerobic soil conditions required for denitrification which will have potential implications for both in situ NO_3-N and infiltrating floodwater NO_3-N (Triska, 1989; Maltby *et al.*, 1991).

Evidence as to the possible consequences of surface water inputs on denitrification comes from a number of sources. Hanson *et al.* (1994) observed a marked increase in measured denitrification rates from surface soil samples following a 5cm summer rainfall event in a riparian system near Kingston, Rhode Island, USA. Brunet *et al.* (1994) have sought to quantify the deposition of fine sediments and associated changes in floodplain water quality during large flood events on the River Garonne, France. They estimated that the combined storage of particulate organic N, the adsorption of NH_4-N and denitrification of NO_3-N in shallow standing water resulted in as much as a 2% loss in terms of the total N budget for the river. Maltby *et al.* (1991) measured increased rates of denitrification in soils of the River Culm, Devon, following inundation and attributed these to the increasingly anoxic soil conditions and the supply of NO_3-N in the infiltrating floodwater.

The possible consequence of floodwater input can be summarised as:

- *providing a NO_3-N source*
- *providing a C source*
- *redistributing in situ sources of C and NO_3-N within the soil profile*
- *providing the elevated soil moisture conditions required to initiate denitrification*

The highly spatially and temporally dynamic nature of floods make quantitative investigations into the effects of flood water on both *in situ* and stream-borne NO_3-N dynamics at the reach scale an inherently problematic undertaking using a methodology based on field sampling (eg Maltby *et al.*,

1991, Maltby *et al.*, 1996; Brunet *et al.*, 1994). However, this currently represents the only available method.

There exists a need, therefore, for a methodology which can be applied to quantitatively assess the NO3-N loading capacity of floods and the buffering potential of floodplain soils during floods.

2.4 The opportunity for an integrated approach

The discussion into the numerical modelling of floodplain flow and floodplain NO_3-N dynamics illustrates that many of the limitations in contemporary floodplain research stem from the current inability to represent the floodplain as an integrated hydrological system. The discussion presented above highlights;

- *The requirement for 2D finite element representation of floodplain hydraulic processes commensurate with the spatial and temporal resolution required for investigations into (a) flood flow characteristics and (b) hydraulically driven NO_3-N dynamics.*

- *The need to represent subsurface hydrology within 2D hydraulic models to enable the effects of infiltration to be incorporated within model prediction and to facilitate the investigation of hydraulically driven NO_3-N dynamics within the floodplain environment.*

It is clear therefore that there is a need for a new conceptual approach to modelling hydraulically driven processes operating on the floodplain and that the opportunity for such an approach can be provided through the coupling of a state-of-the-art 2D finite element hydraulic model with a model describing floodplain hydrology.

2.5 Introduction to the research objectives and research strategy

This section begins with a statement of the research objectives and then considers how the research is to be undertaken.

The solution identifies the development of a state-of-the-art 2D finite element hydraulic model to include infiltration as the next step forward in extending the physical representation of floodplain hydraulic models which will enable the interaction between surface processes, both hydrological and chemical, to be modelled. The discussion identifies the two areas of current research interest that are to be investigated by way of the coupled model, namely the effect of the floodplain soil

moisture store on flood model prediction and the effect of flood events on floodplain NO_3-N dynamics. The specific research objectives are:

(1) ***To couple a physically-based, distributed 2D finite element hydraulic model to an infiltration model for application to the floodplain environment at a high spatial and temporal resolution.***

(2) ***To determine the impact of infiltration on 2D hydraulic model flow prediction.***

(3) ***To identify the dominant processes which determine the fate of NO_3-N in floodplain buffer systems during the winter and to incorporate these within the structure of the floodplain model developed in (1).***

(4) ***To examine the contention that flood events represent high denitrification flux periods in floodplain soils in terms of (i) the loss of in situ soil NO_3-N and (ii) the input and subsequent loss of infiltrating floodwater NO_3-N.***

2.5.1 Research strategy

The research strategy adopted in accordance with these aims is illustrated in the flow diagram presented in Figure 2.8 and discussed in greater detail throughout the remainder of this chapter.

2.5.1.1 Development of a theoretical framework for an integrated approach to modelling floodplain hydraulics, hydrology and NO_3-N chemistry.

The current state of research in the floodplain has been reviewed in terms of the requirement for a more integrated approach to modelling surface and subsurface flows. It is suggested that such a development underlies a more detailed understanding of hydraulically driven floodplain processes. Existing models of floodplain flow have been found to be lacking in terms of their representation of floodplain hydrology while catchment hydrology models, although they often represent the links between surface and subsurface hydrology, fail to adequately represent floodplain flow processes at the spatial and temporal resolution required for detailed process analysis in the floodplain environment. An argument for the development of an existing physically based, distributed 2D finite element flood model to account for infiltration is advanced as a novel conceptual approach to modelling floodplain hydrology and necessary pre-requisite to a more accurate numerical representation of flow and associated processes in the floodplain environment.

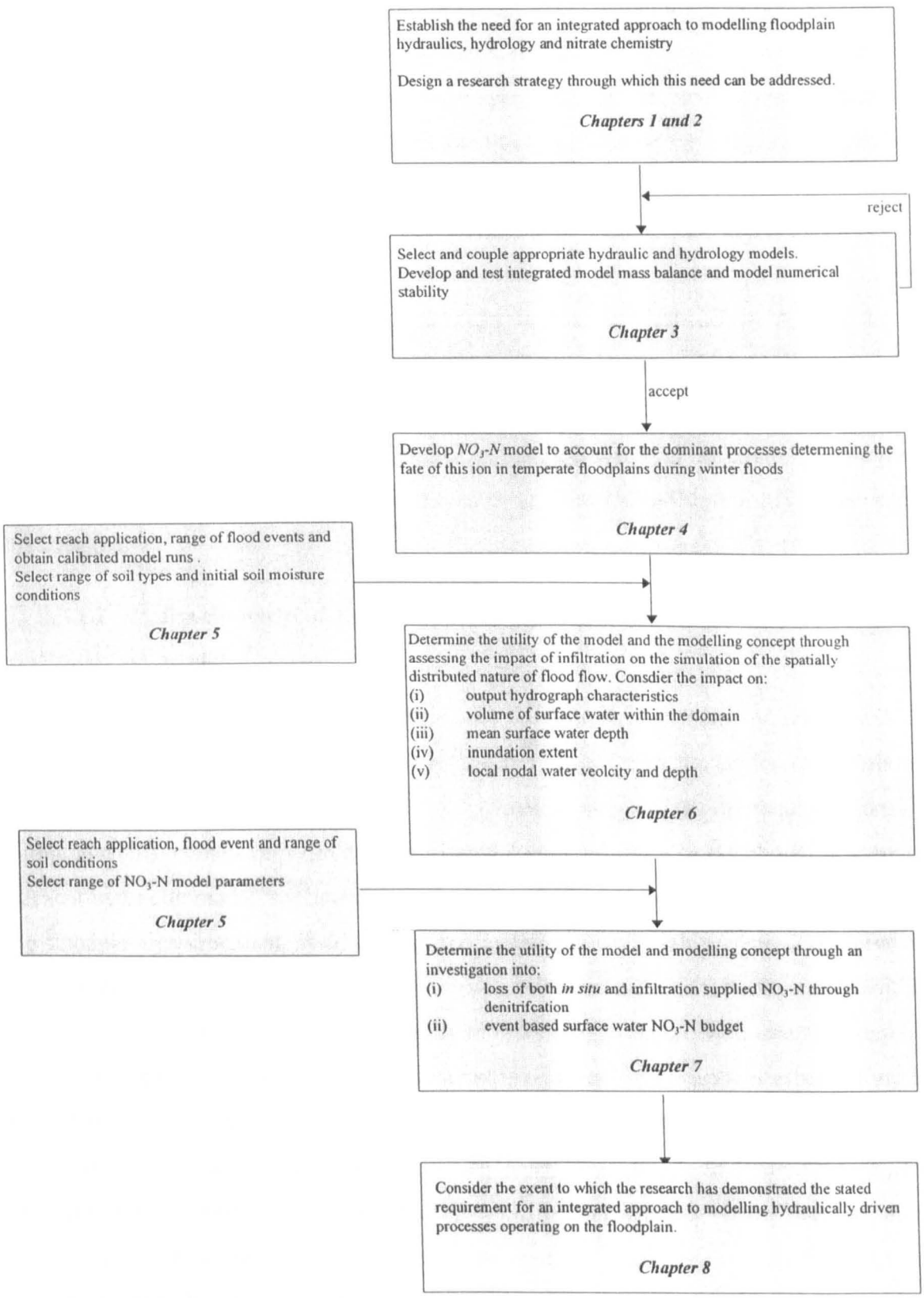

Figure 2.8 Flow diagram representing the proposed research.

As numerical representations of the dominant physical processes occurring in the modelled environment, physically based distributed models provide a structure in which spatially and temporally variable inputs can be accommodated and where output is spatially referenced (Collison, 1993). Indeed, physically based models are necessarily distributed because the equations on which they are defined generally involve one or more space co-ordinates and as such have the ability to represent the spatial pattern of hydrological conditions within the modelled environment, whether this is the entire catchment or the floodplain. As the flow processes within the floodplain are complex and highly spatially and temporally variable a physically based approach lends itself to the requirements of the research in a way that a lumped parameter model could not. The physically based approach enables the interaction between surface and subsurface flow to be modelled effectively as it allows spatially variable physical properties, such as soil moisture, to be described (modelled) at a high resolution (both temporal and spatial). It is envisaged that fluctuations in soil moisture storage will influence the capacity of surface water to infiltrate. The arguments for developing a physically based hydraulic model to account for infiltration have been addressed in this Chapter.

2.5.1.2 Development of a physically based integrated floodplain hydraulic-hydrology model.

This stage of the research is concerned primarily with the development and testing of the coupled hydraulic-infiltration model. This section necessarily begins with the choice of models to be used and is based on the following: (i) the intended model application, (ii) the required model input and output and (iii) model compatibility. For example, with reference to the choice of a suitable finite element hydraulic model, applicability to the research depends upon the model ability to represent the floodplain environment, at an appropriate spatial and temporal resolution, in terms of (i) both the longitudinal and lateral floodplain topographic gradients, (ii) floodplain topography, (iii) floodplain and channel friction and (iv) channel morphology. Again, with reference to the hydraulic model, consideration of model input requirements represents an important aspect of model choice. Physically based models often have considerable parameterisation data requirements including: (i) upstream and downstream hydrometric data, (ii) floodplain and channel friction data, (iii) floodplain and channel topographic data and (iv) floodplain and channel slope data. Additional data requirements can include aerial photographs of inundation extents, records of former high water marks and other historical data for model validation. These are just a few examples of the factors that must be considered when choosing a hydraulic model for the research. Importantly, choice of an infiltration model requires consideration of the dimentionality at which this process is to be represented.

UNIVERSITY OF BRISTOL LIBRARY

This stage also includes testing of the coupled model, the aim of which is to demonstrate model function in the new model construct. These aspects are addressed in *Chapter 3*.

2.5.1.3 Development of a NO_3-N model applicable to the floodplain environment

In *Chapter 4* the development of the NO_3-N model is addressed. The Chapter begins with a review of NO_3-N processes within the floodplain and identifies those which are dominant in determining the fate of NO_3-N within this ecosystem. From this review a conceptual model is advanced from which a numerical model is developed with reference to contemporary modelling strategies and incorporated within the structure of the integrated floodplain-hydrology model.

2.5.1.4 Parameterisation of the hydraulic, hydrological and NO_3-N models

Prior to running the model simulations both the choice of model reaches and the range of soil environments to which the model will be applied must first be identified. Consideration of the environments should include floodplain extent (size of floodplain within the catchment), soil types and initial soil moisture conditions (seasonally controlled), all of which are likely to be major determinants in the size of the floodplain soil water sink. In lowland floodplains where the soils have developed in alluvium and inundation extents are often considerable both spatially and temporally, infiltration losses are likely to be significant, at least initially. However, where the floodplain is limited in extent (bounded by steep hillslopes), the subsoils are impermeable or previously saturated then losses are expected to be small. These considerations are important for both aspects of the study. Where inputs to the soil sink are small then the effect of infiltration on both flood wave attenuation and denitrification are also likely to be minimal, the converse will be true where these losses are large. The choice of suitable test reaches for model application is linked closely with the choice of hydraulic model and relate both to the physical nature of the reach itself and the availability of data required for paramaterising and running the model. The physical nature of a reach includes flooding frequency and magnitude, floodplain topography, channel morphology and floodplain and channel gradients. In terms of the physical attributes of a reach, its suitability is very much dependant upon the capabilities of the hydraulic model chosen (2.5.1.2). As an example, the choice of a reach with complex channel morphology is unsuitable if the hydraulic model chosen is incapable of representing this spatially or if it is incapable of solving the equations of flow under rapid directional change. The choice of a suitable reach also extends to include data availability. Model paramaterisation is addressed in *Chapter 5*.

2.5.1.5 Application of the coupled hydrology model to an investigation of the impact of infiltration on floodplain surface flow characteristics

In order to determine the effect of infiltration on flood model prediction and to establish the utility of the modelling concept the model is applied to a range of soil environments in which both soil

type and initial soil moisture content are varied. The range of conditions is chosen to represent the environments of interest - these being lowland temperate floodplains during the winter months. These issues are dealt with in *Chapter 6.*

2.5.1.6 Application of the integrated hydrology-nitrate model to assess the implications of flooding on in situ soil and flood water NO_3-N

The model is applied to a range of NO_3-N model parameter combinations to assess utility of the model concept through an investigation into the effects of flood water induced denitrification on in situ NO_3-N loss from floodplain soils and the loss of NO_3-N from infiltrating floodwater. Of interest is model response (sensitivity) to in situ NO_3-N concentration, the denitrification rate constant and soil hydraulic conductivity. These issues are addressed in *Chapter 7.*

2.5.1.7 Identification of requirements for future work

Following model development and application, matters arising from either of these stages are identified along with recommendations for future model development and application. The runs in sections 2.5.1.5. and 2.5.1.6. are designed to provide a commentary on the modelling concept developed in the thesis thus the results of these simulations will be examined with this in mind. These issues are discussed in *Chapter 8.*

2.6 Conclusions

The need for an integrated approach to floodplain process modelling has been established. State-of-the-art 2D finite element hydraulic models are identified as the most suitable platforms from which to develop such an integrated approach to modelling floodplain hydrology as they offer high spatial and temporal resolution of surface processes in two-dimensions (eg flow, topography) and an existing and well tested platform from which to include infiltration and a NO_3-N model.

While current finite element hydraulic models assume a zero flux condition at their surface boundary their structure (finite element) makes them suitable for further development. Indeed, the significance of hillslope inputs to 2D finite element hydraulic models has recently been investigated (Charlton, 1995; Bates *et al.*, 1996). Relaxing the zero flux surface boundary enables an exploration of the significance of the floodplain infiltration sink on predicted flood characteristics and the influence of flood inundation on NO_3-N processes within the floodplain. Consideration is also given to the possibility of using and/or developing catchment hydrology models for the same purpose. However, a review of these models reveals that while many of these already represent the catchment in three-dimension (see for example the SHE model (Abbott *et al.*, 1986)) they have a poor spatial representation of floodplain flow and are unable to accurately represent floodplain topography.

However, development of these models is continuing and it is possible that the latest generation of SHE models (MIKE SHE - MIKE 11) might soon incorporate a 2D representation of channel flow. Such a development, however, is beyond the scope of this research.

The range of environments over which infiltration is likely to be significant in terms of both flood flow characteristics and denitrification is outlined and it is suggested that infiltration will only have significant effects in some floodplains environments and conditions of soil type and initial soil moisture status. The magnitude of the effect under different conditions of soil type and soil moisture status will be investigated.

Chapter 3 now considers the development of the coupled, physically based hydraulic-hydrology model which forms the basis of the research.

Development of an integrated floodplain hydraulic - infiltration model

3.1 Introduction and Chapter Objectives

Chapter 2 identifies the development of an existing physically based 2D finite element hydraulic model as the most appropriate platform from which to construct a integrated approach to modelling surface and subsurface floodplain hydrology. This Chapter describes the development of such a model.

Accordingly, this Chapter is divided into four main parts. The first of these considers the choice of a suitable 2D hydraulic model. Factors which are instrumental in this choice have been discussed in the previous Chapter and include the applicability of the model to the floodplain environment, the representation of the moving flux boundary and the amenability of the model to coupling, which requires consideration of the model structure, the manner in which source terms are accommodated in the mass continuity equation and the spatial and temporal resolution of the model. The second part of the Chapter considers the choice of a suitable infiltration model. Again, this choice is based upon a number of criteria including the dimensionality at which the process is represented, the nature of the surface boundary, mass conservation, model structure and amenability to coupling and the temporal resolution of the model. The third section deals with the mechanics of the model coupling. Following a description of the coupling of the hydraulic and hydrology models this section describes the development of a soil moisture mass balance which accounts for the spatially and temporally variable nature of water within the floodplain soil. In the final section a series of simulations are run to establish whether surface boundary relaxation has been achieved in a numerically stable manner.

3.2 Choice of a 2D hydraulic model platform

Until recently the application of 2D finite element techniques to free surface flow problems has been confined to a limited number of specialised cases. Finite element techniques were developed as tools to aid in the solution of complex problems in engineering, mathematics and physics (Chung, 1978) and were first applied by engineers in the aerospace industry (Turner *et al.*, 1956). Since then the technique has been applied to a wide spectrum of problems including that of hydraulics research. Initial application to free surface flow problems was restricted to the analysis of small scale problems such as detailed flow patterns near structures and river confluence studies (Gee *et al.*, 1990). In these cases the scale of interest was small and the computational domain remained fully inundated during the simulation. Application to tidal, estuarine and floodplain studies required two advances in 2D finite element techniques; firstly, a modification to enable accurate representation of the moving flux boundary (ie surface wetting and drying cycles) within the domain and secondly, the application of finite element methods to hydrodynamic problems on a scale larger than had previously been attempted (Gee *et al.*, 1990). The problem of representing moving flux boundaries within finite element models of free surface flow has been the focus of considerable recent interest (King and Roig, 1988; Defina *et al.*, 1994; Hervourt and Van Haren, 1996) and it has been the development and implementation of methods designed to represent this problem that has enabled the successful application of finite element models to studies of tidal flats, estuaries and river floodplains.

3.2.1 Modelling Moving Flux Boundaries in 2D Finite Element Models

2D finite element models developed to solve the shallow water equations began as fixed boundary models with limited application to tidal, estuarine and fluvial hydraulic problems (eg RMA-2, Norton *et al.*, 1973). Such models are of use where the modelled environment remains fully inundated and where the boundary conditions can be represented by either a depth of water or a mass flux specified over time. More recently, 2D finite element models have been developed to explicitly account for tidal cycles and floodplain inundation processes, a development that has been encouraged, in part, through a growing requirement for models which can represent a moving boundary for environmental applications (Hervouet and Van Haren, 1996). Tidal flats and floodplains present an interesting problem in that within a pre-determined domain elements may be variously wet, dry, or partially wet. Elements which are either fully wet or dry present few computational difficulties, it is elements in the transitional state which are partially wet which present computational difficulties and for which solutions have been sought. As summarised by Leclerc *et al.* (1990), the difficulty lies in developing a technique for obtaining a non-stationary boundary which avoids or limits violations of the mass and momentum equations. A number of approaches have been adopted to tackle this problem including element exclusion, deforming grid

techniques and methods in which the governing equations themselves are modified.

3.2.1.1 Element Exclusion and other simple techniques

Early attempts to incorporate a moving flux boundary involved simply eliminating dry element from the computational domain adopting the so called 'element elimination' procedure. In a modification to the RMA-2 model (King and Norton, 1978), King and Roig (1988) adopted an element elimination procedure to simulate water inundation and evacuation. Elements were dropped from the computational domain when the water depth at one node in the element fell below a predetermined minimum while elements entered the computational domain once every node associated with an element achieved a predetermined minimum depth. The criteria by which elements are included within, or excluded from, the computation results in both poor representation of the flow boundary as an irregular wetting front and numerical instability as large volumes are impulsively lost or gained in the solution as elements are included or dropped from the modelled domain. Figure 3.1(a) illustrates the wetting boundary resulting from an element exclusion technique. The method is non mass conservative as the residual water volume present on a drying element is lost immediately from the total domain volume following the reduction of water depth below a minimum at only one node. A similar, though converse, problem of mass conservation is associated with re-wetting where a potentially considerable volume is added to the element before all nodes achieve the minimum required depth for element inclusion. Both mass conservation errors and poor wetting and drying front representation can be minimised through defining small elements that follow the bathymetric contours but such an approach increases computational effort and applies greater detail where it is least required - greater detail is more usefully applied where both depth and velocity gradients are greatest, for example at river meanders and not across floodplains and tidal flats.

The element exclusion technique represents perhaps the simplest solution to the problem of moving flux boundaries. Other simple techniques have been reviewed by both Lynch and Gray (1978) and Leclerc *et al.* (1990). Lynch and Grey (1978) identify two further approaches which can be employed essentially to circumvent the moving boundary problem. The first of these uses an imagined ridged wall at the calculated position of the moving boundary to determine the position of the flux boundary for the next time step as illustrated in Figure 3.1(b). The actual position of the boundary is calculated by extrapolating the water level calculated on the ridged wall to the shoreline. This technique suffers from a lack of mass and momentum conservation and fails where significant shoreline movements are encountered. The second technique employs a modified bathymetric representation for the zone influenced by the moving boundary in which the bottom topography is modified to represent a series of steps leading up the shore line, as illustrated in Figure 3.1(c). Using this so called 'staircase' representation entire elements may be switched on or

off instantaneously depending on the calculated water depth as in the element exclusion method. This method allows for improved mass conservation but non-conservation of momentum leads to undesirable oscillations caused by the impulsive movement of the boundary.

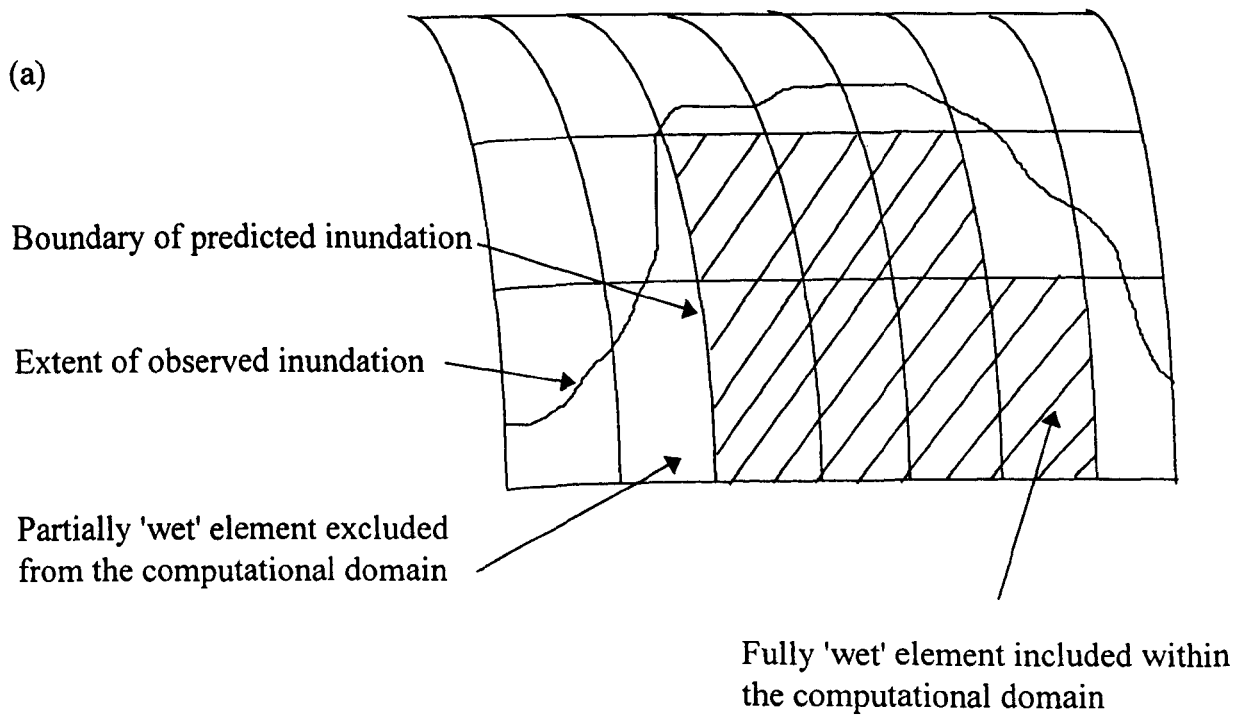

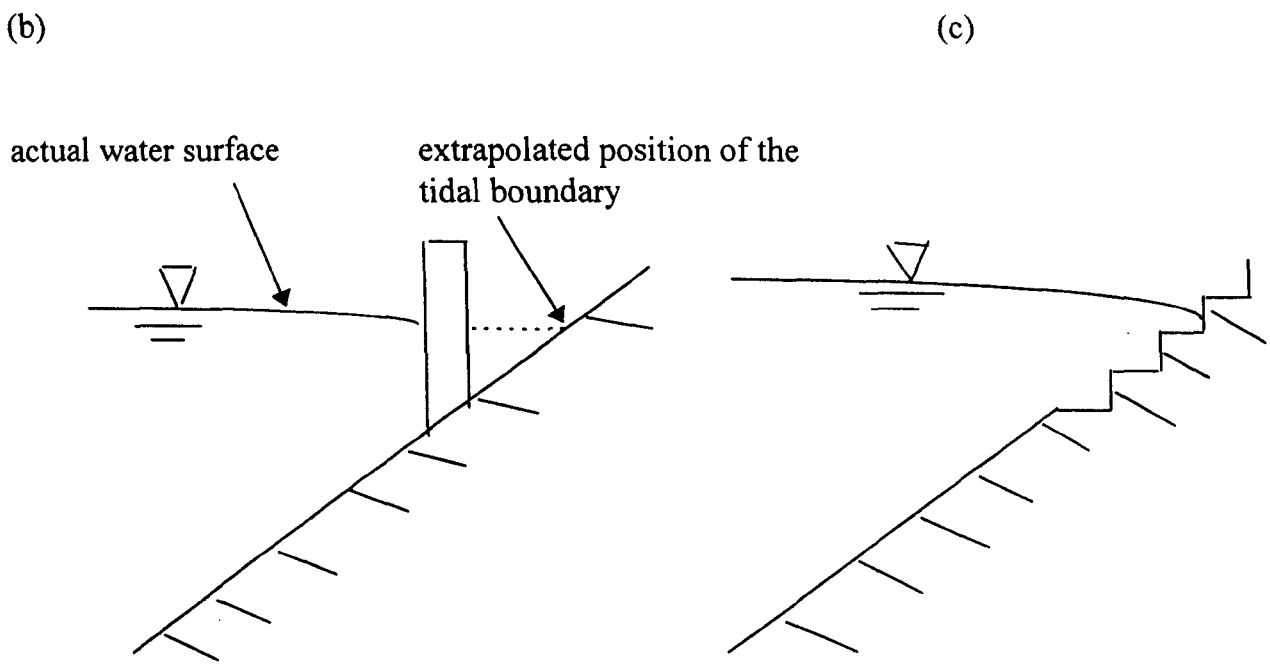

Figure 3.1 Illustration of three discontinuous approaches used to represent the moving flux boundary problem in 2D finite element hydraulic models: (a) representation of an irregular boundary by element exclusion methods (after Anderson and Bates, 1994), (b) specification of an artificial vertical barrier on the flooding boundary (after Leclerc *et al.*., 1990) and (c) the bathymetric 'staircase' approximation (after Leclerc *et al.*, 1990).

3.2.1.2 Deforming Grid techniques

Kawahara and Umetsu (1986) and Lynch and Gray (1978) present techniques for representing moving flux boundaries using a deforming finite element grid. The deforming grid technique has found considerable application in materials engineering and has also been applied to the problem of representing tidal flats. The technique computes the position of the flux boundary at each time step by deforming or rezoning the domain elements. Nodes move according to the computed flux boundary but maintain their initial connectivity until the mesh becomes unacceptably distorted due to accumulated node movement at which point the domain is rezoned. This method suffers from a need for 'excessive' grid detail at those locations where the moving flux boundary is expected but where the velocity and depth gradients are generally small. Where node movement is necessary, considerable computational effort is required, thus although the deforming grid technique eloquently represents the moving flux boundary, where grid re-alignment is required it is highly computationally inefficient.

3.2.1.3 Modification of the shallow water equations

The solution lies in a method that conserves both mass and momentum without complicating the computational procedure or increasing the computational time. Such a method has been developed recently in which the shallow water equations themselves are modified for elements at the moving flux boundary that are partially wet. This approach has been developed for a number of recent 2D finite element hydraulic models for application to environmental problems involving moving flux-boundaries. A selection of these are reviewed:

The 2D finite element model RMA-2 (Norton *et al.*, 1973) was developed originally with fixed boundaries and was later modified to include an element elimination procedure for application to tidal flats. The model was further developed by King and Roig (1988) to allow elements to gradually change from wet to dry states and *vice versa*. The model retains a fixed mesh but modifies the governing equations for partially wet elements using a scaling coefficient, termed the domain coefficient, to achieve a smooth transition between wet and dry states. Partially dry elements are retained within the computational grid until all of the nodes associated with a given element are dry and partially dry elements re-enter the solution domain when one elemental node reaches a given minimum depth, this has the effect of minimising mass discontinuities. RMA-2 achieves this through the implementation of a scaling factor which scales the elemental simulated water volume to a 'true' water volume associated with partially wet elements for each time step. The user is requires to specify a bottom elevation which lies below the lowest possible water surface elevation and to pre-define the volume coefficient, which is then a function of the water surface elevation at each domain node. The volume scaling coefficient is equal to unity for completely inundated elements and less than one for partially wet elements.

A similar technique to that of King and Roig (1988) is used by Defina *et al.* (1994). Two scaling parameters, η and H, are introduced to modify the Saint-Venant equations for flow over partially dry elements. In the mass balance calculation the scaling coefficient, η, applied to the element is a function of the free surface elevation, h. The elemental volume available to flow is calculated using two variables; the mean bottom elevation for the element , h_f, and the threshold depth, Y_{lim}, which represents the difference between the highest ground elevation and h_f (see Figure 3.2). When the free surface elevation, h, falls to the maximum bottom elevation within the element, $h_f + Y_{lim}$, the flow domain begins to dry. Completely dry conditions are assumed to occur once h falls below $h_f - Y_{lim}$. The scaling coefficient η is calculated as a function of h, once h falls below $h_f + Y_{lim}$, and represents the 'wetted percentage' of the element available to flow, as represented in Figure 3.2. Where the domain element is fully wet then η is equal to one and has no effect upon the mass balance calculation. The momentum equations are modified by the scaling coefficient H which is also dependant upon Y_{lim}. The parameters η and H take account explicitly, though synthetically, of the ground unevenness and are both dependant upon the value of Y_{lim}.

This dependence upon Y_{lim} determines that the effectiveness of the model depends very much upon the accuracy of the estimation of this parameter. For flood propagation following a hypothetical river bank collapse D'Alpaos *et al.* (1994) illustrated that a doubling of Y_{lim} from 0.3 to 0.6m resulted in an average celerity[1] increase of over five times, from $0.5ms^{-1}$ to $2.8ms^{-1}$. This sensitivity of the model to Y_{lim} illustrates the importance of being able to accurately estimating this parameter, an area that the authors suggest requires further research.

TELEMAC2D (Hervouet and Van Haren, 1996) offers two radically different options for treating tidal flats and floodplains. The first of these consists of removing all elements which are not entirely wet from the calculations (an element exclusion technique) and the second maintains partially wet elements within the solution domain and corrects for those terms, such as the free surface gradient, which are rendered false. These various representations of the wetting front are illustrated in Figure 3.3. Figure 3.3(a) represents the actual free surface and Figure 3.3(b) the situation which results when neither of the modifications are adopted. In this case, partially wet elements are retained

[1] Celerity describes the velocity of a wave relative to the velocity of the fluid. Celerity, C_g, of a gravity wave in shallow water is given by

$$C_g = (gY)^{1/2}$$

where g is the acceleration due to gravity and Y is the water depth.

within the solution domain and the model interpolates a spurious lateral free surface across the element resulting in both spurious free surface flows and mass balance errors. Figure 3.3(c) illustrates the effect of employing the element exclusion technique, which is non-mass conservative (see section 3.2.1.1). A more accurate representation is provided through a better approximation of the lateral free surface slope in partially dry elements as illustrated in Figure 3.3(d). Within each domain element a check is conducted to test for the presence of dry nodes. If the bed elevation for a particular node Z_{f2} with depth h_2, within an element is greater than the water surface elevation $(Z_{f1}+h_1)$ at one of the other nodes associated with that element then a new water surface elevation (z) for the dry node is defined in the momentum equation as:

$$z_2 = Zf_1 + h_2 \qquad 3.1$$

This leads to more realistic representation of the elemental lateral free surface elevation in the momentum equation resulting in a more realistic representation of the flow velocities in floodplain areas. As only the momentum equation is modified model mass conservation is unaffected.

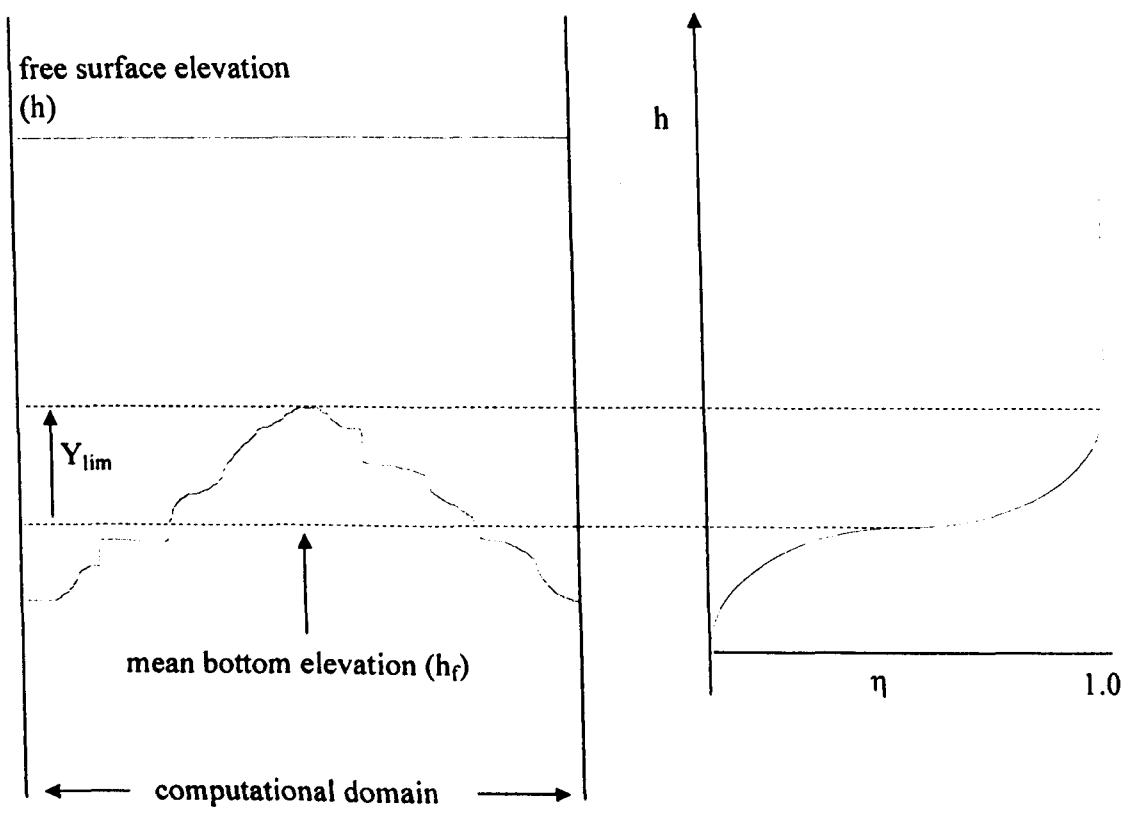

Figure 3.2 Representation of the scaling factor employed by Defina and D'Alpaos. Percentage of wetted area η as a function of free surface elevation (after Defina and D'Alpaos, 1994).

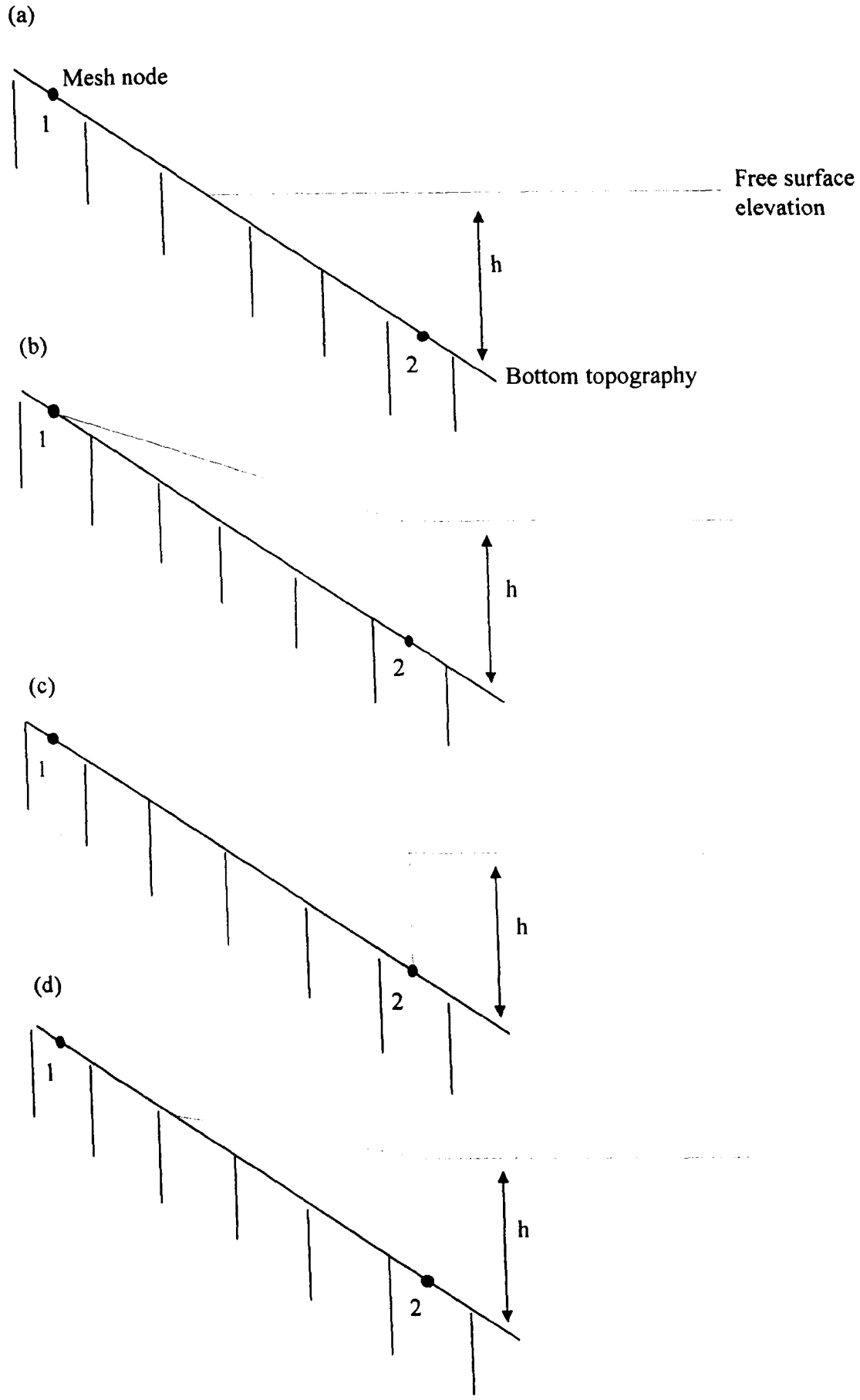

Figure 3.3 Schematic representation of the elemental water surface elevation for floodplain areas in TELEMAC2D: (a) actual free surface on a partially wet element; (b) interpolated free surface (no modification for partially wet areas); (c) element exclusion technique; (d) modified free surface elevation based on an average elemental depth.

The simulation of a moving flux boundary represents perhaps the single most important development in 2D hydraulic models in terms of their application to inundation modelling. However, it is important to remember that all of the methods discussed above represent approximations of a complex system and vary in their success. Element elimination techniques are simple and computationally efficient, if excessive grid specification is not applied to the floodplain, yet suffer from poor representation of the moving flux boundary and computational instability. Deforming grid techniques represent the moving flux boundary faithfully yet are complex and can require considerable computational effort. Both of these methods have recently been superseded by techniques which modify the governing equations and which are able to successfully represent moving flux boundaries in areas of low lateral gradient at low additional computational cost. The methods used by King and Roig (1988) and D'Alpaos *et al.* (1994) are complicated in their requirement for the provision of scaling parameters which are difficult to obtain and should be spatially distributed throughout the floodplain for maximum effect. TELEMAC2D offers a simpler alternative without the requirement for additional parameterisation.

3.2.2 Reach Scale Model Application

The second advance identified as having enabled the application of 2D finite element models to floodplains has been the move from small to large scale application. Until recently the application of 2D finite element solutions to free surface flow problems has been largely restricted to small scale reach problems (for example, to reaches of river a few river widths long) and cases where the river channel flow has rarely been resolved separately from floodplain flow (Gee *et al.*, 1990). However, as there is no theoretical limit to the size of elements used it has been possible to apply the technique to large scale problems. Gee *et al.* (1990) describe an application of the RMA-2 model to a 24km reach of the River Fulda in Germany. Their investigation demonstrates the ability of this model to predict the depth and lateral extent of surface water during flood events at this scale. Charlton (1995) described an application of the RMA-2 model to a 14km river reach in Devon, UK. Bates *et al.* (1995) demonstrate similar capabilities of the TELEMAC2D model for a 11km reach of the River Culm, UK while D'Alpaos *et al.* (1994) demonstrate the suitability of their 2D finite element model for predicting spatially distributed water depth and velocities for a 10km reach of the River Brenta, Italy. The suitability of 2D finite element models to reach scale applications is thus well documented.

3.2.3 Choice of a suitable finite-element model for floodplain application

TELEMAC2D, RMA-2 and the model developed by Defina *et al.* (1994) have a proven ability in the floodplain environment. Use of the model by Defina *et al.* (1994) is currently limited by an inability to accurately determine values for the parameter Y_{lim} to which the model shows

considerable sensitivity (D'Alpaos *et al.*, 1994). Both RMA-2 and TELEMAC2D have been successfully applied to river flood simulations; RMA-2 by Gee *et al.* (1990), Baird *et al.* (1992), Bates *et al.* (1992) and Charlton (1995) and TELEMAC2D by Bates *et al.* (1995), Bates *et al.* (1996) and Hervouet and Van Haren, (1996).

RMA-2 and TELEMAC2D are similar in many aspects. Both models solve the second-order partial differential equations for the depth-averaged fluid flow derived from the 3D Navier-Stokes equations. This results in a set of equations consisting of an equation for mass continuity and two force-momentum equations which will be discussed later in reference to the model chosen for the application. However, TELEMAC2D offers a number of advantages over RMA-2 relating to the solver technique, the wetting and drying algorithm (as discussed above), boundary specification and model structure. For example, TELEMAC2D has a more accurately defined downstream output condition where water depth (h) is specified, according to an observed stage reading, and velocity is free to vary resulting in a predicted output discharge which is then available for comparison with observed discharge. RMA-2 employs a rating curve as a downstream boundary condition which is used to derive water depth (h) and velocity (v) from an estimated discharge (Q). Errors associated with the rating curve established at the downstream boundary are therefore incorporated within the model predictions of depth and velocity.

Accordingly, TELEMAC2D is chosen as the hydraulic template from which the integrated floodplain hydraulic - infiltration model will be developed. A more detailed description of TELEMAC2D now follows.

3.3 TELEMAC2D

3.3.1 Introduction

TELEMAC2D (Hervouet and Van Haren, 1996) was developed at the Laboratoire National d'Hydraulique (LNH) of the Direction des Etudes et Recherches of Electricité de France (EDF) as a general purpose finite element model for free surface flows in rivers, estuaries and coastal areas. The code solves the depth-averaged free surface flow equations such that the main results at each node of the computational mesh are the depth of water (h) and the depth-averaged velocity components (u and v). The code is able to account for the following phenomena relating to hydraulic flow:

- propagation of long waves, including non-linear effects,
- wetting and drying of intertidal zones;

- bed friction;
- the Coriolis effect;
- impact of meteorological conditions such as atmospheric pressure and wind;
- areas of injection or extraction of liquid with or without an input of momentum;
- turbulence;
- supercritical and subcritical flows;
- influence of temperature and salinity on water density, including the effect of horizontal density gradients;
- lunar tides.

The model has many fields of application including marine, estuarine and fluvial hydraulic problems. Application in marine environments includes the sizing of port structures, studies into the effect of building submersible dikes or dredging, the impact of coastal waste discharges and the study of thermal plumes in coastal regions. Application to riverine environments include the hydraulic impact of construction (bridges, weirs), and the study of dam breaks (Hervouet and Van Haren, 1996) and river flooding (Bates *et al.*, 1996; Hervouet and Van Haren, 1996).

3.3.2 The TELEMAC2D Model System

The TELEMAC2D code, representing the central solver, is part of a suite of computational software and associated pre- and postprocessors which comprise the TELEMAC2D model system. The system comprises all of the software modules, except for a mesh generator, required for constructing and running an application beginning with an initial digitisation of bathymetric data and ending with the hydraulic simulation itself. The complete TELEMAC2D model system is illustrated in Figure 3.4 and briefly described in the following paragraph. The SINUSX software is used in conjunction with a digitising tablet to acquire and store bathymetric and boundary data for the proposed application. It is also able to receive data directly from files. Bathymetric data are processed in SINUSX and output in a form suitable for STBTEL. STBTEL combines these data with a mesh of triangles or quadrilaterals produced by one of a number of commercially available automatic mesh generators which results in a file which is input into the TELEMAC2D code, which performs the hydraulic calculations. STBTEL interpolates the depths provided by SINUSX to give a bed elevation at each node of the mesh and at the same time conducts a number of mesh consistency checks, including the identification and elimination of overlapping elements in the mesh which can arise during mapped meshing. A number of commercially available mesh generators are available of which I-DEAS was used to generate the meshes used for the purposes of this research. I-DEAS allows two meshing options; free meshing and mapped meshing. Free meshing refers to what is essentially the default meshing option in which mesh size and shape (tending to equilateral triangles) is determined by the code itself while mapped meshing allows

for user defined distortion of the finite element mesh. Such user involvement is essential to specify elemental geometry in channel areas in riverine applications where a well defined ratio of element length to width is required for model stability. It is also useful where large elements are adequate, for example on a floodplain of low slope angle, where computational efficiency can be enhanced. Post processing of the hydraulic model simulation results is accomplished using the graphical and data analysis package RUBENS.

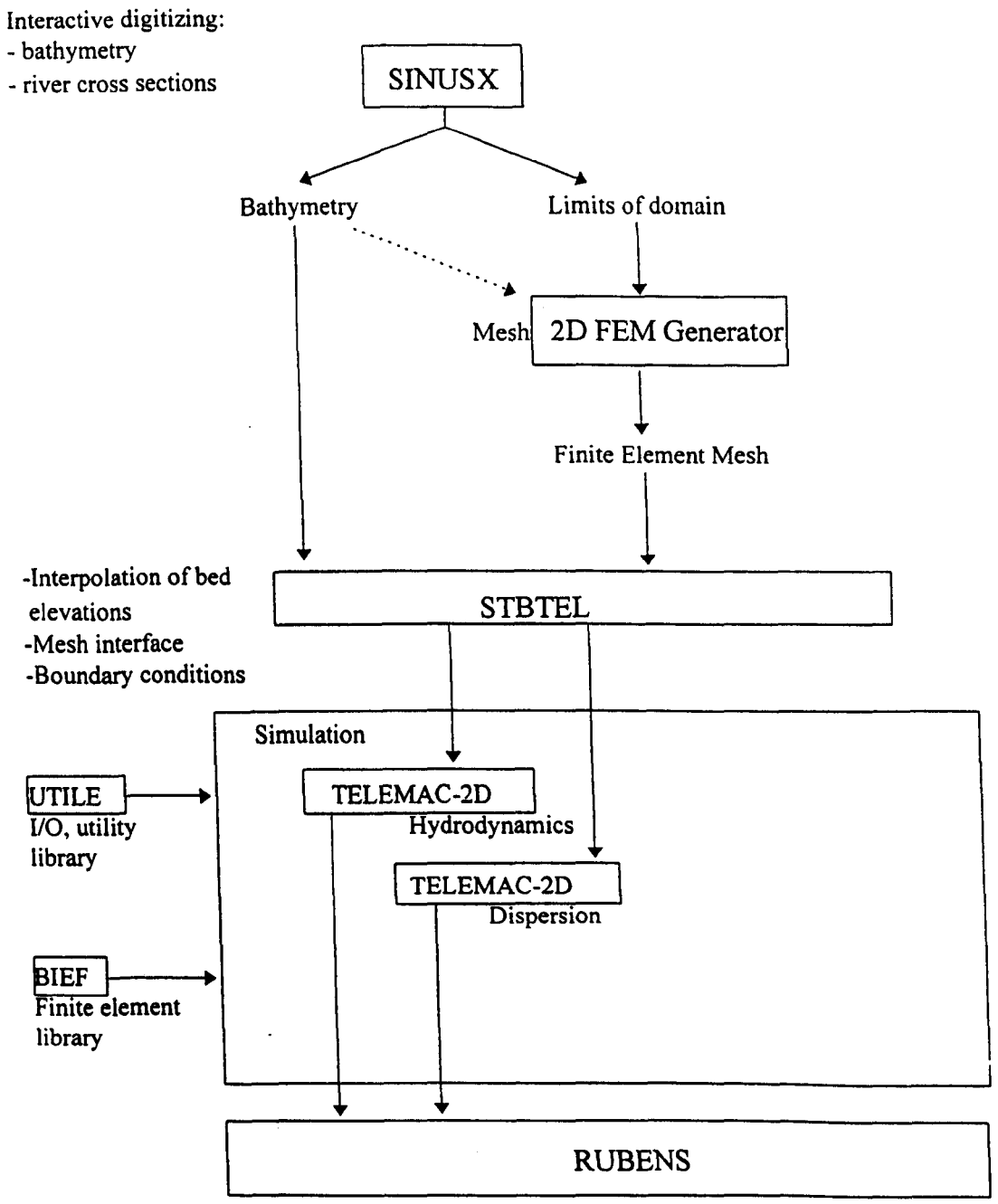

Figure 3.4 Flow diagram representing the individual components of the TELEMAC2D model system.

3.3.3 The TELEMAC2D Code

TELEMAC2D is a depth average model which solves the 2D Shallow Water equations (SWE), otherwise known as the Saint-Venant equations derived from the 3D Navier-Stokes equations, to give a value for water depth and depth averaged velocity at each node in the domain.

As the Saint-Venant equations are derived by taking vertical averages, certain assumptions are required to account for non-linearity in terms such as velocity and density. The requirements of the Saint-Venant equations are that:

- The fluid is Newtonian (The water is incompressible);
- The water pressure is hydrostatic (The water column is well mixed with no significant density variation or stratification);
- That vertical flow components are negligible (Vertical velocities are neglected in the Saint-Venant equations);
- The effective lateral stresses can be represented by an isotropic (usually constant) eddy viscosity;
- That bed stresses can be modelled using a linear or quadratic friction law.

Application of the Saint-Venant equations will only result in acceptable solutions where these conditions are met. Indeed, all of these conditions are commonly met in rivers where the flow is incompressible and vertical accelerations are usually negligible (Cooper, 1996).

The TELEMAC2D code solves three hydrodynamic equations simultaneously, one representing mass continuity and two force-momentum equations, presented here in conservative form:

(i) equation of mass continuity:

$$\frac{\partial h}{\partial t} + \mathrm{div}(\mathbf{Q}) = 0 \qquad 3.2$$

(ii) force-momentum equations:

$$\frac{\partial Q_x}{\partial t} + \mathrm{div}\left(\mathbf{u}Q_x\right) = -hg\frac{\partial Z}{\partial x} + hF_x + \mathrm{div}\left(hv_t\mathbf{gradu}\right) \qquad 3.3$$

$$\frac{\partial Q_y}{\partial t} + \mathrm{div}\left(\mathbf{u}Q_y\right) = -hg\frac{\partial Z}{\partial y} + hF_y + \mathrm{div}\left(hv_t\mathbf{gradv}\right) \qquad 3.4$$

where h is water depth, t is time, Q_x and Q_y represent linear discharge in m^2s^{-1} (equal to hu and hv respectively), u is the first component of velocity in the Saint-Venant Equation, v is the second component of velocity in the Saint-Venant Equation, g is gravitational acceleration, Z is the elevation of the free surface, F_x and F_y represent the depth-averaged source terms of the momentum equation in u and v respectively.

Source terms in the continuity and momentum equations:

In the case of a source or sink, such as infiltration, the right hand side of the continuity equation is no longer zero but equal to a term '*Sce*' (representing 'source'). Equation 3.2 is now rewritten as:

$$\frac{\partial h}{\partial t} + \mathrm{div}\left(\mathbf{Q}\right) = Sce \qquad 3.5$$

where Sce is expressed in ms^{-1} and is positive for an influx of water into the domain.

Expressed according to finite element notation and taking infiltration as an example, the local discharge, Q_{el}, (m^3s^{-1}), associated with an element i is calculated according to the following equation:

$$Q_{el_i} = \int_{el_i} Sce_i \varphi_i d\Omega \qquad 3.6$$

Where φ_i represents the test function (which assumes the value 1 at node *i*) and $d\Omega$ represents a differential element (m^2). Infiltration integrated over the entire domain (Q_{global}) is thus the sum of Q_{el} calculated for all domain elements.

The contribution of source terms is also considered in the momentum equations (Equations 3.3 and 3.4) and includes the effects of surface friction (specified according to either Chezy, Strickler or Manning coefficients), wind, corriolis force and atmospheric pressure. These are expressed as vector components *Mt(x)* and *Mt(y)* (where *Mt* stands for 'Momentum') with dimensions m^2/s^2 . However, in the specific case of infiltration, these terms are assumed to be zero.

Turbulent flows are considered in TELEMAC2D by employing a mean flow concept which averages instantaneous velocities over time to give mean motion only. In this formulation an additional term, the Reynolds stress, is added to the governing equations to represent the increased internal shear stress on mean flow produced by velocity fluctuations. To estimate this additional unknown (the Reynolds stress) and to make the governing equations mathematically tractable, a model of turbulence is introduced. TELEMAC2D adopts two methods, the Boussinesq approximation and a more complex two equation κ - ε turbulence closure model. In the Boussinesq approximation the Reynolds stress is assumed to be the product of the depth-mean velocity gradient and an exchange coefficient ε, dimensionally similar to the coefficient of viscosity and termed the eddy viscosity.

3.3.4 The TELEMAC2D Solution Scheme (Algorithm implementation)

TELEMAC2D employs a finite element method in which the grid can comprise linear triangles or quadrilaterals, but not a mixture of these. The governing partial differential equations are solved at each node and shaping functions are employed to describe the variability of the state functions (water depth and velocity) within each elemental area. This is achieved by assuming that the state variables vary within each element according to a prescribed manner. TELEMAC2D uses linear functions to describe inter-elemental variability for all state variables. Shaping functions are defined

UNIVERSITY OF BRISTOL LIBRARY

for each node and are specific to that node where they assume a value of one. At all other nodes they assume a value of zero. The influence of the shaping function diminishes as the distance from the node increases but the cumulative effect is to produce a linear surface in the elemental space between the two nodes. Whether applied in 1, 2 or 3D the principle remains the same and the shaping functions do no more than interpolate between the grid values. As such it is possible to obtain a value for the state variables for any point within any element within the computational domain for 1, 2 and 3D finite element domains.

A number of solver techniques are available to TELEMAC2D including:

- a fractional step method using the method of characteristics for the advection terms and a Galerkin method for the propagation and diffusion terms in the equations;

- several variants of the Streamline Upwind Petrov Galerkin (SUPG) method (Brooks and Hughes, 1982);

- a hybrid scheme which combines the characteristics and SUPG methods.

TELEMAC2D employs a fractional step method to solve the governing equations where advection terms are solved initially followed by propagation, diffusion and source terms which are solved together in a second step. For the advection step several schemes are available. In previous applications to river flood simulations the method of characteristics has been applied to successfully (Bates *et al.*, 1995). To ensure mass conservation the Streamline Upwind Petrov Galerkin (SUPG) method has been applied for the advection of h in the continuity equation. The SUPG method employs a modification to the standard Galerkin weighted residuals method to account for spurious node-to-node oscillations (wiggles) (Brooks and Hughes, 1982). This combination of solver techniques has been shown to work for river flood conditions (Bates *et al.*. (1995); Hervouet, *pers comm*) and shall similarly be used in the research.

3.3.4.1 Numerical stability

Numerical schemes are often subject to stability criteria related to the Courant number given in 1D as:

$$Cr = u\frac{\Delta t}{\Delta x} \qquad 3.7$$

where Cr is the Courant number, u is the velocity component in the y Cartesian direction, t is time and x is the mesh size (distance in the y direction).

While the stability of explicit schemes is generally dependant upon the Courant number remaining below one, the implicit nature of TELEMAC2D means that this, in theory, is not the case. Courant numbers may indeed exceed 50 (Hervouet and Janin, 1994) but in doing so computational time increases. However, although theoretically not a requirement of model stability, smaller Courant numbers have been shown to improve numerical stability (Smith, *pers comm*) and to improve computational efficiency (Bates *et al.*, 1995).

3.3.5 Model Parameterisation

Prior to running a TELEMAC2D application a number of input data requirements must first be met. The user is required to provide data to establish the finite element mesh, in this case representing the floodplain, hydrodynamic data to satisfy the upstream and downstream boundaries and floodplain friction data. An integral part of model set-up is prescribing boundary conditions at each of the boundary points within the model. The various types of boundary condition may be combined to prescribe boundary conditions of any physical type, including the input and output boundaries for a flood hydrograph. The finite element mesh is constructed in conjunction with topographic data such that mesh sizing and location is consistent with breaks in topography, including channels and steep slope gradients. Meshing is performed according to the two options outlined in (3.3.2). TELEMAC2D accepts inflow and outflow data at the two boundaries in the form of hypothetical or observed hydrographs. Floodplain friction values are input as Manning's n, Strickler or Chezy. Model parameterisation is considered further in *Chapter 5*.

3.3.6 model validation

TELEMAC2D has been comprehensively validated in a number of studies on river flooding. The code (TELEMAC2D version 3.0, the code used in this research) has been independently validated by Cooper (1996) for marine, estuarine and riverine application and was shown to successfully simulate flow occurring at a river confluence where good agreement was found between the model predicted water level and observed water level in a reduced scale physical model. As an example of an application to a purely riverine application the report turns to a paper by Bates *et al.* (1994) in which good agreement was found between computed flows and inundation area and the observed downstream output and inundated area. Indeed, further work has illustrated the applicability of this

code to the simulation of river flood conditions (for example see Bates *et al.*, 1996; Hervouet and Van Haren, 1996).

3.4 Representing Infiltration

The discussion now turns to the selection of a suitable model to represent infiltration.

Infiltration is the entry of water into a soil through the surface boundary. Generally, it refers to the vertical movement of water downwards through the profile as a front under the combined driving forces of gravity and matric potential in response to the supply of surface water. In response to a supply of water in excess of the saturated permeability, the rate of infiltration into a soil is generally observed to decline over time until a constant rate is reached, a rate determined by the saturated hydraulic conductivity of the soil (Hillel, 1971). This pattern has been attributed to a number of effects including; (i) a gradual deterioration of soil structure and the consequential partial sealing of the soil profile by the formation of a dense, less permeable, surface crust, (ii) a consequence of reduced porosity resulting from the swelling of clay minerals during wetting and (iii) as a result of air entrapment within soil pores which is subsequently prevented from escaping. However, in most cases the overriding effect is one of a decreasing mean matric suction gradient as infiltration proceeds and the wetting front passes further into the soil. The suction gradient decreases until finally the gradient in the upper part of the profile is negligible, leaving the constant gravitational gradient in effect as the only remaining force moving the water down profile. Since this has a value of unity, it follows that the flux tends to approach the saturated hydraulic conductivity of the soil as a limiting rate.

The infiltration process has been described mathematically both empirically and mechanistically. The empirical approach to developing an infiltration model consists of finding a mathematical function whose shape fits the observed infiltration rate as a function of time followed by an attempt at a physical explanation (Jury *et al.*, 1991). However, empirical models take no account of the actual physical processes occurring within the soil and as such provide little insight into the process of infiltration itself. Mechanistic models, on the other hand, are derived from the physically based water flow equations, deriving ultimately from Darcy's Law (Equation 3.11). Mechanistic, physically based models provide considerable insight into the infiltration process where, through model parameterisation, account can be taken of those factors which directly control the movement of water through the soil profile which includes; hydraulic conductivity, hydraulic potential and hydraulic gradient. Where the model is sufficiently complex, account can also be taken of the relationship between hydraulic conductivity and soil moisture content through the use of empirically derived relationships such as that of Millington and Quirk (1959) (Equation 3.14) to

account for both saturated and unsaturated soil water flow.

Physically based infiltration models offer numerous advantages over their empirical counterparts and accordingly a physically based model is chosen for the research.

Where water is supplied to an isolated finite soil surface area the resulting process is generally three-dimensional in nature (Philip, 1983) with the downward flux dominating through the combined effects of hydraulic gradient and gravity. The extent to which the vertical component dominates in determining the overall pattern of flow is also influenced by the texture of the soil (Brady, 1990) with vertical flow dominating in coarser textured soils. Two-dimensional flow results from the supply of water to a semi-circular irrigation channel and the same is true where vertically infiltrating water meets a less permeable soil layer within the soil profile (Brady, 1990). However, where infiltrating water from various disparate wetted surfaces coalesces, the resulting flow reduces to purely one-dimensional infiltration (Philip, 1983). This has significant implications for the representation of infiltration resulting from the inundation of large areas of floodplain.

3.4.1 The physical basis behind modelling infiltration

A quantitative study into the hydraulic behaviour of soil depends upon the availability of data for two fundamental hydrologic properties; the relationship between soil water potential and soil water content and the relationship between soil hydraulic conductivity and either soil water potential or soil water content. It is to the provision of these data that the discussion now turns.

3.4.1.1 The soil suction-moisture relationship

The suction-moisture curve (also known as the *soil water-retention curve*, *water release curve*, *water release characteristic* and *soil water characteristic*) defines the unique relationship that exists between soil moisture content and soil moisture suction (tension) for a given soil. Water retention within a soil is a product of the combined effects of capillarity, adsorption and osmosis in the presence of semi-permeable membranes which act to bind the water to the soil. Capillary forces result from surface water tension at the interface between the soil air and the soil water. Molecules in the liquid are attracted more to each other than to the water vapour molecules in the air, resulting in a tendency for the liquid surface to contract. For a given viscosity and surface tension, water will be held more strongly in smaller pores than large ones hence, as the water content of the soil decreases, the larger pores empty at lower suctions than the smaller pores. Soil water can also be adsorbed on to the surfaces of soil particles due manly to electrostatic forces in which the polar water molecules are attached to the charged faces of the solids. These forces are only effective at close range thus only very thin films of water can be held in this way and the relative importance of this effect increases as the pore size decreases. Both the capillary and adsorption forces exert a

tension or suction (a negative pressure relative to atmospheric pressure) on the soil water. Together these forces are termed the matric suction. A third force acting to retain water in soils results from the presence of dissolved solutes in the soil water and is termed the osmotic pressure. Though generally of lesser importance than the matric potential, it can be important in some circumstances and results from the pressure exerted by the difference in solute concentrations across a permeable membrane (eg plant root). The total suction holding water in soil is the sum of the matric and osmotic forces. In sandy soils capillary binding dominates while in clays it is adsorptive (and osmotic) binding which dominates.

To initiate water movement from a given pore size within the soil matrix at a given water viscosity requires the application of a suction opposite and equal to the pressure exerted by the above forces acting to retain the soil water. This pressure required to initiate the movement of the water is dependant upon the pore diameter, and to a certain extent the mineralogy of the soil (Hendrix, 1990). It can be appreciated therefore that the pore size distribution of a soil will be important in determining the shape of the suction-moisture curve. This is exemplified in Figure 3.5 which shows typical suction-moisture curves for a sand and clay soil. Sandy soils are typified by relatively uniform pore size which means that once a threshold suction value, termed the air-entry value, is exceeded the majority of pores empty rapidly and the soil water content decreases rapidly over a relatively small change in suction. In clay soils the situation is very different. The change in soil moisture content decreases slowly as the suction increases and this can be attributed to the relatively uniform pore-size distribution associated with clays. Indeed, it is this relationship between soil pore size distribution and soil mineralogy which has been employed to derive the suction-moisture curves of soils without recourse to experiment.

However, these relationships are rarely (if ever) the simple functions illustrated above and are complicated by both soil structure (Hillel,1980) and hysteresis (Topp, 1969; Topp and Miller, 1966; Jaynes, 1990). The suction-moisture relationship is complicated by the observation that for a given soil suction the observed water content is a product of both the soil moisture 'history' and the soil suction. For the same suction the associated water content will be greater for a drying soil than for a wetting soil and the difference can be quite considerable (Jaynes, 1990). The non-uniqueness in these functions is termed hysteresis. Hysteresis is present in all soils but very few data for soils exists and those which do have primarily been derived from laboratory studies on re-packed column (Jaynes, 1990). Almost no data are available relating to the magnitude of the effect in field soils and in practice, given the many problems associated with measuring the suction-moisture curve accurately, the hysteresis phenomenon is usually ignored in hydrological studies (Hillel, 1980). However, the relatively small effect of hysteresis will be masked by other soil factors with considerably greater influence upon the flow of water through soil, including, for example,

hydraulic conductivity, which is inherently variable and may fluctuate by an order of magnitude or more (Jaynes, 1990) for a given soil.

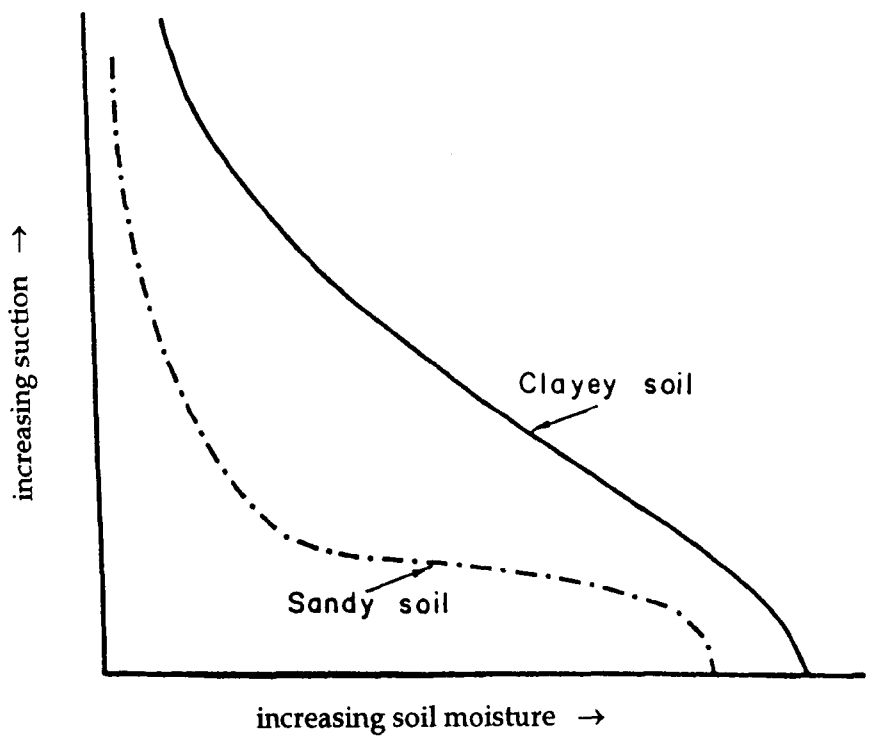

Figure 3.5 An illustration of the effect of texture on soil water retention - suction-moisture curves for a sand and clay soil (after Hillel, 1980).

Data pertaining to the suction-moisture curve may be obtained through both laboratory and field measurement and through a number of empirical methods. The high cost and time consuming nature of laboratory and field based investigations has resulted in a number of efforts to estimate soil moisture retention from easily measured soil properties such as soil texture, organic matter and clay content and soil structure. These methods are generally based on statistical analysis (eg Gupta and Larson, 1979) or the development of algebraic functions which describe smooth curves through measured soil moisture retention data. Of the algebraic functions Hendrix (1990) identified those

developed by Brooks and Corey (1966) and Van Genuchten (1980) as being the two most commonly used. The relationship developed by Van Genuchten (1980) is presented in the following equation:

$$\frac{\theta-\theta_r}{\theta_s-\theta_r}=\left[\frac{1}{\left\{1+(ah)^n\right\}}\right]^m \qquad 3.8$$

where θ_s is the saturated water content, θ_r is the residual water content, h is soil water tension and a, n and m are parameters which determine the shape of the suction-moisture curve.

Subsequently, a number of authors have developed statistical relationships between easily measurable soil properties and the parameters used to develop the algebraic functions discussed above with the result that these parameters are available for different soil types and classes (for example see Wosten and Van Genuchten (1988) and Carsel and Parrish (1988)).

3.4.1.2 The soil moisture-hydraulic conductivity relationship

The second stage in quantifying soil hydraulic properties is the determination of the relationship between soil moisture content, or soil suction, and hydraulic conductivity. Again, this relationship can be experimentally derived or through the use of a number of existing mathematical methods such as that developed by Millington and Quirk (1959). The well known Millington-Quirk algorithm can be used to mathematically transform a known soil suction-moisture curve into a hydraulic conductivity-soil moisture curve, an example of which is presented in Figure 3.6. The Millington-Quirk algorithm is explored further later in the Chapter with reference to the model used in the research.

3.4.2 Model Chosen

A 1D model is chosen to represent infiltration and subsequent redistribution of water within the soil profile based on the observation that flow essentially reduces to 1D infiltration below the influence of the surface boundary (Philip, 1983). Although such a representation precludes the description of lateral flow components, it is considered suitable for the research for the following reasons:

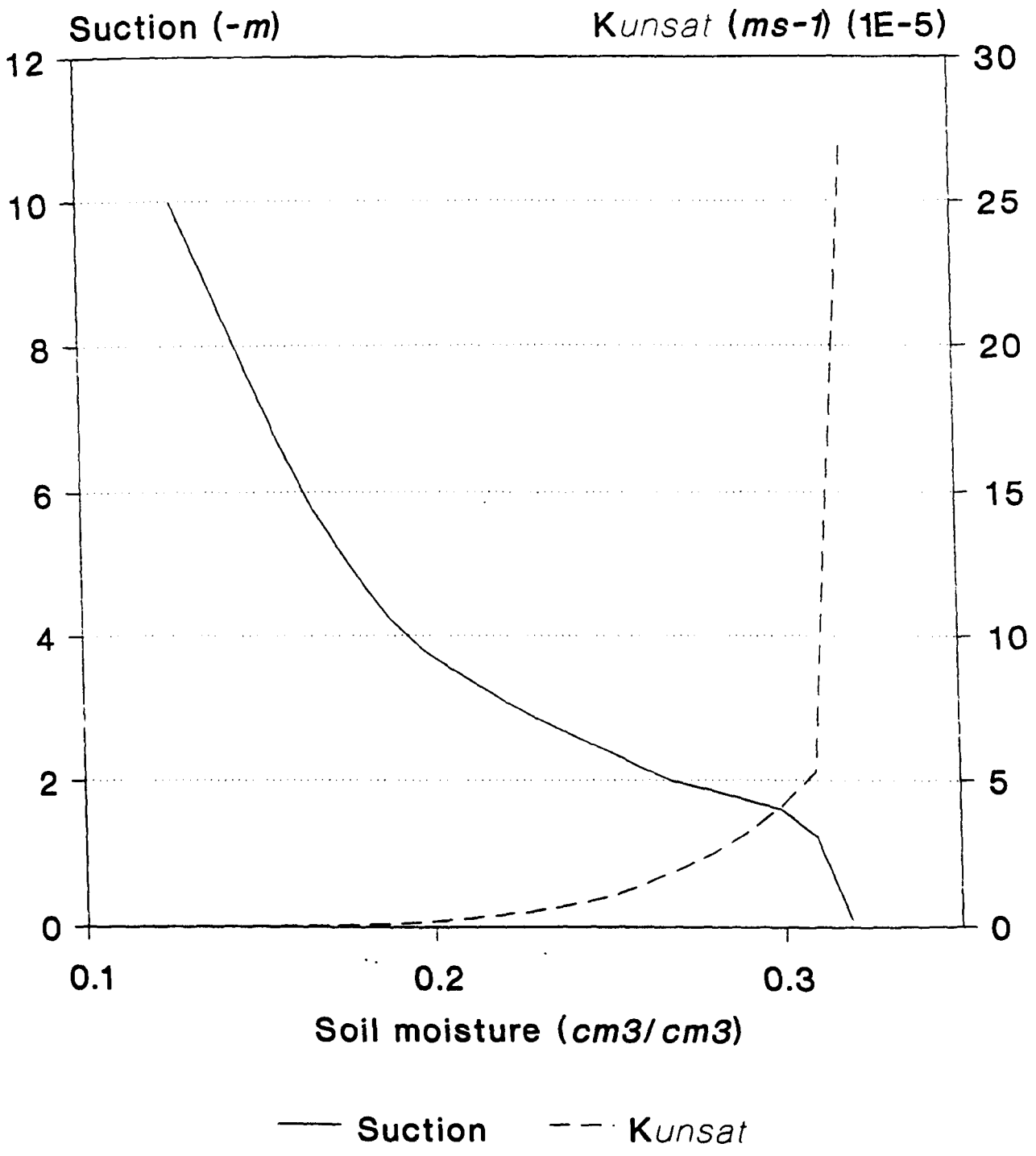

Figure 3.6 Example of a suction-moisture curve and associated unsaturated hydraulic conductivity characteristics derived using the Millington-Quirk algorithm (after Davie, 1992)

- Lateral subsurface flows driven by floodplain topographic gradients are likely to be relatively small compared to vertical flows resulting from hydraulic gradients through the soil profile, especially when considered over the relatively short flood periods over which the simulations are to be run.

- A 1D representation offers the simplest approach to addressing the need to represent the floodplain as a hydrologically integrated system. Increasing the dimensionality to 2- or 3D will result in a substantial increase in the complexity of the problem both in terms of the structure of the model and the computational demands and is beyond the requirement of this initial investigation. Where infiltration following inundation is predominantly vertical, representation beyond 1D is not required.

Inconsistencies in the permeability of the soil profile can result in lateral flow components developing and this is also true of relict channels within floodplain sediments which have been shown to generate preferential flow pathways (Haycock and Burt, 1993). 1D representation of infiltration would be unable to represent such processes thus the soil profiles considered here are homogeneous throughout and include no variability in texture.

The model chosen to represent infiltration for the purposes of this research is a physically based 1D block centred finite difference scheme which solves the Richards equation for saturated-unsaturated vertical flow. There have been a number of significant applications of this model which have allowed its configuration and testing in a range of environments. The model was originally developed as a modified version of the flood forecasting model HYMO (Williams and Hann, 1972) to enable flood prediction in unguaged catchments and to allow for the spatial variability of catchment soil characteristics. The scheme was designed to replace the original model which used an empirically derived, catchment specific, curve for predicting precipitation excess leading to catchment runoff. The model has been used to predict flood hydrographs for a number of catchments and storms in the USA. Since its conception, the model has undergone several modifications and has been applied to a number of different environments in both one and two dimensions.

Anderson and Howes (1985) coupled the model with a stability analysis routine and applied it to model slope failure in the humid tropics. Lloyd (1990) developed the model to consider slope hydrology and stability in 2D and applied the model to slopes in Malaysia. Collison (1993) extended the 2D slope stability model to incorporate the mechanical effects of vegetation through a vegetation slope cover model, again, this was then applied to slopes in the humid tropics. The model

has also been applied to slopes in temperate regions. Brooks (1991) used the hydrology-stability model in 1D form to determine the role of shallow failures in slope development over geological time in a study of the interactions between pedogenesis and hillslope hydrology. The 2D hydrology-stability model was applied to a similar study by Brooks *et al.* (1993). The model has been utilised in a variety of soil types and conditions ranging from freely drained deep tropical soils to shallow temperate soils experiencing impeded drainage (see Table 3.1). In each of these environments the model has been demonstrated to function effectively.

Author	**Model spatial dimension**	**Climatic Zone (and soil types where known)**
Anderson and Howes (1985)	1D	Humid Tropics (Hong Kong)
Lloyd (1990)	2D	Humid Tropics (Malaysia)
Brooks (1991)	1D	Temperate (Scotland) (freely draining podzol)
Collison (1993)	2D	Humid Tropics (Malaysia)
Brooks *et al.* (1993)	1D	Temperate (Scotland)

Table 3.1 Summary of the range of climatic zones and soil types to which the infiltration model (as both 1D and 2D) has been applied.

3.4.3 Model Structure

The model structure is illustrated in Figure 3.7. The model describes the soil column as a series of stacked cells, up to a maximum of 20, distributed within three soil layers which can be parameterised to represent different physical soil conditions describing distinct soil horizons. Water can enter the soil column as precipitation (or from water stored as surface water) through the top boundary and can leave the soil column through the bottom boundary as drainage or the top boundary as an evaporative loss

Evaporation is initiated when precipitation is zero and is described according to equations 3.9 and 3.10 which account for daytime and nigh time evaporation rates respectively:

(i) t = 6 am to 6 pm:

$$e = e_{max} \cdot \frac{\sin(2\pi t)}{86400} \qquad 3.9$$

(ii) t = 6 pm to 6 am:

$$e = 0.01 e_{max} \qquad 3.10$$

where t is equal to time in seconds from an assumed sunrise at 0600 and e_{max} represents the maximum midday evaporation rate. Equation 3.9 describes evaporation between 0600 and 1800 hours by way of a sine curve with a maximum at midday. Equation 3.10 describes evaporation occurring between the hours of 1800 and 0600 which is set at a constant rate of $e_{max}/100$. Evaporation comes into effect when the surface is receiving zero precipitation and results in a loss of water from either the surface water store or the soil column at a rate determined by equations 3.9 and 3.10. These achieve only a crude representation of evaporation, and no account is taken of transpiration. Where evapotranspiration is a significant process in determining the water balance of the soil then application of the model is potentially limited; however, for winter floodplain conditions where evapotranspiration rates are expected to be low this representation is adequate.

Infiltration and subsequent vertical redistribution of water within the soil column is described by the Richards equation (1933), a non-linear partial differential equation derived from Darcy's law in combination with the principle of continuity. For one dimensional flow Darcy's law is as follows:

$$q = -K\frac{dH}{dx} \qquad 3.11$$

where q represents discharge per unit area, K denotes hydraulic conductivity, and dH/dx is the hydraulic gradient. Darcy's law is combined with the continuity equation which can be summarised in the following way:

$$\frac{\partial \theta}{\partial t} = -\frac{\partial q}{\partial x} \qquad 3.12$$

where θ represents the volumetric water content. The Richards equation is derived by combining equations 3.11 and 3.12 and represents flow through the soil as a non-linear partial differential equation which in one dimensional form is described as:

$$\frac{\partial \theta}{\partial t} = -\frac{d}{dx}\left[K\frac{\partial H}{\partial x}\right] \qquad 3.13$$

An explicit finite-difference approximation is used to solve the flow equation. The model simulates the effect on soil moisture conditions of precipitation, evaporation and surface water detention. For each time step water arriving at the surface boundary as precipitation will either wholly enter into the top cell when the precipitation rate is less than or equal to the calculated infiltration capacity or will be partitioned between infiltration and a user defined surface water store in cases where precipitation rate is greater than the soil infiltration capacity. In instances where both the infiltration capacity and the surface water store capacity are exceeded, runoff is initiated and this water is lost to the system. Flow through the bottom boundary is either determined by the conductivity of the bottom cell in the soil column or set to equal zero. Flow through the boundary between adjoining cells is determined by the average hydraulic conductivity of the two cells and is weighted according to cell thickness. For cells attaining saturation, the rate of flow equals the saturated hydraulic conductivity. Otherwise, flow velocities are a function of soil moisture content and are determined through the relationship between soil moisture content and hydraulic conductivity.

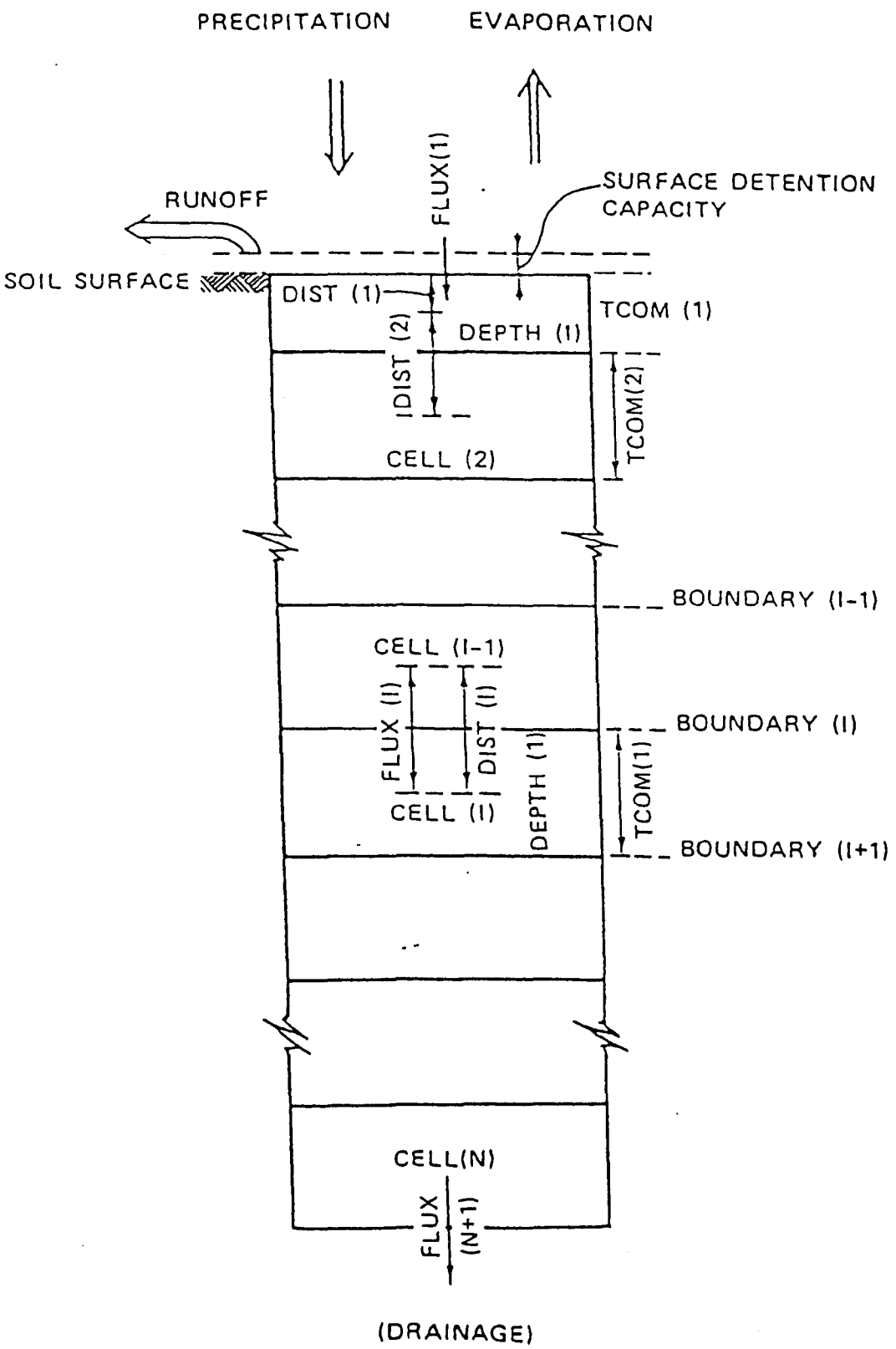

Figure 3.7 Structure of the one dimensional infiltration model

The relationship between soil moisture and hydraulic conductivity is difficult to obtain by experiment in all but the saturated condition but it can be derived from the soil moisture characteristic curve using a number of empirically derived models. The infiltration model adopts the method established by Millington and Quirk (1959), the so called Millington and Quirk Method, which is summarised in the following equation:

$$k(\theta)_i = k_s\left(\frac{\theta_i}{\theta_s}\right)^p \frac{\sum_{j=1}^{m}\left[\left(2_j+1-2_i\right)\psi_j^{-2}\right]}{\sum_{j=1}^{m}\left[\left(2_j-1\right)\psi_j^{-2}\right]} \qquad 3.14$$

where $k(\theta)_i$ corresponds to the unsaturated hydraulic conductivity at a moisture content θ at a point i on the suction-moisture curve, k_s represents the saturated hydraulic conductivity, θ_s is the saturated soil moisture content, ψ_j is the soil suction at moisture content θ_i, m represents the number of equally sized moisture content increments included on the soil moisture characteristic curve and p is a constant.

Following each simulation a water balance check is initiated to test for volumetric discrepancies arising from model instability, which may result from Courant numbers exceeding 1.0 (see Equation 3.7). The following mass balance equation is invoked at the end of each simulation;

$$BAL_I = (W_{(f)} - W_{(i)}) - (I - E - D) \qquad 3.15$$

where $W_{(i)}$ represents the initial soil column water mass, $W_{(f)}$ is the final water mass, I represents total infiltration input, E represents total evaporative loss, D represents total drainage and $BAL_{(I)}$ represents any numerical error resulting from model instability.

3.4.3.1 Parameterising the infiltration model

Initially, the soil is discretized into a finite number of layers and cells. The number and size of cells chosen defines the depth of soil to be modelled. Upto three physically distinct layers (horizons)

within the soil profile can be defined. This allows for the inclusion of distinct horizons within the soil profile for which distinct suction-moisture relationships and saturated hydraulic conductivities can be specified. Values for the saturated and initial soil moisture content of each of the three layers must also be specified along with suction-moisture curve data for each of the three soil horizons.

3.5 Model Coupling

Sections 3.3 and 3.4 introduce and describe the two models to be used. This section details the linking of the two models to provide the hydrological research platform discussed in *Chapter 2*. Model coupling implies taking two or more models, each of which represents an individual system processes, or set of processes, and linking them such that together they represent a greater part of the complete system. As such, model coupling requires consideration of a number of important aspects, the first of which being the choice of a coupling strategy based on a conceptualisation of the physical process interaction.

This section begins by conceptualising the interaction between inundating and infiltrating water in terms of an appropriate coupling strategy and goes on to describe the model coupling itself.

3.5.1 Process Conceptualisation

Process interaction in environmental systems may be conceptualised, for the purposes of model building, as either partially or fully interactive. Where the system of interest comprises one process which has an effect on a second but the second has no effect on the first then process interaction is partial. Both Charlton (1995) and Bates *et al.* (1996) adopted such a scheme in studies into the significance of hillslope runoff on flood characteristics in which hillslope runoff effected floodplain hydraulics, inputs being directly applied to the hydraulic model, but floodplain hydraulics had no effect upon hillslope processes. In fact, floodwater may well influence hillslope inputs through the supply of water to partially contributing areas at the base of hillslopes adjoining the floodplain but for the purposes of the study undertaken these feedback effects were not considered. Semi-interactive coupling schemes have a number of advantages over fully interactive schemes associated primarily with ease of implementation and, importantly, computational efficiency. However, where the system comprises two processes that are fully interactive, where the first effects the second and the second has a feedback effect on the first, then a fully interactive model coupling is required. Such a scheme is adopted here to represent the effect of infiltration on flood inundation, and likewise the effect of inundation on infiltration.

3.5.2 Compatibility of TELEMAC2D and the infiltration model to the coupling strategy

The interactive coupling strategy envisaged requires that TELEMAC2D and the infiltration model

are consistent with this aim in terms of their boundary conditions and mass conservation, temporal resolution and general model structure. These aspects are now considered for each model:

Boundary conditions and mass conservation: TELEMAC2D can accommodate infiltration losses at each node in the computational domain and account for these, in terms of mass conservation, through the continuity equation (Equation 3.5). The infiltration model accommodates inputs through a surface boundary which responds to both precipitation and ponded surface water and in which mass balance is accounted for through equation 3.15.

Temporal resolution: Both TELEMAC2D and the infiltration model require short time steps to maintain computational stability. TELEMAC2D is consistently run using 2 second time steps for flood simulations (Bates *et al.*, 1995) while the explicit nature of the infiltration model requires a similar iteration period to ensure stability, though this also depends upon the cell size chosen and the physical properties of the soil, specifically hydraulic conductivity.

Model structure: The TELEMAC2D structure, which has been referred to earlier (section 3.3), allows for modifications to nodal parameters through the use of subroutines. Such a structure lends itself to the incorporation of the infiltration model within the TELEMAC2D structure from where it can be accessed for each simulation time step and node while maintaining model efficiency.

Both models are compatible with the coupling strategy proposed. The discussion now turns to the development of the infiltration model as a subroutine of the TELEMAC2D code.

3.5.3 Model coupling and integrated model structure

Functionally, the infiltration model can be divided into two parts. The first of these comprises initial functions which are executed only once at the beginning of the simulation and include reading of the initial conditions input file, checks on this input data, calculation of the suction-moisture curves and initialisation of model variables. The second part of the model comprises the main computational body of the code which provides the hydrological simulation. In order to optimise model efficiency these two distinct parts of the infiltration model are separated into two exclusive subroutines, the first, termed subroutine *1DINIT*, comprising those functions which require execution only once within any simulation and a second, termed *1DMODEL*, comprising the 'hydrological' function of the model which must be called for each node and at each time step during a simulation. When future reference is made to the infiltration model it refers to these two subroutines.

Within TELEMAC2D the 1D infiltration model is required to respond to fluxes across its surface

at each domain node. The driving force for fluxes across the surface boundary is provided by inundation, precipitation or evaporation which are likely to be spatially and temporally heterogeneous over the domain during a simulation. This heterogeneity in nodal hydrology must be represented by the 1D infiltration model and is achieved using the subroutine structure of TELEMAC2D. Each time the infiltration model is called values relating to that node, calculated at the previous time step, are used to calculate the new hydrology at that node and the results are stored in 2D arrays in subroutine PROSOU, located higher in the programme structure, ready for the next time step.

This offers the most computationally elegant method as the infiltration model operates within the structure of TELEMAC2D and no changes are made to TELEMAC2D itself. The structure of the coupled model, in terms of the subroutine linkage and resulting data flow, is illustrated in Figure 3.8.

An idealised representation of the model structure resulting from the coupling is represented in Figure 3.9. TELEMAC2D defines the spatial extent of the floodplain, its topography, roughness and hydraulics while the infiltration model renders the floodplain surface responsive to inputs through infiltration, from both inundating water and precipitation, and losses through evaporation.

3.6 Developing a mass balance to represent the coupled model

An integral part of hydraulic and hydrological models is a mass balance which is incorporated to verify that the change in domain moisture storage, as surface water in a hydraulic model and soil moisture in an infiltration model, can be accounted for by the difference in inputs and outputs to the system according to the general equation:

$$\textit{Change in storage} = \textit{inputs} - \textit{outputs} \qquad 3.16$$

This section begins with an outline of the TELEMAC2D mass balance calculation and then describes the development of a floodplain soil moisture mass balance to account for the spatially and temporally variable fluxes across the floodplain surface boundary, a pre-requisite to model application.

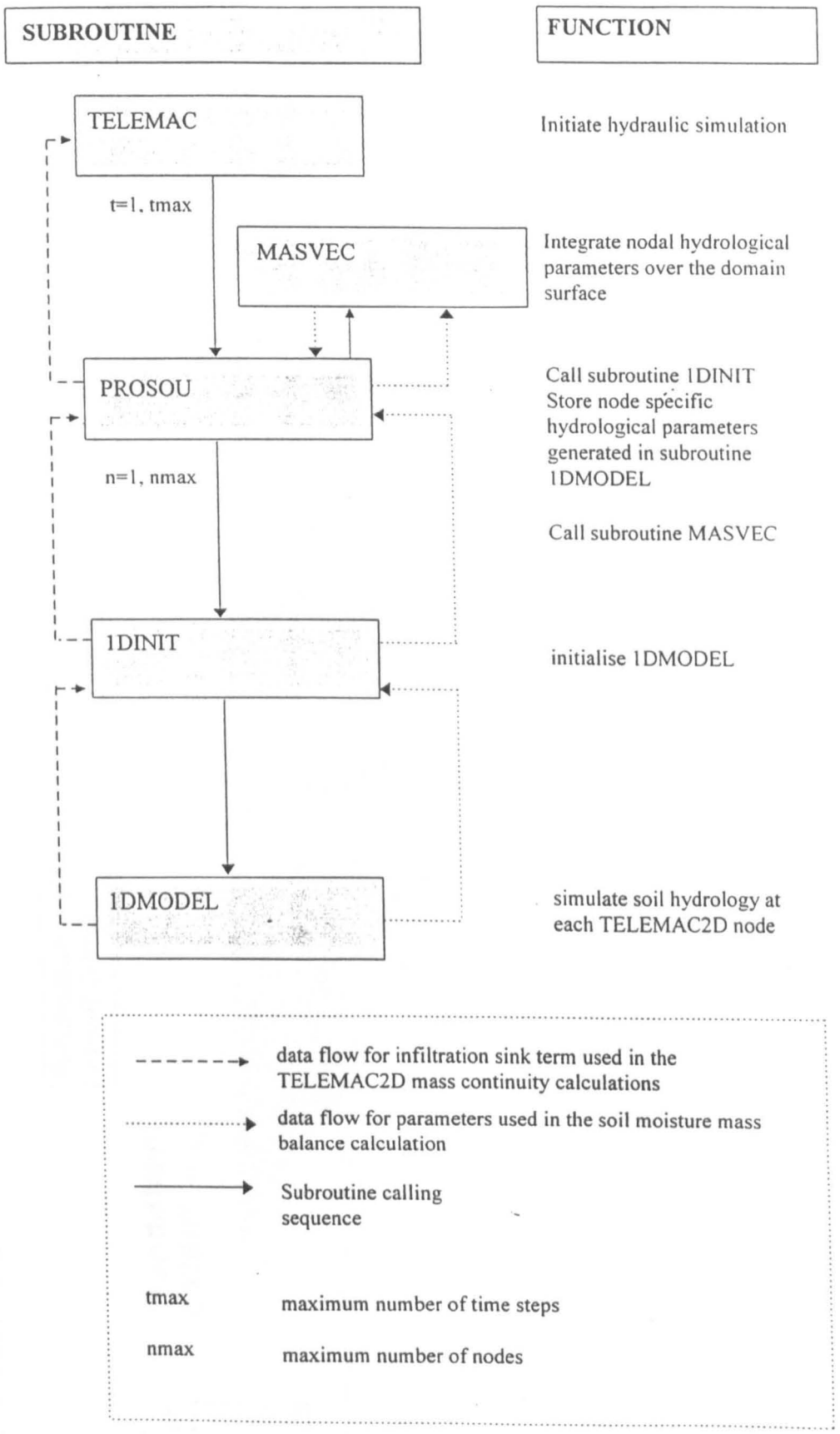

Figure 3.8 Schematic of the infiltration model subroutines within the TELEMAC2D model structure.

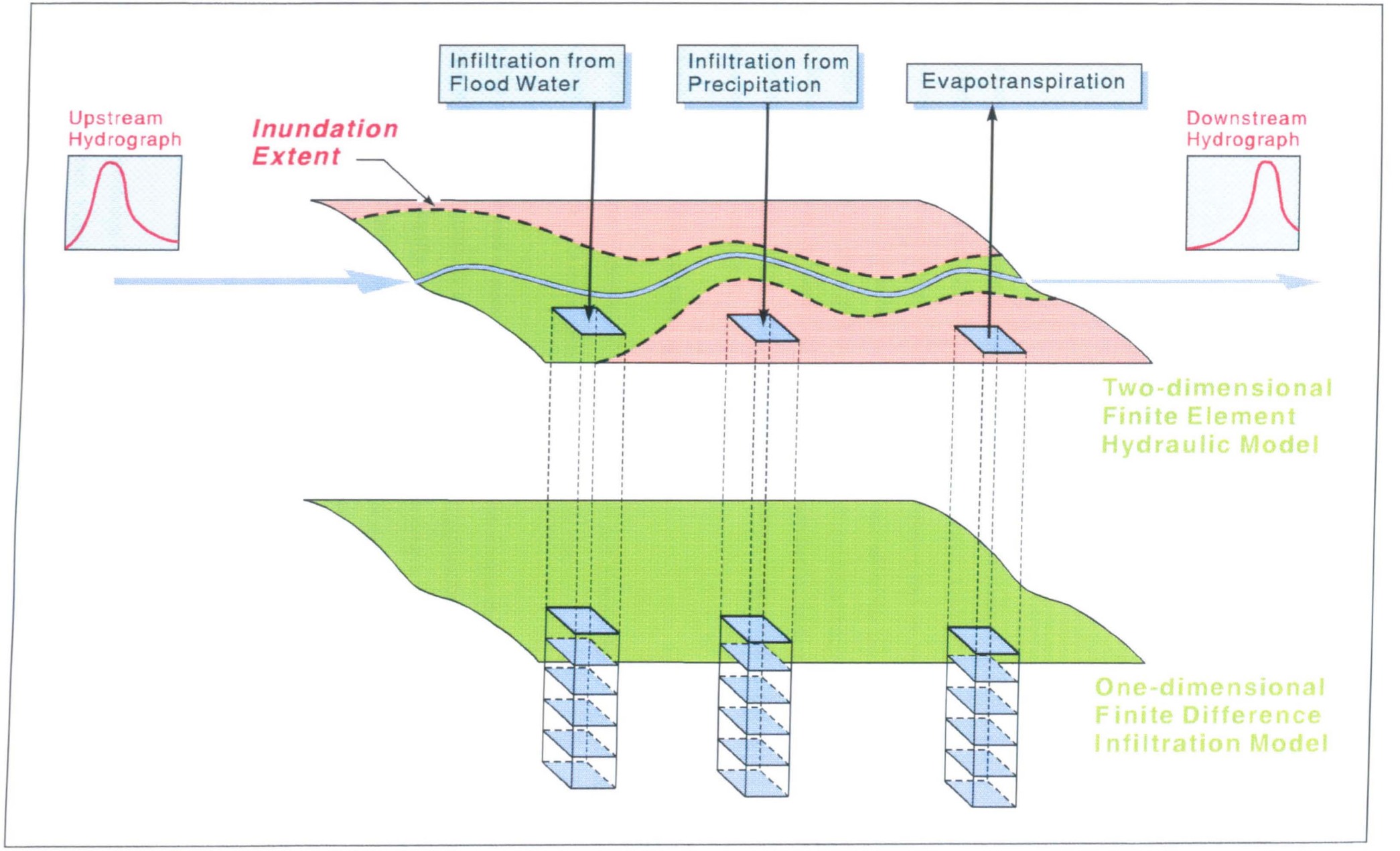

Figure 3.9 Idealised representation of the coupled floodplain hydrology model.

3.6.1 The TELEMAC2D mass balance

The TELEMAC2D mass balance is calculated according to the following equation:

$$BAL_2 = (V_{(f)} - V_{(i)}) - (V_{(in)} - V_{(s)}) \qquad 3.17$$

where $V_{(i)}$ represents the initial volume of water within the modelled domain, $V_{(f)}$ is the final water volume within the modelled domain, $V_{(in)}$ represents the difference between the total volume of water input across the upstream model boundary during a simulation and the total volume of water output across the downstream boundary and $V_{(s)}$ is the volume added by the source term. BAL_2 represents the total volume lost through internal TELEMAC2D numerical errors. Terms $V_{(i)}$ and $V_{(f)}$ represent domain volumes at the beginning and end of the simulation while the remaining terms represent volumes integrated over the simulation. A mass balance is presented at the end of each simulation according to Equation 3.17.

3.6.2 Development of a Domain Mass Balance

A water balance calculation is developed for the floodplain soil domain based on the balance equation which appears in the 1D infiltration model (Equation 3.15).

Equation 3.15 is now developed to account for water fluxes and storage changes occurring over the domain as a whole. This represents a departure from the 1D application of the equation in which inputs and outputs are temporally but not spatially variable to what is essentially a 3D application, spatially defined by the computational domain, in which inputs and outputs are both temporally and spatially variable. As an example, while one node is inundated an adjacent node might be losing water across its surface boundary through evaporation or receiving water from precipitation at a rate determined by that of the precipitation which might be lower than that at the inundated node. Such a hydrologically dynamic situation determines that the hydrological characteristics of each domain node will potentially be unique and this must be represented in the mass balance.

A mass balance representation is achieved using equation 3.15 and by modifying the way in which each parameter is treated. Firstly, the parameters are stored in 2D arrays in the subroutine PROSOU (see Figure 3.8) which ensures node specific characteristics are maintained. Secondly, at the first simulation time step an integrated soil moisture volume is calculated using the subroutine

MASVEC which employs an equation similar to Equation 3.6 except that in this case the term *Sce* is replaced with the required parameter value (in this case W_i). Following the final simulation time step MASVEC calculates a final domain integrated soil moisture volume and at each intervening time step domain integrated values of I (infiltration), E (evaporation) and D (drainage) are calculated and stored cumulatively. In this way the parameters required for the domain soil moisture mass balance are generated.

The domain integrated parameter values for W_f, W_i, I, E and D which now carry the suffix $_{tot}$ (representing total) can now be used to calculate the domain mass balance as represented by Equation 3.18:

$$BAL_3 = (W_{(ftot)} - W_{(itot)}) - (I_{(tot)} - E_{(tot)} - D_{(tot)}) \qquad 3.18$$

where $W_{(ftot)}$ represents the final domain soil moisture content, $W_{(itot)}$ is the initial domain soil moisture content, $I_{(tot)}$ represents the cumulative domain infiltration, $E_{(tot)}$ represents the cumulative domain evaporation and $D_{(tot)}$ the cumulative domain drainage.

As an example: Taking the case of infiltration and assuming that infiltration is occurring at the same rate at each of the nodes in the computational domain then the following occurs. The flux calculated at each node is passed to MASVEC and integrated over the domain area represented by that node, the same occurs for each node and results in a value of infiltration for the domain for that time step. Cumulative nodal values of infiltration allow for the calculation of integrated infiltration totals at the end of a simulation. Taking this one step further, assuming that half of the domain is inundated and the remaining half is experiencing evaporation then for each node MASVEC receives a value of infiltration flux or evaporative flux loss. These are integrated and summed for the time step and represent total domain infiltration and total evaporative loss, for that time step. Cumulative values of total infiltration and evaporation are also maintained for the mass balance calculation. The same is true for precipitation and drainage and values for initial and final domain soil moisture storage.

Essentially, these modifications facilitate the move from a mass balance representing a single nodal point to a mass balance representation of the entire domain hydrology through the treatment of each node as an independent entity and the use of the subroutine MASVEC for the integration of the mass balance parameters over the domain area. In this way the volumetric fluctuations in domain

storage can be fully accounted for.

Two additional mass balance checks are performed, one for the domain precipitation (Equation 3.19) and the other for domain infiltration (equation 3.20). These are calculated according to the principle used to calculate BAL_3 and similarly use the subroutine MASVEC to spatially and temporally integrate the equation parameters.

Domain precipitation mass balance:

$$BAL_4 = P_{(tot)} - (P_{w(tot)} + I_{d(tot)} + R_{(tot)}) - E_{(tot)} \qquad 3.19$$

where $P_{w(tot)}$ represents the cumulative precipitation on inundated (wet) areas, $I_{d(tot)}$ is the cumulative infiltration from dry areas (ie precipitation derived), $P_{(tot)}$ is cumulative precipitation, $R_{(tot)}$ is cumulative runoff and $E_{(tot)}$ has been previously defined. These parameters represent cumulative values integrated over the domain area over the duration of the simulation.

Domain Infiltration mass balance:

$$BAL_5 = I_{(tot)} - (I_{w(tot)} + P_{d(tot)} + R_{(tot)}) \qquad 3.20$$

where $P_{d(tot)}$ represents precipitation falling on dry areas and the other parameters have been previously defined.

At the end of each TELEMAC2D simulation results of the three mass balance checks are output together with the TELEMAC2D mass balance previously discussed in section 3.6.1.

3.7 Model testing and analysis

In order to determine whether surface boundary condition relaxation can be achieved in a numerically stable manner the integrated model is subjected to a series of test simulations.

3.7.1 Testing the TELEMAC2D and soil moisture mass balance

A series of tests are undertaken to determine firstly the TELEMAC2D response to infiltration through the TELEMAC2D mass balance and secondly the response of the soil moisture domain mass balance to spatially variable surface fluxes.

3.7.1.1 Response of the TELEMAC2D mass balance to infiltration losses

A simple 'reservoir' domain was chosen for testing the TELEMAC2D mass balance. The 'reservoir' has a length of 500m and a width of 100m. The boundary conditions are impermeable to the flow of water, except for the relaxed surface boundary, which is able to respond to fluxes. The domain topography is assumed to be flat. The simple mesh used is illustrated in Figure 3.10. This test domain was chosen to allow the effects of infiltration on the TELEMAC2D mass balance to be determined under controlled conditions which would not be possible using a complex, dynamic flood case in which the number of inundated and dry nodes fluctuates with each time step. The reservoir application chosen facilitates easy control of the domain parameters where, for example, it is possible to specify the extent of dry and inundated areas to fully investigate the mass balance effect and it also offers computational efficiency as the meshed domain comprises only 315 nodes and 543 elements.

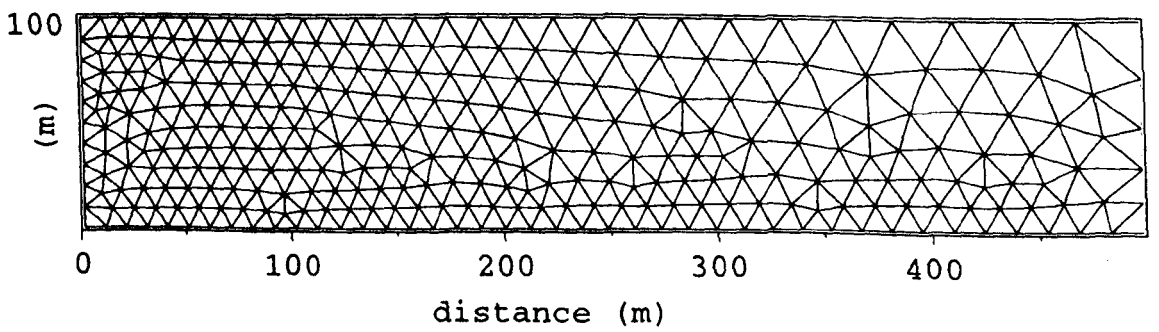

Figure 3.10 Illustration of the mesh used for the simple 'reservoir' test case.

The TELEMAC2D mass balance was tested under four different initial conditions described in Test 1 to Test 4.

Test 1: TELEMAC2D mass balance with relaxed surface boundary:

The reservoir was set-up with a uniform initial water depth of 1.0m over the domain resulting in a total volume of 50000m^3. A constant infiltration rate of $5.0x10^{-6}$ ms^{-1} was specified at the surface boundary of the infiltration model (this was set to override the model calculated infiltration rate) and the simulation was run for 2000s. The volumetric loss calculated by TELEMAC2D and appearing in the TELEMAC2D mass balance can then be compared to a loss calculated manually using the known simulation parameters.

Test 2: TELEMAC2D mass balance with impermeable surface boundary:

The simulation set-up was the same as for Test 1. The infiltration subroutine was not called thus the surface boundary condition remained impermeable.

Test 3: TELEMAC2D mass balance with permeable surface boundary, hydraulic conductivity set to zero:

The simulation was set-up as for Test 2 except here the infiltration routine was called but infiltration was prohibited by a hydraulic conductivity value set to zero. This test was introduced to eliminate the possibility that erroneous effects are introduced simply by calling the infiltration routine.

Test 4: TELEMAC2D mass balance with relaxed surface boundary for a 'dynamic' simulation.

The simulation set-up was as Test 1, except here inundation is specified over only half of the domain, the remainder of the domain remains dry and precipitation is set to zero. The surface boundary condition is relaxed over the entire domain. It is not possible to impose an inundated condition on exactly half of the domain, however, it is possible to specify a close approximation in the TELEMAC2D subroutine CORFON. Subroutine CORFON allows user specified modifications to the bathymetric data, which in this case allowed the domain to be split into two regions, one of high and one of low topography. By imposing an initial depth of water to cover the entire domain and allowing an initialisation period during which this water flowed to the area of lower topography, a mass balance test where approximately only half of the domain is inundated and

experiencing infiltrating can be conducted. Figure 3.11 illustrates the domain topography used in this test.

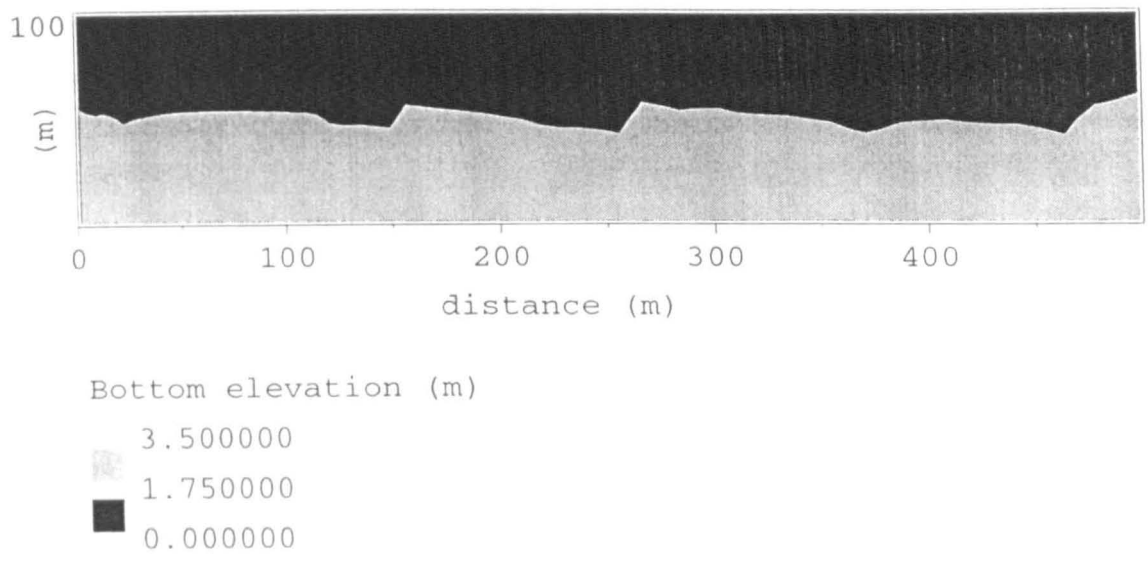

Figure 3.11 Illustration of the domain topography used in test 4.

The results of the four tests are presented in the Table 3.2.

Test	Initial surface water volume	final surface water volume	total floodwater derived infiltration	TELEMAC2D numerical error	calculated flood derived infiltration volumetric loss	calculated infiltration rate
1	50000.0	49500.0	500.0	-0.5×10^{-9}	500.0	5.0×10^{-6}
2	50000.0	50000.0	0.0	0.0	0.0	0.0
3	50000.0	50000.0	0.0	0.0	0.0	0.0
4	23459.2	23185.3	249.9	23.95	250.0 (estimated)	5.0×10^{-6}

Table 3.2 TELEMAC2D mass balance results for Tests 1 to 4.

The results clearly demonstrate the correct functioning of TELEMAC2D under the conditions tested. Under fully inundated conditions, the results from Test 1 confirm that the volume lost through infiltration, as determined by TELEMAC2D, match those calculated manually. Furthermore, dividing the total volume lost by the surface area of the domain and the duration of the

simulation gives an infiltration rate which matches that of $5.0x10^{-6}$ ms^{-1} set in the infiltration model. Tests 2 and 3 confirm that with no infiltration the mass loss to TELEMAC2D is zero. Test 3 illustrates that by calling the infiltration subroutine no erroneous effects are introduced into TELEMAC2D. Finally, Test 4 illustrates that when the surface boundary is relaxed over the entire domain but only half of the domain is inundated then only water lost from the inundated area is considered in the TELEMAC2D mass balance equation. In this case the infiltration loss calculated is roughly half of that calculated for the fully inundated domain and approximates that calculated manually which corresponds to the area inundated. The larger TELEMAC2D internal error associated with this calculation is a product of the method used to define a partially wet domain surface in which large topographic slopes are produced resulting in high water velocities. These tests illustrate that the data (infiltration rate) provided by the infiltration model is (i) being passed to TELEMAC2D and (ii) results in the correct volumetric loss as determined by the mass balance. However, these losses are necessarily artificial in that the flux across the surface boundary is set. This is required to perform the mass balance checks, otherwise the value of flux would vary with each time step according to the soil moisture content of the top cell and verification of the TELEMAC2D mass balance would be impossible.

3.7.1.2 Response of the domain mass balance to variable source inputs

The following series of tests were devised to demonstrate the response of the domain mass balance to surface inputs derived from different sources. Total domain infiltration represents the sum of infiltration derived from inundation plus that resulting from precipitation. Where there is no precipitation, total domain infiltration is equal to that derived from inundation alone and *vice versa*. Where the domain is partially inundated and experiencing precipitation at the same time, total domain infiltration will be the sum of the infiltration arising from these two sources. The following tests were devised to illustrate (i) the correct spatial partitioning of infiltration according to the area inundated or receiving precipitation and (ii) that, where the total infiltration is derived from two sources, only that derived from the inundated area is used in the TELEMAC2D mass balance calculation.

The same test reservoir is employed for these tests as was used for Tests 1 to 4 however the flux across the surface boundary is not overridden in these simulations by a specified rate as was the case in Tests 1 to 4. Instead, the flux is determined by the hydraulic gradient across the surface boundary and is therefore temporally dynamic. The soil column is parameterised to represent an 'idealised' silty loam with an initial soil moisture content of 80% of saturation. Derivation of the input parameters for the infiltration model are discussed in greater detail in *Chapter 5*. In all of the following simulations inundation is specified for only half of the domain by employing the technique discussed with reference to Test 4.

Test 5 and Test 6: TELEMAC2D mass balance with relaxed surface boundary (hydraulic conductivity not imposed):

These tests are duplicates of Tests 1 and 4. Total infiltration to the floodplain derived from inundation is determined with no precipitation inputs. However, while the infiltration rate is specified in tests 1 and 4, in tests 5 and 6 it is not.

Test7: TELEMAC2D mass balance with impermeable surface boundary:

Test7 is designed to determine the mass balance effect when the floodplain is experiencing inundation and precipitation but the hydraulic conductivity is set to zero. The domain is set-up as in Test 6.

Test 8: TELEMAC2D mass balance with floodplain experiencing inundation and precipitation (precipitation rate set at greater than maximum infiltration rate):

Test 8 is designed to test the TELEMAC2D mass balance when the floodplain is exposed to a combination of infiltration derived from both inundating water and precipitation. The domain is set-up as in Test 6 and the precipitation rate set at a rate greater than the maximum infiltration capacity.

Test 9: TELEMAC2D mass balance with floodplain experiencing inundation and precipitation (precipitation rate set lower than maximum infiltration rate):

Test 9 is designed to determine the effect on mass balance when precipitation falling on half of the domain is set at a rate below the maximum infiltration capacity. The test is set-up as for Test 6 but the precipitation rate was set at a value less than the maximum infiltration capacity.

The results of the five tests are presented in Table 3.3(a).

The results of this series of tests demonstrate the correct partitioning of infiltrating water between that derived from inundation and that derived from precipitation. Tests 5 and 6 simply repeat Tests 1 and 4 but the infiltration rate is not set in the latter. Tests 5 and 6 provide the controls against which the other simulations in this series are compared. It is not possible to verify the infiltration figures for this dynamic case (as the flux across the surface boundary is variable over time). Test 7 confirms that the total infiltration is zero when the domain is neither inundated or subject to precipitation. Tests 8 and 9 demonstrate the effect on total infiltration when the precipitation rate is varied. Where the precipitation rate is greater than the infiltration capacity then total infiltration is

the same as that under a fully inundated domain, as expected. Where the precipitation rate is less than the infiltration capacity then total infiltration is reduced to that derived from the inundated zone plus that derived from precipitation, which is equal to the total precipitation falling on the non-inundated domain area. These tests confirm the two points raised above, namely that (i) correct spatial partitioning of infiltrating water is achieved between that derived from inundating water and that derived from precipitation, and (ii) that where the total infiltration is derived from two sources, only that derived from the inundated area is employed in the TELEMAC2D mass balance calculation.

As the rate of infiltration across the surface boundary in Tests 5 to 9 is not previously prescribed, it is possible to comment on the mass errors associated with changes in domain soil moisture. These are presented in Table 3.3b and illustrate that this aspect of the model remains numerically stable throughout.

Test	Initial surface water volume	Final surface water volume	Total floodwater derived infiltration	TELEMAC2D error	Total floodwater and rainfall derived infiltration	Total precipitation derived infiltration
5	50000.0	49383.3	616.7	0.38	616.7	0.0
6	23459.2	23126.9	308.2	23.9	308.2	0.0
7	0.0	0.0	0.0	0.0	0.0	0.0
8	23459.2	23126.9	308.2	23.9	616.7	308.5
9	23459.2	23126.9	308.2	23.9	313.2	5.0

Table 3.3(a) TELEMAC2D mass balance results for Tests 5 to 9

Test	BAL_3 (the domain soil moisture mass balance - Equation 3.18)
5	$4.58x10^{-11}$
6	$1.17x10^{-11}$
7	-4.18x10-^{11}
8	$4.58x10^{-11}$
9	$4.58x10^{-11}$

Table 3.3(b) The domain soil moisture mass balance for Tests 5 to 9

3.8 Conclusions

In *Chapter 2* the most appropriate methodology for developing an integrated approach to modelling floodplain hydrology was identified as one in which a 2D finite element hydraulic model offering unparalleled spatial representation of surface flow processes is coupled with a physically based model representing infiltration. In *Chapter 3* this has been accomplished through the interactive coupling of a 1D finite difference infiltration model with the state-of-the-art distributed finite element hydraulic model, TELEMAC2D.

In the coupling achieved TELEMAC2D determines both the spatial and temporal resolution at which surface hydraulic processes and infiltration is represented (in plan) while the physically based infiltration model provides the spatial description of the floodplain soil hydrology in 1D with depth. Importantly, the nature of the finite element approach allows for considerable flexibility in the spatial representation of both surface flow and the 'density' with which infiltration is represented.

The model structure allows for the uniqueness of the hydrology associated with each domain node to be maintained throughout the simulation and to be integrated within a domain soil moisture mass balance. Thus at the end of each simulation data relating to both the TELEMAC2D and integrated soil moisture mass balances is provided. Numerical stability of the coupled floodplain hydrology model is demonstrated through a series of test simulations which investigate the effect of infiltration on both the TELEMAC2D mass balance and the floodplain soil moisture mass balance. The results of these test simulations support the application of the coupled model to the more complex floodplain cases to be investigated in later Chapters.

Modelling nitrate dynamics in the floodplain

4.1 Introduction and Chapter Objectives

The importance attached to simulating the transport and transformation of NO_3-N within soils is reflected in the large number of models dedicated to describing these processes. The N-cycle is complex and dynamic to the degree that in some areas it is not yet fully understood and before a model dedicated to simulating the behaviour of NO_3-N within the floodplain N-cycle can be developed, in accordance with the research aims, the place of this ion within the system as a whole must first be identified. Only then can those processes which dominate in its fate be identified and incorporated within a model structure.

Accordingly, this chapter begins with a review of the floodplain N cycle throughout which particular attention is paid to those processes that determine the fate of the NO_3-N ion within the floodplain soil system. Following the identification of the major factors influencing the concentration of NO_3-N in the floodplain a conceptual model representing the fate of NO_3-N in floodplain soils is advanced. Following a review of the techniques available for modelling the transport and transformation of NO_3-N in soils at a scale commensurate with the aims of the research, the conceptual model is converted into a deterministic model for use in the research into flood induced floodplain soil NO_3-N processes.

4.2 The Floodplain N-cycle

Before considering the specifics of N cycling in floodplain ecosystems, a generalised N-cycle is presented (see Figure 4.1). The specific rates attached to each of the inputs, outputs and transformation processes will vary between ecosystems and both spatially and temporally within individual ecosystems. The system receives additions of N through atmospheric deposition, both wet and dry, through microbially mediated N_2 fixation, through animal and plant detritus and through anthropogenic inputs intentionally as N fixed in fertilisers and unintentionally through the

products of combustion. Losses of N occur through leaching, predominantly of the NO_3-N anion, surface runoff, erosion, volatilisation of ammonia ($NH_3(g)$), plant and animal removal (which predominates in agricultural ecosystems), and gaseous losses of N_2 and N_2O resulting from the microbially mediated processes of denitrification and nitrification. Within the soil ecosystem a highly active N-cycle operates within which N is utilised to supply the energy and material needs of the microbial population. Nitrogenous organic matter is mineralised through the action of soil microbes releasing NH_4-N which is then available for oxidation to NO_2-N and NO_3-N through microbial nitrification. NH_4-N and NO_3-N are then both available for uptake by plants and immobilisation within microbial biomass.

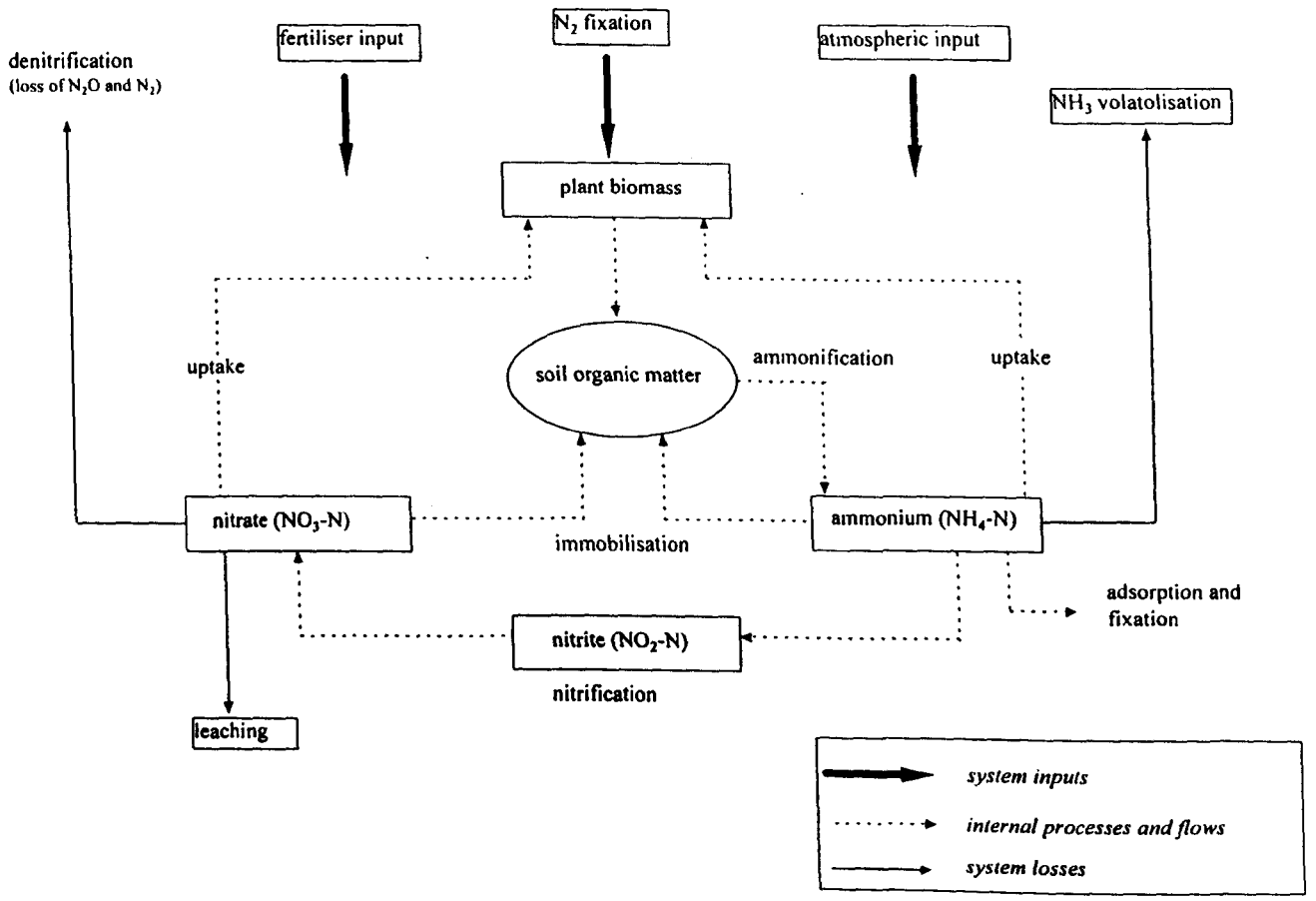

Figure 4.1 The nitrogen cycle.

In mature non-agricultural systems in steady state the N-cycle remains effectively closed and inputs to the system through precipitation and N_2 fixation balance losses through denitrification, volatilisation and leaching. Inputs are also small relative to the annual N-turnover. In contrast, many agricultural ecosystems are comparatively open and sustain N loss through product removal, enhanced leaching, runoff and gaseous losses and the application of fertilisers is required to reinstate the equilibrium. It is the disturbance of the ecosystem equilibrium and the addition of fertilisers to redress it in agricultural systems which has predominantly been responsible for the current economic and environmental concerns relating to *NO_3-N* pollution from farmed land. The inputs, outputs and transformations associated with the floodplain N-cycle are now covered in greater detail with particular attention given to those processes that influence the concentration of *NO_3-N*.

4.2.1 Inputs of N to the floodplain ecosystem

4.2.1.1 Atmospheric additions

N is derived from the atmosphere through both wet (dissolved in rainwater as *NH_4-N*, *NO_2-N*, *NO_3-N*) and dry (gaseous or particulate form) deposition. Of these two pathways, considerably more is known about the first (Haynes, 1986) which is also regarded to be the most significant (Whelan, 1993). The importance of wet deposition as a source of N depends largely upon the location of the receiving area. For instance, while the amount of N added to the soil each year through wet deposition is normally small compared to that added through fertilisers and animal waste in cropped systems or grazed systems, such inputs are potentially significant in replacing the N lost through leaching and denitrification in mature, natural ecosystems (Stevenson, 1982). It is recognised that areas close to industrial centres receive higher levels of dissolved *NO_3-N* in rainwater than do remote, rural areas, due to higher releases of nitrogen oxides from the combustion of fossil fuels. Paul and Clark (1989) suggest a range of input between 5 kg ha^{-1} yr^{-1} of *NO_3-N* in polluted areas to less than 0.5 kg ha^{-1} yr^{-1} in low-rainfall areas far from sources of industrial pollution. Low levels of *NO_3-N* input in areas remote from industrial centres is supported by Atteia (1994). However, due to the considerable variation in the chemical composition of precipitation over large areas compounded by small-scale variations in time and space it is difficult to make generalisations (Haynes, 1986).

Little is known about inputs derived from dry deposition. However, these are known to include ammonia (NH_3) absorption by soils and plants (Denmead *et al.*, 1976) and the uptake of N as *N_2O* and *N_2* by wetland plants (Reddy *et al.*, 1989). It is likely, however, that N derived from dry deposition remain small.

4.2.1.2 Nitrogen fixation

The earth's atmosphere contains a vast supply of N in the form of inert N_2 gas, part of which is made available to higher plants and animals through the N-fixing capability of certain soil microbes. It is estimated that $12.2x10^{-5}$ tonnes of combined nitrogen are made available annually to the biosphere through the process of N-fixation (Burris, 1980) which ensures that this process remains responsible for much of the fertility in agricultural soils, a fact that is especially true in Developing World systems (Stevenson, 1982). The magnitude of N fixed depends upon the availability and activity of the microbes capable of performing the process. These can be divided into the following three main life groups: (i) freeliving nonsymbiotic, (ii) freeliving but in close association with the rhizosphere of plant roots and (iii) those forming symbiotic associations with other plants. The most well known and most agriculturally important relationship is the root nodule forming symbiosis between Rhizobium species and some legumes. Detailed accounts of the various groups, their taxonomy and physiology are given elsewhere (for example, see Havelka *et al.*, 1982). Stevenson (1982) attached such importance to N-fixation that he suggests this process should be added to photosynthesis and respiration as the third basis biochemical process occurring in nature. The significance of N-fixation in floodplain soils will depend primarily upon the vegetation present. If leguminous species are used in the permanent pastures typical of lowland floodplain systems then the potential for N fixation will be dramatically increased.

4.2.1.3 Fertiliser additions (Industrial fixation)

The application of N based fertilisers has increasingly been used to replenish the N loss sustained in agricultural systems, particularly those in the Western World. The use of nitrogen fertilisers in England and Wales has increased considerable since the 1950s, between 1950 and 1980 the increase was 23% and 42% for permanent and temporary grassland (Ross, 1989). On a global scale, inputs of N through fertilisers are thought to fall below those from biological N fixation, representing between 30 and 60%. However, on a local scale this will vary considerably depending upon the rates of fertiliser application and the presence of N-fixing microbes. Where lowland floodplains are used for summer grazing they generally receive fertiliser inputs.

4.2.1.4 Hydrologically mediated inputs

A feature of floodplains which sets them apart in the landscape is their unique hydrology which also mediates N inputs. Floodplains receive hydrologically mediated N inputs through both floodwater and laterally flowing hillslope surface and groundwater. Infiltrating floodwater will carry with it a dissolved load of NO_3-N (Maltby *et al.*, 1991; 1996) while sediment deposition, a feature of lowland floodplain systems (Walling *et al.*, 1992) will deposit N associated with mineral and perhaps more significantly, organic sediments (Brunet *et al.*, 1994). A considerable wealth of research has considered the lateral input of NO_3-N to the floodplain environment both as shallow groundwater

(Groffman *et al.*, 1991, Lowrance, 1992, Haycock and Pinay, 1993, Hanson *et al.*, 1994) and surface flow (Chesheir *et al.*, 1987). Indeed, this research represents much of the literature on buffer zone processes alluded to in *Chapter 2*.

While little is known about the magnitude and significance of the potential floodwater NO_3-*N* input, inputs from the hillslope have been quantified for a number of hillslope-floodplain systems. Lowrance (1992) reported a NO_3-*N* input of 13.52 mgl^{-1} in laterally flowing shallow groundwater from a row-crop corn field receiving 250 Kg N $ha^{-1}y^{-1}$ to a Georgia coastal plain riparian site. Haycock and Pinay (1993) measured winter groundwater NO_3-*N* inputs flowing from a farmed (arable) hillslope to a grass riparian buffer strip in the River Leach catchment (Gloustershire, UK). Observed NO_3-*N* concentrations in the groundwater entering the floodplain were closely related to groundwater flow and fluctuated between approximately 2 mgl^{-1} and 12 mgl^{-1} between December 1989 and February 1990. Hanson *et al.* (1994) measured average NO_3-*N* concentrations in groundwater arriving at a floodplain site from an unsewered residential development of 8 mgl^{-1}.

The magnitude of both floodwater N and hillslope N inputs to the floodplain will depend upon a number of controlling factors including the magnitude and frequency of inundation, the permeability and soil moisture status of the floodplain soils, the predominant hillslope-floodplain hydrological pathways, N removal processes occurring prior to the water arriving at the hillslope-floodplain interface, and the landuse upstream of the floodplain. The behaviour of NO_3-*N* in floodwater exhibits considerable complexity with the result that its concentration varies considerably between catchment river systems and within in the same system during different events (Walling and Foster, 1975; Webb and Walling, 1985). As the pathway by which water reaches the channel will be significant in determining the NO_3-*N* concentration then significant fluctuations in river NO_3-*N* concentrations are likely during storm events when runoff from disparate sources mix in the river (Johnes and Burt, 1993). During floods the concentration of NO_3-*N* may be reduced through the diluting effect of additional water (Walling and Webb, 1986; Johnes and Burt, 1993) or increased through additional inputs due to the flushing of NO_3-*N* (Foster and Walling, 1978; Brunet *et al.*, 1994) which is particularly significant in autumn storms after a prolonged period without rain. Such differences in NO_3-*N* concentrations are thought to reflect the influence of a number of factors including the variations in the rate of mineralisation and nitrification, storm hydrograph characteristics and antecedent soil moisture conditions (Walling and Webb, 1986). Floodwater concentrations therefore may be either greater or lower than their mean values. For the Adour River in Southern France Brunet *et al.* (1994) reported NO_3-*N* concentrations rising above 10mgl^{-1} at two monitoring sites during a June flood. Maltby *et al.* (1991) report NO_3-N concentrations for the River Culm, Devon, ranging from 5 mgl^{-1} to in excess of 8 mgl^{-1} for 1989 while Johnes and Burt (1993) report concentrations of NO_3-*N* for Slapton Wood stream that fall

from approximately 8mg l^{-1} to less than 5 mg l^{-1} during storm discharge (this discharge also exhibits the considerable effect of flushing). The concentration of NO_3-N within floodwater exhibits high variability and may reach in excess of 10mgl^{-1}.

4.2.2 Losses of N from the N cycle

4.2.2.1 Gaseous losses through denitrification

Gaseous loss of NO_3-N through denitrification has been identified as a significant factor in the attenuation of NO_3-N in floodplain buffer zones (see discussion presented in *Chapter 2*) and will be discussed here in detail accordingly. Floodplains are often made up of a patchwork of well- and poorly-drained soils, the later providing conditions favourable to denitrification (Schnabel and Stout, 1994). Under anaerobic soil conditions NO_3-N is subject to two microbially mediated reduction mechanisms (Buresh and Patrick, 1978). The first of these is NO_3-N respiration (also known as *dissimilatory denitrification*) in which NO_3-N functions as an alternative to O_2 as an electron acceptor during microbial respiration, according to the following reduction sequence:

$$NO_3\text{-}N \rightarrow NO_2\text{-}N \rightarrow N_2O\text{-}N \rightarrow N_2 \qquad 4.1$$

for which the reduction half reaction takes the form:

$$NO_3^- + 6H^+ + 5e^- \rightarrow \frac{1}{2}N_2 + 3H_2O \qquad 4.2$$

NO_3-N is reduced first to nitrite (NO_2-N) then to nitrous oxide (N_2O) and finally dinitrogen gas (N_2). The process is described as a dissimilatory reduction as the products of NO_3-N reduction (NO_2 and N_2) are not assimilated but released to the atmosphere.

The second reduction pathway (nitrate assimilation) involves the microbial reduction of NO_3-N to NH_4-N following which NH_4-N can be immobilised in microbial tissue. An important consequence of this process is the retention of N within the ecosystem.

There is also evidence for a purely chemical pathway involving the reduction of NO_2-N to NO, a gas not normally associated with microbial denitrification, N_2O and N_2 (Van Cleemput and Baert, 1984) under acidic soil conditions in a process termed '*chemodenitrification*' (Nelson, 1982). Bollag *et al.* (1973) demonstrated that NO_2-N is unstable in acid solutions and decomposes predominantly to nitric oxide (NO) and nitrogen dioxide (N_2) by way of chemical reaction, while at neutral or alkaline pH NO_2-N reduction was found to be predominantly biological. Van Cleemput and Baert (1984) illustrated that wherever NO_2-N is formed in a soil under acid conditions both soil organic matter and the soil mineral phase can act to stimulate NO_2-N reduction. In conditions favouring the solubility of Fe(III)-compounds and Fe_2^+ formation NO_2-N decomposition was reported even under slightly acidic conditions. Bulla *et al.* (1970) reported chemical NO_2-N decomposition in soils over a wide range of pH values and suggested that copper, iron, magnesium and certain aluminium salts may promote non-enzymatic decomposition of NO_2-N. However, NO_2-N does not usually accumulate in the soil due to its oxidation to NO_3-N by nitrifiers (Howard-Williams and Downes, 1993) thus the source of NO_2-N available for chemodenitrification may be limited under most natural ecosystem conditions. As the contribution of chemical reduction to total denitrification is likely to be small in all but acidic soils this reduction pathway is not considered further.

Of the two microbially mediated pathways there has been little research into the reduction of NO_3-N to NH_4-N (Ross, 1989) resulting in only a limited knowledge of this pathway. Nommick (1956) concluded that under the conditions prevalent in arable soils no, or extremely insignificant amounts, of NH_4-N are produced during denitrification. His conclusions have been both supported and challenged by subsequent authors, many of whom show this pathway to be active under reducing soil conditions. Using labelled NO_3-N (N^{15}), Reddy *et al.* (1982) found that less than 3% of the added N was incorporated into the organic and NH_4-N fractions in soils ranging in pH from 5.6 to 7.5 (supporting the findings of Jordan *et al.*, 1993 and Haycock and Pinay, 1993 in floodplain soils). However, Ponnamperuma (1972) suggested that a substantial proportion of added NO_3-N may, in some submerged soils, be assimilated, and incorporated into the pool of soil organic matter. It is worth noting the work of Stanford *et al.* (1975a) whose research showed a substantial amount of NO_3-N reduction to NH_4-N during anaerobic incubation in glucose amended soils. They suggest that these results seriously challenge the view that NO_3-N reduction (dissimilation) accounts for essentially all NO_3-N reduction in anaerobic soils and conclude that NO_3-N assimilation may be a significant process in some soils. In a study designed to expand upon the work of Stanford *et al.*

(1975), Buresh and Patrick (1978) found that only under very reducing conditions (-260mV) were significant amounts of NO_3-N reduced to NH_4-N. Under such conditions they found that upto 20% of added NO_3-N was converted to NH_4-N following a four day incubation.

Although highly reducing conditions have been reported in anaerobic floodplain soils associated with NO_3-N attenuation (Jordan *et al.*, 1993) associated conversion of NO_3-N to NH_4-N has not been widely reported (Jordan *et al.*, 1993; Haycock and Pinay, 1993). Jordan *et al.* (1993) reported a $0.1 mgl^{-1}$ increase in NH_4-N and dissolved organic nitrogen (DON) concentration along a transect through a deciduous riparian forest which supported both low Eh values (-95 to -260mV) and high NO_3-N attenuation. They conclude that as the increase in concentration of both NH_4-N and DON is only slight, NO_3-N is not being transformed into DON or NH_4-N, but instead is being denitrified and removed through plant uptake.

The practical significance of naturally occurring NO_3-N reduction to NH_4-N may be limited. Buresh and Patrick (1978) point out that NO_3-N which is contained in water which flows into the soil column will normally come into contact with a zone of intermediate reduction where conversion to N_2 rather than NH_4-N is probably favoured before it comes into contact with the most reduced zone of flooded soils. They cite the most likely condition for the conversion of NO_3-N to NH_4-N to be in rice fields during seedbed preparation where a drained soil containing NO_3-N and readily decomposable carbon supply is flooded and intense reducing conditions may develop rapidly enough for the conversion of NO_3-N to NH_4-N. Such an argument may explain the relative unimportance of this process reported in floodplain buffer systems where NO_3-N generally passes gradually into more reducing conditions along flowpaths towards surface water (for example, see Hanson *et al.*, 1994).

The literature exhibits a certain amount of ambiguity over this point but for the purposes of this project nitrate assimilation will not be considered further. The lack of significant NO_3-N conversion to NH_4-N reported in floodplain soils suggests that this process requires no further consideration for floodplain soils. However, its potential significance in highly reducing floodplain soils should not ignored. ***Denitrification will now refer to NO_3-N respiration exclusively.***

Microbially mediated reactions are highly sensitive to the chemical and physical environments in which they occur. Accordingly, the occurrence and rate of denitrification is found to be dependant upon the following five environmental factors: Soil oxygen status, soil moisture content, carbon availability, soil temperature and soil pH. The prevailing combination of these factors determine the extent to which denitrification represents a significant loss of NO_3-N from the system.

Soil Oxygen Status: Oxygen has long been established as an important regulator of the soil denitrification rate. Denitrification is an enzymatically controlled process in which the absence, or at least the reduced availability, of O_2 is a prerequisite for both the synthesis and function of the N oxide reductase enzymes involved. Potential sites for denitrification will only develop in soils where oxygen demand exceeds oxygen supply and the prevailing O_2 concentration falls below the threshold required to initiate denitrification. Such conditions are likely to prevail in sites supporting a respiring microbial population which are concurrently experiencing restricted oxygen diffusion, such as waterlogged soil conditions. These conditions can also develop at the centre of soil structural peds, creating anaerobic 'microsites', which account for the denitrification observed in 'aerobic soils' (Sextone *et al.*, 1985; Tiedje *et al.*, 1984). Anaerobic microsites have not been reported in all well structured soils (Craswell, 1978) while their presence within soil aggregates does not necessarily imply an occurrence of denitrification. Sextone *et al.* (1985) observed that although the presence of anaerobic centres were necessary to support denitrification, not all aggregates with anaerobic centres denitrified. This was thought to imply the presence of additional rate limiting factors including carbon and NO_3-N availability.

The importance of soil oxygen status in determining denitrification activity is understood at the microbial level, however, due to the difficulties in directly measuring the distribution of O_2 concentrations within the soil it has been difficult to directly quantify the control that this parameter exerts over denitrification at increased scales, especially in the field. Increased rates of denitrification have also been correlated positively with increased soil moisture contents and it is this observation which has lead researchers to adopt soil moisture, which is significantly more easy to measure, as a surrogate for O_2 concentrations in the determination of denitrification rates. The influence of water is linked to its role in governing the rate of O_2 diffusion to sites of microbial activity. Indeed, soil moisture content has been widely used as a 'surrogate' for oxygen status (for example, see Whelan, 1993).

Soil Moisture: Denitrification rates have been shown to be closely related to soil moisture content. Both Rolston *et al.* (1984) and Sextone *et al.* (1985) found a close (inverse) relationship between the proportion of soil saturation and the rate of denitrification. The soil moisture level below which denitrification is inhibited will vary according to a number of factors including the rate of microbial O_2 consumption but has been put at between 60% and 80% saturation. Nommik (1956) determined that at 60% soil water saturation denitrification was not detectable while at 80% water saturation denitrification remained strongly inhibited. Ambus and Christensen (1993) also reported complete inhibition of denitrification below 80% water filled porosity in fen soils (26.8% organic-C). Paul and Clark (1989) suggest that for field soils that are not subject to abnormally high O_2 consumption rates that denitrification is insignificant or lacking at moisture levels below 60% of moisture

holding capacity. Similar thresholds for denitrification 'take-off' are reported by Maag and Lind (1992) for the three soil types presented in Table 4.1.

Soil type	volumetric moisture content (%)	Water filled porosity (%)
Sand	30	72
Clay	40	88
Peat	55	75

Table 4.1 Thresholds for the denitrification 'take-off' reported by Magg and Lind (1992).

Once the threshold soil moisture content required to initiate denitrification has been met rates are generally observed to increase dramatically following even small increases in water content following precipitation or flooding (Sextone *et al.*, 1985; Linn and Doran, 1985). Linn and Doran (1985) summarised the relationship between soil moisture content (as water filled pore space) and denitrification rate (as relative microbial activity) over a range of soil moisture contents and their results are illustrated in Figure 4.2. Significantly, their findings illustrate the sensitivity of denitrification rate to soil moisture content which increases by a factor of five between 80 and 90% water filled porosity. The inverse relationship between soil moisture content and denitrification is now universally accepted (Firestone, 1982) and can be explained by the considerably slower diffusion rate of O_2 through soil water ($0.226x10^{-4}$) than through soil air ($0.209cms^{-1}$).

Increasing soil moisture can also result in the redistribution and transport of both NO_3-N and C to denitrifying sites within the soil profile. For example, Sexstone *et al.* (1988) demonstrated a lowering of the coefficient of variation for denitrification rates with increasing soil moisture content. Coefficients of variation were highest in aerobic cores and decreased as the soil moisture content increased and denitrifiers became non-limited by O_2 and substrate supply.

Carbon Availability: The availability of organic carbon (C) is often cited as a major factor influencing the rate of denitrification. Available C within the soil is utilised by denitrifiers for respiration and cell growth and in anaerobic conditions the availability of readily decomposable C will limit the rate of denitrification through C enforced limits on denitrifier population dynamics. As such it is both the presence and quality of soil organic C and the rate at which it is converted to soluble organic C that determines the rate of denitrification in C limited environments. Numerous researchers have reported increased denitrification rates following the addition of organic C to soils

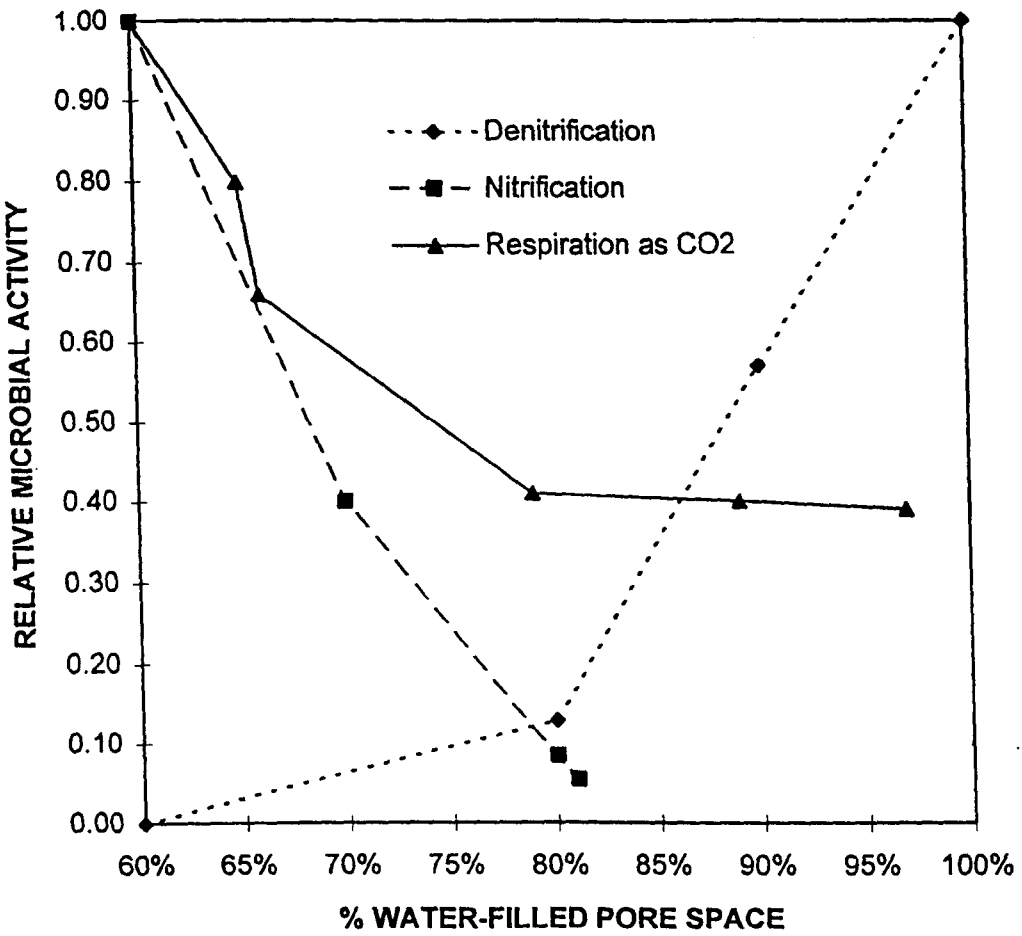

Figure 4.2 The relationship between water-filled pore space and relative microbial activity (after Linn and Doran, 1985).

(Nommik, 1956; Stanford *et al.* , 1975a; Bijay-Singh *et al.*, 1988 and 1989; Myrold and Tiedje, 1985; Reddy *et al.*, 1982; Obenhuber and Lowrance, 1991), while others have reported decreases in denitrification associated with C limitations (Smid and Beauchamp, 1976). While there is general correlation between total soil organic matter (SOM) content and denitrification potential, much better correlation has been found with the supply of easily decomposable organic matter.

In a study of 30 soils of differing carbon content, Stanford *et al.* (1975a), demonstrated NO_3-N loss to be significantly correlated to both soil organic carbon ($r^2 = 0.69$) and soil extracted glucose ($r^2 = 0.82$). For a soil in which NO_3-N was not limiting Myrold and Tiedje (1985) reported that C

availability, through its control of microbial growth, was the dominant factor in determining denitrification capacity. In aquifer environments usually associated with low rates of denitrification, Obenhuber and Lowrance (1991) reported significant decreases in NO_3-N in microcosms of unconsolidated aquifer systems (south-central Georgia, USA) following the addition of a carbon source. Their findings suggest an adaptation of the microbial population to denitrification (large amounts of NO_3-N not usually being present in these environments) and an important effect upon the groundwater concentrations of NO_3-N in unconsolidated aquifers. Hill and Sanmugadas (1985) reported a positive correlation between potential daily NO_3-N loss rates in sediments from three Ontario streams and sediment organic carbon, total N, sediment ammonia and the percentage silt and clay. However, the most significant correlation was with water soluble C which accounted for 67-79% of the variation in NO_3-N loss. Most, but not all authors have reported increased denitrification following the addition of a carbon source. Indeed, Craswell (1979) reported reduced denitrification but increased immobilisation rates in soils receiving carbon additions in the form of straw. He suggested that increased immobilisation was responsible for reducing the availability of NO_3-N for denitrification. Such a situation is likely to occur only where NO_3-N is limiting and the overwhelming bulk of literature reports increased denitrification rates following the addition of a readily available carbon supply.

The generally higher concentration of a readily available supply of carbon in top soils usually means that denitrification is concentrated in the upper soil horizon and the reduction in denitrification rate with depth can be rapid. Numerous examples testify to this stratification of denitrification rate with depth (Lowrance, 1992) and Table 4.3 presents data reported by Oenema and Velthof (1992) for the average contribution to total denitrification measured to a depth of 1m in grassland soil.

Soil depth (m)	Contribution to total denitrification (%)
0-0.05	60
0.05-0.1	13
0.1-0.2	18
0.2-0.4	8
0.4-0.6	1
0.6-1.0	<1

Table 4.2 Contribution of different soil depths to total soil profile denitrification measured to a depth of 1m by Oenema and Velthof (1992) in a number of grassland soils.

Temperature: Temperature is a major factor controlling the rate of denitrification in the field (Stanford *et al.*, 1975b; Jacobson and Alexander, 1980). Denitrification responds directly in

that microbial activity responds exponentially according to the Arrhenius equation and indirectly in that temperature affects both the solubility and speed of diffusion of O_2 in water.

Stanford *et al.* (1975b) determined the 1st order decay coefficient (k) for NO_3-*N* loss (denitrification) for soils at different temperatures. For the range 15 - 35°C, k approximated a doubling for each 10°C rise in temperature (Q_{10} = 2), while above 35°C k was not significantly affected and at 5°C denitrification was reported to be very slow. Jacobson and Alexander (1980) reported no loss of NO_3-*N* during a 7 day incubation at 1°C in a Windsor sandy loam while in glucose amended soil between the temperature of 15 and 30°C Q_{10} was 1.9. While the effect of temperature on the reaction rate is well documented once denitrification has been initiated, there remains much debate regarding the lower temperature limit of the process. While most authors report denitrification occurring at temperatures as low as 1 - 2 °C, but not below, others have found the threshold temperature to be both lower and higher. Craswell (1978) was unable to detect the loss of ^{15}N-labelled NO_3-*N* from cores of Queensland soils (Australia) held under anaerobic waterlogged conditions at 10°C. Dorland and Beauchamp (1991), on the other hand, reported denitrification albeit at reduced rates, at minus 2°C in unfrozen (supercooled) and frozen soils. In poorly drained Pennsylvania floodplain soils Schnabel and Stout (1994) report increased denitrification rates following a rise in soil temperature from the winter low to 5-7°C.

Indeed, the effect of temperature is not simple and has been shown to be complicated by other soil physical and chemical factors including antecedent soil moisture content and available C. Craswell (1978) demonstrated that the effect of temperature on denitrification interacted strongly with that of soil water content. As temperature decreased, the minimum soil water content required for the initiation of denitrification increased. Both Dorland and Beauchamp (1991) and Smid and Beauchamp (1976) have reported increased denitrification rates following increases in available C at a given temperature. Dorland and Beauchamp (1991) found that the rate of denitrification at all temperatures tested was enhanced by the addition of alfalfa as a carbon source. They suggest also that the threshold temperature necessary for the initiation of denitrification may increase as the availability of carbon decreases and that this may offer an explanation as to why some authors have reported the initiation of denitrification to occur only at temperatures above 0°C, in effect, their systems being C limited with respect to temperature.

It has also been suggested (Powlson *et al.*, 1988) that denitrifier populations are adapted to the temperature regimes of their environments such that denitrifiers in temperate soils are able to denitrify at lower temperatures than those in the sub-tropics. These suggestions are based on the results of a comparison of a temperate soil and a sub-tropical soil conducted by Powlson *et al.* (1988) where consistently higher denitrification (and immobilisation) rates were found in the

temperate soils at lower temperatures. Such adaptation by denitrifier populations might explain why some authors (eg Craswell, 1978) have reported little or no denitrification loss at low temperatures while others have reported substantial losses.

pH: Most denitrifying bacteria grow best near neutrality (pH 6 - 8). Denitrification becomes slow but still may remain significant below pH 5 and is negligible or absent below pH 4 (Paul and Clark, 1989).

While denitrification represents a potential sink for NO_3-*N* in most, if not all, ecosystems, it can represent a significant process in floodplains given the prevalence of water within this ecosystem, especially during the winter months when both the hydrological and NO_3-*N* loading of the system are high. Indeed, much of the work on NO_3-*N* attenuation in floodplains has identified the close proximity of the water table to the upper floodplain soils with high denitrification potentials as a major, if not the major, process determining NO_3-*N* loss, assumed to be through denitrification. Estimates of NO_3-*N* loss from floodplains vary.

Maltby *et al.*, (1996) report denitrification losses in the range of 0.026 - 0.67 $KgNha^{-1}d^{-1}$ for the floodplain of the River Torridge in Devon, UK. Schnabel and Stout (1994) report losses of NO_3-*N* attributed to denitrification of 17 to 110 $KgNha^{-1}$ for poorly drained Pennsylvanian soils. The lower losses are for soils receiving no fertiliser N while the higher losses relate to soils receiving 252 $KgNha^{-1}$. This magnitude of loss is consistent with those reported by other authors, including Peterjohn and Correll (1984) for a wooded riparian strip buffering a cropped field and Hanson *et al.* (1994) . Hanson *et al.* (1994) estimated a range of annual denitrification losses from less than 5$Kgha^{-1}$ yr^{-1} for a moderately well drained control site (downstream of undeveloped land) to almost 40$Kgha^{-1}$ y^{-1} for very poorly drained soils receiving N-inputs in groundwater from an unsewered residential development. A summary of denitrification rates reported in the literature for riparian soils, non-riparian agricultural soils and soils under controlled conditions (denitrification potential rates) are presented in Table 4.3. These are presented as reported by the author, as KgN ha^{-1} d^{-1} and $\mu gN\ g^{-1}\ d^{-1}$. For the required conversions, a uniform bulk density of 1.5 and a microbially active soil depth of 10cm are assumed.

Author	Reported denitrification rate	Denitrification rate in KgN $ha^{-1}d^{-1}$	Denitrification rate in $\mu gN\ g^{-1}d^{-1}$
Floodplain soils:			
Haycock and Burt (1993)	740 mg m^2d^{-1}	7.4	4.93
Schipper *et al.* (1993)	1.12 gN m^2d^{-1} (mean) 0.95 gN m^2d^{-1} (median)	11.2 9.5	7.47 6.33
Hanson *et al.* (1994)	<5 - 40 KgN $ha^{-1}y^{-1}$	0.014 - 0.11	$9.13x10^{-3}$ - 0.073
Schabel and Stout (1994)	17 - 110 KgN $ha^{-1}y^{-1}$	0.047 - 0.301	0.031 - 0.201
Maltby *et al.* (1996)	0.026 - 0.67 KgN $ha^{-1}d^{-1}$	0.026 - 0.67	0.017 - 0.447
Agricultural soils:			
Eggington and Smith (1986)	>2 KgN $ha^{-1}d^{-1}$	>2	>1.333
Garwood *et al.* (1986)	80 KgN $ha^{-1}y^{-1}$	0.219	0.146
Colbourn (1992)	0.8 KgN $ha^{-1}d^{-1}$	0.8	0.533
Barraclough *et al.* (1992)	25 (100KgN $ha^{-1}y^{-1}$ input) 75 (750KgN $ha^{-1}y^{-1}$ input)	0.069 0.205	0.046 0.137
Goulding *et al.* (1993)	>1 KgN $ha^{-1}d^{-1}$	>1	>0.667
DNP:			
Bijay-Singh *et al.* (1988)	3.65+/- 0.37 $\mu g\ g^{-1}h^{-1}$ 4.86+/- 0.53 $\mu g\ g^{-1}h^{-1}$ 1.06+/- 0.16 $\mu g\ g^{-1}h^{-1}$ 1.80+/- 0.32 $\mu g\ g^{-1}h^{-1}$	131.4+/- 13.32 174.9+/- 19.08 38.16+/- 5.76 64.8+/- 11.52	87.6+/- 8.88 116.6+/- 12.72 25.44+/- 3.84 43.2+/- 7.68
Bijay-Singh *et al.* (1989)	1.46+/- 0.05 $\mu g\ g^{-1}h^{-1}$	52.56+/- 1.8	35.04+/- 1.2
Cooper *et al.* (1990)	0.013 -0.044 $\mu g\ g^{-1}h^{-1}$ (mineral soil) 0.0004 -1.35 $\mu g\ g^{-1}h^{-1}$ (organic soil)	0.47 - 1.58 0.014 - 48.6	0.312 - 1.056 $9.6x10^{-3}$ - 32.4
Groffman *et al.* (1991)	17208 gN $ha^{-1}d^{-1}$ 15208 gN $ha^{-1}d^{-1}$	17.21 15.21	11.47 10.14
Addiscot *et al.* (1991)	30 Kg $ha^{-1}d^{-1}$	30	20

Table 4.3 Denitrification rates reported in the literature for riparian soils, non-riparian agricultural soils and denitrification potentials presented as losses per hectare and per gram of soil per day.

4.2.2.2 Gaseous losses through ammonia volatilisation

The origin of ammonia gas (NH_3) in the soil is the NH_4-N ion which, under alkaline conditions, is converted to NH_3 in solution from which it can be released into the atmosphere according to the reversible equation:

$$NH_4^+ + OH^- \leftrightarrow NH_3 + H_2O \qquad 4.3$$

Volatilisation will have no direct influence on the NO_3-N concentration of the soil other than by indirectly reducing NH_4-N available for nitrification.

4.2.2.3 Leaching

Of the various forms of soil N only NO_3-N is leached out of the soil in appreciable amounts by percolating water. The movement of NH_4-N ions is restricted by cation exchange on clay and humus while most soil organic N compounds are of low solubility. NO_3-N ions are not absorbed by soils other than those of the humid tropics (Singh and Kanehiro, 1969) and remain in the soil solution where they are susceptible to leaching. Dissolved NO_3-N which passes below the root zone may percolate through porous rocks into an aquifer, or move laterally to rivers through agricultural drains or through a system of naturally occurring channels and fissures, and it is this NO_3-N which is primarily responsible for the pollution of ground and surface waters and which has led to the considerable interest in the nutrient retention capacity of floodplain buffer zones discussed in *Chapter 2*.

The NO_3-N originates from a number of sources, including the mineralisation of soil organic matter, fertiliser N not taken up during the growing season, human activity and atmospheric, predominantly precipitation, inputs. Indeed, as leaching predominates during the winter in Britain (when precipitation exceeds evaporation) NO_3-N which is at risk from leaching is that left in the soil at the end of the cropping season together with that which is mineralised during the autumn and winter (Addiscott *et al.*, 1991). Consequently, increased leaching from agricultural ecosystems adjacent to floodplains will be most prevalent during the winter months when nutrient leaching processes are at their most prevalent and the hydrological loading of the floodplain is at its greatest (for example, see Haycock and Pinay, 1993). Leaching represents a major pathway by which NO_3-N reaches the

floodplain from adjacent land. The theory behind NO_3-N leaching is considered in greater detail in section 4.4.

4.2.2.3 Erosion

The predominant mechanisms of erosion are wind and water and the magnitude of loss generated by these forces are site specific, depending on plant cover (type and density), topography, soil stability and the intensity of the runoff or wind event. Where mass movement of soil is initiated a significant loss of N may occur, though this may indeed represent a transfer from one part of the ecosystem to another, rather than a loss *per se*. In fluvial environments the significance of erosion will depend upon whether the location experiences net loss or net gain of sediment. Indeed, lowland river floodplains might be considered net receivers of sediment where erosional losses are minimal (Walling et al., 1992; Brunet et al., 1994).

4.2.3 Transfers of N within the N-cycle

4.2.3.1 Mineralisation (ammonification and nitrification)

A second important indirect input of NO_3-N to the soil system is that brought about through mineralization. Mineralisation refers to the processes by which nitrogen held in organic form in litter and soil organic matter is returned to the soil in mineral form by ammonification and nitrification. Nitrification is of particular significance here as it represents the pathway by which NH_4-N is transformed to NO_3-N in the soil.

During ammonification organic nitrogen compounds are hydrolysed to NH_4-N through a reaction catalysed by enzymes present in a wide range of heterotrophic microorganisms under both aerobic and anaerobic conditions. The resulting NH_4-N is then available within the soil for immobilisation within microbial tissue, fixation onto cation exchange sites, leaching through the soil profile (but only in soils with very low cation exchange capacities) or, in the presence of oxygen, nitrification.

Nitrification represents the transformation of NH_4-N first to NO_2-N in a reaction mediated principally by the chemoautotrophic genera Nitrosomonas spp, and then to NO_3-N through the action of Nitrobacter spp. The energy generated by these oxidations is used to fix CO_2, the main C source of autotrophic nitrifiers. Both reactions are dissimilatory and require an aerobic environment in which O_2 serves as the terminal electron acceptor. The nitrification reactions may be represented as follows:

The oxidation of ammonium:

$$2NH_4^+ + 3O_2 \rightarrow 2NO_2^- + 4H^+ + 2H_2O \qquad 4.4$$

The oxidation of nitrite:

$$2NO_2^- + O_2 \rightarrow 2NO_3^- \qquad 4.5$$

Combining equations 4.4 and 4.5:

$$NH_4^+ + 2O_2 \rightarrow 2H^+ + H_2O + NO_3^- \qquad 4.6$$

Autotrophic nitrifiers exhibit a relatively narrow species diversity which means that the nitrification process can be greatly influenced by external environmental factors. Nitrification is inhibited both by high soil moisture contents and drought stress (Whelan, 1993). Conditions favourable for NO_3-N accumulation in soils through nitrification have been associated with bare follow where there is a supply of decomposable soil organic matter, the soil is kept free from vegetation, rainfall is limited such that leaching and denitrification are minimised and the soil is moist or subject to cycles of alternate wetting and drying. During winter conditions where soil water content is likely to be high additions of NO_3-N through nitrification are likely to be small, indeed, in near-saturated and saturated soils nitrification rates have been found to be absent or occurring at very slow rates due to a lack of respiratory O_2 (Sabey, 1969; Linn and Doran, 1984) (see Figure 4.2). Inhibition of nitrification during periods of the year experiencing potentially high denitrification and leaching rates may help conserve N in soils through inhibiting the production of NO_3-N.

4.2.3.2 Plant Uptake

As a major component of amino acids, proteins, nucleic acids and chlorophyll, N plays a crucial role in plant productivity. N is usually taken up through the root system as NH_4-N, NO_3-N or urea-N, and there is also evidence that N_2O and N_2 gas can be directly utilised by plants (Reddy *et al.*, 1989). Vegetative uptake of NO_3-N has often been cited as a mechanism for NO_3-N attenuation in floodplain buffer zones. Groffman *et al.* (1992) suggested plant uptake as the likely dominant groundwater sink for NO_3-N during the growing season in a study of three wooded riparian sites near Kingston, Rhode Island and his suggestions have been supported by other authors (Simmons *et al.*, 1992). Plant uptake has also been implicated as a potential NO_3-N removal mechanism even during the dormant winter season in some floodplain riparian systems. Lowrance (1992) concluded that plant uptake was the only available mechanism to explain observed NO_3-N attenuation during winter at the University of Georgia Coastal Plain Experimentation Station.

4.2.3.3 Immobilisation

Immobilisation describes the conversion of mineral-N, usually as NH_4-N (Vinten and Smith, 1993), to organic-N during the decomposition process when microorganisms cannot satisfy their needs from the organic materials on which they are feeding. A major influence therefore on the occurrence and rate of immobilisation is the C:N ratio where a high ratio (low nitrogen content) usually results in increased immobilisation according to the equation:

$$NH_4^+ \,\&\, NO_3^- \leftrightarrow NH_3 + H_2O \qquad 4.7$$

Groffman *et al.* (1992) report NO_3-N attenuation in near surface soils of a riparian forest in Kinston, Rhode Island, during the dormant winter period and implicate immobilisation as well as denitrification in this removal. However, the effects of immobilisation are not widely reported in literature describing riparian zone processes and consequently there are few data with which to quantify the effects of immobilisation in these systems.

4.2.4 Summary

At any one point in space and time a large number of factors act to determine the fate of the NO_3-N ion in a system which is highly complex. Consequently, the concentration of NO_3-N measured in the field exhibits considerable spatial and temporal heterogeneity. The discussion above presents a

review of these processes and highlights those which dominate in controlling the fate of the NO_3-N ion in floodplain buffer systems. These dominant processes are now identified in terms of a conceptual model which will form the basis of the mathematical model presented later in the Chapter.

4.3 A conceptual model for representing NO_3-N in the floodplain

The location and ecosystem structure of floodplains ensures that almost all processes in the 'conventional' N-cycle can occur in close proximity, either spatially or temporally within the floodplain. This is illustrated, for example, in the seasonal wetting and drying of floodplain soils leading to an enhanced potential for ammonification and nitrification. N processes comprising the floodplain N-cycle remain the same, *per se*, as those of the 'conventional' N-cycle presented above but differ in terms of balance and rates. The differences that exist stem largely from the unique hydrology of the floodplain which results from the following influential seasonal events: (i) fluctuating water table which can interact with the C rich upper soil layers, (ii) inputs of both water and substrate (NO_3-N and C) originating from the hillslope and (ii) episodic flood events, all of which may infer profound effects on floodplain hydrology and N chemistry. In section 4.2, the various pathways by which N enters, leaves and is transferred within a generalised floodplain system are identified and the various pathways are quantified in terms of inputs and losses for a number of site specific studies. This section identifies the dominant pathways controlling NO_3-N within the floodplain ecosystem during the winter, drawing on the discussion above, to provide the basis for building a conceptual model for NO_3-N behaviour in floodplain soil. This is achieved by first considering the dominant floodplain hydrological pathways and then the floodplain N processes.

Floodplain hydrology: During the winter months the mean water table elevation is generally close to the soil surface, in some cases meeting it. Additional inputs of water from hillslopes adjoining the floodplain and from flood events will further influence the floodplain hydrology, generally combining to increase soil moisture content. Where these conditions lead to waterlogging and occur in association with a high oxygen demand conditions suitable for the anaerobic pathways of the N-cycle are likely to prevail.

Floodplain N chemistry: The processes responsible for N inputs to the floodplain system are described in section 4.2. Of these the interaction between hillslope derived N in surface and subsurface runoff and riparian zone soils has been the subject of considerable study. The concentration of N , predominantly as NO_3-N, transported to the riparian zone in hillslope runoff depends upon the nature (agricultural system, soil type etc) of the 'donor' area and varies

considerably (see section 4.2.1.4). The effect that inundation has upon wetland water quality, and indeed the quality of riparian soil water quality, is not well known (Howard-Williams, 1985; Burt and Haycock, 1996). Flood events can either import or export N from the floodplain system and the effect is likely to be spatially and temporally heterogeneous. While a slow moving flood wave is likely to deposit parts of its load (nutrient rich sediment) fast moving floodwater is likely to scour the floodplain surface removing both sediment and associated nutrients. Within any one flood event the relative importance of these two processes is likely to vary temporally and spatially across the floodplain. However, in lowland alluvial systems, deposition is generally expected to dominate (Brunet *et al.*, 1994). Where floodwater carries a dissolved load it is reasonable to expect part of this to enter the floodplain soil with infiltrating water (Maltby *et al.*, 1991). Where the concentration of N in the floodwater is greater than that in the soil this will have a concentrating effect, where it is lower it will result in a dilution, although total mass will increase in both cases.

N enters surface water through point and non-point sources. Point sources include effluent from sewage treatment works, silage liquor and liquid runoff from stored manures. Non-point sources describe the diffuse inputs from agricultural land adjacent to streams and rivers which arrives through surface and subsurface runoff. Within streams and rivers N is further cycled between various forms through an aquatic N-cycle which resembles that of its terrestrial counterpart in all but the size of the various N pools. NO_3-N may be assimilated by algae and macrophytes and released through mineralisation of decaying plant matter followed by the oxidation of NH_4-N to NO_3-N. The N content of flood waters will depend upon the relative importance of the various pathways by which water reaches the channel and results in considerable within- and between-catchment variability. Floods also play a potentially important role in transporting both dissolved nutrients and particulate matter through catchments (Mulholland *et al.*, 1981; Brunet *et al.*, 1994). Mulholland *et al.* (1981) concluded that flood events play a major role in the annual phosphorus flux in Creeping Swamp, a coastal plain stream in North Carolina.

High rates of denitrification have been found in waterlogged riparian systems which are also endowed with a supply of organic carbon (for example, see Simmons *et al.*, 1992, Groffman *et al.*, 1992). The reduction of NO_3-N to NH_4-N (nitrate assimilation) is reported to be of limited significance in riparian soils (Jordan *et al.*, 1993; Haycock and Pinay, 1993). The aerobic process of nitrification is suppressed over the winter months by both the prevailing anaerobic conditions and low temperatures which will ensure that any additions of NO_3-N via this process remain small (Sabey,1969, Linn and Doran,1984). Leaching predominates in winter in temperate regions, occurring when inputs of water exceed losses through evapotranspiration and consequently when the hydrological loading of the floodplain riparian zone is at its greatest (Haycock and Pinay, 1993). Plant uptake, a significant process during the active growing season, is generally thought to have

Plant uptake, a significant process during the active growing season, is generally thought to have little effect on the NO_3-N balance during the dormant winter period although this suggestion has been challenged (Lowrance, 1992). Nitrogen fixation exerts an indirect effect upon the NO_3-N budget through the supply of NH_4-N. The effects of immobilisation on NO_3-N concentrations in riparian zone soils is rarely reported although it is undoubtedly occurring (Groffman *et al.*, 1992).

The discussion presented above suggests that during the winter months in temperate regions the fate of NO_3-N is determined by two predominant processes; infiltration and denitrification (Ross, 1989). Accordingly, these two processes form the basis of the conceptual model proposed to represent NO_3-N in floodplain soils which also includes NO_3-N inputs from floodwater. The conceptual model is illustrated in Figure 4.3.

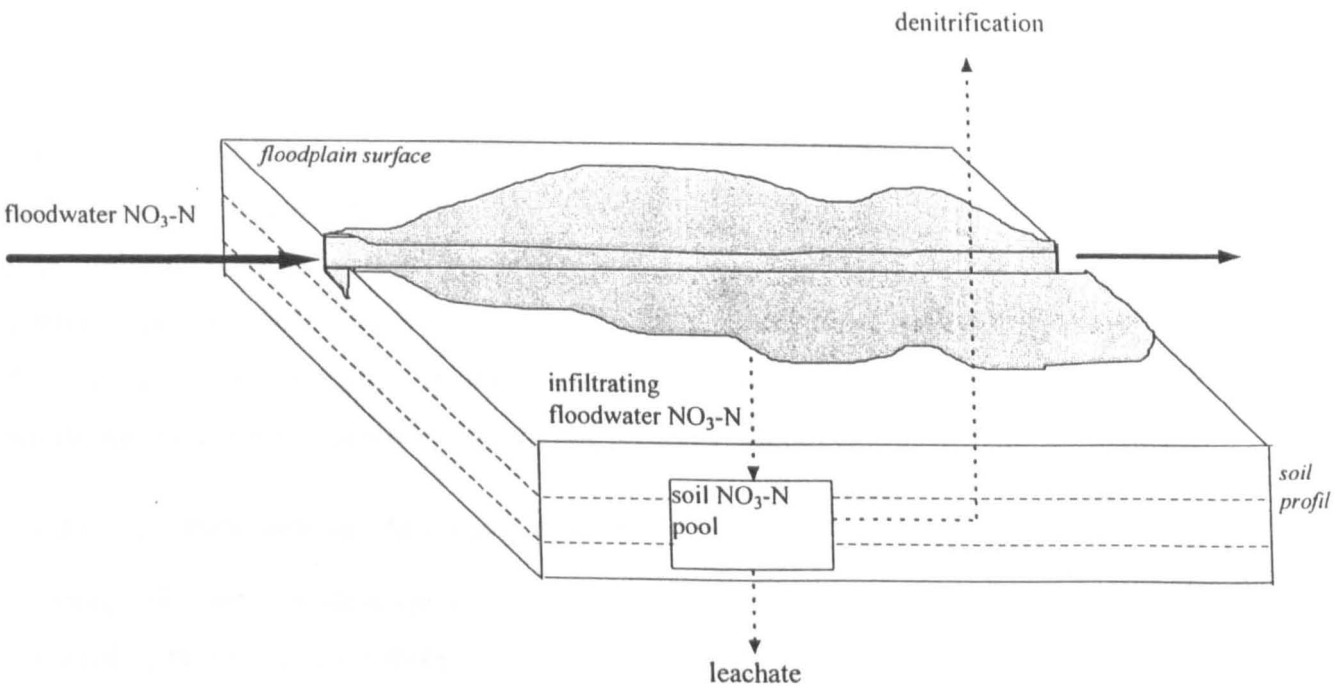

Figure 4.3 Illustration of the conceptual model proposed to represent NO_3-N within the floodplain system.

4.4 Modelling NO_3-N transport and transformations in soil

This section considers the development of the conceptual model presented above into a mathematical model for application to the research. Accordingly, this section begins with a review of the methods available for modelling NO_3-N transport and denitrification in soils and ends with a description of the NO_3-N model and its incorporation within the structure of the existing floodplain hydrology model. A deterministic approach to modelling both NO_3-N transport and denitrification is adopted as this fits in with the deterministic, physically based approach to modelling floodplain flow developed in the previous chapter.

4.4.1 Modelling NO_3-N leaching

Two broad approaches have been applied to the deterministic modelling of solute leaching processes in soils; The first of these, termed mechanistic, incorporates the most fundamental mechanisms of the processes of leaching and solute transport, as presently understood. This means that for a description of leaching the models are based on the physical principles embodied in Darcy's Law for the movement of water in soils and on the equations describing mass flow and diffusion-dispersion for the determination of solute transport. The second approach covers functional models such as those developed by Burns (1974), Corwin *et al.*, (1991) and Burns and Collier (1980) which consist of simplified treatments of water and solute flow which take no account of the fundamental physical mechanisms driving these processes and instead use capacity, or rate, parameters, such as field capacity or wilting point. Deterministic, functional models offer no advantage over mechanistic approaches other than that derived from their relative simplicity. In the present case a mechanistic approach is in place for the description of 1D vertical water flow (in the floodplain hydrology model developed in *Chapter 3*)which can also be applied to the description of NO_3-N transport. Accordingly, the following discussion is limited to a description of the deterministic, mechanistic approach to modelling NO_3-N transport.

4.4.1.1 Deterministic, Mechanistic Models.

In models which are both deterministic and mechanistic solute transport within the soil profile is considered to be the result of three processes; mass flow (convection), diffusion and dispersion. From the (empirical) equations describing these three processes a set of equations has been formulated to describe steady and unsteady state solute flow in soil (Hillel, 1980). These equations form the basis of a considerable literature on solute transport and are derived from the equations of convection, diffusion and mass flow which are developed here according to the discussion presented by Hillel (1980) and Jury *et al.* (1991).

Convection: Convection of soil water (Darcian flow) carries with it a convective flux of solutes which is proportional to their concentration in solution according to the equation:

$$J_c = qc = -c\left(K\frac{dH}{dx}\right) \qquad 4.8$$

where q is equal to $-KdH/dx$ (Darcy's Law, Equation 3.11). q is expressed as a volume of liquid passing through a unit area per unit time, c is a concentration (mass of solute per unit volume of solution) and J_c is therefore expressed as a mass of solute passing through a unit cross-sectional area per unit time. J_c can also be approximated as:

$$J_c = \bar{v}\theta c \qquad 4.9$$

where v denotes the 'apparent velocity' of the soil solution derived from:

$$\bar{v} = \frac{q}{\theta} \qquad 4.10$$

where θ represents the volumetric water content.

Diffusion: Diffusion within the soil solution results from random thermal motion in which the net result of repeated collision and deflection of molecules in the fluid act to equalise concentration

gradients and create a uniform distribution of solute within the soil solution. The rate of diffusion is described by Fick's first law where:

$$J_d = -D_o \frac{dc}{dx} \qquad 4.11$$

where D_0 denotes the diffusion coefficient for solute diffusing in bulk water and *dc/dx* the concentration gradient. This equation can be modified to account for the diffusion occurring in soils where the effective diffusion coefficient is generally less than the diffusion coefficient in bulk water resulting from (i) soil water occupying only a fraction of the total soil volume and (ii) pore tortuosity resulting in greater path lengths for solute diffusion. The diffusion coefficient is replaced by a soil diffusion coefficient, D_s , which is dependant upon both θ and pore tortuosity. The diffusion coefficient is further reduced by factors such as increased fluid viscosity during soil drying and these additional factors are accounted for in the diffusion coefficient D_s , through a single factor, α according to the following equation:

$$D_s = D_o \theta \alpha \qquad 4.12$$

where α accounts for all factors which act to influence the diffusion coefficient such as pore tortuosity and viscosity and $D_o\theta$ accounts for the effect of soil moisture content. Equation 4.11 can now be rewritten as:

$$J_d = -D_s(\theta)\frac{dc}{dx} \qquad 4.13$$

Hydrodynamic dispersion: Hydrodynamic dispersion exhibits the same homogenising effects in solutions exhibiting concentration gradients as diffusion. Motion within the soil solution due to temperature and pressure gradients act to mix the solution reducing concentration gradients. Indeed, hydrodynamic dispersion is analogous to diffusion and is described mathematically in the same way but with a dispersion coefficient, D_h, rather than a diffusion coefficient, D_o. D_h is found to be linearly related to v:

$$D_h = a\bar{v} \qquad 4.14$$

where a is an empirically derived parameter. As the results of both diffusion and dispersion are similar they are often considered to be additive where D_s and D_h are combined to form a single term, the diffusion-dispersion coefficient, D_{sh}, which is therefore a function of both soil water volume, θ and average pore water velocity, v:

$$D_{sh}(\theta,\bar{v}) = D_s(\theta) + D_h(\bar{v}) \qquad 4.15$$

The three mechanisms of solute movement in soil, convection, diffusion and dispersion, represented by equations 4.9, 4.13 and 4.15, can now be combined in a general series of equations to describe solute flux:

$$J = \bar{v}\theta c - \left[D_s(\theta)\frac{dc}{dx} + D_h(\bar{v})\frac{dc}{dx} \right] \qquad 4.16$$

As stated above, diffusion and dispersion cannot be practically separated thus when the diffusion-dispersion coefficient is employed, equation 4.16 becomes:

$$J = \bar{v}\theta c - D_{sh}(\theta, \bar{v})\frac{dc}{dx} \qquad 4.17$$

where J is the total mass of solute transported across a unit cross-section of soil per unit time, D_{sh} is the diffusion-dispersion coefficient (a function of soil moisture content and mean pore water velocity), c is the solute concentration and dc/dx the solution gradient. Equation 4.17 represents steady-state conditions only and for application to more complex dynamic state processes equation 4.17 is combined with the continuity equation:

$$\frac{\partial(c\theta)}{\partial t} = \frac{-\partial J}{\partial x} \qquad 4.18$$

to give:

$$\frac{\partial(c\theta)}{\partial t} = -\frac{\partial(\bar{v}\theta c)}{dx} + \frac{\partial}{\partial x}\left(D_{sh}\frac{\partial c}{\partial x}\right) \qquad 4.19$$

The simplest form of this equation is that for steady-state flow where θ, v and D_{sh} are constant and where the solute neither reacts or adsorbs to the soil solids. In these circumstances, Equation 4.19 becomes:

$$\frac{\partial c}{\partial t} = -\bar{v}\frac{\partial c}{\partial x} + \frac{D_{sh}}{\theta}\frac{\partial^2 c}{\partial x^2} \qquad 4.20$$

This equation is applicable to the transport of inert, non adsorbing solutes such as chloride and bromide ion tracers which do not react chemically with the kinds of ions normally found in soil solution and, being anions, are not attracted to clay or organic matter surfaces (Jury *et al.*, 1991). Where the transport of reacting and, or adsorbing, solutes is described, Equation 4.20 can be modified to include a source/sink term (for examples see Misra *et al.*, 1974a, b; Hillel, 1980; and Jury *et al.*, 1991).

Models employing the CDE are necessarily complex and require considerable parameterisation (Armstrong and Burt, 1993). Indeed, it is often difficult to obtain appropriate values for v, D_s and D_h , but perhaps the greatest problem lies in the values themselves which represent averages applied to soils which may exhibit considerable diversity in, for example, pore water velocity. Indeed, it is becoming increasingly clear that solution of the CDE where the solute concentration, dispersion coefficient and average pore water velocity are averaged over the whole soil may not adequately account for solute transport in all soils (Barraclough, 1989). Indeed, the provision for preferential flow in structured soils is now being incorporated in a number of flow models (Barraclough, 1989; Corwin *et al.*, 1991; Whelan, 1993). Nevertheless, the equation set developed above forms the basis of a considerable number of solute transport models.

4.4.2 Modelling denitrification in soils

Denitrification has been modelled at scales ranging from individual soil aggregates (Arah and Smith, 1989; Arah, 1990) through to the soil profile (Rolston *et al.*, 1984) and on to the field (Whelan, 1993)and ultimately the landscape scale (Groffman and Tiedje, 1991). At the scale of the soil profile, denitrification is generally described using zero-, first-, or second-order kinetic or Michaelis-Menten type models.

The velocity of microbialy mediated reactions is influenced by external environmental factors including temperature, pH, soil moisture and pressure as well as the concentration, or availability, of reactants. Experimentally it has been found that the velocity of a reaction can be simply expressed as a function of the concentration of one or more of its reactants according to the following rate equation:

$$r = k\{\text{reactant(s)}\}^n \qquad 4.21$$

where r denotes the velocity of the reaction, k denotes the rate constant for the reaction and the exponent n denotes the order of the reaction and which, for microbially mediated soil nitrogen reactions, is typically zero or a small integral number, usually 1 or 2.

Zero-Order Reactions: Where the observed reaction rate is unaffected by substrate concentration then the reaction is termed zero-order (n=0). Zero-order kinetics are observed where the substrate is non-limiting or in cases where factors other than substrate concentration, for example a catalyst, determine the reaction rate. Substrate degrades according to the following equation:

$$\frac{dN}{dt} = k \qquad 4.22$$

where N denotes the substrate concentration, t denoted time and k is the rate coefficient.

First-Order reactions: Where the observed reaction rate is found to be linearly proportional to one substrate concentration the reaction is termed first-order and proceeds according to the following reaction:

$$\frac{dN}{dt} = kN \qquad 4.23$$

Second-Order reactions: When the observed rate of a reaction is found to be proportional to the product of the concentrations of two reactants then the reaction is termed second-order and proceeds according to the following equation:

$$\frac{dN}{dt} = kNK \qquad 4.24$$

where K denotes the concentration of the second substrate.

Hyperbolic kinetics (Michaelis-Menten type models): A further equation (relationship) has been developed to describe reaction kinetics which change order during the course of a reaction. Hyperbolic kinetics have been used to describe reactions which at low (limiting) substrate concentrations are 1st order while at higher, non-limiting, concentrations are zero order. When referring to enzymatically mediated reactions the model is described by the Michaelis-Menten equation and has the following form:

$$V_o = \frac{V_{max}[N]}{[N]K_m} \qquad 4.25$$

where N represents the substrate concentration, V_o denotes the reaction velocity, V_{max} represents the maximum reaction velocity, K_m is the substrate concentration at which V_o is equal to 1/2 V_o. V_{max} and K_m define the quantitative relationship between V_o and *[N]* for a simple enzyme catalysed reaction and their values are unique to each reaction under given conditions.

The decay of substrate over time according to zero-order, first-order and Michealis-Menten reaction kinetics are presented graphically in Figure 4.4.

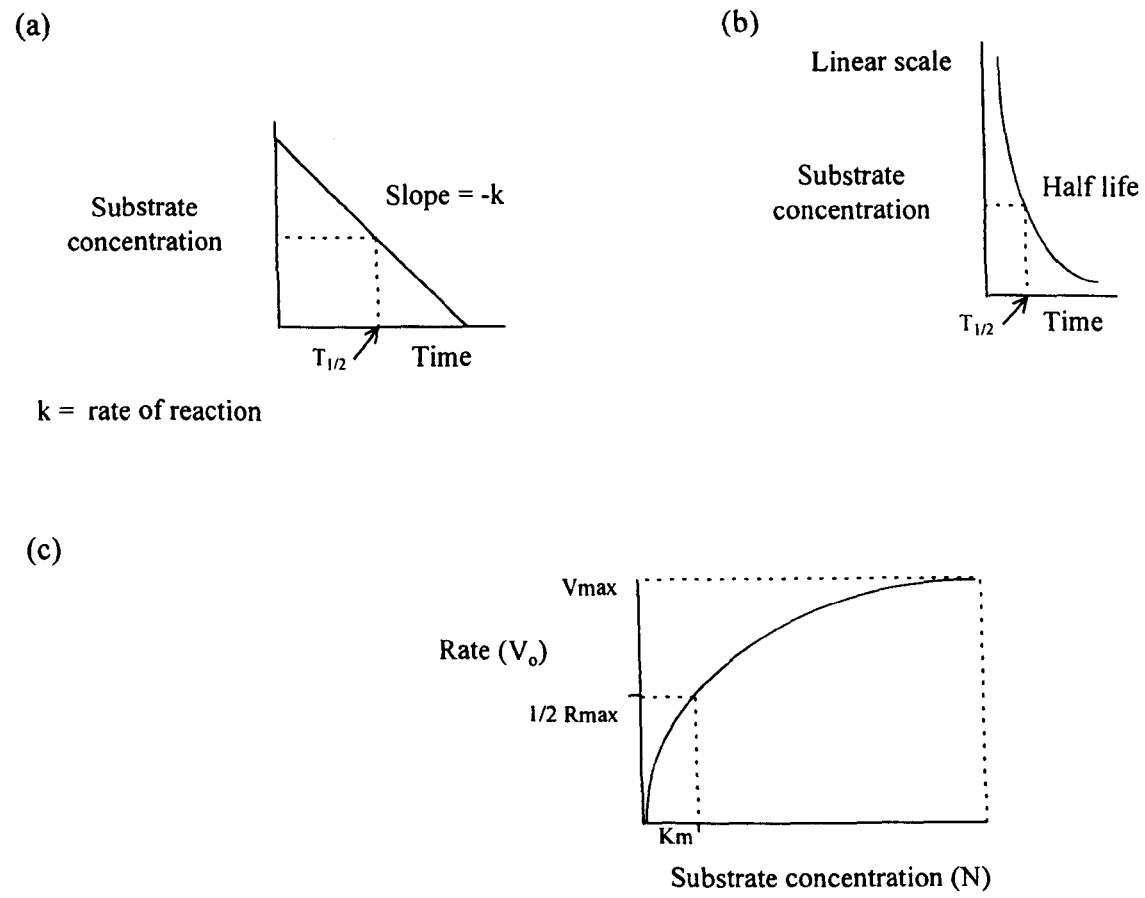

$$V_o = V_{max} = \frac{[N]}{[N]Km}$$

Figure 4.4 Graphical representation of (a) zero (b) first and (c) Michaelis-Menten reaction kinetics.

4.4.3 Development of the *NO_3-N* Model

The conceptual model presented in section 4.3 includes the processes of *NO_3-N* leaching and denitrification and accounts for the input of *NO_3-N* dissolved in floodwater. The processes being considered are both spatially and temporally dynamic over the floodplain and require a high spatial and temporal model resolution to capture this. Models which operate on a daily time step (Whelan, 1993, Jansson *et al.*, 1991)) or adopt the field or small catchment as the base scale unit (Whelan,

1993) cannot adequately represent the rapidly changing and spatially distributed NO_3-N processes associated with the flood wave. The coupled floodplain hydrology model developed in *Chapter 3* provides a high spatial and temporal representation of the floodplain hydrology and in representing infiltration solves the Richards equation for unsaturated flow which is also a requirement of the mechanistic description of solute flow (the CDE). Indeed, as the existing hydrology model provides an appropriate spatial and temporal resolution, solves the Richards equation and provides an existing model structure, the NO_3-N model is developed in association with the 1D infiltration model within the existing structure of the coupled floodplain hydrology model.

4.4.3.1 A model for NO_3-N leaching

The NO_3-N model comprises two parts; a transport component and a denitrification component. The transport component is developed in association with the 1D infiltration model described in Section 3.4.3 and the denitrification component is developed using a kinetic model based on those described in section 4.4.2.

NO_3-N transport: The theory behind modelling solute transport was introduced in section 4.4.1 where it was illustrated that mechanistically, the flux of dissolved solute can be described using two terms: the bulk transport (convection) and the diffusive-dispersive flux of dissolved solute. The convective flux of solute is determined by multiplying a flux of water (as a volume of water passing through a unit area per unit time) by a solute concentration (mass of solute per unit volume of solution) as represented by Equation 4.8. Equation 4.8 employs Darcy's law, which, when combined with the continuity equation, gives in the Richards Equation (Equation 3.13). The Richards equation is solved in the CDE and within the 1D infiltration model to represent water fluxes. The means of calculating water flux (convective flux) is therefore supplied by the existing 1D model which has been previously coupled to the flood hydraulic model (*Chapter 3*). The NO_3-N transport model is therefore developed in association with the coupled floodplain hydrology model.

The model first determines the volumetric flux of water passing between each cell boundary in the soil column (see Figure 3.7) and uses these values to calculate the corresponding NO_3-N flux. In Equation 4.8 this is achieved by multiplying the flux by the concentration of NO_3-N in the source cell. Here the model considers NO_3-N as a mass in each cell, and flux of NO_3-N between cells is calculated by multiplying the fraction of water passing from source to recipient cell by the mass of NO_3-N in the source cell.

The second component of the CDE represents diffusion and dispersion which are often considered together in the diffusive-dispersive coefficient. This term is not accounted for explicitly in the

model but is represented through the assumption of complete solute mixing in each modelled soil cell prior to the next time step. The model further assumes zero anion adsorption.

The model is now illustrated through a description of the processes occurring at each model boundary:

Surface boundary: The model has been developed to respond to precipitation, irrigation and floodwater with associated anion concentrations in units of g/m^3 as inputs across its surface boundary. The mass of anion (M_1 (g)) passing through the surface boundary for each time step is determined as the product of the anion concentration ($C(g/m^3)$) in the supply water multiplied by the volume of that water passing through the surface boundary ($V_1(m^3)$) for each time increment. Thus:

$$M_1 = CV_1 \qquad 4.26$$

Solution of the Richards equation (Equation 3.13) determines the volume of water passing through the surface boundary into cell one for each time step while the concentration of solute in the supply water (precipitation, irrigation and floodwater) is determined prior to the model simulation. The mass of anion entering cell 1 (M_1) calculated according to equation 4.26 is then assumed to mix with any mass already present in this cell (P_1) obtaining equilibrium and a new mass (N_1) according to the following equation:

$$N_1 = M_1 + P_1 \qquad 4.27$$

Internal and bottom model boundaries: Solute is transferred from cell one to cell two in association with the convective water flux between the two cells. Again, solution of the Richards equation will determine the volume of water (V_2) passing between cell one and two but this time the mass (M_2) of anion passing between cells is calculated as:

$$M_2 = \frac{V_2}{V_{cell_1}} N_1 \qquad 4.28$$

where V_{cell1} represents the cell water volume (cm^3) of cell one, the cell from which the anion originates.

Mass M_2 enters cell two and is assumed to attain equilibrium with NO_3-N already present in this cell (P_2) resulting in a new cell mass, N_2, according to the following equation:

$$N_2 = M_2 + P_2 \qquad 4.29$$

The process is repeated until the bottom boundary is met where flux of water is determined according to the gravity flow assumption and the flux of NO_3-N according to the following equation:

$$M_x = \frac{V_x}{V_{cell(x-1)}} N_x \qquad 4.30$$

where M_x represents the flux of NO_3-N leaving the bottom cell, V_x represents the volume of water leaving the bottom cell, $V_{cell(x-1)}$ represents the volume of cell x-1 and N_x is the mass of NO_3-N in cell x.

The sequence of calculations performed by the model means that all water and NO_3-N fluxes between cells are calculated prior to the calculation of the net changes in cell NO_3-N mass. The explicit nature of the infiltration model means that unstable model solutions will result in both water and NO_3-N mass balance errors.

4.4.3.2 A kinetic model for denitrification

Denitrification is assumed to occur in the upper soil layer only (represented by cell 1 in the model, see Figure 3.7) and to obey 1st-order reaction kinetics. Restricting denitrification to the upper soil layer is consistent with the findings of numerous studies that show consistently higher denitrification rates associated with upper soil layer and that these decline rapidly with depth (see section 4.2.2.1).

Denitrificaton has been described as following zero-order (Duffy *et al.*, 1975), 1st-order (Chesheir *et al.*, 1987; Phillips, 1989a, b), 2nd-order kinetics (Rolston *et al.*, 1984) and Michaelis-Menten kinetics (Arah and Smith, 1989; Jansson *et al.*, 1991; Whelan, 1993). It is generally described, however, as following first-order kinetics with respect to NO_3-N for the range of concentrations usually encountered within soils.

An important feature of the model is that the rate coefficient for denitrification is considered as a variable rather than a constant. This is introduced to account for the influence of soil moisture content on the denitrification rate as discussed by Linn and Doran (1985) and illustrated in Figure 4.2. The influence of soil moisture content on denitrification is accounted for through the inclusion of a dimensionless rate function, f_w , in equation 4.23 to give the following representation of denitrification:

$$\frac{dN}{dt} = kf_wN \qquad 4.31$$

where f_w represents the dimensionless water function which is determined according to the following equation:

$$f_w = bk + (1 - bk)^{(-(100-sat)^t)} \qquad 4.32$$

Where *bk* represents the background denitrification rate and *sat* represents the percent soil moisture content of cell 1. By varying the value of *s* in the exponent the shape of the soil moisture function curve can be adjusted to match available data. Figure 4.5 illustrates the curves resulting from values of *s* of 2, 5, 10 and 20.

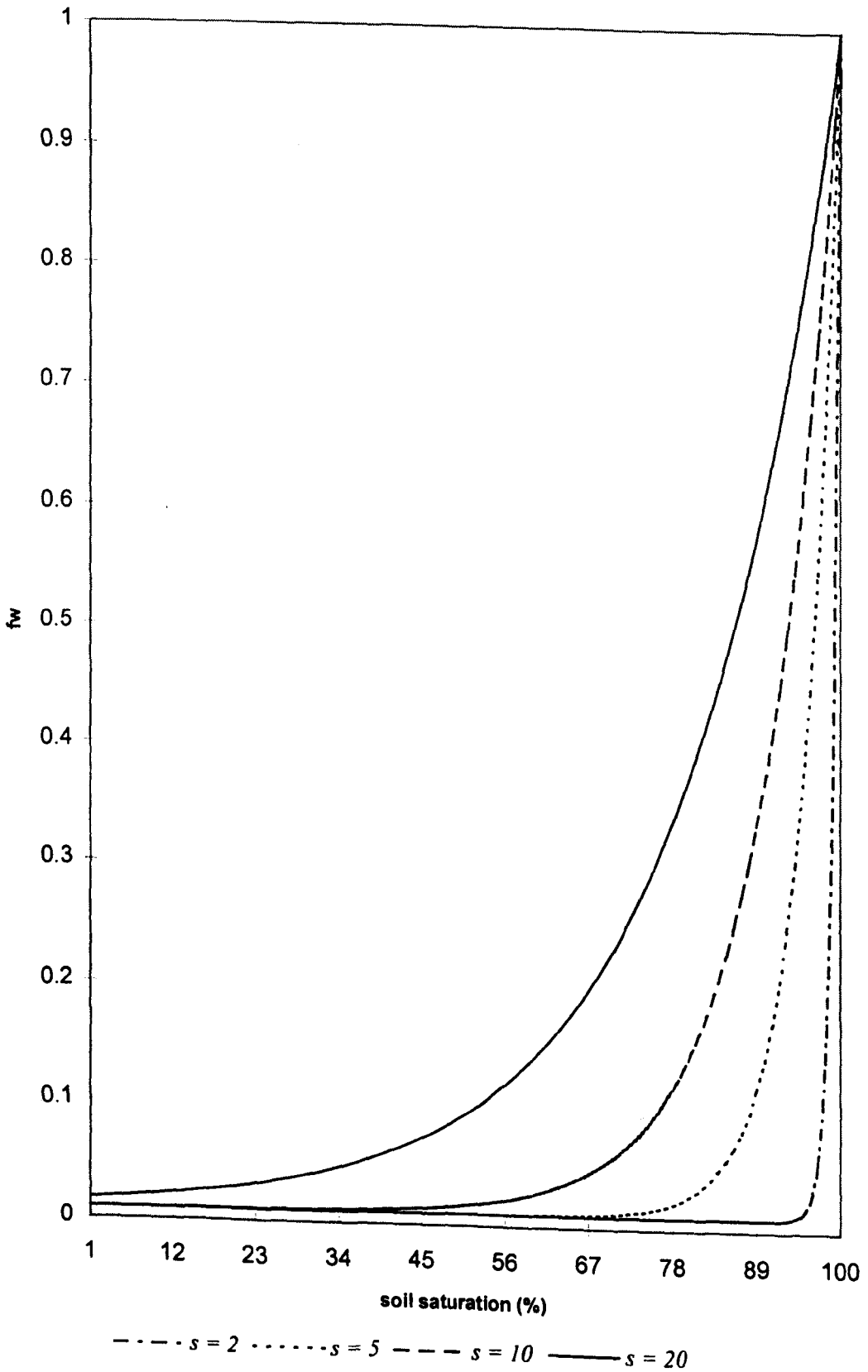

Figure 4.5 Moisture response function used for denitrification in the model with a range of values for *s*.

Of those factors likely to be significant in affecting denitrification rates during floodplain inundation soil moisture fluctuations are considered to be the most important. Floodplain topsoils are generally non-limiting in terms of available carbon; thus, for the purposes of this research carbon availability is not considered in the rate equation. The effect of transient soil temperatures has also been included in denitrification kinetic equations (eg Rolston *et al.*, 1984) but is not included in the current model as temperature is considered to be invariant during the relatively short simulations proposed. However, the model structure allows for the inclusion of diurnal temperature effects if required.

4.4.4 NO_3-N Mass Balance

A NO_3-N mass balance has been introduced into the model to account for inputs, losses and changes in NO_3-N storage according to the following equation:

$$BAL_{NO3} = (N_f - N_i) - (N_{input} - N_{leach} - N_{dn}) \qquad 4.33$$

where N_f represents the final domain NO_3-N mass, N_i represents the initial domain NO_3-N mass, N_{input} represents the total input of NO_3-N during the simulation (through floodwater), N_{leach} represents the total loss of NO_3-N in leachate and N_{dn} represents the total denitrification loss. All parameters in Equation 4.33 are calculated nodally and integrated using the TELEMAC2D subroutine MASVEC to represent domain values[1]. NO_3-N mass balance results are presented following each simulation.

4.5 Model Sensitivity

It is evident from the structure of equation 4.31, the 1st-order kinetic equation chosen to represent denitrification, that the mass of NO_3-N denitrified will depend not only upon the NO_3-N concentration but also upon the value of the rate constant, k_1, and the dimensionless soil water function, f_{wl}. The extent to which the model is sensitive to k_1 is now investigated.

[1] For a full description of the function of this subroutine see section 3.6.2 where it is described with reference to the domain soil moisture mass balance.

Sensitivity is a measure of the effect of change in one factor on another factor (McCuen, 1973). Sensitivity analysis performs an important function by describing quantitatively the dependence of model output upon varying model input. Sensitivity analysis can be employed at various times during model development and can provide an important diagnostic tool during model verification (eg - checking programme operation). Anderson and Howes, (1988) identify three uses to which a sensitivity analysis can be usefully applied during model verification: firstly, to demonstrate that in response to representative variation in model input and parameter values, theoretically realistic behaviour is expected. Secondly, to illustrate that the model is sufficiently sensitive to represent actual variation in the prototype system and finally, to identify those model parameters or inputs to which the model is most sensitive. The results of such an analysis will identify whether or not the model is performing as expected in terms of expected sensitivity to different inputs and will be important in identifying those input parameters to which the model is highly sensitive. The results of such an analysis have far reaching consequences for model parameterisation, data collection, variability in input data and model application.

4.5.1 Sensitivity of the nitrate model to k_1

As a first step in the analysis a representative range of denitrification rate constant values is required against which model sensitivity can be assessed. The list of values presented in Table 4.4 were obtained from a literature search which covered a range of environments.

Author	Denitrification rate constant (k) (hr^{-1}, unless otherwise specified)	Temperature (°C)	Comments
Misra *et al.* (1974a)	0.001 - 0.002	19.5+/10.5°C	Columbia silt loam (2% organic C). The k values were used in a convective transport equation to match observed soil column results. Lower k values were associated with higher O_2 levels.
Misra *et al.* (1974b)	(i) 0.0016 0.015 0.014 0.01 (ii) 0.035 0.04 0.045	(i) 19.5°C 20% O_2 5% O_2 0.5% O_2 0.5% O_2 (ii) 34.5°C 20% O_2 5% O_2 0.5% O_2	Denitrification rate constants determined for a Columbia silt loam under different O2 and temperatures through matching experimental and simulated results.

Table 4.4 Denitrification rate constants for a range of environments derived from a literature search.

Stanford *et al.* (1975a)	0.001-0.04	35°C	Rate constants determined (by experiment) for 30 soils of varying organic-C content.
Stanford *et al.* (1975b)	(i) 0.0015 - 0.1 0.0044 - 0.0153 0.0113 - 0.0375 (ii) 0.0017 - 0.1596* 0.0013 - 0.0906	(i) 15°C 25°C 35°C (ii) range 5 - 45°C	10 soils selected from Stanford *et al.* (1975a) covering a broad range of characteristics (texture, % organic-C, pH) (i) 8 soils incubated anaerobically with added glucose (ii) 2 soils incubated anaerobically with added glucose. (* = Hagerstown silt loam, 1.64% C, glucose assumed to be non-limiting)
Selim and Iskandar (1981)	0.01	not specified	Simulation for Windsor sandy loam. Model developed to simulate nitrogen transformations, sensitivity to k not investigated and the value of this parameter was set low.
Rolston *et al.* (1984)	0.000168 - 0.0006 day^{-1}	23°C	High k values used in simulations of cropped plots reflecting carbon additions and increased O_2 demand from plant roots. Low k assumed for uncropped plots.
Chescheir *et al.* (1987)	range: 0.0157 - 0.0284 mean: 0.0205	not specified	North Carolina. High organic mineral soils. Fitted 1st order decay equations to field NO_3-N data. Variability between and within sites and between sampling dates. k was highest in June and lowest in February.
Kalvarachchi and Parker (1988)	0.002 & 0.006	not specified	Values of 0.002 chosen to be in keeping with values reported in the literature. 0.006 chosen to represent denitrification in a wastewater drainfield, Virginia, USA.
Phillips (1989b)	0.0115	not specified	Chosen to represent denitrification rate in a 1st -order decay equation in a water quality detention-time model.

Table 4.4 (continued)

The denitrification rate constants presented in Table 4.4 cover a range from 2.5×10^{-5} h^{-1} (Rolston *et al.*, 1984) to 0.1596 hr^{-1} (Stanford *et al.*, 1975b). Although this is by no means an exhaustive list it

provides an indication of the range of values associated with this parameter. For the purposes of the sensitivity k_1 will be varied from $1.0x10^{-5}$ and $1.0x10^{-1}$, which approximates the range identified in Table 4.4.

Water and NO_3-N transport are simulated for a clay and a silty loam for which $K_{(sat)}$ and saturated soil moisture conditions were, $5.56x10^{-7}$ and $1.25x10^{-6}$ ms^{-1} and 0.38 and 0.45 cm^3/cm^3 respectively. The derivation of the parameters for these soils is discussed in detail in *Chapter 5*. The total depth of the soil was 60cm which is divided into 3 layers, each of two cells, 10cm in depth. The soil layers were assumed to be identical both physically and hydrologically and to have a uniform initial soil moisture content of 80% saturation. Each simulation was of 100 hours duration with a ponded water condition at the surface boundary and a gravity flow condition at the bottom boundary. In each simulation an initial mass of 10g NO_3-N was specified in the top cell of the model with no further additions of NO_3-N. f_w is maintained at a value of 1.0. The results of the simulations are illustrated in Table 4.5.

The results demonstrate a high degree of model sensitivity to k_1 which is also related to soil type. It is not unexpected that the model exhibits considerable sensitivity to k_1 given the form of the denitrification equation and the assumption of a saturated condition in the top cell (a necessary condition) for these simulations where the loss of nitrate is related to NO_3-N mass alone through the rate constant in Equation 4.31. The model demonstrates an increase sensitivity to k_1 with decreasing saturated hydraulic conductivity. This is illustrated in Table 4.5, columns 3 and 5, by the greater differences between the results for the k_1 values tested in the Clay compared to those in the Silty Loam. This can be explained as a function of residence time, which is greater in the Clay which has the lower saturated hydraulic conductivity. The considerable range of k_1 values found in the literature and the extent of the model sensitivity to this parameter highlights a potential parameterization difficulty which will be considered in the *Chapter 5*.

Denitrification rate constant (k_1)	**Soil**			
	Clay		**Silty loam**	
	Total NO_3-N lost (100hr simulation) (g)	Difference	Total NO_3-N lost (100hr simulation) (g)	Difference
0.1	4.5		3.9	
0.01	0.9	3.6	0.6	3.3
0.001	0.1	0.8	0.06	0.54
0.0001	0.02	0.08	0.006	0.054

Table 4.5 Results illustrating the effect of denitrification rate constant on NO_3-N loss.

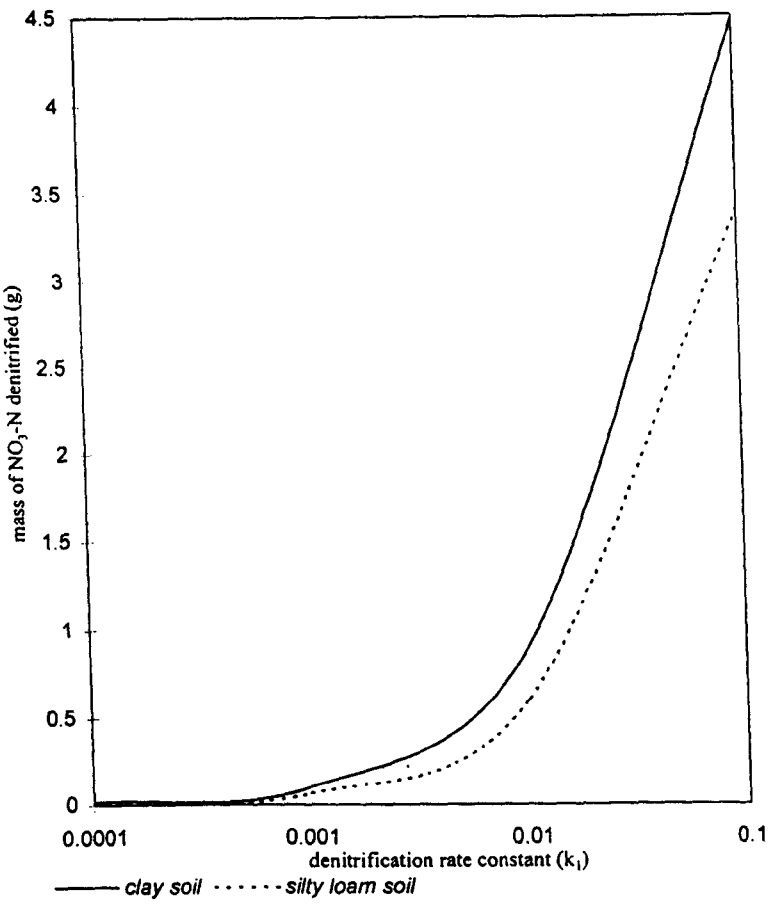

Figure 4.6 Nitrate model sensitivity to the denitrification rate constant, k_1.

4.6 Conclusions

The Chapter details the development of a model for describing *NO_3-N* transport and transformation in a multi-layered soil for application to lowland floodplain soils during temperate climate winters. The model allows for additions of *NO_3-N* across the surface boundary through infiltrating floodwater (and precipitation) and for denitrification which is restricted to the uppermost soil layer. The model derives its convective flux through the solution of the Richards equation while advection-dispersion is accounted for through the assumption of complete mixing of *NO_3-N* within model cells during each time step. Denitrification is described as obeying 1st-order reaction kinetics and explicit account is taken of the relationship between denitrification rate and soil moisture content through a dimensionless soil moisture function.

The model is found to be highly sensitive to the denitrification rate constant, k_1, over a range of values derived from the literature pertaining to both experimental results and values used in models of denitrification.

The deterministic nature of the model allows for a high spatial and temporal resolution in the representation of NO_3-N transport and denitrification. This representation is consistent with the nature of the floodplain environment where changes in soil moisture content, surface boundary conditions and the supply of NO_3-N are also highly variable in space and time. The model structure also allows for the inclusion of additional N-processes at a later stage.

Incorporation of the nitrate model within the structure of the existing floodplain hydrology model allows each floodplain mesh node to maintain a unique distribution of NO_3-N within its associated soil column which is then integrated within a domain NO_3-N balance. As was the case for the representation of floodplain hydrology, the nature of the finite element approach allows for considerable flexibility in the 'density' with which NO_3-N processes can be represented.

Selection and Paramaterisation of a Reach Application

5.1 Introduction and Chapter Objectives

The utility of the coupled floodplain hydrology-nitrate model developed in Chapters 3 and 4 is investigated in Chapters 6 and 7 through the application of the model to a 'quasi-real' test reach. This Chapter describes the development of this application in terms of model parameterisation and set-up.

Accordingly, the Chapter is divided into three main sections, each dealing with a specific aspect of model parameterisation and set-up: The first of these describes the test reach chosen for the application based on an examination of the physical nature of the reach, data availability and inundation history and goes on to consider model parameterisation, set-up and the generation of calibrated control model runs. The second section covers the selection of appropriate soil types for the reach and the corresponding parameterisation of the infiltration model. The third section discusses the parameterisation of the NO_3-N model which relates specifically to the choice of appropriate denitrification rate constants and parameterisation of the dimensionless water function.

The aim of this Chapter is therefore to provide the reach application which will form the test platform (template) for Chapters 6 and 7 along with the parameterisation of both the infiltration and nitrate models.

5.2 Parameterisation data for hydraulic model set-up

5.2.1 Reach selection

Implicit within the selection of a suitable reach is that it meets certain minimum criteria which relate on the one hand to the well specified limits of the model (see *Chapter 3*, section 3.3) and, on the other hand, to the overall suitability of the site to the research objectives which requires, for instance, that the reach has a recorded history of inundation. There are few reaches where all of the necessary requirements, both physical and data, can be met, especially relating to the provision of suitable quality hydrometric data. Given these constraints a reach was chosen which has previously been modelled successfully using the RMA-2 hydraulic code (Bates *et al.*, 1992; Charlton, 1995). The site selected is an 11km reach of the river Culm, Devon, lying between Woodmill and Rewe. The location of the site is given in Figure 5.1 and a description of the site and the availability of data pertaining to the model requirements are now considered in the remainder of this section.

Site description: The River Culm forms an eastern (left bank) tributary of the River Exe whose confluence is approximately 3km north of Exeter. The river originates in the Blackdown Hills on the Somerset-Dorset boarder and drains a catchment of approximately 276km^2. The river has a total length of 55km which in its lower reaches meanders through a well developed floodplain averaging 450m in width. Channel flow is contained within a gravel bed channel approximately 12m wide with banks of approximately 1m high composed largely of fine alluvial material. Bankfull discharge at Woodmill is approximately 26m^{3}s^{-1}. Channel topography has been modified at two locations along the reach through the construction of mill races at Silverton and Hele. The floodplain itself has also been modified a number of features including a railway embankment, a motorway embankment, a number of smaller roads and bridges and a number of buildings. These features on the floodplain will serve to complicate the flood characteristics observed. During the winter months the reach is subject to frequent overbank flows with extensive winter flooding occurring on average 6 times annually where typical inundation depth measured at the middle reaches varies from 40cm for the mean annual flood to 70 cm for the fifty year flood. A gauging station was established at Woodmill in 1962 by the then Devon River Authority while at Rewe a recorder maintained by Exeter University provides stage data.

5.2.2 Hydraulic model data requirements and data availability for the Culm site

The parameterisation requirements of TELEMAC2D were outlined in *Chapter 3*. In summary, the hydraulic model requires an observed input hydrograph for the upstream boundary (m^{3}s^{-1}) and observed stage at the downstream reach (m). The minimum requirement for model calibration a is an observed downstream hydrograph. The model also requires a description of floodplain

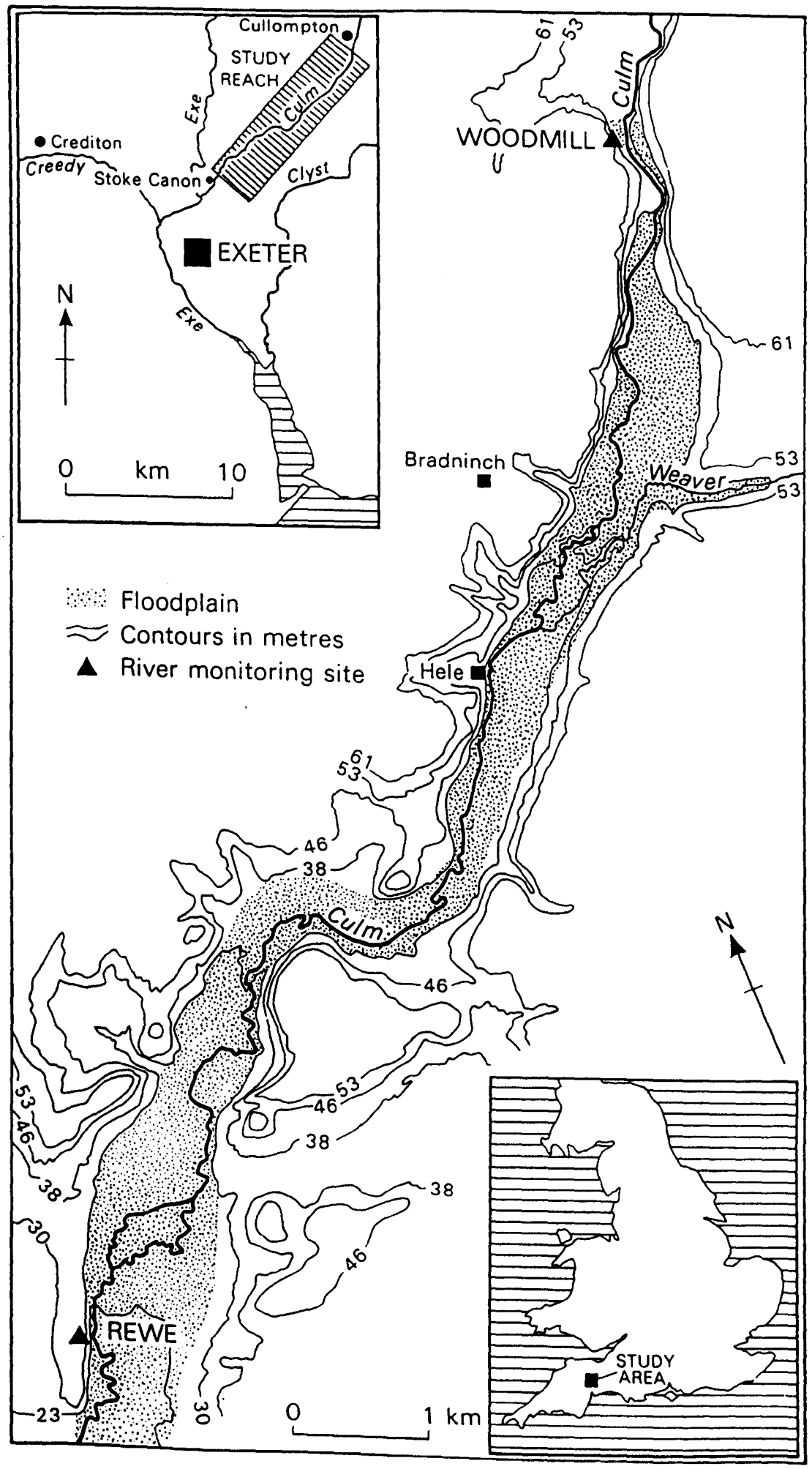

Figure 5.1 Location of the River Culm reach.

topography, boundary delineation and surface friction data. The availability and provision of these data for the Culm site are now reviewed:

5.2.2.1 Hydrometric data

The Culm site is well provided for in terms of hydrometric data. The gauging stations at Woodmill and Rewe record stage data at 0.25 hourly intervals with a record extending back many years. A full compound channel rating curve is available for both sites, an essential requirement as out of bank flows are to be measured, according to the following general equation:

$$Q = A + B(h)^c \qquad 5.1$$

where Q represents discharge, h is water depth and A, B and c are empirical coefficients.

A full compound channel rating curve has been established by the NRA for the entire cross-section at Woodmill, providing data for both in-channel and out-of-bank flow, and which have been described by Bates *et al.* (1992) to be reasonable accurate. The gauging station at Rewe provides stage data only thus for model calibration purposes an out-of-bank stage-discharge rating curve was developed for this site by Bates *et al.* (1992) using the slope-area method in which flows were estimated using detailed topographic survey data and the Manning formulae (Equation 5.2). The resulting curve, illustrated in Figure 5.2, is approximated to three segments corresponding to in-channel, bankfull, and out-of-bank flow conditions. However, this curve is likely to represent only an approximation of the stage-discharge relationship at Rewe due to procedural errors responsible for inaccuracies in the relationship in the order of +/- 20% (Bates *et al.*; 1992; Martin and Myers, 1991), or even greater (Walling, *pers comm*). Indeed, establishing stage-discharge relationships is inherently problematic. Herschy (1978) illustrated that the accuracy of the stage-discharge relationship for within bank flow is at best +/- 10% and this error is likely to increase once out of bank flows are encountered through errors in the cross-section dimensions, more variable cross-section flow velocities and energy dissipation at the interface between bank and floodplain flow. Where out of bank flows are measured across a known and stable cross-section (eg Woodmill) these errors can be minimised, but where the cross-section is less well defined or unstable over time, and the rating curve is developed using the slope-area method, there is considerable potential for error in

the derivation of the stage-discharge relationship. The possible errors associated with the stage-discharge relationship at Rewe are discussed in later sections.

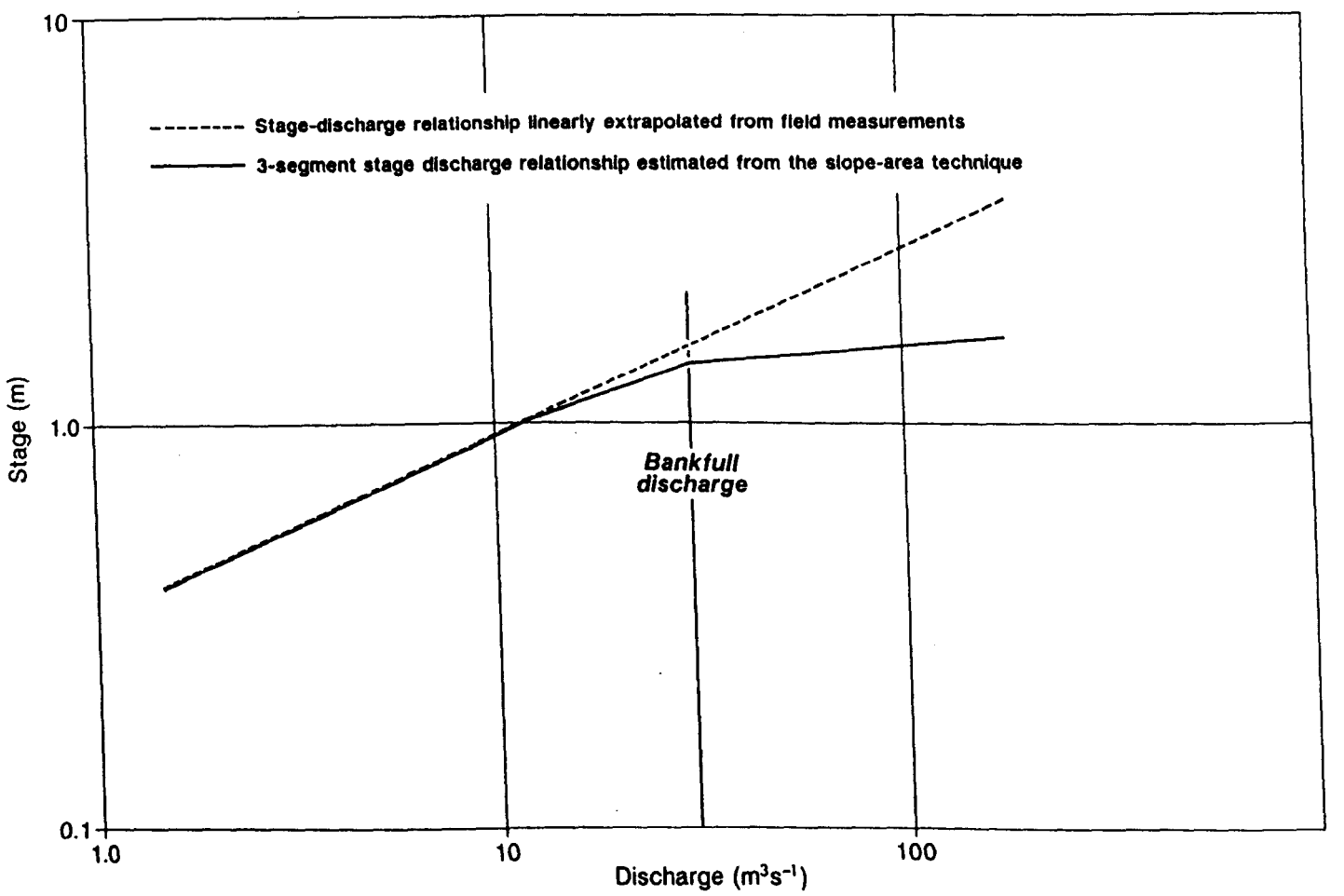

Figure 5.2 The three-stage rating curve derived for the Rewe gauging station on the River Culm (after Bates *et al.*, 1992).

5.2.2.2 Floodplain topographic data

Topographic data for the study site were provided by Bates *et al.* (1992) using 1:2500 and 1:25000 scale OS maps, cross-sections and bench marks. The OS 1:2500 maps provided the boundary delineation and channel morphology data while the OS 1:25000 scale maps provided contour data. Cross-sections were measured at the upstream and downstream extremities of the reach and at four intermediate locations along the reach where data were considered to be sparse. Eleven bench marks were used to fix channel bed, providing a fix on the channel long profile, and floodplain elevation. The topographic representation of the reach is relatively simple with the floodplain considered to be essentially planar, yet it has been of sufficient detail to accurately simulate flood events (Bates *et al.*, 1992; Charlton, 1995).

5.2.2.3 Floodplain friction data

The relationship between flow velocity and the roughness and hydraulic geometry of the flow surface can be summarised by the Manning Formula:

$$V = \frac{1.49}{n} R^{2/3} S^{1/2} \qquad 5.2$$

where V is the mean velocity (in fps), R is the hydraulic radius (in ft), S is the slope energy line, and n is the coefficient of roughness (Manning's n).

TELEMAC2D requires a value of friction to be associated with each node in the computational domain specified as a value of Manning's n, Chezy or Strickler (where the Strickler coefficient is 1/n). In choosing values of friction the greatest difficulty lies in selecting the appropriate values for the flow problem. Indeed, there is no exact method of selecting friction coefficients. In effect, the choice of a friction coefficient relies on an estimate of the resistance to flow for a given condition and this will be highly variable, depending on a number of sometimes interdependent factors which includes the following, discussed with reference to Manning's 'n': (i) surface roughness represented by the size and shape of the grains of material forming the wetted perimeter (generally, fine grains result in a relatively low value of n and course grains in a high value of n), (ii) vegetation, which may also be regarded as a form of surface roughens and which reduces the capacity of the channel

and retards flow, (iii) channel irregularity which comprises irregularities in wetted perimeter and variations in cross section, size and shape along the channel length, (iv) fluctuations in stage and discharge where the friction coefficient in most streams decreases with increases in stage and discharge. However, when flow leaves the channel that part of the flow on the floodplain experiences an increase in friction compared to the channel which is dependant upon the floodplain vegetation or surface condition. Channel and floodplain friction is also subject to seasonal variation according to aquatic and terrestrial plant growth cycles.

An understanding of the basic relationships between roughness and those factors associated with the flow problem under consideration provides the first step in selecting an appropriate value of n. The second stage in selecting appropriate roughness coefficients normally involves use of a table of roughness values, such as that presented by Chow (1959), a selection of which relating to the floodplain environment are illustrated in Table 5.1. Selection of friction values in this way provides the starting point for model parameterisation from which adjustments can be made.

The selection of friction coefficients for the TELEMAC2D simulations developed here derives from the selection of Manning's n values for the RMA-2 1 in 1 year simulation (Bates *et al.*, 1992) discussed earlier for which ten roughness classes were identified based on an assessment of floodplain vegetation types from photographic images. RMA-2 allows a roughness coefficients to be associated with each model element providing a highly spatially distributed friction surface. When the mesh was converted for use with TELEMAC2D the friction representation was simplified to include only two roughness classes, one for the channel nodes and one for the floodplain nodes. These coefficients were chosen from the ten roughness classes specified for the RMA-2 model. Calibration of TELEMAC2D for the two events was then achieved by varying these roughness coefficients and the final values chosen are presented in Table 5.2.

The Culm reach between the gauging stations at Woodmill and Rewe is adequately represented in terms of the data requirements of TELEMAC2D, providing a high quality hydrometric data set, topographic and surface friction data and well defined floodplain boundary delineation. These data are now incorporated within the model set-up which is discussed in the following section.

5.3 Hydraulic model set-up for the Culm reach

The procedure for hydraulic model set-up is discussed in *Chapter 3* (section 3.3) and summarised in Figure 3.4, beginning with digitising the floodplain boundaries and topography and finishing with the hydraulic simulation. This section is concerned with setting-up the model for the Culm reach to

Type of Channel and description	Minimum	Normal	Maximum
Floodplains			
Pasture, no brush			
(i)Short grass	0.025	0.030	0.035
(ii)High grass	0.030	0.035	0.050
Cultivated areas			
(i) No crop	0.020	0.030	0.040
(ii) Mature row crops	0.025	0.035	0.045
(iii) Mature field crops	0.030	0.040	0.050
Brush			
(i) Scattered brush, heavy weeds	0.035	0.050	0.070
(ii) Light brush and trees, in winter	0.035	0.050	0.060
(iii) Light brush and trees, in summer	0.040	0.060	0.080
(iv) Medium to dense brush, in winter	0.045	0.070	0.110
(v) Medium to dense brush , in summer	0.070	0.10	0.160
Trees			
(i) Dense willows, summer straight	0.110	0.150	0.20
(ii) Cleared land with tree stumps, no sprouts	0.030	0.040	0.050
(iii) Same as above, but with heavy growth of sprouts	0.050	0.060	0.080
(iv) Heavy stand of timber, a few down trees, little undergrowth, flood stage below branches	0.080	0.10	0.120
(v) Same as above, but with flood stage reaching branches	0.10	0.120	0.160

Table 5.1 Values of the Roughness Coefficient n for floodplain environments (from Chow, 1959).

provide the calibrated control runs for Chapters 6 and 7. This begins with the selection of suitable flood events from the NRA data set, discusses the provision of a mesh for the reach and concludes with a discussion of the calibrated control model runs.

5.3.1 Choice of flood events

Two flood events of widely differing hydraulic characteristics (recurrence frequency) are chosen to allow the model to be tested over a range of hydraulic conditions. Two flood events have been chosen from the NRA data base; a 1 in 1 year event occurring on 30/01/90 with a maximum discharge of 65.8 m^3s^{-1} and a total volumetric input of 2205579.8 m^3 (both measurements relate to Woodmill) and a 1 in 5 year event beginning on the 26/01/84 with a maximum discharge of 108.78 m^3s^{-1} and a total discharge of 5763319 m^3 (again, both measurements were taken at the Woodmill gauging station) The flood frequency relationship is based on data from the NRA relating maximum discharge to return period.

Data from the Woodmill and Rewe gauging stations, which are recorded at 0.25 hour intervals, were interpolated to provide data at 2 second intervals suitable for TELEMAC2D simulations. Two files

are created for each TELEMAC2D simulation; the first comprises the input flow data (m^3s^{-1}) from Woodmill and the second the stage data (m) from Rewe. A third file is created containing discharge data for Rewe for calibration purposes generated using the rating curve illustrated in Figure 5.2.

5.3.2 Mesh generation

The mesh used in the Culm simulations originates from an application using the RMA-2 model (Bates *et al.*, 1992; Charlton, 1995). The mesh has subsequently been successfully modified for use with TELEMAC2D (Bates *et al.*, 1994; Bates *et al.*, 1996, Price *et al.*, 1997)). The original mesh generation procedure, a description of which can be found in Bates *et al.* (1992), adopted the following broad criteria. The mesh was configured as a continuum of triangular and quadrilateral elements designed to minimise sharp changes of slope within elements and potentially unstable situations where large volumes of water flow into small elements. Maximum element size was limited to 150 by 150m, with an average element size substantially less than this. This represents an increase in spatial resolution over previous applications (eg Gee *et al.*, 1990) but also represents a trade-off between the need to model the complex nature of the Culm floodplain topography and the need to maintain acceptable computing requirements. In addition to these more general requirements, four additional properties were included in the mesh design. Firstly, the triangular channel formulation adopted by Gee *et al.* (1990) which was found to over predict the velocity vectors was replaced by a trapezoid channel representation. Secondly, the requirement for more detailed modelling of bankside roughness was met by defining a strip of elements running along either side of the channel. Thirdly, the mesh was designed such that its longitudinal lines tended to run parallel to the channel ensuring a smooth advance and recession of floodwater. Finally, lateral lines were set-up to cross the reach in a straight line perpendicular to the long axis in order to minimise the front width used in the calculations which had the effect of increasing solution efficiency. The mesh includes a number of more complex floodplain features, including a mill race at Silverton and Hele, a railway embankment and a 1km long bifurcation at the downstream end of the reach.

Steady state flow test simulations performed by Bates *et al.* (1992) identified a number of problems with the initial mesh. The simulations were found to be unstable and to show poor continuity and convergence in areas where large volumes of water were flowing into small elements, areas of steep lateral or longitudinal slope, sharp changes in the direction of flow and in the region of the four complex floodplain structures (as above). The instability was identified as being associated with excess topographic representation in these areas which was modified accordingly and resulted in a series of further guidelines for future mesh generation. These included an upper limit of 110° for channel meanders, a maximum longitudinal channel drop of 2m/km, lateral changes in elevation of

less than 3m between adjacent nodes and floodplain topographic representation relating to overall form rather than microscale structures of the size 1 - 10m.

The mesh has successfully been applied to a 1 in 1 year, a 1 in 5 year and a 1 in 12 year flood event using the RMA-2 model (eg Bates *et al.*, 1995; Charlton, 1995) where a close correspondence has been found between the observed and simulated downstream hydrographs. Results of the simulations with RMA-2 illustrate (i) good correspondence between observed and simulated hydrograph peak timing and (ii) the spatial and temporal dynamics of flood inundation at a high level of resolution.

The initial impetus behind applying the original Culm mesh developed for RMA-2 to TELEMAC2D was for a comparison between the behaviour of the two models (Bates *et al.*, 1995). The RMA-2 mesh based on a mixture of triangular and quadrilateral elements is not suitable for TELEMAC2D which requires meshes comprising a single elemental geometry which may be linear triangular or bi-linear quadrilateral with three or four nodes respectively. The mesh was developed for use with TELEMAC2D through the use of a simple procedure in which all quadrilateral elements were split into triangles. This method has been used to generate a mesh for the 11km Culm reach which has been successfully applied to a number of storm events using TELEMAC2D (Bates *et al.*, 1995; Bates *et al.*, 1996; Price *et al.*, 1997). The resulting mesh comprises 1130 nodes and 2019 elements. The advantage of using this mesh for the research in this thesis is that it has been fully validated through application to a number of flood simulations. It is of relatively low spatial resolution and incorporates a relatively low level of topographic representation yet it provides an ideal test reach for the research having been previously applied and of low computational requirement. The mesh is illustrated in Figure 5.3.

5.3.3 A strategy for obtaining calibrated model runs

Calibrated model runs for the 1 in 1 and 1 in 5 year events are required to provide the control hydraulic simulations for Chapters 6 and 7. There are a number of criterion for assessing the 'goodness-of-fit' or calibration of simulated hydrographs when compared with observed data ranging from subjective, visual methods to objective techniques using statistical functions[1]. The criteria adopted here is essentially a subjective matching of the timing of the simulated and observed hydrograph output. This procedure is widely used for model calibration (Gee et al, 1990; Charlton, 1995; Bates et al, 1996; Hervouet and Van Haren, 1996) as timing of the peak discharge, which is assumed to occur with the peak stage, often represents the most reliable identifiable feature of the hydrograph. Matching peak timing also benefits from being a relatively simple technique,

[1] See Green and Stephenson (1986) for a discussion of a range of criteria for assessing the 'goodness-of-fit' between observed and predicted hydrographs.

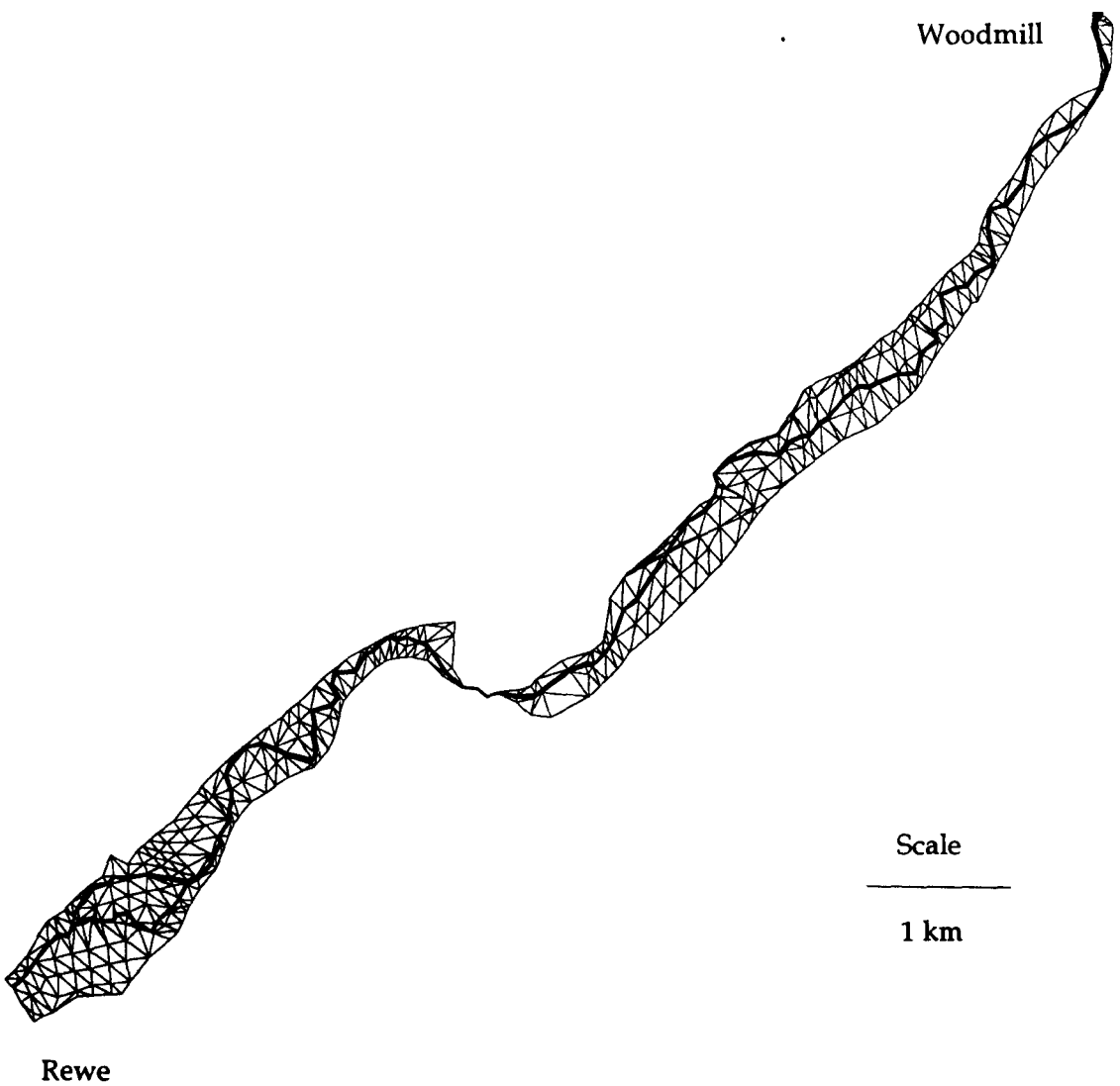

Figure 5.3 The 11km Culm 2D finite element mesh developed for TELEMAC2D.

avoiding the complexity of a statistical method such as best fit, and presents a well defined criteria against which to calibrate the model.

Calibration is a two-stage process. During the first stage the model is run to obtain an initial condition from which the dynamic simulation, stage two, is run. Stage two involves running the dynamic simulation and optimising the phase of the predicted output hydrograph until it matches that of the observed output hydrograph. Model calibration is now considered for the two flood events.

5.3.3.1 The starting condition (initial condition)

A number of methods are available for creating the starting conditions for this class of problem. The most common, the steady-state method, fixes both the upstream (input) and downstream (output) boundaries to their respective flow and stage values for the beginning of the ensuing dynamic simulation. The simulation is run until a steady-state condition is achieved where the simulated downstream discharge corresponds to the imposed upstream input. This method represents the one most commonly used but suffers from a potential problem where non-physical conditions are imposed at the downstream boundary during the initial phase of the dynamic simulation. This condition remains until the input hydrograph has travelled the length of the reach and the output discharge once again matches the imposed stage. The steady-state initial condition is appropriate where stable lead-in flow and stage data are available and can be used to generate the initial conditions, or where lead-in data are not available.

A second method, which can be termed 'dynamic', employs the actual flood data (discharge and stage) to generate the initial conditions. Here the upstream and downstream boundaries are varied according to the observed hydrograph data. This method ensures that the upstream and downstream boundary conditions are temporally consistent and avoids the potential problem of specifying non-physical conditions at the downstream boundary.

The steady-state method was employed to generate the initial conditions for the 1 in 1 year simulation while the complex nature of the 1 in 5 year flood hydrograph, which includes a smaller event (1 in 1 year) immediately prior to the 1 in 5 year event, necessitated the use of a dynamic initial condition for this case.

5.3.3.2 Calibrated flood events

Previous work with RMA-2 and TELEMAC2D has demonstrated the importance of floodplain friction is a major determinant in flood flow characteristics. Increasing the value of friction slows the flood wave, retards the hydrograph peak and decreases the peak discharge while decreasing the

friction coefficient has the converse effect. This parameter is used extensively for model calibration and is used here to obtain the best possible correspondence between the timing of the predicted and observed peak outflow discharges.

For each node on the reach a value of friction is specified according to whether the node is located on the floodplain, the channel or the 'reservoir' located at the end of the reach and calibration is achieved through varying the friction values for each of these areas. The friction values associated with each area used to obtain the calibrated runs are presented in Table 5.2, the calibrated model runs are illustrated in Figures 5.4 and 5.5 and statistics relating to these are presented in Table 5.3. The statistics give information on the difference in peak timing between predicted and observed hydrographs, the difference in the magnitude of peak discharge between simulated and observed and the difference in total flood volume between simulated and observed for the two simulations. Figure 5.6 illustrates the modelled inundation extent for the two events plotted at three hourly intervals throughout the two simulations.

Flood event	Floodplain friction (Strickler coefficient with Manning's n in brackets)	Channel friction (Strickler coefficient with Manning's n in brackets)	'Reservoir' friction (Strickler coefficient with Manning's n in brackets)
1 in 1 year event	12 (0.083)	40 (0.025)	60 (0.0166)
1 in 5 year event	12 (0.083)	40 (0.025)	60 (0.0166)

Table 5.2 Strickler coefficients used to obtain the calibrated Culm 1 in 1 and 1 in 5 year flood simulations.

Event	Simulation	Total discharge volume (m^3)	% difference	Peak discharge (m^3s^{-1})	% difference	Time to peak discharge (s)	% difference
Culm 1 in 1 year		1875571.0		70.28		46778.0	
Culm 1 in 5 year		5039942.6		67.48		59398.0	
	Control1	1857139.9	-0.98	62.97	-10.4	47238.0	+0.98
	Control2	7202713.5	+42.91	107.57	+59.4	63718.0	+7.27

Table 5.3 Calibration statistics for the calibrated Culm 1 in 1 and 1 in 5 year flood simulations.

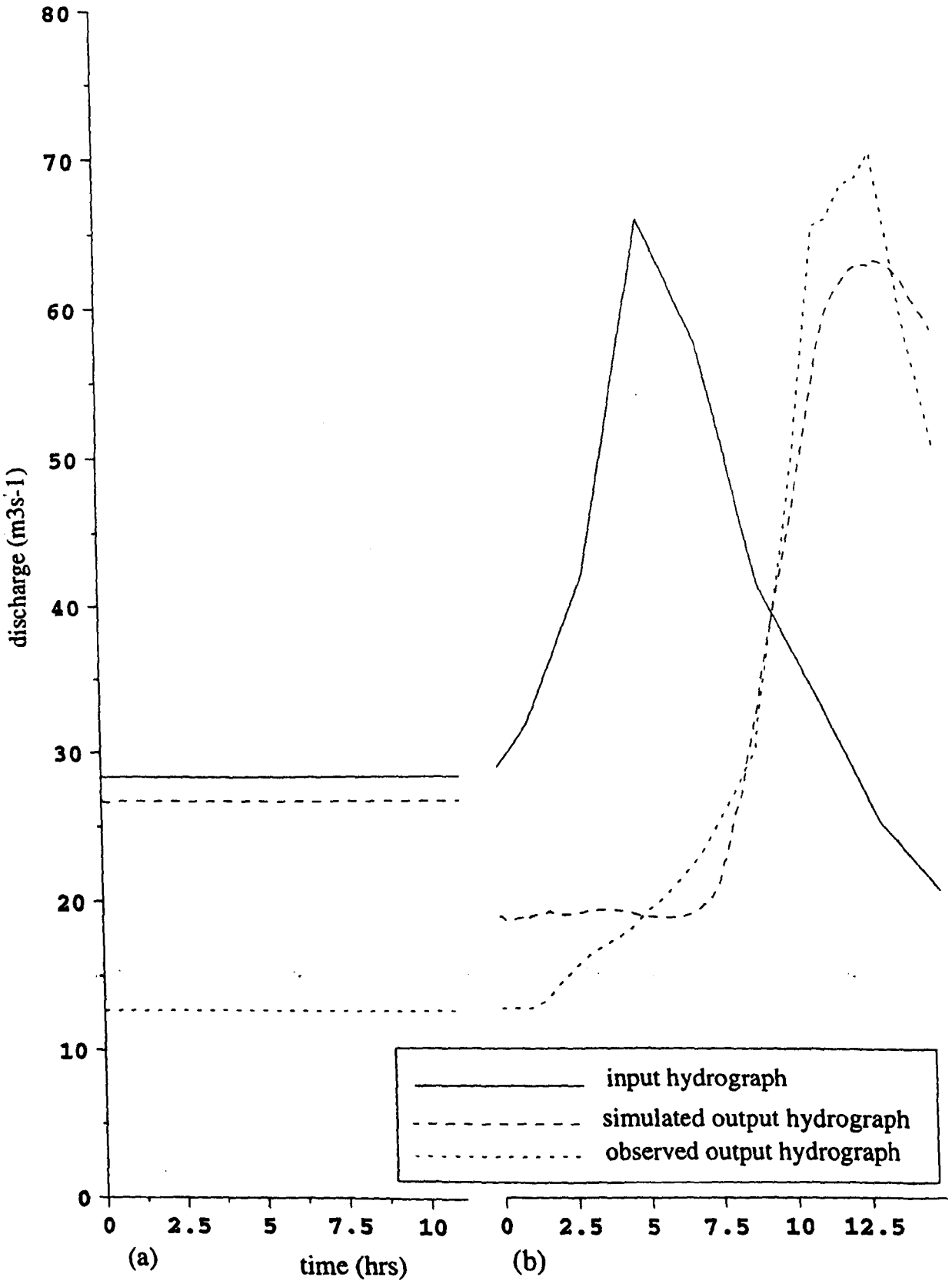

Figure 5.4 The calibrated 1 in 1 year Culm flood simulation (a) starting condition (b) dynamic 1 in 1 year flood simulation.

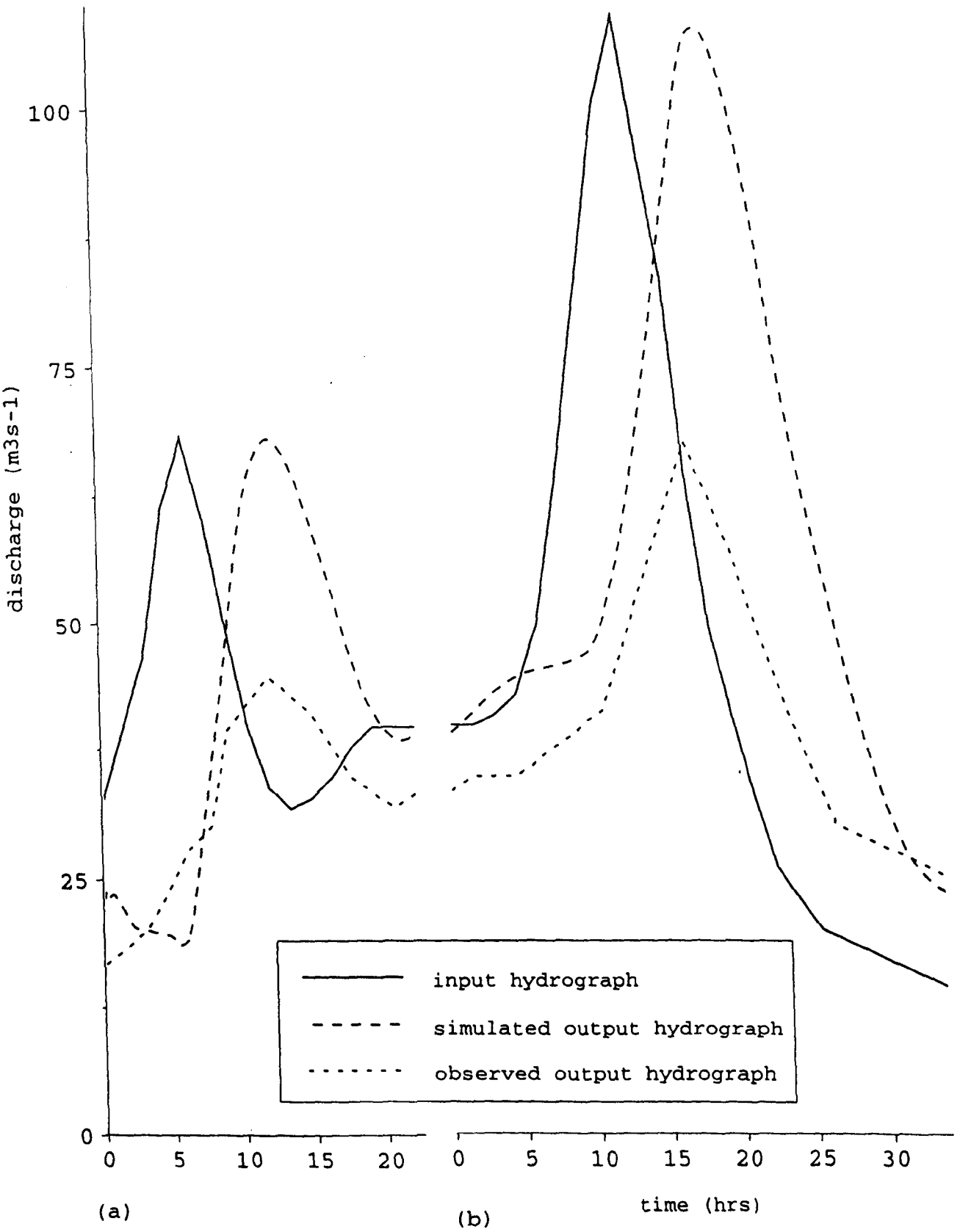

Figure 5.5 The calibrated 1 in 5 year Culm flood simulation (a) starting condition (b) dynamic 1 in 5 year flood simulation.

(a)

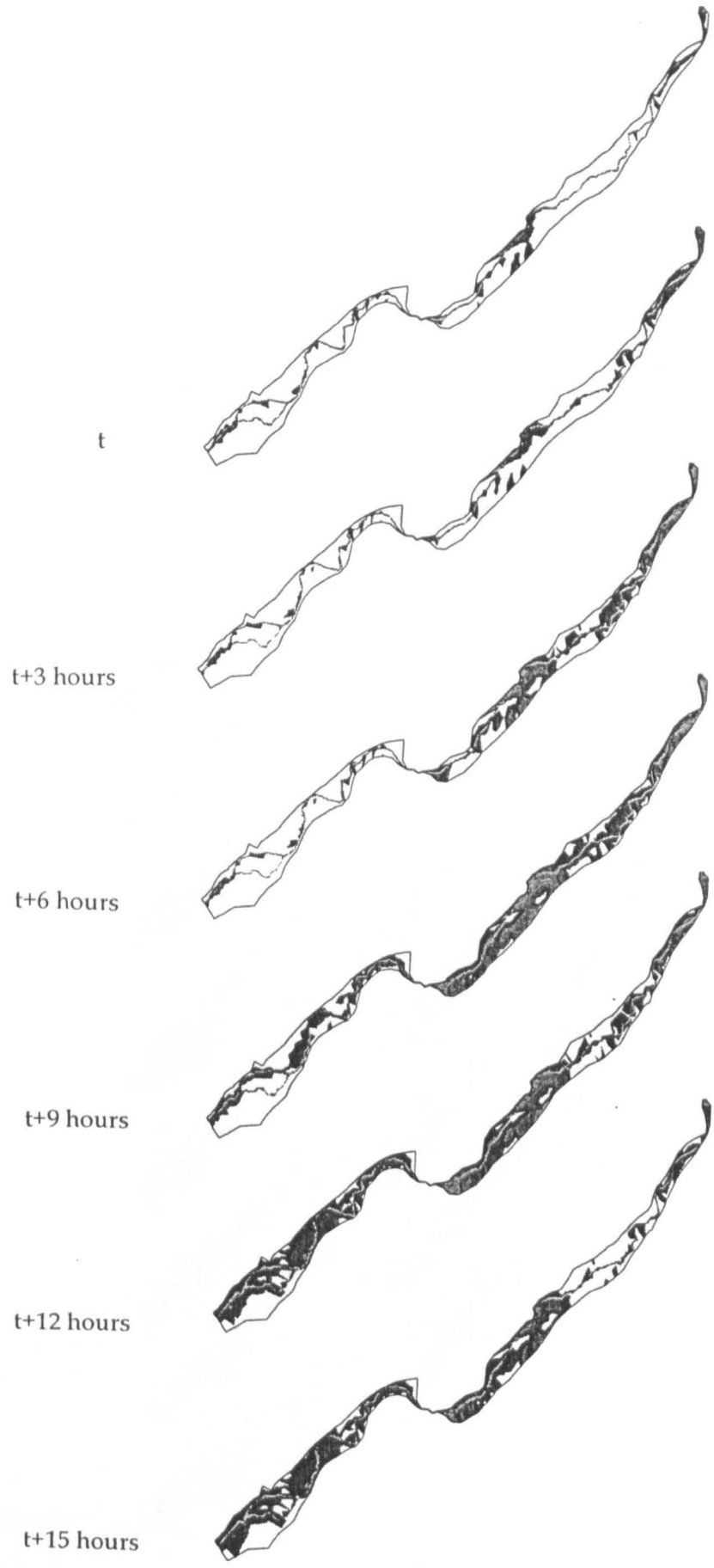

Figure 5.6 Modelled inundation extent at 3 hourly intervals throughout the (a) Culm 1 in 1 and (b) 1 in 5 year simulations.

(b)

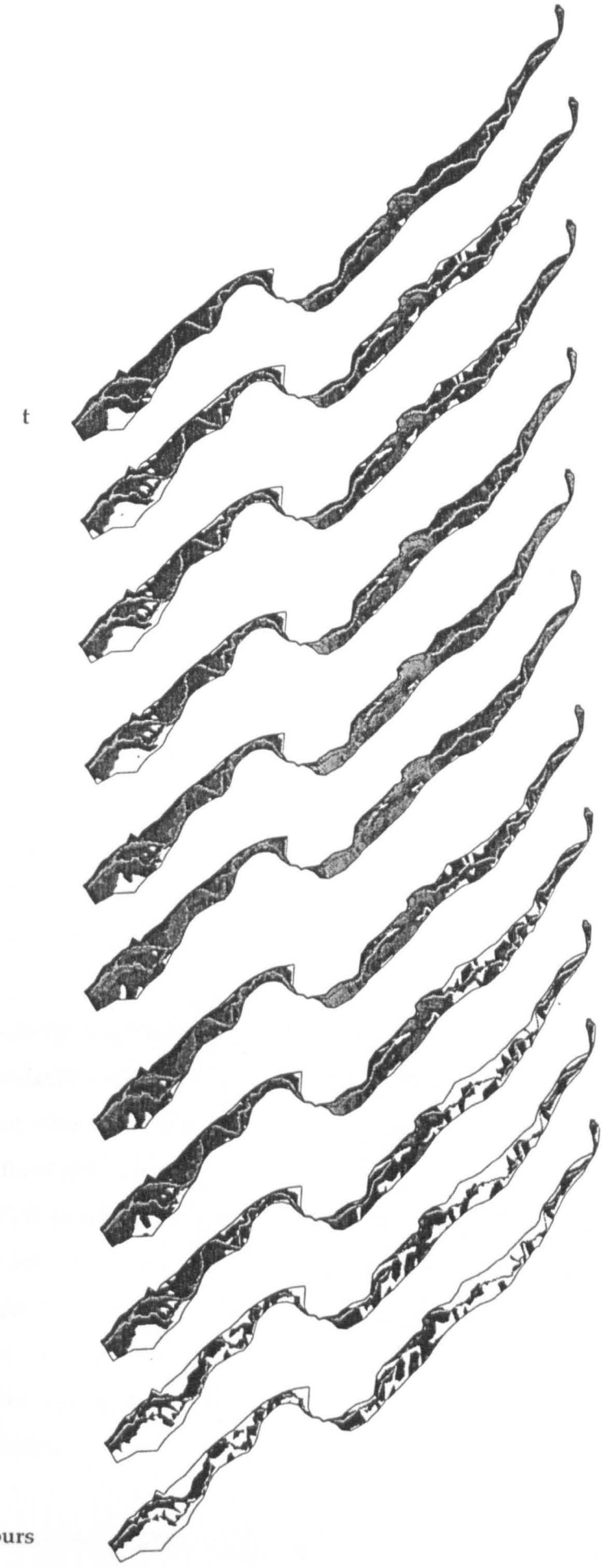

Figure 5.6 (continued)

5.3.3.3 The calibration issue

Although the criterion used to assess model calibration is the 'goodness-of-fit' between the predicted and observed output hydrographs, consideration should also be given to the general correspondence between the two hydrographs over the simulation in terms of simulated flow magnitude and general hydrograph shape. An inspection of Figures 5.4 and 5.5 illustrates that while the calibration was adequate for both simulations in terms of peak timing, the correspondence between predicted and observed flows was less satisfactory for the 1 in 5 year event. This is now considered in terms of the suitability of the runs to the proposed application.

The calibration achieved for the Culm 1 in 1 year event is reasonably good in that the timing to peak is within 460 seconds (+0.32%) of the observed peak discharge and the magnitude of the peak differs by -7.31 m^3s^{-1} (-10.4% of the maximum). Indeed, this falls within the expected uncertainty with which discharge can accurately be measured (Herschy, 1978).

The success of the calibration achieved for the Culm 1 in 5 year event is less accurate in both peak phase (4320 s) and peak discharge (- 40.09 m^3s^{-1}). There are a number of possible reasons for this:

- It is likely that errors discussed in the stage-discharge relationship at Rewe will be significant. It is expected that the uncertainty in the relationship will increase with increasing discharge and with overbank flow (Walling, *pers comm.*) thus while the relationship is reasonably accurate for the smaller 1 in 1 year event it is less so for the larger 1 in 5 year event.

- The simulations are possibly experiencing storage routing problems. It is possible that TELEMAC2D is not accurately accounting for mass storage fluctuations in the domain during the 1 in 5 year simulation where in reality the storage of water on the floodplain would partly account for the reduced flood peak discharge and reduced total volumetric output observed. It is possible that TELEMAC2D is not accurately accounting floodplain storage which could be an effect of the interaction between flow and floodplain topography, which for the larger 1 in 5 year event is not well represented. For example, the larger flood wave associated with the 1 in 5 year event will interact with a greater storage potential on the floodplain which is not represented in the model topography. Such a flow routing problem will result in an over estimate of the predicted flow.

It is probable that the difference between the observed and predicted output discharge in the 1 in 5 year simulation is a manifestation of these two factors. However, this does not preclude the use of this event in *Chapter 6* where the semi-theoretical approach adopted will consider differences between model predictions, both in terms of those measured at the downstream boundary and those

which are spatially distributed over the domain surface, with and without infiltration. This event illustrates the problems associated with relying on an observed output hydrograph as the sole method of calibration for distributed models such as TELEMAC2D. This issue is returned to in *Chapter 8*.

The result of section 5.3 is the provision of the hydraulic model platform upon which the subsequent research rests. The calibrated simulations provides two control simulations against which the significance of infiltration loss will be determined in *Chapter 6* and the 1 in 1 year simulation which will form the basis of the investigation in *Chapter 7*.

5.4 Parameterisation of the infiltration model for the Culm application

The infiltration model itself was introduced in *Chapter 3* (section 3.4) where the parameterisation requirements were also identified. The infiltration model has been previously applied and parameterised in sections 3.7 and 4.5 and the basic principles underlying the derivation of the parameterisation data have been discussed (section 3.4). Aside from the physical aspects of model parameterisation, which include the depth of soil to be modelled, the number of soil horizons (layers) and cells, the basic requirement of model parameterisation is the derivation of the suction-moisture relationship for each soil used. A number of techniques used for determining this relationship have been discussed previously (section 3.4.1).

This section now describes the derivation of the suction-moisture relationship for the soils chosen to represent those of the Culm application and the range of initial soil moisture values to be used. The section begins with a description of the soils of the Culm floodplain.

5.4.1 Soils of the Culm Floodplain

The soils which have developed in the alluvium along the floodplains of the Exeter district are typically young and have inherited the texture of the parent material from which they were derived (Clayden, 1971). They have been classified into soil groups according to the degree of gleying, which is a measure of the influence of groundwater in the upper 1m of the soil. The following discussion is based on the findings of the Soil Survey of England and Wales (Findlay *et al.*, 1984; Clayden, 1971).

Soils that exhibit little gleying in the upper 90 cm are termed brown warp soils. Those with evidence of considerable mottling in the lower horizons below 50 cm are classed as gleyed brown warp soils while those having profiles which are gleyed throughout are classes as ground water gley soils. The brown warp and gleyed brown warp soil groups are further divided into soil series

according to texture. In all, seven soil series and three complexes are described by Findlay *et al.*. (1984). Two soil groups have been mapped for the lower reaches of the River Culm floodplain, which includes the area covered in this study. These are brown warp soils of the Exe series, present for about 1km upstream of the confluence with the River Exe and gleyed brown warp soils of the Clyst complex which extend upstream beyond the reach of interest. Soils from the Exe series are typified by a brown silt loam surface horizon of fine subangular blocky structure which extends to 90cm and below. The soils are rarely affected by ground water moving to within 90cm of the surface although intermittent waterlogging is evident. The most widespread variant of the series are gleyed brown warp soils which are associated with minor topographic depressions. The soil are described as having a ***silty loam*** or ***silty clay loam texture***. The second soil group associated with the Culm are those of the Clyst complex. The complex is dominated by reddish brown stoneless clays of the Clyst series exhibiting a limited extent of gleying above 40cm. The alluvium of the River Culm in which the Clyst complex soils have developed exhibits a variable composition with clayey and fine loamy textures predominating. Coarser textured soils are also common along with stratified profiles with clay loams interbedded with loams, sandy loams or loamy sands. The floodplain is dominated by gleyed brown warp soils but groundwater gleys also occur. The Clyst complex soils exhibit variability in texture but can be generalised as ***stoneless clays***.

The two soil groups identified for the River Culm floodplain (Clayden, 1971) are also common throughout the Exeter region floodplains and are also typical of British lowland floodplains in general.

Land use on the floodplain reflects the frequent occurrence of inundation and wet soil conditions in the winter months. As such the land is predominantly reserved for cattle and sheep grazing during the summer months, together with hay and silage production. Nevertheless, the permanent pasture receives fertiliser inputs of NPK.

The soils described cover a range of textural characteristics which range from clay through to silty loam. These two soils are chosen to represent the subsurface condition in the floodplain hydrology model and provide a basis for the derivation of hydraulic properties required to parameterise the infiltration model. It is to the derivation of these parameters that the discussion now turns.

5.4.2 Determining the suction-moisture relationship for the floodplain soils

A number of different methods for determining the suction-moisture curve for soils were discussed in *Chapter 3* (section 3.4). Of these the van Genuchten model, represented by Equation 3.8, was selected as the most appropriate. The suction-moisture relationship for the clay and silty loam soils are determined, by application of the van Genuchten model, using parameter values previously

determined for these soil types by Carsel and Parrish (1988). The means and standard deviations for the model parameters for the two soil types are presented in Table 5.4.

Soil texture	θ_s (cm^3/ cm^3)		θ_r (cm^3/ cm^3)		Ks (cm/ day)		a (cm^{-1})		n (-)	
	mean	std	mean	std	mean	std	mean	std	mean	std
Clay	0.38	0.09	0.068	0.034	4.8	10.1	0.008	0.012	1.09	0.09
Silty Loam	0.45	0.08	0.067	0.015	10.8	29.5	0.02	0.012	1.41	0.12

Table 5.4 Means and standard deviations of the Van Genuchten model parameters for a clay and silty loam soil. (from Carsel and Parrish, 1988). θ_s represents the saturated water content, θ_r represents the residual water content and *a* and *n* are parameters which determine the shape of the curve.

The resulting suction-moisture curves are presented in Figure 5.7. The mean values are used to generate the curves and no account has been given to the potential effect of the standard deviations.

5.4.3 Antecedent soil moisture

The infiltration model requires antecedent soil moisture conditions to be set at the beginning of each simulation. The range of possible soil moisture values will be bound by the maximum and minimum soil moisture contents encountered in each soil. The maximum amount of water that a soil can hold, the saturated water content, is determined by the total porosity of the soil (total pore space). Yet this condition is rarely met in the field as air entrapment, even in flooded or submerged soils, will reduce the total pore space available to water. Typical values for soil moisture content at saturation range from 40 to 60% of soil volume. Soils that have drained under gravity reach a moisture content termed the field capacity (10 - 55% of soil volume), a value which can be further substantially reduced by transpiration through plant roots which reduce the moisture content to the permanent wilting point, equivalent to -15,000cm of matric suction, and at which point soil water occupies between 5 and 35% of the soil volume. Soil moisture can be reduced still further by evaporation until the air-dry state is attained, but this will be of little significance to the research proposed. Practically, the possible antecedent soil moisture conditions (volumes) are bounded by that at saturation and that at the permanent wilting point. The initial soil moisture values for this research will be chosen to represent conditions during late autumn through to Spring and are therefore at the higher end of the spectrum. Two initial values are chosen to represent soil moisture conditions at the beginning of each simulation: 80% and 95% of saturation.

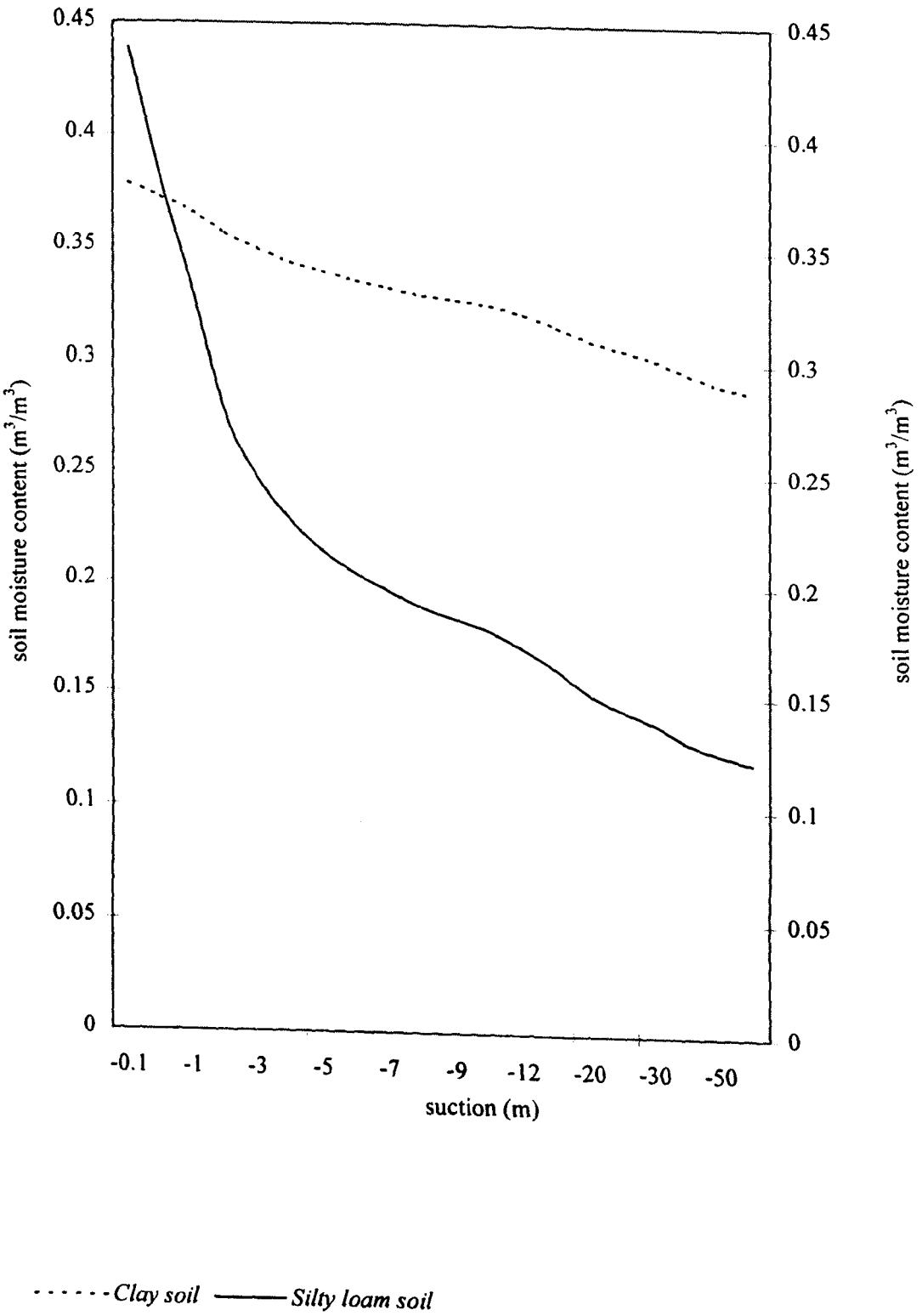

Figure 5.7 Suction-moisture curves for the clay and silty loam soils derived by application of the Van Genuchten model using model parameters derived by Carsel and Parish (1988).

5.5 Parameterisation of the nitrate model

The parameterisation requirements of the nitrate model has been discussed in *Chapter 4*. Prior to each simulation values are required for (i) the in situ NO_3-N mass, (ii) the floodwater NO_3-N concentration, (iii) rainwater NO_3-N concentration (if required), (iv) the denitrification rate constant and (v) the form of the dimensionless soil moisture function. In *Chapter 7* values for each of these will be required. This section is concerned with the provision of suitable denitrification rate constants for the research and a suitable form of the soil moisture function. These issues are now considered.

5.5.1 Obtaining representative values for the denitrification rate constant (k_1)

The importance of the denitrification equation rate constant, k_1, in determining denitrification loss is established in *Chapter 4* (Section 4.5) in terms of model sensitivity. The sensitivity of the model to this parameter implies that careful consideration should be given to selecting values for k_1. Three methods are available for selecting k_1 values. Firstly, k_1 can be determined through experimentation (Stanford *et al.*, 1975a; Reddy *et al.*, 1982) . The second method relies on selecting suitable values of k_1 from the literature. This has commonly been the case where denitrification rate constants are required for model parameterisation (eg, Kaluarachchi and Parker, 1988; Philips, 1989a;b; Chesheir *et al.*, 1987) and extends to the selection of rate constants for other N-transformation processes. The third method involves an iterative method in which the model is run using different k_1 values until the predicted loss corresponds to known losses for a particular system. As field analysis has not been undertaken as part of this research, the denitrification rate constants used have been selected using a combination of methods two and three (literature search and iterative fitting). Initially a literature search was conducted to obtain values of k_1, the results of which have previously been presented in Chapter 4 (Table 4.4). The literature survey provides a starting point from which the choice of suitable values can begin.

Selection of suitable k_1 values for the research was achieved by first selecting a range of k_1 values from Table 4.4 and then running a series of simulations in which these values were applied and comparing the NO_3-N losses generated with the denitrification loss data for floodplain/riparian soils presented in *Chapter 4* (Table 4.3). This method of first reviewing the literature and then finding appropriate values through fitting model results to reported results allows for: (i) an appreciation of the range of k_1 values available for model parameterisation and the context for their use and (ii) conformation that the denitrification rates produced by the k_1 values selected for the research match, to a reasonable degree, published denitrification data from floodplain/riparian systems.

The denitrification rate constant values presented in Table 4.4 cover a range of between $2.5x10^{-5}$ h^{-1} (Rolston *et al.*, 1984) and $0.1596h^{-1}$ (Stanford *et al.*, 1975b) and demonstrates the considerable range of rate constants associated with this process. Although this is by no means an exhaustive list it does provide an indication of the range of rate constants used by authors researching in a range of soil types and conditions and as such represents a starting point for model parameterisation.

The iterative fitting of the rate constants found in the literature to literature cited denitrification losses for floodplains and riparian zones presents a number of problems. Most measurements of denitrification are made under transient conditions of aeration, carbon availability, temperature and, to a lesser extent pH, which means that the resulting values of loss are dependant upon the prevailing combination of these factors as discussed in *Chapter 4*. Unless the model can accurately reproduce the transient conditions under which these values were derived, which it cannot, then such comparisons are not possible, though they may still prove useful. However, reported measurements of denitrification potential provide data which can be used more readily for comparison. Denitrification potential represents the maximum rate of denitrification for a given system in which all factors are non-limiting. By assuming that k_1 represents the maximum rate of denitrification for the system (and setting $f_w = 1.0$) then it is possible to replicate these conditions in a series of model runs and to compare predicted losses of NO_3-N with measured DNP rates from the literature. The remaining problem here is that in all simulations the concentration of NO_3-N will remain limiting, while in the determination of DNP this is not usually the case. The results of a literature search for DNP values is presented in Table 5.5.

Two sets of simulations were conducted and reported as Test 1 and Test 2.

Test 1 uses a simple model written specifically for this test in which 10g of NO_3-N is subject to denitrification for 24 hours according to the rate equation (4.31), where f_w is set to equal 1.0 (thus assuming fully anaerobic conditions) and k_1 assumes the values 0.1, 0.01, 0.001, 0.0001 and 0.00001. The results are presented Table 5.6.

Test 2 investigates losses under a number of transient conditions using the coupled floodplain hydrology-nitrate model. Again, the rate equation (4.31) is used and f_w is set to equal 1.0. The series of rate constants used are the same as for Test 1 as is the initial mass of NO_3-N in the top soil cell.. Three different transient conditions are simulated: (a) the model is set up such that no input occurs through the surface boundary. The results from these simulations should closely match those of Test 1, though they should be slightly smaller due to a small loss of NO_3-N leached from cell 1. (b) flood conditions are simulated at the surface boundary and floodwater has a NO_3-N concentration is set to

zero (c) flood conditions are again assumed at the surface boundary but this time with a concentration of 10mgl^{-1} NO_3-N. The results of the simulations are presented in table 5.6.

Author	Soil type	location/land use	Reported DNP
Bijay-Singh *et al.* (1988)	Halstow/Fedburn Series (poorly drained)	Devon. Grassland	3.65+/-0.37μgN $g^{-1}h^{-1}$ (field moist samples)
	(as above)	(as above)	4.86+/-0.53μgN $g^{-1}h^{-1}$ (air-dried samples)
	Frilsham Series (freely drained)	Berkshire. Grassland	1.06+/-0.16μgN $g^{-1}h^{-1}$ (field moist samples)
	(as above)	(as above)	1.80+/-0.32μgN $g^{-1}h^{-1}$
Bijay-Singh *et al.* (1989)	Frilsham series (freely drained)	(as above)	1.46+/-0.05μgN $g^{-1}h^{-1}$
Groffman *et al.* (1991)	Enfield silty loam	Tall fescue	17208gNha^{-1}d^{-1}
	(as above)	Reed Canary grass	15208gNha^{-1}d^{-1}
Cooper *et al.* (1990)	Mineral		0.013-0.044μgN $g^{-1}h^{-1}$
	Organic		0.0004-1.35μgN $g^{-1}h^{-1}$

Table 5.5 Potential denitrification rates (DNP) derived from the literature.

	Test 1	Test 2	Test 2	Test2
rate constant	**NO_3-N loss ($\mu gNg^{-1}\ hr^{-1}$)**	**(a) ($\mu gNg^{-1}\ hr^{-1}$)**	**(b) ($\mu gNg^{-1}\ hr^{-1}$)**	**(c) ($\mu gNg^{-1}\ hr^{-1}$)**
0.00001	$2.3x10^{-2}$	$2.3x10^{-3}$	$6.0x10^{-4}$	$6.7x10^{-4}$
0.0001	0.02	$2.3x10^{-2}$	$6.0x10^{-3}$	$6.7x10^{-3}$
0.001	0.2	0.2	$6.0x10^{-2}$	$6.7x10^{-2}$
0.01	2.1	2.0	0.6	0.6
0.1	8.9	8.8	3.8	4.3

Table 5.6 Results from Tests 1 and 2 designed to investigate the mass of NO_3-N lost with different k_1 values under a series of conditions.

Examining the results from Test 1 first, the greatest loss (8.9 $\mu gNg^{-1}h^{-1}$) correspond to a rate constant set at 0.1 and exceeds all DNP losses reported in Table 4.4. The loss of 2.1 μgNg^{-1} hr^{-1} for k_1 = 0.01 is comparable to the maximum DNP rate reported for organic riparian soils by Cooper (1988) of 1.35μgNg^{-1} hr^{-1}. For mineral riparian soils Cooper (1988) reports a range of between 0.013 and 0.044 $ugNg^{-1}$ h^{-1} which corresponds to the result generated for a k_1 value of 0.0001 in Test 1. For a poorly drained grassland in Devon (Halstow/Tedburn Series) Bijay-*Singh et al.* (1988) reports losses of 3.65 +/- 0.37 μgNg^{-1} hr^{-1} for field moist and 4.86 +/- 0.53 μgNg^{-1} hr^{-1} for air dried soils and lower values for a freely drained Berkshire grassland (Frilsham Series) of 1.06 +/- 0.16 μgNg^{-1} hr^{-1} for field moist and 1.80 +/-0.32 μgNg^{-1} hr^{-1} for air dried soils. All values reported by Bijay-Singh *et al.* (1988) and Bijay-Sing *et al.* (1989) correspond to a k_1 value of between 0.01 and 0.1 in Test 1. The results suggest that NO_3-N losses associated with DNP rates correspond to high rate constants of the order 0.01 to 0.1. However, the major unknown in this study remains the initial concentration of NO_3-N within the micobially active layer.

Considering these results in terms of those reported for riparian soils (not DNP) in Table 4.3 suggests that lower denitrification rate constants are operating in these environments. The rates of NO_3-N loss reported by both Haycock and Burt (1993) and Schipper *et al.* (1993) correspond with a loss in Test 1 associated with a rate constant of 0.001 while those reported by Hanson *et al* (1994), Schnabel and Stout (1994) and Maltby *et al.* (1996) correspond to losses in Test 1 associated with rate constants at or below 0.00001. However, it must be remembered that the losses reported by these authors represent average values which will be lower than the maximum rates occurring.

The results from Test 2 are now considered: Test 2(a) shows similar, though slightly smaller, rates of denitrification when compared to Test 1. This is expected due to the small loss of NO_3-N from the microbially active cell 1 to cells lower in the profile which reduces the amount of NO_3-N available to denitrify. Test 2(b) illustrates the leaching effect of floodwater. The initial 10g of NO_3-N in cell 1 is leached from this cell under the influence of the surface flux. Test 2(c) again illustrates the leaching effect of floodwater but also the effect of the addition of NO_3-N from the infiltrating floodwater. As such the rates of denitrification are higher in Test 2(c) than Test 2(b) but in both cases these remain lower than in Test 2(a). In terms of reported denitrification losses the same pattern applies here as was found for Test 1. Rates of loss associated with DNP studies compare with the higher rate constants used in Test 2 while rates of loss reported for riparian soils (not DNP) compare to those generated by the lower rate constants used in Test 2.

The choice of rate constants for parameterisation of the nitrate model in *Chapter 7* will be based upon the discussion above and based on the observation that actual rates will generally be lower than DNP values but higher than non-DNP values reported for riparian soils.

5.5.2 Obtaining a suitable form for the soil moisture function, f_w.

The soil moisture function was introduced in *Chapter 4* and is represented by Equation 4.32. The form of this dimensionless function, which ranges from a pre-determined minimum background value to a maximum of 1.0, is dependant upon the value of s in the exponent. Figure 4.5 illustrates the shape of the curve for four values of s. The response of denitrification rate to increasing soil moisture content was discussed in section 4.2.2.1 and in remaining consistent with the general pattern observed, a value of 5 for s in equation 4.32 is chosen for all runs undertaken in *Chapter 7*.

5.8 Conclusions

In this Chapter three main objectives have been realised. Firstly, a suitable reach to which the coupled floodplain hydrology-nitrate model can be applied in Chapters 6 and 7 has been selected. The 11 km reach of the River Culm chosen has a record of previous inundation, a substantial hydrometric data set and has been successfully applied in previous modelling studies using the 2D finite element model RMA-2 (Bates *et al.*, 1992; Charlton, 1995). Two flood events, a 1 in 1 and a 1 in 5 year, have been selected and run using the above reach to provide calibrated control simulations for the investigations in Chapters 6 and 7.

Secondly, two soil types have been identified as representing those most commonly associated with lowland floodplain alluvial deposits - a clay and a silty loam. Parameterisation data for these two soils has been derived relating to the suction-moisture curves, saturated moisture contents, saturated hydraulic conductivities and initial soil moisture contents which have been chosen to represent a range typical of temperate winter conditions.

Finally, a suitable range of denitrification rate constant (k_1) values and a suitable form of the soil moisture function curve has been identified for use in *Chapter 7*. Selection of k_1 values is based on a two stage process during which a range of values were first obtained from the literature and then these were run using the coupled floodplain hydrology model to determine their correspondence with published DNP rates and denitrification rates. This provides an indication as to the suitability of the k_1 values reported in the literature.

Hydraulic model response to infiltration

6.1 Introduction and Chapter Objectives

In this Chapter the significance of relaxing the surface boundary of the TELEMAC2D finite element hydraulic model over a range of soil types and conditions is addressed through the consideration of a number of aspects of model prediction. Accordingly, the aim of this chapter is to assess both the utility of the coupled floodplain hydrology model and the impact of infiltration on flow prediction.

The arguments for investigating the effects of infiltration on 2D finite element hydraulic model prediction are set out in *Chapter 2* while the coupled floodplain hydrology model to be employed in the research is described and developed in *Chapter 3*. The range of soil parameter values over which the coupled floodplain hydrology model is to be applied have been chosen to represent those conditions typical of lowland alluvial floodplain environments as discussed in *Chapter 5*. Indeed, in *Chapter 5* the River Culm hydraulic model template which provides the test cases for this Chapter is developed along with the infiltration model parameterisation data.

This Chapter begins with an introduction to the simulations which form the basis of the investigation together with a summary of the range of soil conditions to be investigated. Consideration is then given to the manner in which the results are to be analysed. The bulk of the Chapter is occupied by the analysis itself during which the significance of infiltration on hydraulic model prediction is investigated according to two general themes. The first of these considers the domain integrated effect of infiltration on hydraulic model output, measured in terms of (i) the output hydrograph, (ii) the volume of surface water within the domain, (iii) the mean surface water depth and (iv) inundation extent. The second considers the localised effects of infiltration through an analysis of water depth and velocities at selected nodes taken from two cross-sections across the reach. The Chapter concludes with a consideration of the effects of infiltration on model numerical stability and mass conservation.

6.2 Simulations undertaken

The simulations in this Chapter are undertaken to investigate 2D hydraulic model response to infiltration to:

determine the impact of infiltration on 2D hydraulic model flow prediction.

In accordance with this objective the range of soils and soil conditions over which the coupled floodplain hydrology model is to be applied have been identified in *Chapter 5* as has the reach template and control simulations which form the basis of the investigation.

6.2.1 Model Parameterisation

Infiltration model: For the purpose of this investigation the clay and silty loam soils identified in *Chapter 5* are used. Both soils are of 60cm depth and are divided into three layers which are assumed to be homogeneous throughout in terms of their physical characteristics. Thus within each soil each layer assumes an identical suction-moisture curve and saturated hydraulic conductivity, the data for which are presented in Table 5.4 and the resulting suction-moisture curves are illustrated in Figure 5.7. Vertical homogeneity is also assumed for initial soil moisture content, of which two initial values were chosen, 80% and 95%, the choice of which was discussed in *Chapter 5*. Gravity flow is assumed to account for flow at the bottom boundary which occurs at a rate determined by the conductivity of the bottom cell. Water is therefore 'lost' from the system into an assumed aquifer underlying the floodplain soil. The two soil types and two initial soil moisture conditions chosen for the investigation generate four possible combinations of initial conditions for the floodplain infiltration model:

Soil type	Initial soil moisture content (%)
Clay	80% and 95%
Silty loam	80% and 95%

Table 6.1 The four possible combinations of initial conditions for the floodplain infiltration model.

Precipitation does not occur during any of the simulations while the maximum evaporative rate is set at $6.0x10^{-8}$ ms^{-1}.

Hydraulic model: Hydraulic model parameterisation was covered in *Chapter 5* where the test reach and the two flood events were identified and calibrated runs for these established. The simulations run in this analysis use these events in combination with the infiltration model parameterisation identified in Table 6.1. The resulting series of simulations are discussed in the following section.

6.2.2 Simulations

The simulations undertaken are listed in Table 6.2. These consist of two control runs, one for each of the Culm events investigated (Culm 1 in 1 year and Culm 1 in 5 year), in which the models were run with impermeable surface boundaries. The results from these simulations are presented in *Chapter 5* (section 5.3.3.2) together with statistics relating to the calibrations achieved for each event (Table 5.3). These runs are identified in Table 6.2 as *Control01* and *Control02*. Additionally, four further simulations were undertaken for each calibrated event in which each of the four soil conditions presented above (Table 6.1) were used. Thus, for each control run the four additional runs were: (i) sitly loam soil, 80% initial saturation , (ii) silty loam soil, 95% initial soil saturation, (iii) clay soil, 80% initial soil saturation and (iv) clay soil, 95% initial saturation. These are identified in Table 6.2 as *Clay01*, *Clay02*, *Clay03* and *Clay04* for the clay soil and *Sil01*, *Sil02*, *Sil03* and *Sil04* for the silty loam soil. A further 8 simulations were undertaken using the Culm 1 in 1 year event in which the hydraulic conductivity used in the original runs (*Clay01*, *Clay02*, *Sil01* and *Sil02*) was first increased by one order of magnitude and then decreased by one order of magnitude for both soil types and initial soil moisture conditions. These runs are identified in Table 6.2 as *Clay05*, *Clay06*, *Clay07*, *Clay08*, *Sil05*, *Sil06*, *Sil07* and *Sil08*.

Each simulation is assigned a code in Table 6.2 and is referred to by this code in all tables hereafter). For clarity, when reference is made to a simulation in the text this code is cited together with an identification of the soil type (ie clay (Clay) or silty loam (Sil)) and its initial soil moisture content (ie 80 or 95% of the saturation value). Thus, simulation *Sil02* refers to an event run on the silty loam at 95% initial saturation and will be referred to in the text as *Sil02* (substrate *Sil(95)*).

Simulation code	inundation event	surface boundary condition	soil type	initial soil moisture content (%sat)	$K_{(sat)}$
Control01	Culm 1:1 year	impermeable	-	-	-
Control02	Culm 1:5 year	impermeable	-	-	-
Clay01	Culm 1:1 year	relaxed	Clay	80%	$5.56x10^{-7}$
Clay02	Culm 1:1 year	relaxed	Clay	95%	$5.56x10^{-7}$
Clay03	Culm 1:5 year	relaxed	Clay	80%	$5.56x10^{-7}$
Clay04	Culm 1:5 year	relaxed	Clay	95%	$5.56x10^{-7}$
Sil01	Culm 1:1 year	relaxed	Silty loam	80%	$1.25x10^{-6}$
Sil02	Culm 1:1 year	relaxed	Silty loam	95%	$1.25x10^{-6}$
Sil03	Culm 1:5 year	relaxed	Silty loam	80%	$1.25x10^{-6}$
Sil04	Culm 1:5 year	relaxed	Silty loam	95%	$1.25x10^{-6}$
Clay05	Culm 1:1 year	relaxed	Clay	80%	$5.56x10^{-6}$
Clay06	Culm 1:1 year	relaxed	Clay	80%	$5.56x10^{-8}$
Clay07	Culm 1:1 year	relaxed	Clay	95%	$5.56x10^{-6}$
Clay08	Culm 1:1 year	relaxed	Clay	95%	$5.56x10^{-8}$
Sil05	Culm 1:1 year	relaxed	Silty loam	80%	$1.25x10^{-5}$
Sil06	Culm 1:1 year	relaxed	Silty loam	80%	$1.25x10^{-7}$
Sil07	Culm 1:1 year	relaxed	Silty loam	95%	$1.25x10^{-5}$
Sil08	Culm 1:1 year	relaxed	Silty loam	95%	$1.25x10^{-7}$

Table 6.2 Simulations undertaken for the sensitivity analysis.

An additional loose-leaf copy of this table is available in the back cover of the thesis for easy reference throughout this chapter. A full summary of the TELEMAC2D and soil moisture mass balance data generated for each simulation is presented in Appendix 1.

6.2.3 Methods of Analysis

The analysis essentially takes the form of a sensitivity analysis in which the effects of changing soil type and initial soil moisture on hydraulic model output are determined. As alluded to in the introduction to this Chapter, the results are analysed according to two general themes. The first of these seeks to determine the significance of infiltration on model prediction through an analysis of the following four model outputs:

- ***The output hydrograph;***
- ***The volume of surface water within the domain;***
- ***The mean surface water depth;***
- ***The modelled floodplain inundation extent.***

These predicted model outputs can be considered to be the result of a combination of factors occurring over the domain as a whole where, for example, the mean surface water depth is a product of the combined effects of hydraulic model parameterisation acting over the entire domain surface. It is the effect of infiltration that is to be analysed here. Similarly, the output hydrograph, although calculated at the downstream boundary of the model, is a product of the hydraulic characteristic of the domain as a whole, of which infiltration is one process. As such, these model outputs are termed 'integrated'. All of the simulations presented in Table 6.2 are analysed in this section and the effects of infiltration are measured with reference to the control runs (*Control01* and *Control02*).

The second part of the analysis considers the localised effects of infiltration through a detailed analysis of the Culm 1 in 1 year event. This is done by first locating two cross-sections along the reach, one at the upstream end and another located at the downstream end, and then comparing water depth and flow velocity at two nodes, one floodplain and one channel, from each of the two cross-sections.

6.3 The effect of infiltration on integrated hydraulic model output

The effect of infiltration on the predicted output hydrographs, the volume of surface water within the domain, the mean surface water depth and inundation extent of the simulations in Table 6.2 is now considered:

6.3.1 The effect of infiltration on the predicted output hydrograph

In this section the effect of infiltration on the model predicted output hydrograph is addressed.

There are a number of ways in which the predicted output hydrograph, measured at the downstream model boundary, might respond to infiltration including; *(i)* a change in total volume, *(ii)* a change in time to peak discharge and *(iii)* a change in peak discharge rate. The simulations presented in Table 6.2 are analysed in terms of these three factors and the results are presented in Tables 6.3 and 6.4 and Figures 6.1 and 6.2. Each of these aspects of the simulated hydrograph are now considered in turn:

Simulation code	total simulated discharge volume (m^3)	% difference in discharge volume	time to peak discharge (s)	% difference in time to peak discharge	peak discharge (m^3s^{-1})	% difference in peak discharge
Control01	1857139.9	-	47238	-	62.97	-
Control02	7202713.5	-	63718	-	107.57	-
Clay01	1708358.0	-8.0	47238	0.0	61.06	-3.04
Clay02	1777205.8	-4.3	47238	0.0	61.06	-3.04
Clay03	6912967.2	-4.0	63918	+0.31	105.47	-1.96
Clay04	6995775.7	-2.9	63898	+0.28	105.86	-1.59
Sil01	1652312.6	-11.0	47258	+0.04	58.70	-6.77
Sil02	1700851.7	-8.4	47258	+0.04	58.71	-6.77
Sil03	6706802.8	-6.9	64058	+0.53	103.34	-3.94
Sil04	6769149.6	-6.0	64038	+0.50	103.54	-3.75
Clay05	1230127.9	-33.8	48778	+3.26	43.76	-30.5
Clay06	1804995.2	-2.8	47378	+2.96	62.04	-1.48
Clay07	1288024.2	-30.6	48278	+2.20	44.15	-29.89
Clay08	1837823.7	-1.0	47238	0.0	62.56	-0.65
Sil05	773629.3	-58.3	50318	+6.52	25.76	-59.08
Sil06	1808675.2	-2.6	47238	0.0	61.84	-1.79
Sil07	794291.7	-57.2	50318	+6.52	25.86	-58.92
Sil08	1833518.8	-1.3	47238	0.0	62.40	-0.91

Table 6.3 Table of results depicting the manner in which infiltration influences the predicted hydrograph in terms of predicted discharge, time to peak and peak discharge

(i) Predicted discharge volume (m^3): In all simulations run with a relaxed surface boundary condition, total predicted discharge volume is less than the corresponding control discharge volume. The following analysis first considers those simulations in which average $K_{(sat)}$ values were used and secondly, those in which $K_{(sat)}$ was varied by an order of magnitude about the mean.

With reference to runs *Clay01* to *Clay04* and *Sil01* to *Sil04* initially, it is evident that, in terms of total volume lost to infiltration, measured in m^3, the losses for the 1 in 5 year event are consistently

greater than those for the 1 in 1 year event. This is not unexpected given the relative magnitude of the two events, both in terms of size and duration (see Table 5.3). For example, a maximum loss of 204827.3m^3 for simulation *Sil01* (1 in 1 year event; substrate *Sil(80)*) compares with a maximum loss of 495910.7m^3 for the 1 in 5 year event, run with the corresponding substrate. The loss for the 1 in 1 year event is less than half that of the 1 in 5 year event. A rather more informative measure is that of relative loss which is gained by expressing the loss associated with each simulation as a fraction of the corresponding control simulation output (the predicted output hydrograph). These results are presented in Table 6.3. Relative losses (losses expressed as a fraction of predicted output) are found to be greater for the 1 in 1 year event. For comparative runs, losses on the silty loam substrate are consistently greater than for those run on clay. For the Culm 1 in 1 year event infiltration losses generated by simulation *Sil01* (substrate *Sil(80)*) and *Clay01* (substrate *Clay(80)*) are -11.0% and -8.0% respectively while for the Culm 1 in 5 year event the equivalent losses are -4.0% (substrate *Clay(80)*) and -6.9 (substrate *Sil(80)*).

As expected, losses are also found to be consistently greater for simulations beginning with an 80% soil moisture content compared to 95%. For the 1 in 1 year event the losses associated with simulations *Sil01* (substrate *Sil(80)*) and *Sil02* (substrate *Sil(95)*) are -11.0% and -8.4% respectively and for the 1 in 5 year event are -6.9% and -6.0% for the corresponding simulations. The greatest loss, measured as a percentage of the control simulation discharge, is associated with the 1 in 1 year event, simulation *Sil01* (substrate *Sil(80)*), while the smallest is associated with the 1 in 5 year event, simulation *Clay04* (substrate *Clay(95)*). The results are consistent with those expected where total infiltration loss increases with both an increasing $K_{(sat)}$ and decreasing initial soil moisture content. Lower initial soil moisture contents result in both an initially greater potential soil moisture store and higher infiltration fluxes due to initially greater hydraulic gradients across the surface boundary. Indeed, in all of the simulations the pattern observed complies with the expected results where: *Sil01* > *Clay01*, *Sil03* > *Clay03*, *Clay01* > *Clay02*, *Clay03* > *Clay04*, *Sil01* > *Sil02 and Sil03* > *Sil04*.

A consideration of the total infiltration loss alone conceals an interesting pattern in the model response which is illustrated in Figure 6.1 which suggests that the relative importance of initial soil moisture content and saturated soil hydraulic conductivity in determining infiltration loss changes during the course of the simulation. In both events (see Figure 6.1), while the predicted discharge for simulation *Clay02* and *Clay04* (substrate *Clay(95)*) remains above those of simulations *Sil01* and *Sil03* (substrate *Sil(80)*) throughout the 1 in 1 and 1 in 5 year simulations respectively, the curves tracing the output discharge for simulations *Clay01* and *Clay03* (substrate *Clay(80)*) and

(a)

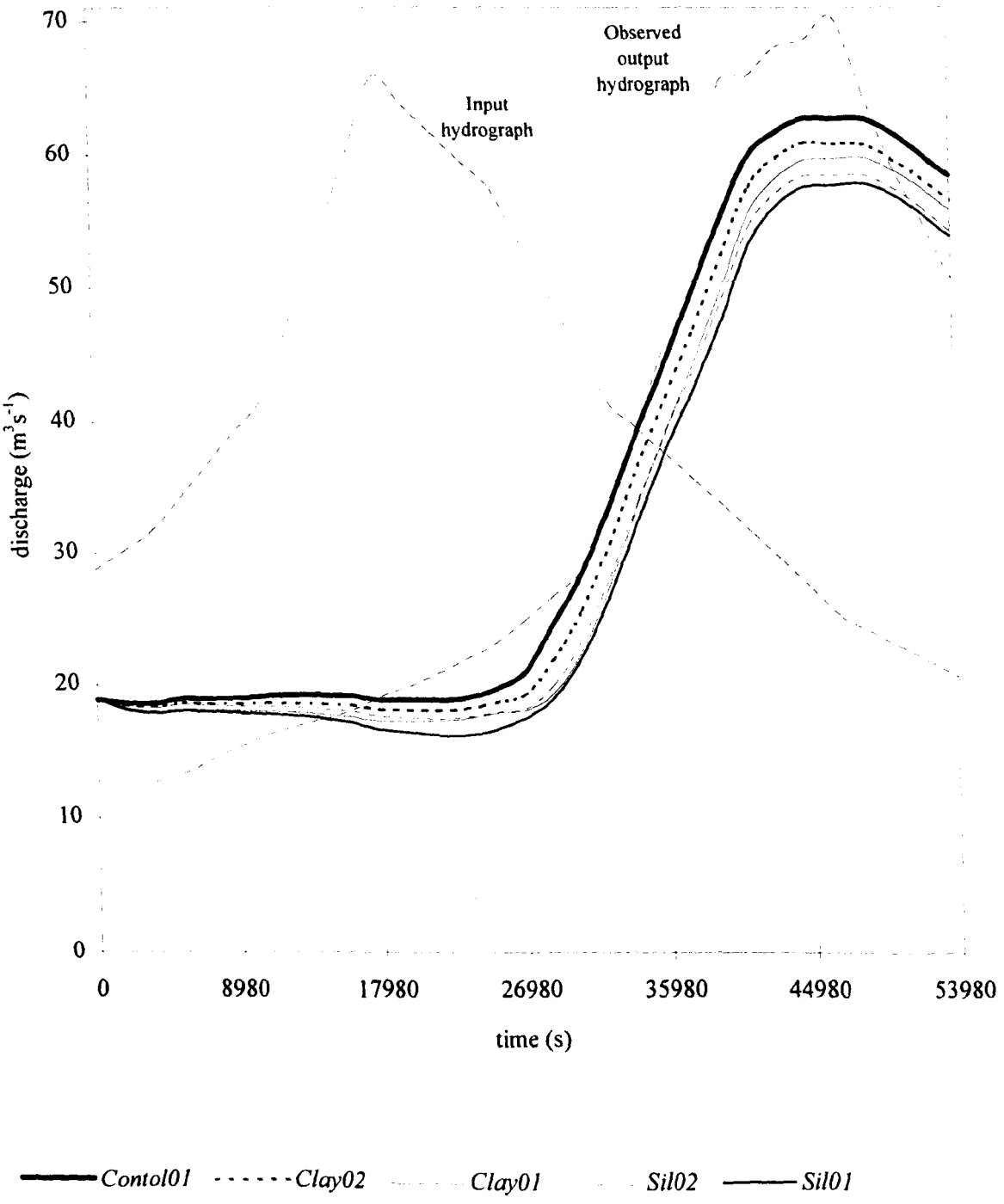

Figure 6.1 Illustration of the impact of infiltration on the predicted output hydrograph of TELEMAC2D. (a) Culm 1 in 1 year simulation with relaxed surface boundaries showing the input hydrograph, observed output hydrograph, the predicted output hydrograph (*Control01*) and the predicted hydrographs for simulations *Clay01*, *Clay02*, *Sil01* and *Sil02*. (b) Culm 1 in 5 year simulation with relaxed surface boundaries showing the input hydrograph, observed output hydrograph, the predicted output hydrograph (*Control02*) and the predicted hydrographs for simulations *Clay03*, *Clay04*, *Sil03* and *Sil04*.

(b)

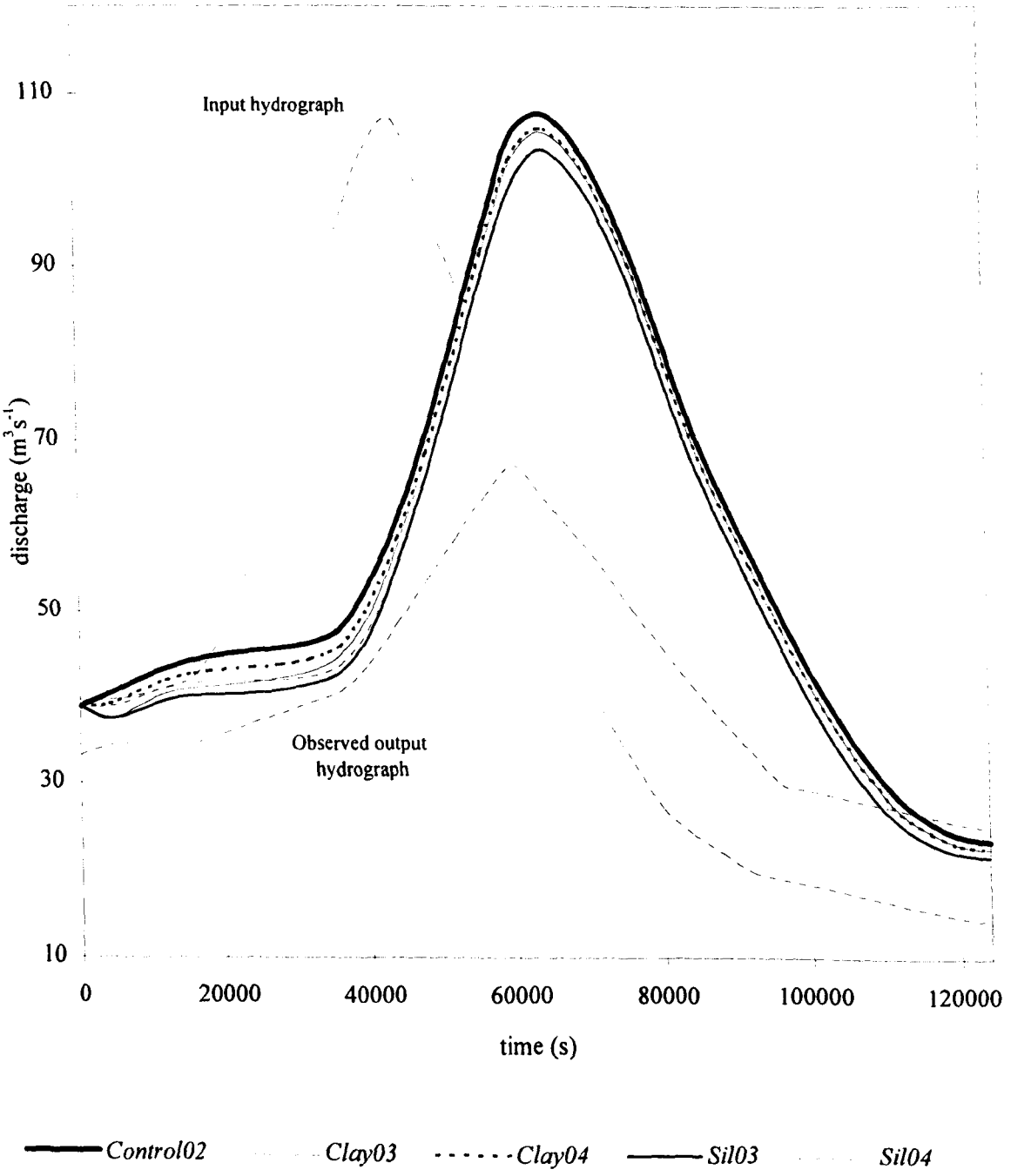

Figure 6.1 (continued)

simulations *Sil02* and *Sil04* (substrate *Sil(95)*) intersect during the course of each simulation. For both events the predicted output discharge for simulations run on the *Clay(80)* substrate begin below those run on the *Sil(95)* substrate but intersect after approximately 36000 seconds for the 1 in 1 year event and approximately 26000 seconds during 1 in 5 year event. This can be explained by an initial dominance of the lower soil moisture content in driving the infiltration flux across the surface boundary (this greater flux derives from the greater total potential gradient across the surface boundary), the importance of which decreases as the water content of the soil increases. As the water content of both soils increases and the difference between them diminishes, $K_{(sat)}$ becomes the more important determinant in the infiltration flux rate and the curve tracing the output discharge for the *Sil(95)* substrate falls below that of the curve for *Clay(80)* substrate (ie volumetric loss to the *Sil(95)* substrate exceeds that to the *Clay(80)* substrate).

Table 6.3 also presents the results from simulations *Clay05 to Clay08* and *Sil05* to *Sil08* in which variations in $K_{(sat)}$ were investigated (see also Figure 6.2). The results presented above, for simulations employing mean $K_{(sat)}$ values, illustrate that the greatest losses, for both events, are associated with the silty loam substrate at 80% initial soil moisture saturation while the lowest losses are associated with the clay soil at 95% initial saturation. Thus these two soil conditions represent the two extremes of model response over the conditions chosen. The effect of varying $K_{(sat)}$ is considered for the simulations representing these two extremes in order to determine the maximum and minimum effects on model response associated with variations in this parameter. Thus, the results for simulations *Clay07* (substrate *Clay(95+)*), *Clay08* (substrate *Clay(95-)*), *Sil05* (substrate *Sil(80+)*) and *Sil06* (substrate *Sil(80-)*) only are considered. The results illustrate that discharge at the downstream boundary responds non-linearly. Losses are lower than those for the mean values where $K_{(sat)}$ is decreased (simulations *Sil06* < *Sil01* & *Clay08* < *Clay02*) but are considerably greater where $K_{(sat)}$ is increased (simulations *Sil05* > *Sil01* & *Clay07* > *Clay02*). The maximum reduction in predicted discharge for the silty loam substrate was -58.3% (simulation *Sil05*; substrate *(Sil(80+)*) and the maximum for the clay was -30.6% (simulation *Clay07*; substrate *Clay(95+)*).

The discussion above presents infiltration losses in terms of the model predicted output hydrograph. A further insight into the significance of infiltration may be gained through a consideration of infiltration loss as a fraction of the input hydrograph. Table 6.4 presents the losses for each simulation in terms of their respective input hydrographs. The results conform to the general pattern found above with greatest losses associated with the silty loam substrate and lower initial soil moisture content. Considering runs *Clay01* to *Clay04* and *Sil01* to *Sil04* initially, the greatest loss, as a percentage of total input volume, is 9.3%, associated with simulation *Sil01* (1 in 1 year event;

substrate *Sil(80)*) and the lowest is 3.59% associated with simulation *Clay04* (1 in 5 year event; substrate *Clay(95)*). Where variations in $K_{(sat)}$ are investigated, the greatest loss is associated with simulation *Sil05* (substrate *Sil(80+)*) and reaches 49.1% of the total input hydrograph volume. In all cases infiltration losses associated with the input hydrographs are slightly lower than those calculated with reference to the predicted hydrographs (for example, -9.3% compared to -11.0% for simulation *Sil01* (substrate *Sil(80)*). This reflects the relative size of the input and simulated hydrographs.

Simulation code	total input volume (m^3)	difference between simulated output and respective control output (m^3)	% difference (in terms of input hydrograph)
Control01	2205579.8	-	-
Control02	5763319.0	-	-
Clay01	-	148781.9	-6.8
Clay02	-	79934.1	-3.6
Clay03	-	289746.3	-5.0
Clay04	-	206937.8	-3.6
Sil01	-	204827.3	-9.3
Sil02	-	156258.2	-7.1
Sil03	-	495910.7	-8.6
Sil04	-	433563.9	-7.5
Clay05		627012.0	-28.4
Clay06		52114.7	-2.4
Clay07	-	569115.7	-25.8
Clay08	-	19316.2	-0.9
Sil05	-	1083510.6	-49.1
Sil06	-	48464.7	-2.2
Sil07		1062848.2	-48.2
Sil08		23621.1	-1.1

Table 6.4 Table of results in which total volume lost through infiltration is expressed as a percentage of the total volume input

(ii) Time to peak discharge (m^3s^{-1}): Time to predicted peak discharge is the criterion by which model calibration is most usually assessed, thus changes in this feature of model behaviour have far reaching implications for model use. The following analysis first considers those simulations in which average $K_{(sat)}$ values were used and secondly, those in which $K_{(sat)}$ was increased and then decreased by an order of magnitude. The results relating to time to peak for the simulations undertaken in this analysis are presented in Table 6.3.

Considering simulations *Clay01* to *Clay04* and *Sil01* to *Sil04* initially, infiltration loss has a minimal effect on time to peak in all cases resulting in a maximum effect of +340 seconds (+0.53 %) for simulation *Sil03* (1 in 5 year event; substrate *Sil(80)*). For the two 1 in 1 year simulations *Clay01* (substrate *Clay(80)*) and *Clay02* (substrate *Clay(95)*) no difference in time to peak was

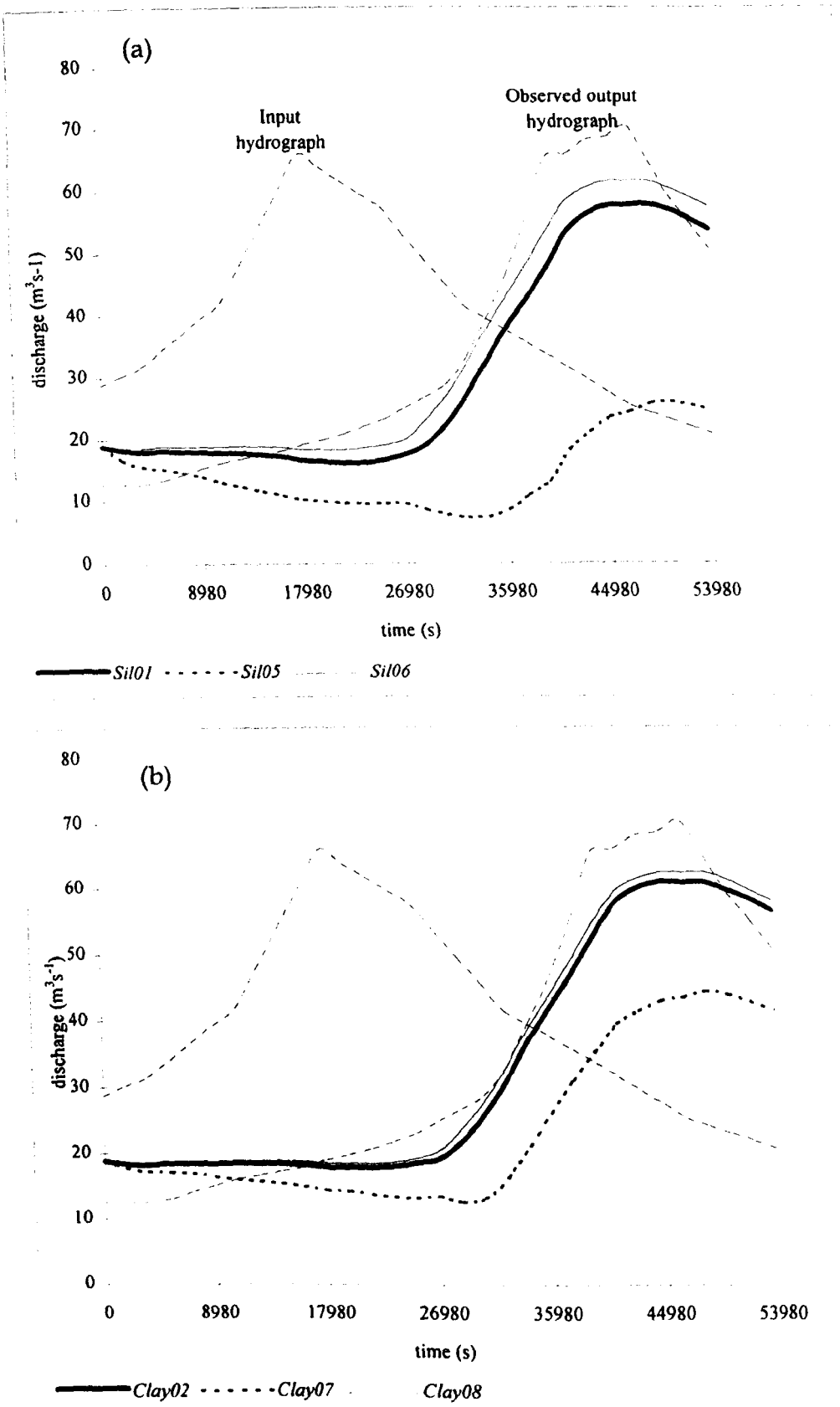

Figure 6.2 Culm 1 in 1 year simulation with relaxed surface boundaries showing the effect of variability in the hydrology model parameter $K_{(sat)}$ on predicted hydrograph charateristics. (a) illustration of the input hydrograph, observed output hydrograph and simulated output hydrographs for simulations *Sil01*, *Sil05* and *Sil06*. (b) illustration of the input hydrograph, observed output hydrograph and simulated output hydrographs for simulations *Clay02*, *Clay07* and *Clay08*.

observed when compared to their corresponding control simulation (*Control01*). For the corresponding runs on the silty loam substrate, *Sil01* (substrate *Sil(80)*) and *Sil02* (substrate *Sil(95)*) the resulting difference was marginal, amounting to 20 seconds for both. For the 1 in 5 year event the greatest effect was +340 seconds for simulation *Sil03* (substrate *Sil(80)*) and the smallest change, 180 seconds, was associated with simulation *Clay04* (substrate *Clay(95)*).

A comparison of the two flood events illustrates that while the overall differences are minimal, for corresponding simulations they are greater for the larger flood event, thus the increase in time to peak for simulation *Sil03* (1 in 5 year event; substrate *Sil(80)*) is greater than that for simulation *Sil01* (1 in 1 year event; substrate *Sil(80)*) while that for simulation *Clay03* (1 in 5 year event; substrate *Clay(80)*) exceeds that of simulation *Clay01* (1 in 1 year event; substrate *Clay(80)*). For the Culm 1 in 1 year event initial soil moisture content has no discernible effect upon time to peak however, for the Culm 1 in 5 year event, time to peak is found to increase with decreasing initial soil moisture content. Thus an increase in time to peak of 0.31% for simulation *Clay03* (substrate *Clay(80)*) compares to an increase of 0.28% for simulation *Clay04* (substrate *Clay(95)*) while an increase in time to peak discharge of 0.53% for simulation *Sil03* (substrate *Sil(80)*) compares to an increase of 0.50% for simulation *Sil04* (substrate *Sil(95)*). However, none of these differences are significant.

The pattern observed for the 1 in 5 year event is more evident than that for the 1 in 1 year event. For the 1 in 5 year event both an increase in $K_{(sat)}$ and a decrease in the initial soil moisture content results in an increase in time to peak discharge. For the 1 in 1 year event an increase in time to peak discharge results only from an increase in $K_{(sat)}$. However, the results do illustrate that an increase in the potential infiltration rate (resulting from an increase in $K_{(sat)}$ and, for the 1 in 5 year event, a decrease in initial soil moisture content) increases the extent to which the flood wave is attenuated which results in an increase in the time to the simulated peak discharge. The lack of model response to initial soil moisture content observed for the 1 in 1 year event must derive from the character of the flood wave and its interaction with the floodplain soils. It might be expected that the greatest attenuation of the flood wave occurs where water is moving onto previously non-inundated areas where hydraulic gradients are greatest. The loss of water will therefore be enhanced where initial soil moisture conditions are lower. However, Figure 5.6 suggests that such an explanation cannot be used to explain the observed lack of model response to lower initial soil moisture observed for the 1 in 1 year event as the initial condition simulation for this event leaves the floodplain less inundated than that of the 1 in 5 year event. Nevertheless, the lack of model response to initial soil moisture content observed for the 1 in 1 year event must derive from the character of the flood wave and its interaction with the floodplain soil.

Increasing $K_{(sat)}$ has a more marked effect upon time to peak for both the Silty loam and Clay substrates. Again, the results relate to the 1 in 1 year event and only the two substrate conditions which generate the extremes in model response are considered. Comparing runs *Clay07* (substrate *Clay(95+)*), *Clay08* (substrate *Clay(95-)*), *Sil05* (substrate *Sil80+)*) and *Sil06* (substrate *Sil(80-)*) shows a marked effect upon the time to peak for both the silty loam and clay soils where $K_{(sat)}$ is increased by one order of magnitude. This effect is greatest for the Silty loam substrate and amounts to 3080 seconds (0.855hr) for simulation *Sil05* (substrate *Sil(80+)*) and 1040 seconds (0.28hrs) for simulation *Clay07* (substrate *Clay(95+)*). The explanation for these results is the same as that given for those simulations run with mean $K_{(sat)}$ parameter values. The phase difference for the calibrated 1 in 1 year Culm event is 460 seconds (0.127 hrs) (see Table 5.3). The need for possible recalibration is considered further in section 6.3.1.1. Where $K_{(sat)}$ is increased by an order of magnitude for both the clay and silty loam soils, no difference in time to peak is recorded when compared to the corresponding control simulation.

(iii) Peak discharge (m^3s^{-1}): Peak discharge is reduced in all simulations run with infiltration. The following analysis first considers those simulations in which average $K_{(sat)}$ values were used and secondly, those in which $K_{(sat)}$ is varied. The results relating to peak discharge for the simulations undertaken in this analysis are presented in Table 6.3.

Considering runs *Clay01* to *Clay04* and *Sil01* to *Sil04* first, the greatest reduction in peak discharge is associated with the silty loam soil, where, for example, for the 1 in 1 year event a difference of -6.77% for simulation *Sil01* (substrate *Sil(80)*) compares to a difference of -3.04% for simulation *Clay01* (substrate *Clay(80)*). A similar pattern is found for the 1 in 5 year event where a difference of -3.94% for simulation *Sil03* (substrate *Sil(80)*) compares to -1.59% for simulation *Clay04* (substrate *Clay(80)*). The influence of initial soil moisture content is not apparent in any of the Culm 1 in 1 year simulations, but in the 1 in 5 year simulations decreasing initial soil moisture content results in a lowering of the peak volume discharge where a reduction in total peak discharge for simulation *Sil03* (substrate *Sil(80)*) of -3.94% compares to -3.75% for simulation *Sil04* (substrate *Sil(95)*) and a reduction of -1.59 for simulation *Clay04* (substrate *Clay(95)*) compares to a reduction of -3.75 for simulation *Sil04* (substrate *Sil(95)*). The results for peak discharge are broadly consistent with expected pattern with the model illustrating greater sensitivity to the silty loam than the clay and, for the 1 in 5 year Culm event, sensitivity increases with decreasing initial soil moisture. However, no difference in peak discharge between the two initial soil moisture contents was found for the Culm 1 in 1 year events. The same explanation can be offered to describe the observed reduction in peak discharge as was given to describe the retardation in time to peak

discharge in the previous section. As the potential for infiltration increases so does the reduction in simulated peak discharge. Again, while this is clearly observed in the four 1 in 5 year simulations, for the 1 in 1 year simulations it is true only for $K_{(sat)}$. A similar explanation can be given to account for the observed lack of model sensitivity to changes in initial soil moisture content for the 1 in 1 year runs as has been given previously.

Runs *Clay07* and *Sil05* illustrate the impact of increasing $K_{(sat)}$ on the peak volume which for simulation *Clay07* (substrate *Clay(95+)*) is reduced by 29.89% and 59.08% for simulation *Sil05* (substrate *Sil(80+)*).

The results of this first part of the analysis, in which aspects of the predicted flood hydrograph are considered demonstrate that infiltration has little effect upon hydrograph peak timing but can result in significant effects upon total flow volume and the magnitude of the discharge peak. In all cases, the maximum effect is associated with the substrate most amenable to infiltration, the silty loam at 80% initial saturation.

The effect of infiltration on time to peak is of particular significance given the role of this parameter in model calibration (see *Chapter 5*, section 5.3). While the effect is minimal for those simulations in which 'average' $K_{(sat)}$ values are considered generating a maximum effect of +340 seconds for simulation *Sil03* (1 in 5 year event on substrate *Sil(80)*) the effect is considerably greater where $K_{(sat)}$ is increased by an order of magnitude. The acceptable phase error in time to peak will be dictated according to the particular study. The errors in time to peak associated with the two control simulations used in this study were 460 seconds (0.98%) for the 1 in 1 year event and 4320 seconds (7.3%) for the 1 in 5 year event. Although large, the error associated with the 1 in 5 year event was deemed acceptable given the aims of this research in which relative effects are considered. If, as a bench mark, an error of plus or minus one hour is assumed then none of the simulations performed for this analysis require recalibration. The maximum peak time shift is 3080 seconds which falls short of the necessary shift required for recalibration.

An indication of the significance of infiltration induced changes in peak predicted discharge can be gained from a comparison of the results in this study with those obtained from a study into the impact of mesh resolution and the type of numerical solver on model prediction using the Culm 1 in 1 year recurrence interval flood event used in this study. An increase in mesh resolution from 2019 elements (as in the mesh used in this study) to 9800 elements has been found to increase the predicted flow of the control simulation (Figure 5.4) by 2.9%. This compares to an increase in peak

discharge which ranges from -3.04% for simulations *Clay01* and *Clay02* (substrates *Clay(80)* and *Clay(95)*) to -6.77% for simulations *Sil01* and *Sil02* (substrates *Sil(80)*) and *Sil(95)*). Only marginal effects, smaller than those reported for the increase in mesh resolution, were found for a change in the solver technique used (Bates *et al.* (1996). The potential magnitude of the effects suggests that the relaxation of the surface boundary can be an important control on model prediction generating results which are comparable with the need to refine numerical solution techniques and mesh discretization which currently occupies a key component of research into flood inundation prediction (see for example Molinaro and Natale, 1994).

However, while the effects of infiltration are significant in the context of changes to hydrograph characteristics generated by changes in mesh resolution and solver techniques, such effects are subsumed within inaccuracies inherent in flood flow measurement. In *Chapter 5* the errors associated with the stage records at Rewe were discussed and it was suggested that these could be 10% at best for in bank and over 20% for out-of-bank flood flows. Where such errors persist it is therefore not possible to quantitatively assess the impact that infiltration has on model prediction in terms of the predicted output hydrograph. By ignoring infiltration this process has been accounted for in the calibration procedure. Thus, these results illustrate a potentially significant deficiency in model process representation which requires, under certain environmental conditions, inclusion in a physically based model such as TELEMAC2D.

Where variations in $K_{(sat)}$ are considered the effects are correspondingly magnified or reduced. In all cases where $K_{(sat)}$ was increased the discussion above applies except that the magnitude of the effects are increased. This is evident in the results.

6.3.2 The effect of infiltration on the storage of surface water

In this section the loss of surface water through infiltration is examined in terms of its effect on: (i) the volume of floodplain surface water during each event and (ii) timing to the peak domain water volume. The results are presented in Table 6.5 and Figures 6.3 and Figure 6.4.

(i) Volume in domain:

The volume of surface water in the domain at any one time during the course of a simulation is lower in those simulations with a relaxed surface boundary. The following analysis first considers those simulations in which average $K_{(sat)}$ values were used and secondly, those in which $K_{(sat)}$ was increased and then decreased by an order of magnitude. The results relating to volume in the domain for the simulations undertaken in this analysis are presented in Table 6.5.

Simulation code	total mass in domain	difference (%)	time to peak (s)	difference (%)	peak volume (m^3)	difference (%)
Control01	$7.28x10^{11}$	-	35798	-	1754000.3	-
Control02	$1.95x10^{12}$	-	55018	-	2627569.6	-
Clay01	$7.09x10^{11}$	-2.8	36378	+1.6	1710524.9	-2.48
Clay02	$7.18x10^{11}$	-1.5	35958	+0.4	1729079.0	-1.42
Clay03	$1.92x10^{12}$	-1.6	55058	+0.02	2602209.2	-0.97
Clay04	$1.93x10^{12}$	-1.1	55038	+0.01	2606769.7	-0.79
Sil01	$7.08x10^{11}$	-3.8	36138	+0.9	1688832.0	-3.72
Sil02	$7.01x10^{11}$	-2.9	35918	+0.3	1700852.0	-3.03
Sil03	$1.895x10^{12}$	-2.7	55038	+0.01	2578361.7	-1.87
Sil04	$1.90x10^{12}$	-2.4	55018	0.0	2580814.8	-1.78
Clay05	$6.39x10^{11}$	-12.3	36678	+2.4	1529759.6	-12.78
Clay06	$7.22x10^{11}$	-1.0	36018	+0.6	1739907.1	-0.8
Clay07	$6.49x10^{11}$	-11.0	35918	+0.3	1545544.5	-11.88
Clay08	$7.26x10^{11}$	-0.4	35879	+0.2	1748277.0	-0.33
Sil05	$5.56x10^{11}$	-23.7	35658	-0.4	1292845.7	-26.29
Sil06	$7.22x10^{11}$	-0.9	35878	+0.2	1738745.6	-0.87
Sil07	$5.61x10^{11}$	-23.1	35718	-0.2	1317181.0	-24.9
Sil08	$7.26x10^{11}$	-0.4	35878	+0.2	1746359.6	-0.44

Table 6.5 Table of results relating to volume in the domain, time to peak domain volume and peak domain volume.

A consideration of runs *Clay01* to *Clay04* and *Sil01* to *Sil04* shows the greatest reduction in floodplain surface water volumes over the range of soil conditions tested to be associated with the 1 in 5 year events, which is consistent with the findings reported in section 6.3.1 for the flood hydrograph volumes and is expected given the larger total volume of water passing through the floodplain system (see *Chapter 5*, Table 5.3). Similarly, where these losses are presented relative to their respective control simulations, the greatest differences are then found to be associated with the Culm 1 in 1 year event with a maximum of -3.8% for simulation *Sil01* (substrate *Sil(80)*) and a minimum of -1.1% for simulation *Clay04* (1 in 5 year event; substrate *Clay(95)*). The results are again consistent with the expected greater volumetric losses associated with the silty loam substrate and lower initial soil moisture contents. For example, for the 1 in 1 year event a loss of -3.8% for simulation *Sil01* (substrate *Sil(80)*) compares to a loss of -2.8% for simulation *Clay01* (substrate *Clay(80)*) and for the 1 in 5 year event a reduction of -2.7% for simulation *Sil03* (substrate *Sil(80)*) compares to a loss of -1.6% for simulation *Clay03* (substrate *Clay(80)*). The following order of sensitivity can be established where *Sil01>Sil02>Clay01>Clay02* & *Sil03>Sil04>Clay03>Clay04*. The pattern identified in section 6.3.1 in which the curves depicting discharge volume for *Clay(80)* and *Sil(95)* transect is also identifiable in Figure 6.3(a&b) and can be explained according to the same mechanisms.

Increasing $K_{(sat)}$ has a marked effect upon the volume in the domain for both the Silty loam and Clay substrates. The discussion presented here relates to the 1 in 1 year event and to the two substrate conditions which have been shown to generate the extremes in model response (see section 6.3.1). A comparison of runs *Clay07* (substrate *Clay(95+)*), *Clay08* (substrate *Clay(95-)*), *Sil05* (substrate *Sil(80+)*) and *Sil08* (substrate *Sil(80-)*) illustrates a marked effect upon the mass of surface water for both the silty loam and clay soils where $K_{(sat)}$ is increased by one order of magnitude. This effect is greatest for the Silty loam substrate and amounts to -23.7% for simulation *Sil05* (substrate *Sil(80+)*) and -11.0% for simulation *Clay07* (substrate *Clay(95+)*). Where $K_{(sat)}$ is decreased by an order of magnitude for both the clay and silty loam soils the losses are smaller than those for their corresponding 'mean parameter' runs (*Clay02* and *Sil01*).

(ii) Timing of the maximum volume in the domain:

The effect that infiltration confers upon the timing of the peak domain surface water volume is discussed first with reference to those simulations in which average values of $K_{(sat)}$ are employed and secondly to those where $K_{(sat)}$ is varied. The results, presented as time to peak and percentage difference in time to peak, calculated with reference to the respective control runs, are presented in Table 6.5.

Considering runs *Clay01* to *Clay04* and *Sil01* to *Sil04* the time to peak volume is observed to increase through the effects of infiltration in all cases but one (*Sil04*; 1 in 5 year event, substrate *Sil(95)*). The increase is inversely related to both $K_{(sat)}$ and initial soil moisture content (thus the increase in time to peak is observed to increase with lower $K_{(sat)}$ values and lower initial soil moisture values). For example, for the 1 in 1 year event, an increase in time to peak of +1.6% (580s) for simulation *Clay01* (substrate *Clay(80)*) compares to an increase of +0.9% (340s) for simulation *Sil01* (substrate *Sil(80)*) while the increase of +1.6% for simulation *Clay01* compares to an increase of +0.4% (160s) for simulation *Clay02* (substrate *Clay(95)*). The greatest increase is associated with the 1 in 1 year simulation *Clay01* (substrate *Clay(80)*) while no difference is registered for the 1 in 5 year simulation *Sil04* (substrate *Sil(95)*). The results illustrate that infiltration results in only small shifts in the timing of the peak surface water storage volume.

The results for this first series of simulations demonstrate that as the opportunity for infiltration increases, through an increase in $K_{(sat)}$ and a decrease in initial soil moisture saturation, the positive shift in the timing of the peak volume in the domain decreases.

(a)

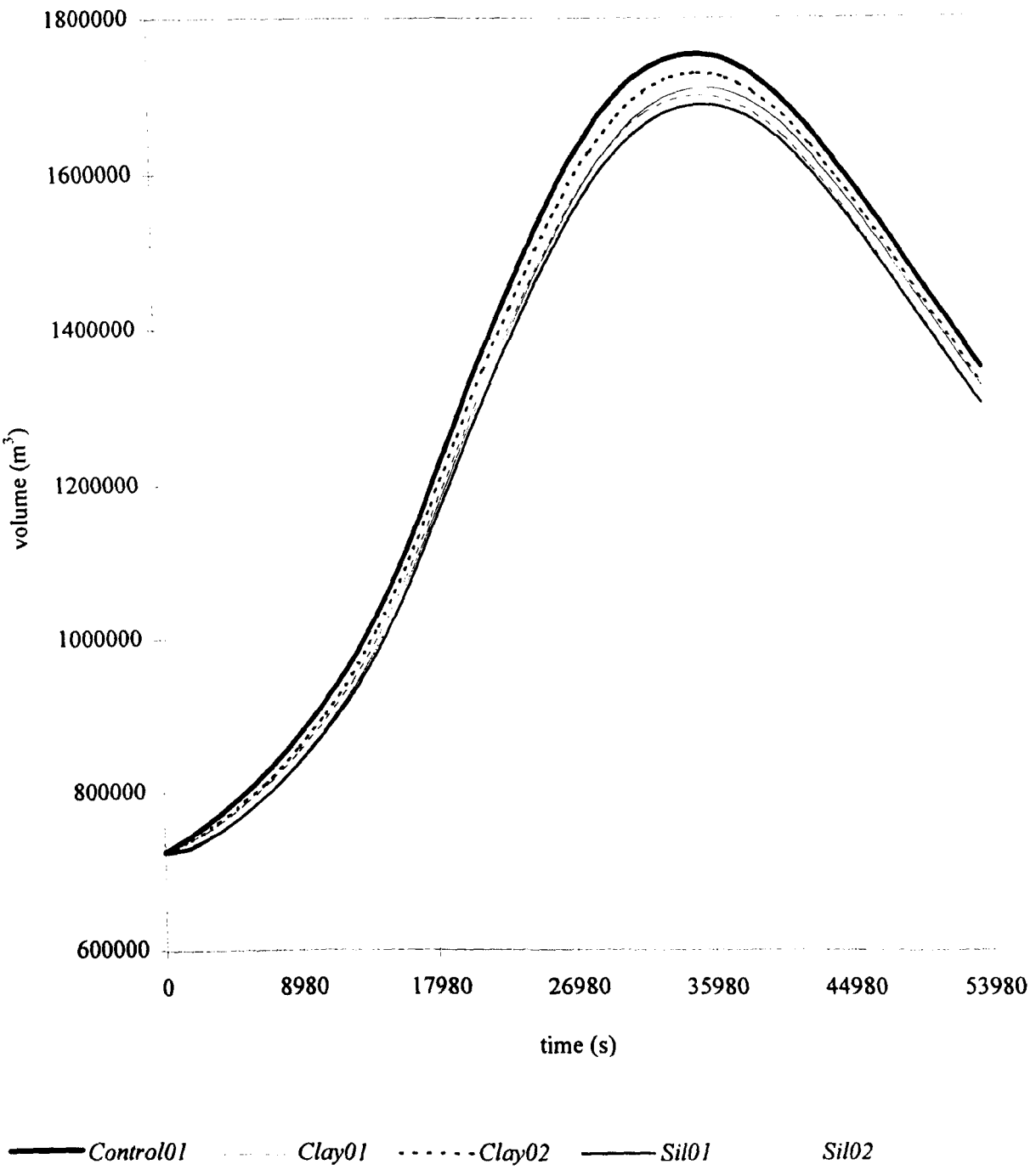

Figure 6.3 Illustration of the impact of infiltration on TELEMAC2D simulated floodplain surface water volume. (a) Culm 1 in 1 year simulations with relaxed surface boundaries showing predicted volume in the domain for simulations *Control01*, *Clay01*, *Clay02*, *Sil01* and *Sil02* (b) Culm 1 in 5 year simulations with relaxed surface boundaries showing predicted volume in the domain for simulations *Control02*, *Clay03*, *Clau04*, *Sil03* and *Sil04*.

(b)

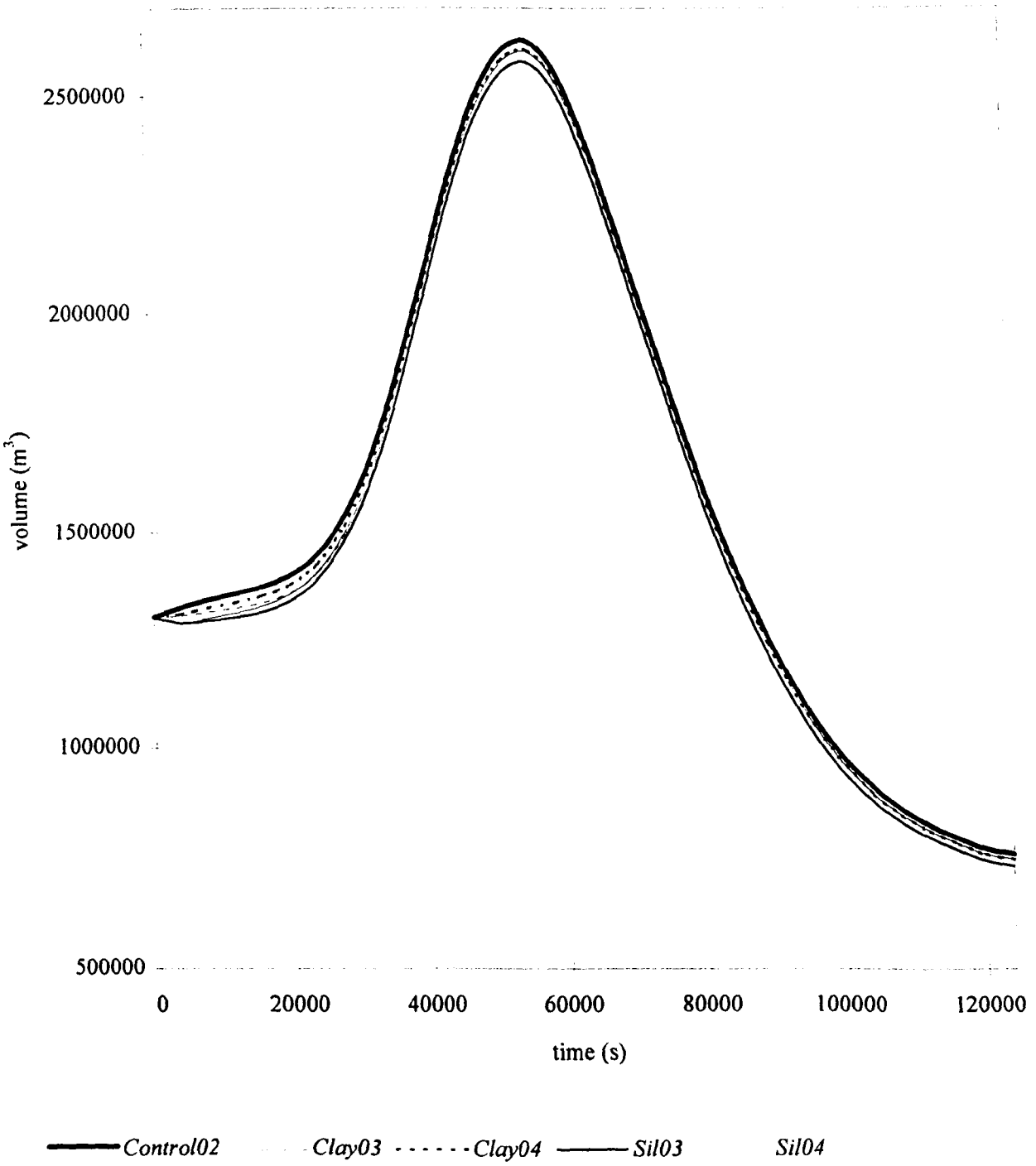

Figure 6.3 (continued)

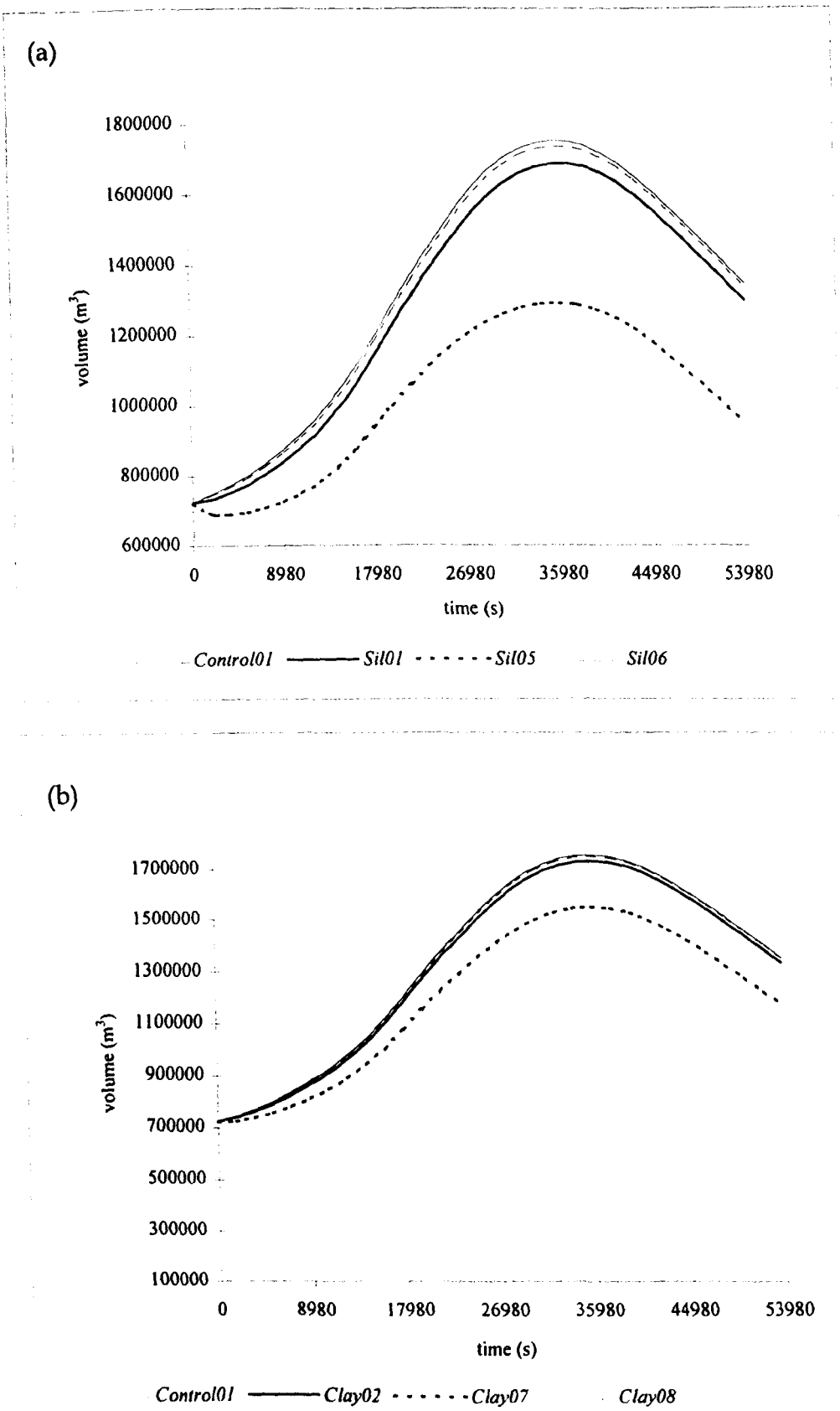

Figure 6.4 Culm 1 in 1 year simulation with relaxed surface boundaries showing the effect of variability in the hydrology model parameter $K_{(sat)}$ on predicted floodplain surface water volume. (a) illustration showing the predicted domain volume for simulations *Control01*, *Sil01*, *Sil05* and *Sil06*. (b) illustration showing the predicted domain volume for simulations *Control02*, *Clay02*, *Clay07* and *Clay08*.

When the results from the simulations in which $K_{(sat)}$ is varied are considered the pattern observed suggests that the mechanisms involved in determining time to volume in domain peak are complex. Indeed, the results from this series of simulations do not conform to the general pattern identified above. These results relate to the 1 in 1 year event only. Where the simulations employing the *Clay(95)* substrate are considered, according to the pattern observed above it might be expected that the shift in peak would be less positive for simulation *Clay07* (*Clay(95+)*) and more positive for simulation *Clay08* (*Clay(95-)*) when compared to simulation *Clay02*. However, in both cases the shift is less positive than that for simulation *Clay02* and is less positive for *Clay08* than *Clay07*. For the Silty loam soil the peak shift is less positive for both simulations *Sil05* (substrate *Sil(80+)*) and *Sil06* (substrate *Sil(80-)*) but here the shift in peak for *Sil05* (*Sil(80+)*) is negative (-0.4%; -140s).

The greatest losses of surface water volume are associated with the silty loam substrate at 80% initial saturation and amount to -3.8% for the 1 in 1 year event and -2.7% for the 1 in 5 year event. The changes in time to peak for all simulations, including those in which $K_{(sat)}$ is increased, are small, however, the results suggest that the controls determining the timing of the peak surface water domain volume and, indeed, the pattern of surface water volume during an event are complex.

Time to peak floodplain surface water storage is determined by the balance between the domain (floodplain) inputs and outputs which are easy to define for the control simulations where the volume of water in the domain increases where inputs exceed outputs and decreases where outputs exceed inputs. The inputs and outputs being well defined as the input and output hydrographs. Where infiltration represents an additional loss to the system the balance between input and outputs as defined by the control case is no longer valid. An additional factor must be considered; that of the reduction in the volume in the domain itself. A reduced output discharge will act to shift the peak to the right (positive) as input (which is not affected) remains greater than output for longer. However, as it is volume in the domain which is being considered here, there will be an effect on this mass brought about by infiltration which is occurring over the whole domain surface area and this will act to reduce the volume in the domain over the whole area. Where this effect is greater than the effect of reduced output, the peak will shift less to the right and indeed, under some circumstances, might even shift to the left. This appears to be the result of simulation *Sil07* where the timing of the peak shifts to the left decreasing the time to peak surface water volume by 140 seconds.

6.3.3 Effect of infiltration on mean water depth

In the following section the effect of infiltration on mean surface water depth is considered.

The results are presented as the difference between water depths for simulations run with relaxed surface boundaries and their respective control simulations. This is necessary given the small differences in mean water depth between the various simulations. The results are presented in Figure 6.5 for the Culm 1 in 1 and 1 in 5 year events.

For the 1 in 1 year Culm event the difference in recorded mean water depth associated with simulation *Sil01* (substrate *Sil(80)*) is consistently greater than the other three simulations for all but the initial part of the simulation. The maximum single difference recorded reaching 0.023m at 28000 seconds. Conversely, the difference in recorded mean water depth associated with simulation *Clay02* (substrate *Clay(95)*) remains consistently lower than the other three simulations in this series. The curves for simulations *Sil02* (substrate *Sil(95)*) and *Clay01* (substrate *Clay(80)*) intersect between 34000 and 36000 seconds, initially the curve for simulation *Sil02* lies below that of simulation *Clay01* (ie the difference in mean water depth is initially lower for simulation *Sil02* than for simulation *Clay01*). Again, this is consistent with the pattern observed for both the predicted discharge hydrograph (section 6.3.1) and the volume of water in the domain and can be explained according to the same mechanisms. A similar pattern is observed for the 1 in 5 year event.

For both events the general pattern observed is of an increasing difference in mean water depth which peaks and then diminishes. For both flood events the initial increase in the difference in mean water depth is greatest for the two soils at 80% initial saturation but as the simulation proceeds the effect of initial soil moisture saturation diminishes and the curves representing the same soil types converge, this is especially evident for the Culm 1 in 5 year simulations (see Figure 5.6(b)) and is a result of the longer duration of these simulations.

The greatest difference in mean water depth is associated with the silty loam substrate at 80% initial saturation for both events while the smallest is associated with the Clay substrate at 95% initial saturation. These results are consistent with those found earlier with maximum volumetric losses being associated with the silty loam at a lower initial soil moisture content. The maximum difference in mean water depths (derived through the comparison of each simulation and its respective control) might be expected to coincide with the rising limb of the hydrograph when water is spilling onto the floodplain and the potential for infiltration is at its greatest. Figure 6.6, in which the difference in mean water depth for the silty loam substrate at 80% initial saturation is plotted together with the curve depicting the total volume in the domain for both events, supports this suggestion. The greatest difference is concurrent with increasing surface water volume but the greatest difference peaks prior to the peak in surface water. This is to be expected as the greatest

effects will result when both infiltration potential and the potential for an increase in inundated area are at their greatest.

(a)

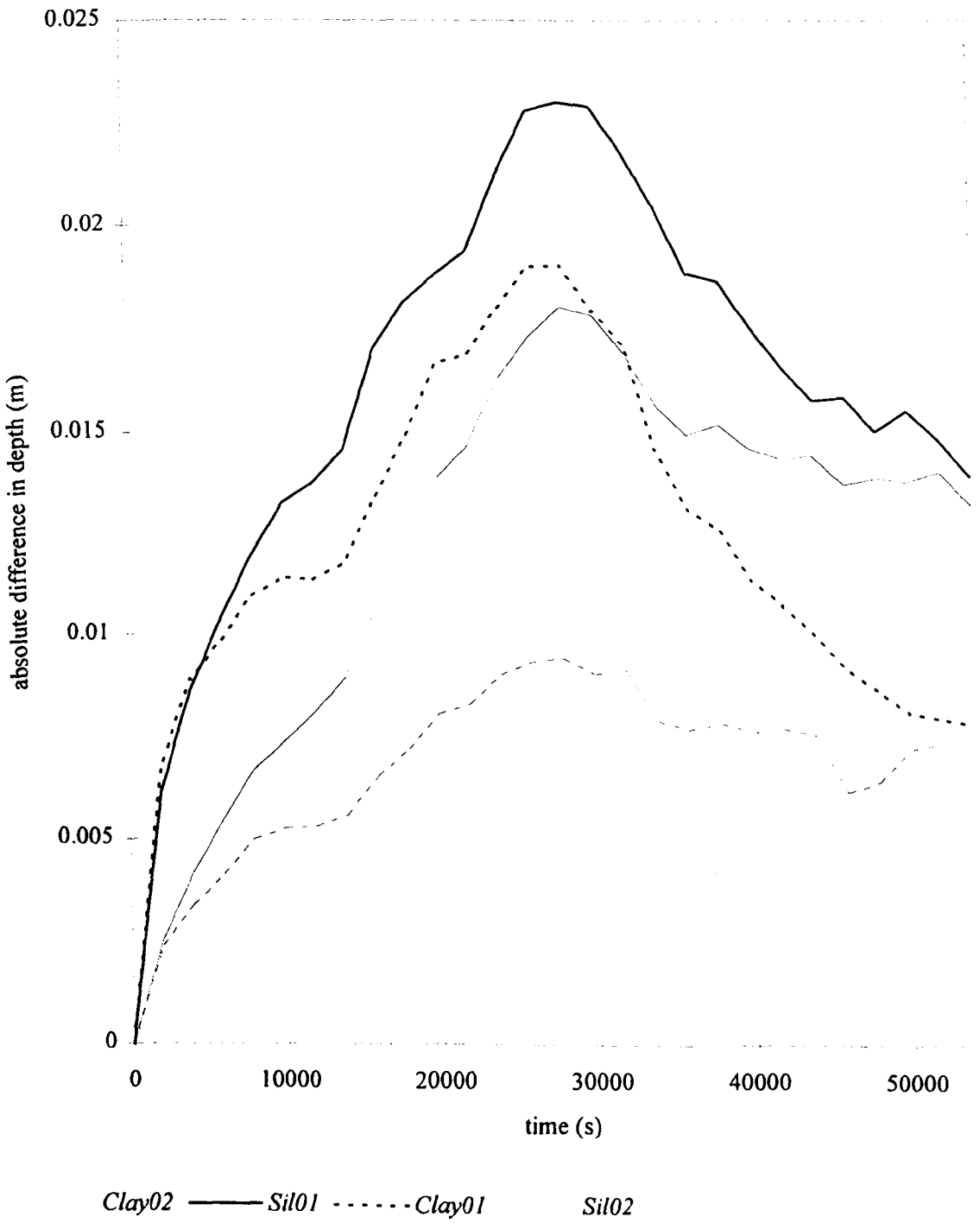

Figure 6.5 Illustration of the impact of infiltration on predicted mean surface water depth. (a) difference in the mean water depth between *Control01* and simulations *Clay01, Clay02, Sil01* and *Sil02* for the 1 in 1 year flood event. (b) difference in the mean water depth between *Control02* and simulations *Clay03, Clay04, Sil03* and *Sil04* for the 1 in 5 year flood event

(b)

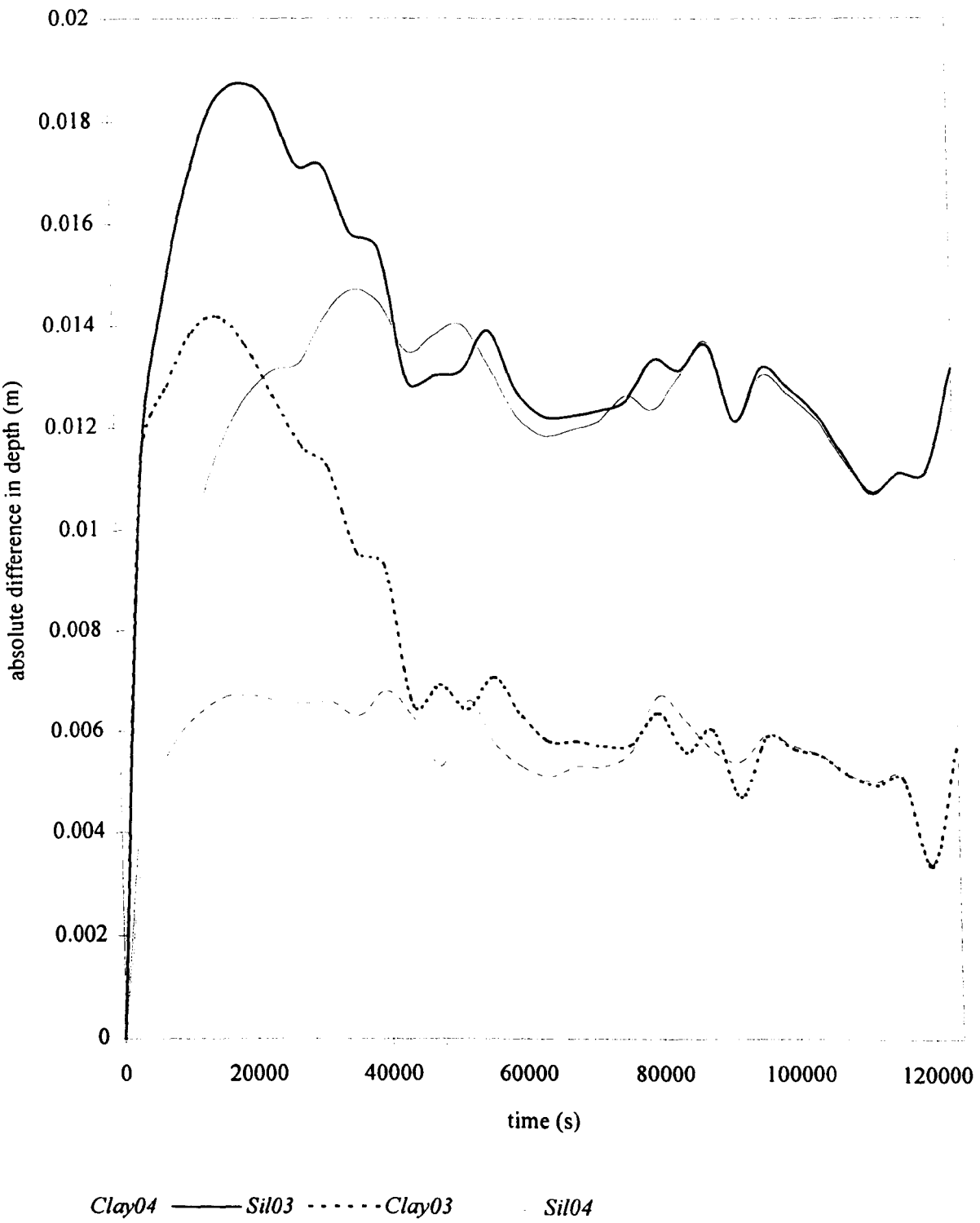

Figure 6.5 (continued)

(a)

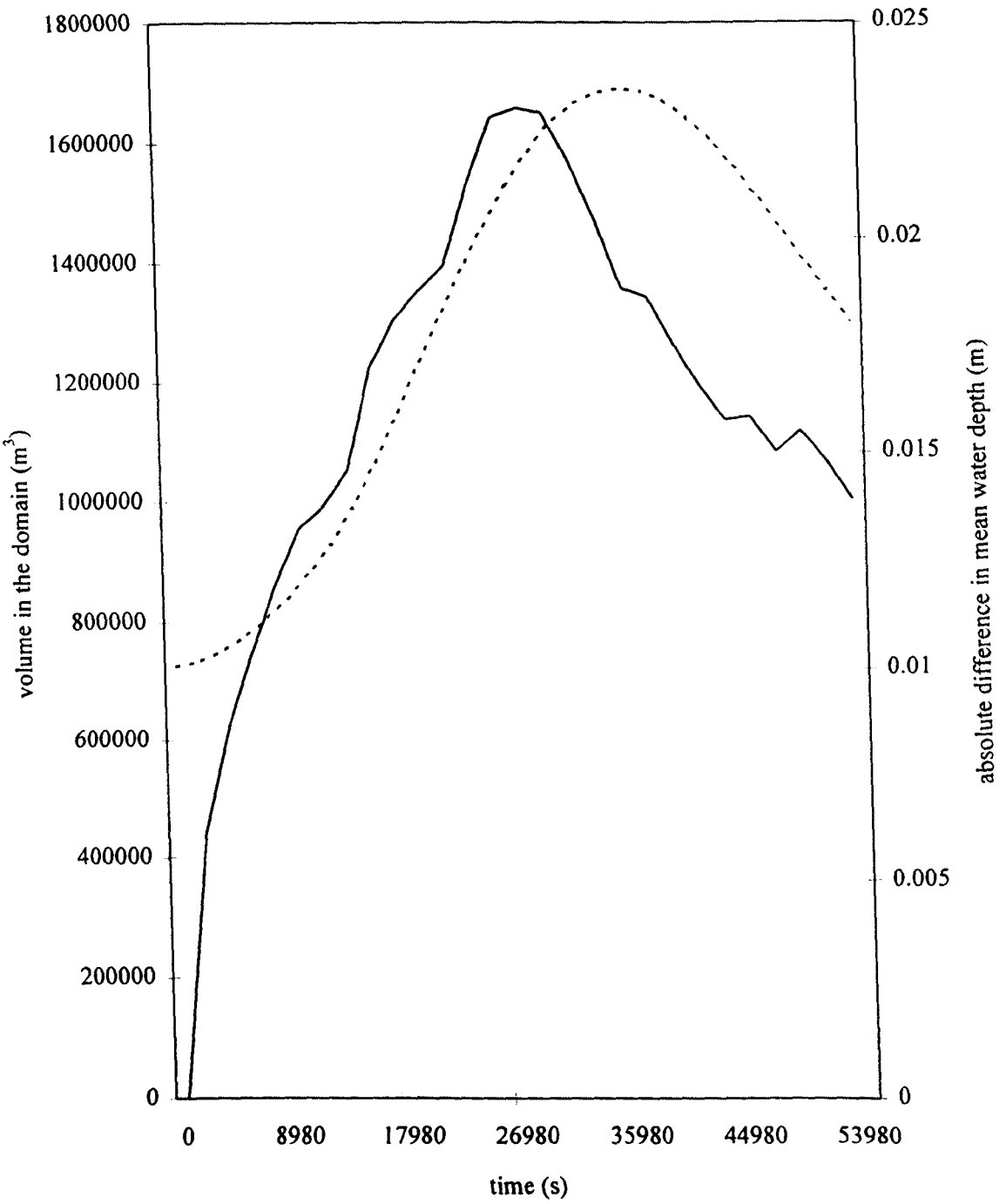

Figure 6.6 (a) Difference in mean water depth between simulations *Control01* and *Sil01* for the 1 in 1 year event illustrated together with the volume in the domain for the same event (b) Difference in mean water depth between simulations Control02 and Sil03 for the 1 in 5 year flood event illustrated together with the volume in the domain for the same event.

(b)

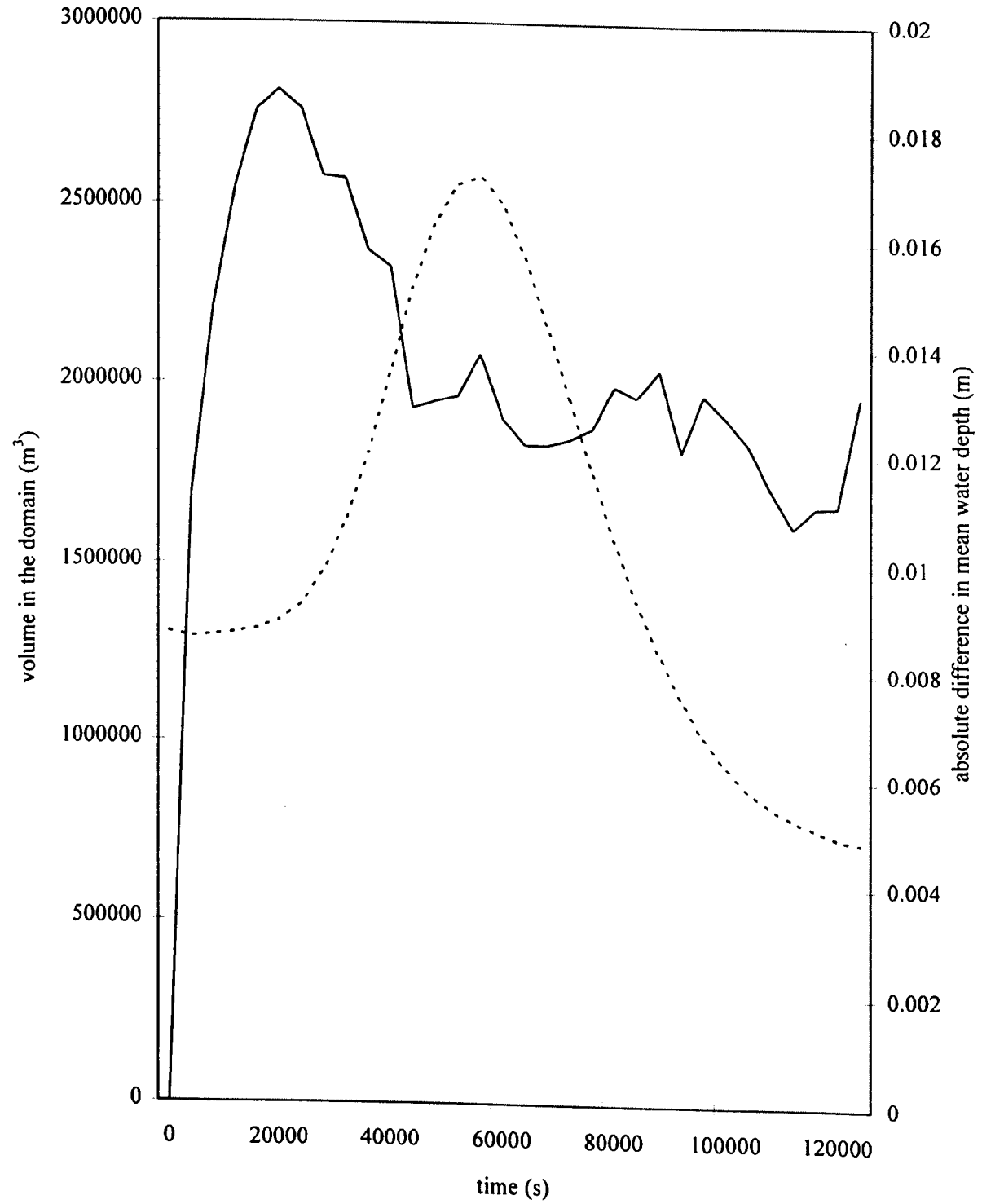

Figure 6.6 (continued)

6.3.4 Effect of infiltration on inundated area

In the following section the effect of infiltration on the predicted inundated area is addressed.

The difference in simulated inundated area between the control simulations and those associated with the substrates which have consistently been shown to provide the greatest range in results, *Sil(80)* and *Clay(95)*, are presented in Figure 6.7 for the 1 in 1 and 1 in 5 year events and in Table 6.6 and Figure 6.8 for selected times during each event.

These simulations were chosen as they represent the two extremes of infiltration potential (eg see Table 6.3) which suggests they will respectively produce the greatest and smallest effect upon floodplain inundation extent. The results illustrate that inundation extent is reduced over the range of conditions tested and that the extent of this reduction is related to the potential for infiltration. For both events illustrated in Figure 6.7 inundation extent for the control simulations remains above that for the test simulations run with infiltration. Inundated area is consistently lower for the simulations run on the *Sil(80)* substrate when compared to those run on the *Clay(95)* substrate although this pattern in reversed on occasion. It is expected that the observed reduction in surface water volume (section 6.3.1) and mean surface water depth (section 6.3.3) will result in a reduction in the extent of inundation and that this will be related to the potential of the floodplain to infiltrate.

simulation code	difference in inundation area after 25% of simulation	difference in inundation area after 50% of simulation	difference in inundation area after 75% of simulation	difference in inundation area after 100% of simulation
Clay02	-0.46	-0.87	-0.32	-1.53
Sil01	-1.46	-2.66	-0.3	-3.16
Clay04	-0.24	-0.35	-0.19	-0.06
Sil03	-5.06	-0.6	-2.66	-0.81

Table 6.6 Inundation extents and infiltration induced differences in inundation extent at five intervals through the simulation for selected 1 in 1 and 1 in 5 year events.

The results in Table 6.6 present a 'snap shot' record of inundation extent during each of the simulations selected at times which represent 25%, 50%, 75% and 100% of the total simulation duration. In each case inundation extent is lower for those simulations run with a relaxed surface boundary when compared to their corresponding control simulation. In all cases but one, (simulation *Clay02* (substrate *Clay(95)*) compared with simulation *Sil01* (substrate *Sil(80)*) at 75% through the simulation), predicted inundation extent is lower for simulations run on the *Sil(80)*

(a)

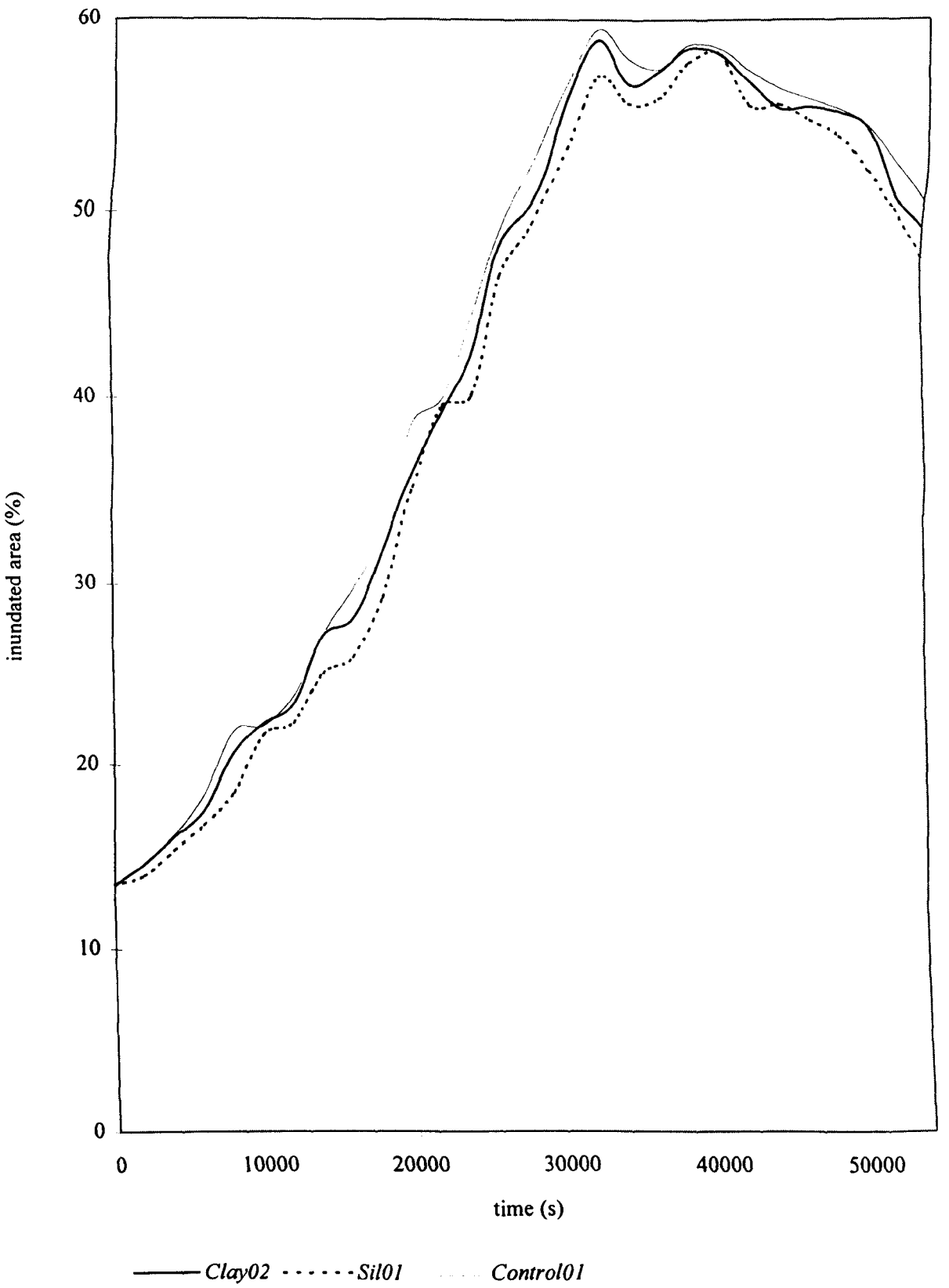

Figure 6.7 Illustration of the impact of infiltration on simulated inundation extent. (a) difference in model simulated inundated area for the 1 in 1 year flood simulations *Sil01* and *Clay02* and the control simulation, *Control01* (b) difference in model simulated inundated area for the 1 in 5 year flood simulations *Sil03* and *Clay04* and the control simulation, *Control02*.

(b)

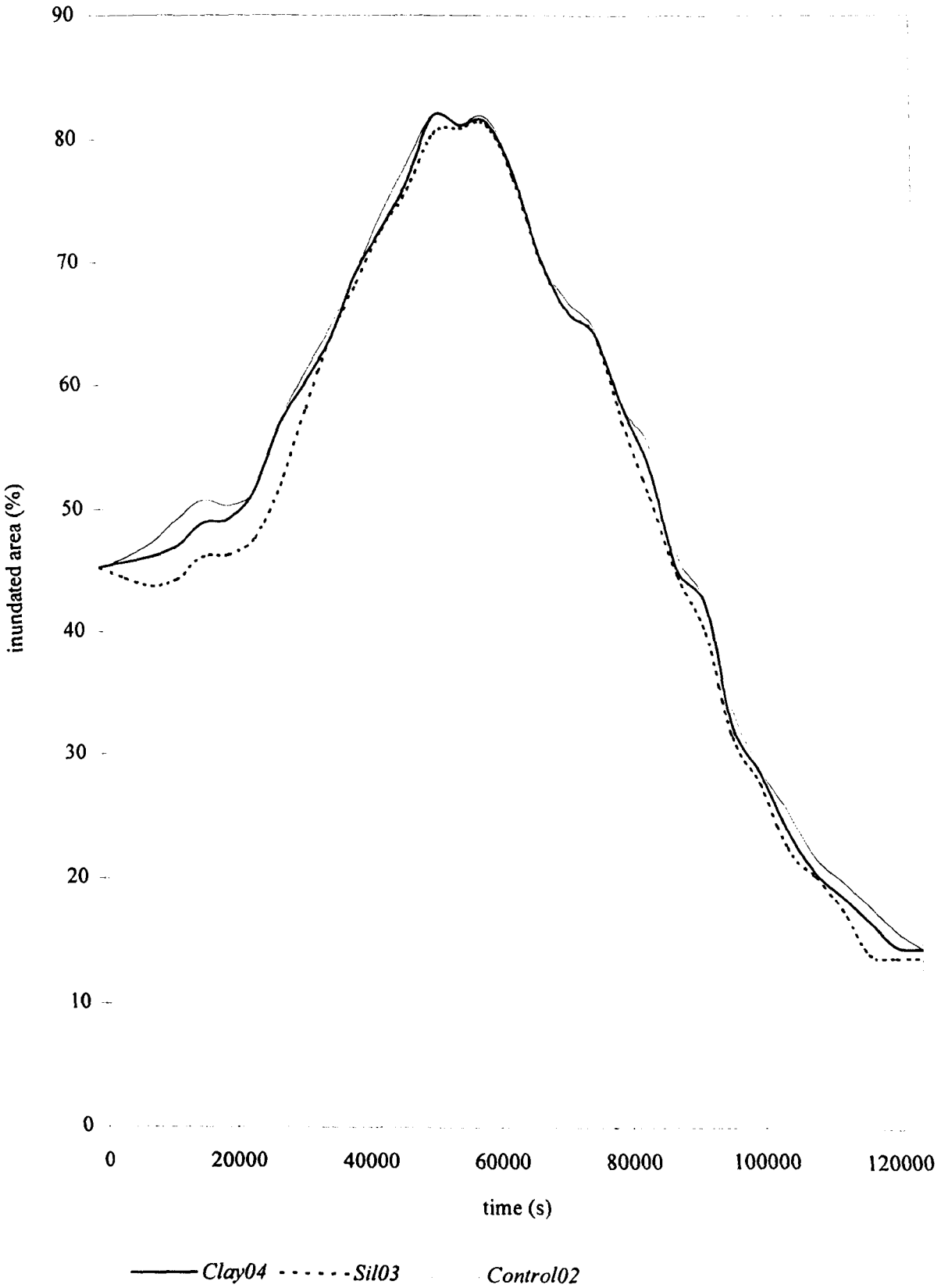

Figure 6.7 (continued)

substrate. The greatest difference (-5.06%) is associated with the 1 in 5 year event after 25% of the run with the *Sil(80)* substrate while the smallest difference (-0.06%) is associated with the same event for the *Clay(95)* substrate at the end of the simulation. The difference in inundation extent between the control simulations and those run on the *Sil(80)* substrate for both events are presented for a selected area of the reach in Figure 6.8 at time intervals during the simulations corresponding to those presented in Table 6.6.

The greatest difference in inundation extent between the control and test simulations is expected to coincide the rising limb of the flood hydrograph when water is moving onto the floodplain and the soils are at their driest. Under these conditions water is most able to infiltrate, driven by the higher gradients in hydraulic potential. The 1 in 5 year event conforms to this pattern (see Figure 6.7(b)) but the 1 in 1 year event exhibits considerable variability. Continuing the argument, the smallest difference in mean water depth might be expected to coincide with the greatest volume of surface water on the floodplain when water is no longer moving onto 'dry' soil with a high capacity for infiltration and what water remains on the floodplain occupies previously inundated areas. Such a pattern is evident in the results presented in both Table 6.6 and Figure 6.7. For the 1 in 1 year event the greatest differences occur at the beginning and end of the simulation while the smallest is at 40000s which compares to a maximum surface water volume at 36138 seconds. For the 1 in 5 year event the greatest difference in inundated area is at the beginning of the simulation and the smallest at 60000s (see Figure 6.7(b)), which compares to a maximum surface water volume at 55038 seconds (see Figure 6.3(b)). Plotting the mean difference in inundation extent against mass in the domain for each of the simulations supports this suggestion, though the pattern is more consistent for the 1 in 5 year event. Plots of the mean difference in inundation extent against mass in the domain for each of the simulations are presented in Figure 6.9.

6.4 Local implications of infiltration on hydraulic model prediction

The analysis presented in 6.3 discusses results which pertain to the behaviour of the floodplain hydraulics in a general sense, but provides no insight into the hydraulic behaviour at single floodplain nodes. The analysis now turns to consider the implication of infiltration on water depth and flow velocities in a 'localised' context, first by choosing two cross-sections across the Culm floodplain reach and then by considering water depth and flow velocity at two nodes from each cross section, one located on the floodplain and the other in the channel. The approach benefits the study in two ways, firstly, through an investigation of the implied assumption that the integrated hydraulic behaviour reported in section 6.3 is indeed a function of the nodal effect and secondly by

considering the relationship between infiltration, water depth and flow velocity on a local scale. Although the integrated hydraulic behaviour represents the sum of the nodal values, it is possible

(a)

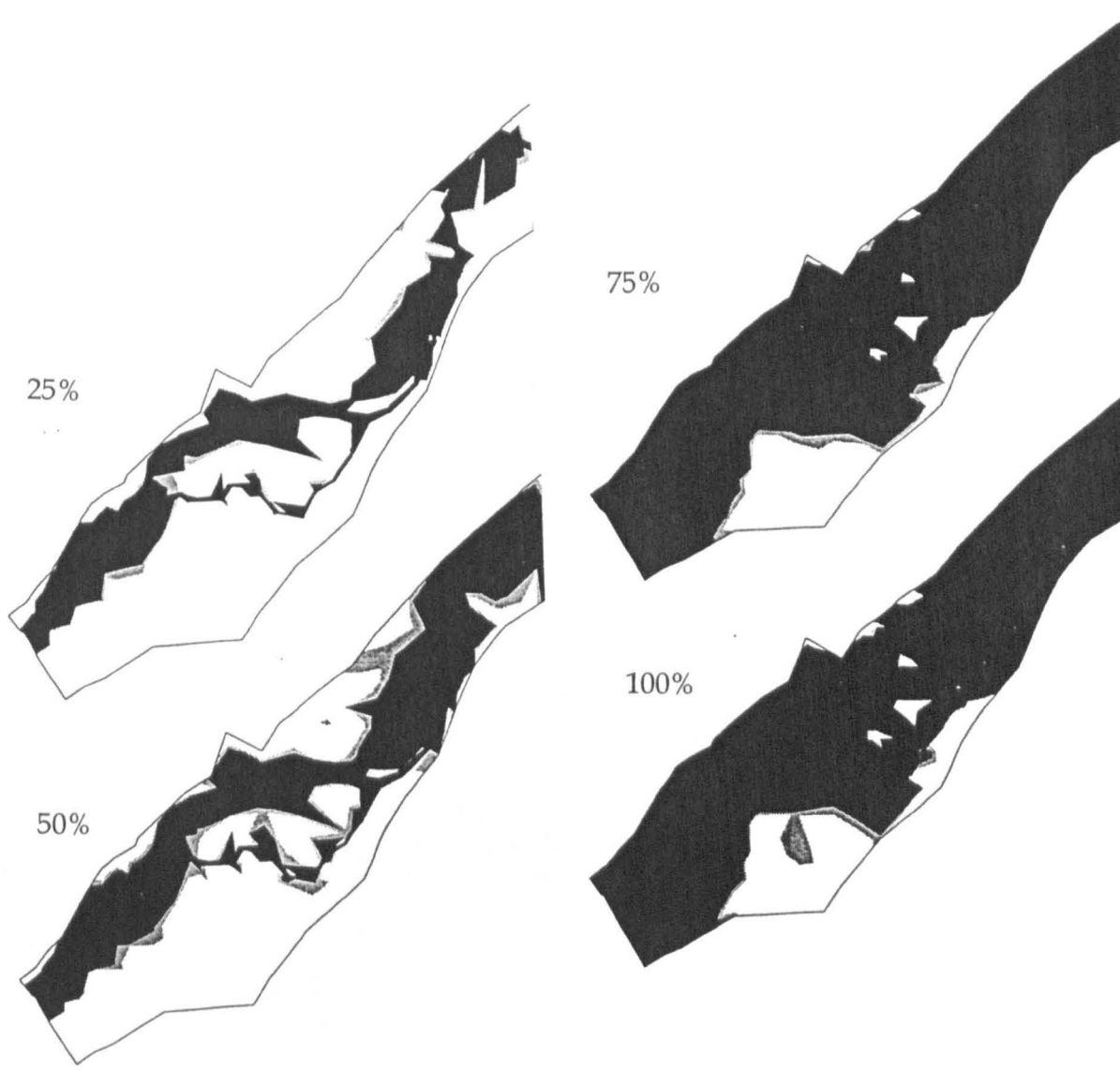

Figure 6.8 (a) Difference in model predicted inundation extent between simulations *Control01* and *Sil01* for the 1 in 1 year event for a section of the River Culm reach at 25%, 50%, 75% and 100% of the simulation run time (b) difference in model predicted inundation extent between simulations *Control02* and *Sil03* for the 1 in 5 year event for a section of the River Culm reach at 25%, 50%, 75% and 100% of the simulation run time. The light grey area represents inundation extent for the control simulations, the black area represents inundation extent for the simulations run with infiltration.

(b)

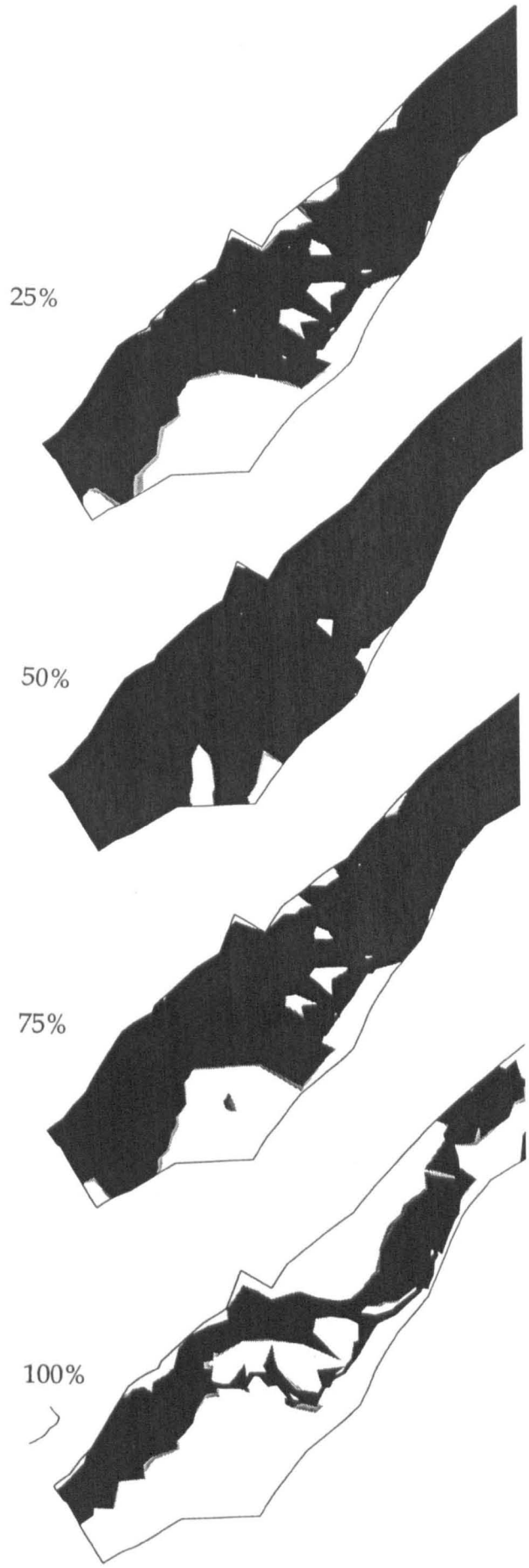

Figure 6.8 (continued)

(a)

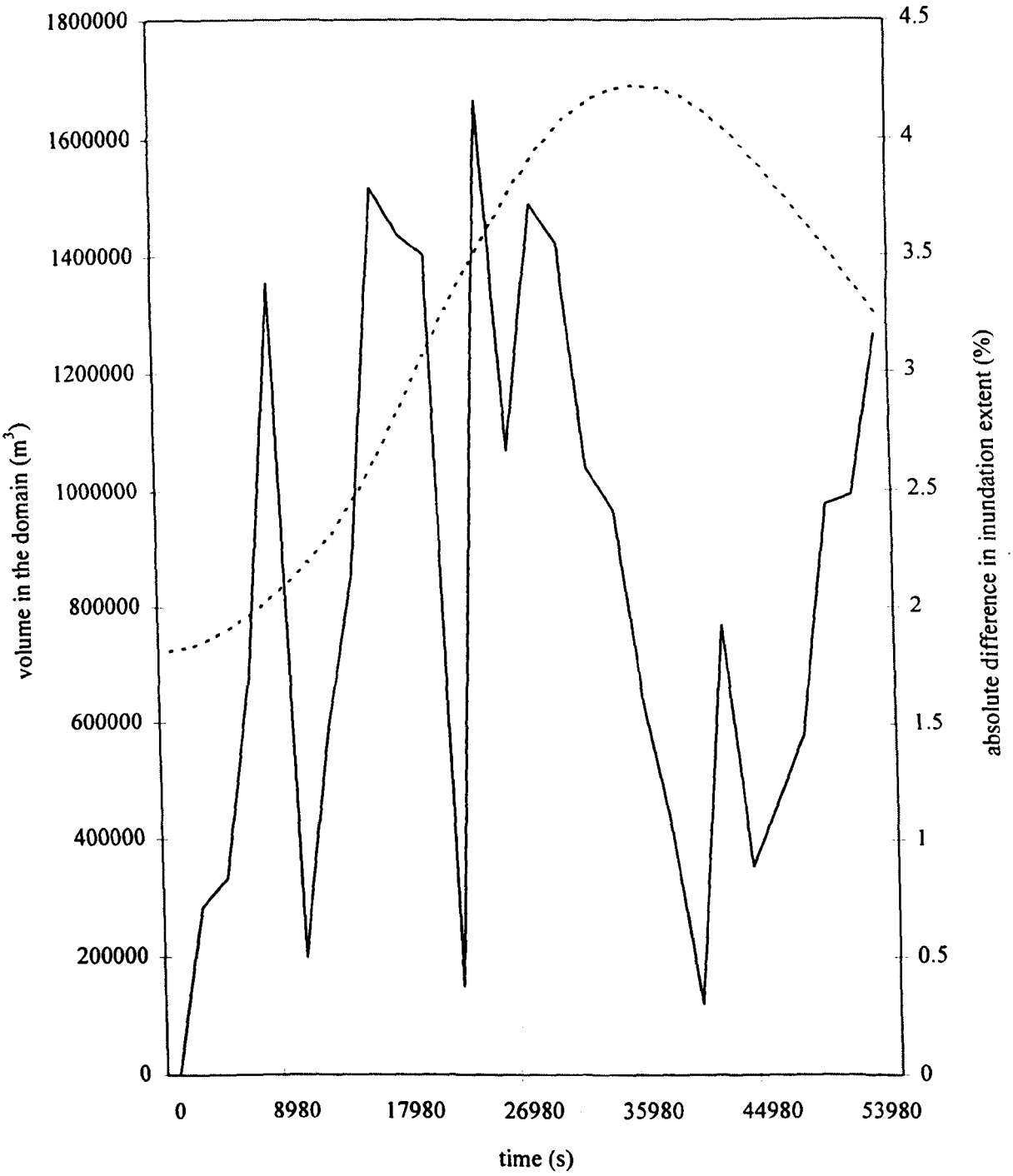

Figure 6.9 (a) Illustration of the difference in inundation extent between *Control01* and simulation *Sil01* together with a plot of total volume in the domain for the 1 in 1 year event (b) illustration of the difference in inundation extent between *Control02* and simulation *Sil03* together with a plot of total volume in the domain for the 1 in 5 year event.

(b)

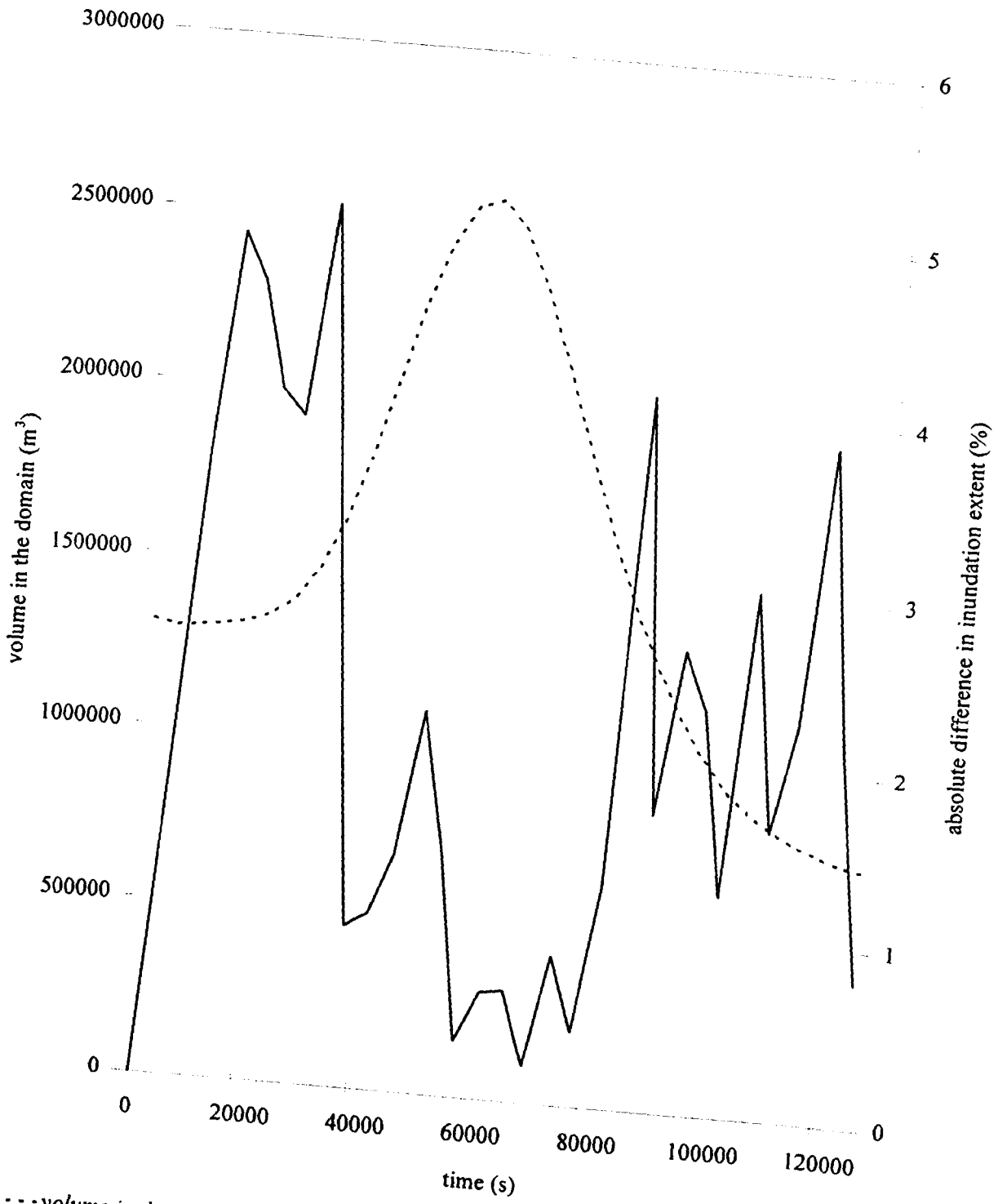

Figure 6.9 (continued)

that these integrated effects are the product of unrepresentative hydraulic behaviour on the floodplain thus the analysis conducted here is an essential part of the full analysis undertaken in this Chapter.

During this part of the investigation the results from simulation *Sil01* (1 in 1 year event run with substrate *Sil(80)*) only are analysed. This run was chosen as it has consistently been found to generate the greatest differences relative to the control run.

6.4.1 The effect of inundation on flow velocities at selected floodplain and channel nodes

Two cross-sections were chosen for the analysis, one located at the upstream and the other at the downstream end of the reach. The cross-sections, identified in Figure 6.10, were chosen to represent two distinct regions of the reach where full inundation occurred during the 1 in 1 year simulation.

Four nodes were selected for the analysis, two from each of the two cross-sections identified in Figure 6.10. One channel and one floodplain node were selected from each cross-section for which water depth and flow velocity data are presented in Figure 6.11 as the difference between the nodal value for the *Sil01* simulation and the corresponding control run (*Control01*).

The data in Figure 6.11 represent the two floodplain nodes 155 and 840 located at the upstream and downstream cross sections respectively and the two channel nodes, 159 and 835, positioned at the upstream and downstream cross sections respectively. The results demonstrate both between and within-site variability in the data.

The results illustrate that between sites (ie upstream vs downstream) the greatest differences in both water depth and velocity are found at the downstream site (nodes 835 & 840). For the downstream site the maximum recorded difference in velocity in the channel is 0.0604ms^{-1} at 30000 seconds (node 840) while the maximum difference recorded on the floodplain is 0.0926 ms^{-1} at 24000 seconds (node 835). For the upstream site the maximum difference recorded in the channel is 0.02018 ms^{-1} at 10000 seconds (node 159) and on the floodplain is 0.02969 ms^{-1} at 6000 seconds (node 155).

Within site patterns show that the greatest difference in flow velocity is recorded at the floodplain node for both sites (nodes 835 and 155). At the upstream cross-section, a reduction of 0.02018 ms^{-1} at the channel node compares to a reduction of 0.02969 ms^{-1} at the floodplain node while the difference at the downstream cross-section is 0.06037 ms^{-1} and 0.09259 ms^{-1} respectively. The maximum reduction in velocity is time synchronous with the maximum reduction in water depth for

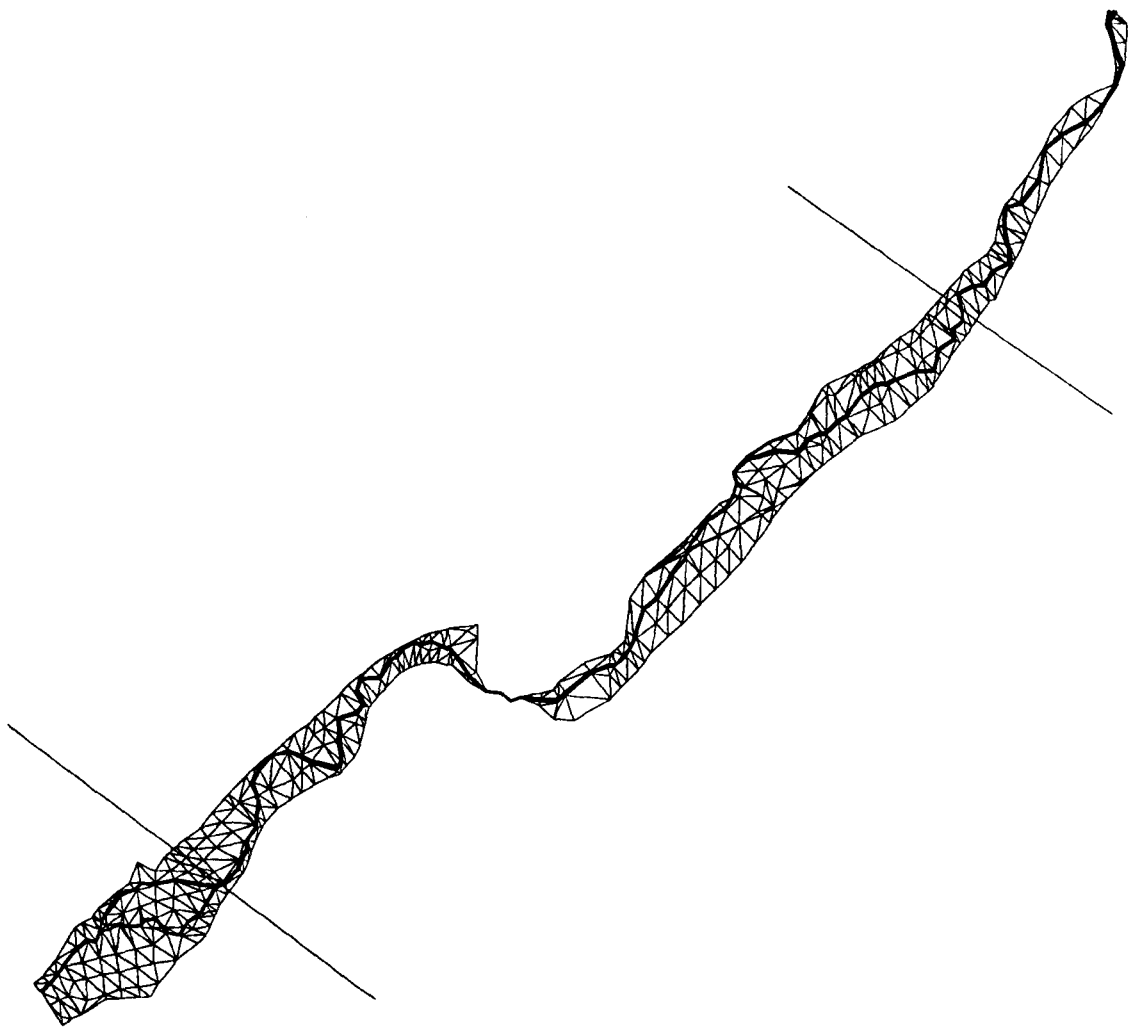

Figure 6.10 Location of the two cross-sections from which the floodplain and channel nodes are selected for the analysis into the impact of infiltration on nodal water depth and velocity.

all but the upstream floodplain node (node 155) where the maximum difference in velocity occurs 2000 seconds later than the maximum reduction in water depth. At both sites the maximum reduction in floodplain velocities and depths occurs earlier than that recorded for the channel. With respect to velocity, at the upstream site this difference amounts to 4000 seconds (6000s for the floodplain and 10000s for the channel) and at the downstream site it is 6000 seconds (24000s for the floodplain and 30000s for the channel).

The greatest difference in nodal water depth and velocity occurs when water is moving onto the floodplain and is therefore seen to occur earlier at the two upstream nodes (155 and 159). The peak reduction in velocity at the floodplain nodes is consistently greater than at the channel nodes. This can be explained in terms of the relatively greater effect that a reduction in water depth has on flow velocity on the floodplain where the depth of water is considerable lower than in channel. Although the greatest reduction in flow velocity occurs at the floodplain node, the greatest reduction in water depth is not associated with the upstream floodplain node, although it is at the downstream location.

6.5 Model stability and mass conservation

Acceptable numerical stability and mass conservation for both the hydraulic and hydrological components of the floodplain hydrology model was demonstrated in *Chapter 3* (section 3.7) for what were essentially non-dynamic simulations. The following section considers the extent to which numerical stability and mass conservation is maintained following the relaxation of the surface boundary during the dynamic simulations undertaken in this Chapter. These two measures of model performance are instrumental in determining the reliability of the model predictions with infiltration.

There are a number of ways in which model stability can be investigated including an examination of the model mass balance, an analysis of the impact of infiltration on model predictions and a comment on the overall success of the model runs where completion of a run implies model stability.

Appendix 1 presents a summary of the mass conservation data relating to both the surface and subsurface hydrology components of the integrated model for the runs undertaken in this chapter. The effect of infiltration on the TELEMAC2D numerical error are small. Indeed, in simulations run with a relaxed surface boundary, this error is slightly reduced due to the lower volume of water passing through the floodplain. Mass balance errors associated with the subsurface hydrology component of the model are insignificant and range from $+6.79 \times 10^{-13}$ for simulation *Clay08* (1 in 1 year event, substrate *Clay(95-)*) to -3.09×10^{-4} for simulation *Sil04* (1 in 5 year event, substrate *Sil(95)*).

Numerical stability is further illustrated through an analysis of the effects of infiltration on model prediction. In Figures 6.1 and 6.2 the simulated output hydrographs respond in a stable manner and in the expected sequence (ie the greatest impact on predicted discharge at the downstream boundary is associated with the soil supporting the highest infiltration potential in all cases). In addition, the magnitude of the effect is not unreasonable. Similar results are obtained in section 6.4 where the

(a)

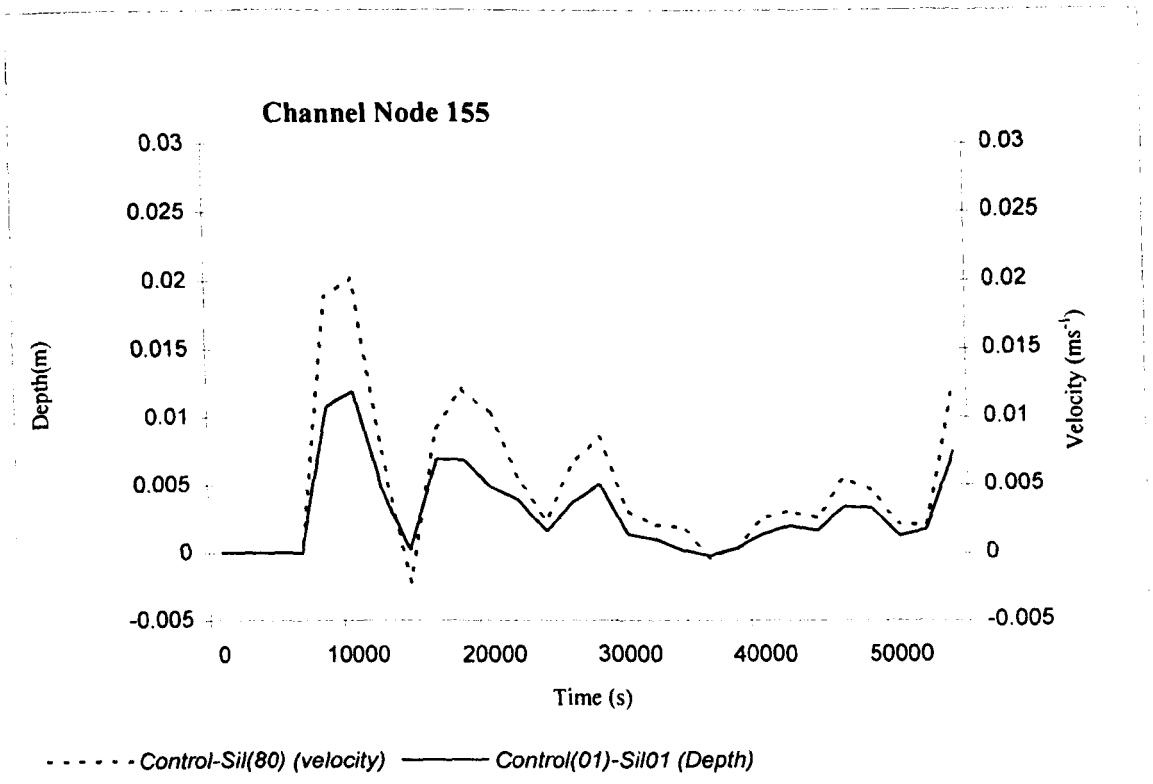

(b)

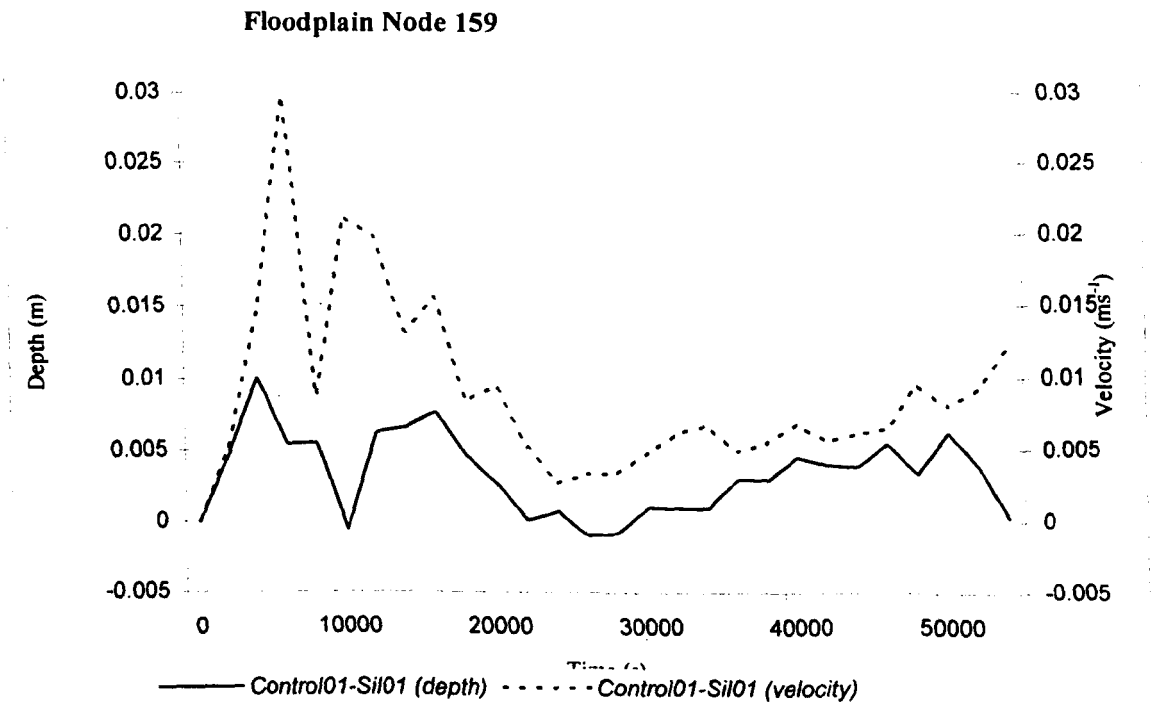

Figures 6.11 Illustration of the impact of infiltration on nodal water depth and velocity. (a) The difference in simulated water depth and velocity between simulations *Control01* and *Sil01* for the 1 in 1 year event at the channel node 155. (b) as for (a) but for floodplain node 159. (c) the difference in simulated depth and velocity between simulations *Control02* and *Sil03* for the 1 in 5 year event at the channel node 835. (d) as for (c) but for floodplain node 840.

(c)

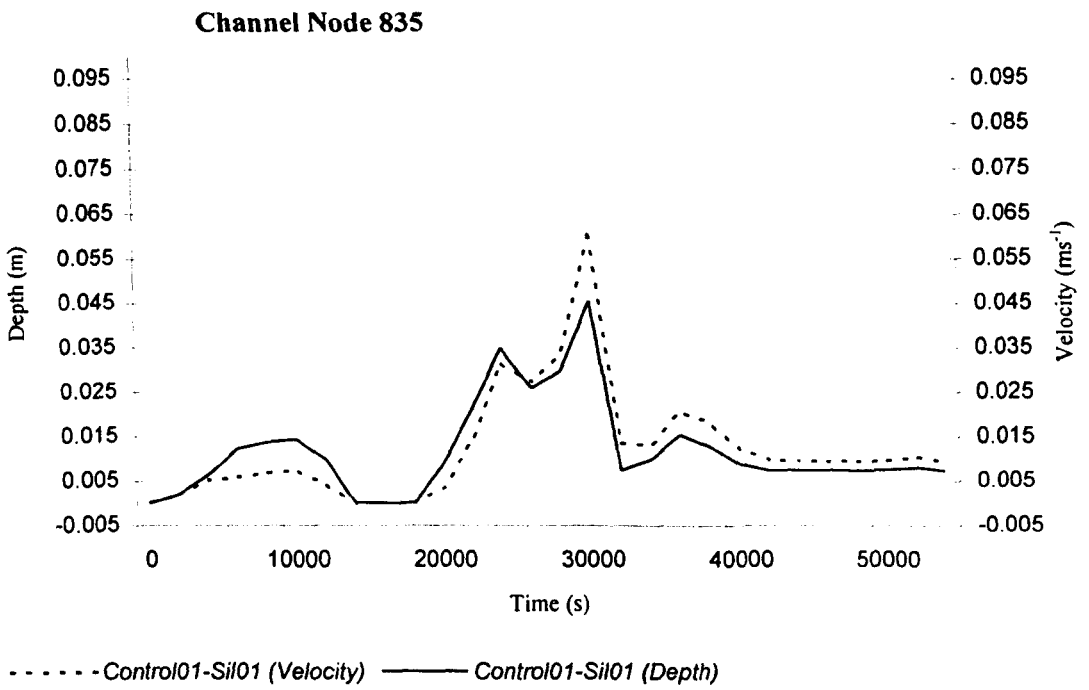

(d)

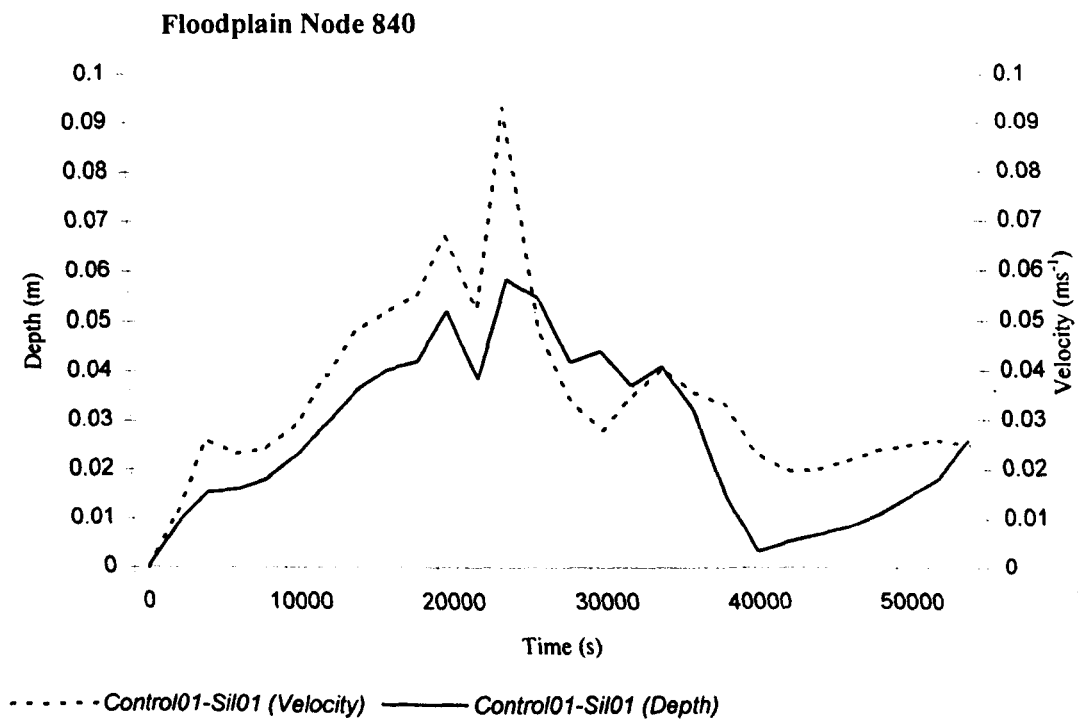

Figure 6.11 (continued)

impact of infiltration on nodal flow velocity and water depth is considered. Again, the results appear to be numerically stable and the magnitude of the effect is not unreasonable. Similar model stability was demonstrated in *Chapter 3* where the infiltration rate was specified across the surface boundary.

Finally, numerical stability is implied by the successful completion of the runs where numerical instability will generally cause the model to crash mid-run.

The discussion presented above and the data presented in Appendix 1 illustrate that for the runs undertaken in this chapter the coupled floodplain hydrology model remains numerically stable. Thus a numerically viable model coupling has been achieved.

6.6 Conclusions

In *Chapter 2* it was suggested that the predictive power of 2D finite element hydraulic models for floodplain flow was compromised through their inability to represent infiltration. Relaxation of the surface boundary of TELEMAC2D has been shown to impact on a series of model prediction characteristics and to result in changes, some of which are potentially significant.

For example, a silty loam substrate at 80% initial soil moisture content and a $K_{(sat)}$ of 1.25×10^{-6} reduced the total discharge volume of a 1 in 1 year flood event by 11.03% and the peak discharge by 6.77%. These effects are relevant both to hydraulic modelling itself and to those disciplines which rely upon the accurate prediction of flood hydraulics, which includes; catchment geomorphology, floodplain planning and floodplain sedimentology.

It is beyond the scope of this thesis to examine the potential variability in all model parameters consistent with a full sensitivity analysis. Instead, the research has concentrated on a relatively narrow parameter range considered to represent a lowland floodplain environment for which soils typical of a the River Culm, Devon, were used. The results have demonstrated considerable variability in model response even within this narrow parameter range (eg a range of $K_{(sat)}$ values from 1.25×10^{-5} to 5.56×10^{-8}). The results suggest that if the model were applied to environments with higher $K_{(sat)}$ and lower initial soil moisture contents this would result in a considerably greater impact on flood flow prediction. Such a situation, for example, might be envisaged where the model is applied to semi-arid environments.

The results throughout demonstrate the significance of the distributed modelling approach adopted. This is illustrated with reference to the change in relative importance of initial soil moisture content

and $K_{(sat)}$ in determining model response to infiltration and, furthermore, how the spatially distributed nature of the flood event impacts on this. Initial soil moisture content exerts its greatest influence at the beginning of each simulation where lower initial soil moisture contents generate high hydraulic gradients across the surface boundary. As the simulation progresses and differences in soil moisture contents between soils are reduced, differences in $K_{(sat)}$ assume the dominant role in determining the rate of infiltration. This is seen clearly in Figure 6.5 which illustrates the difference in mean water depth between each simulation and their respective controls for both the 1 in 1 and 1 in 5 year events.

Recently, a number of other attempts have been made to increase (improve) the physical representation of 2D hydraulic models for flood flow prediction, including, the solution of the 3D version of the 2D Saint-Venant equations (Hervouet and Van Haren, 1996) and the consideration of hillslope runoff within the hydraulic model solution (Charlton, 1995). Other research has considered the impact of changes in the 2D finite element mesh resolution and solver technique on model prediction. The results presented in this Chapter suggest that the floodplain soil moisture store should be included in any consideration of floodplain surface flow. However, while the effects resulting from infiltration have been shown to be significant with reference to the control simulations, a quantitative assessment of the impact of infiltration on the simulated hydrograph cannot be undertaken with reference to the observed output hydrograph due to the significant errors associated with the derivation of the later. The effects of infiltration are therefore effectively subsumed within the potentially large errors in the observed output hydrograph within the existing calibration procedure. The implications for calibration are returned to in *Chapter 8*.

An investigation into the nitrate loading and buffering capacity of flood flow in the floodplain environment

7.1 Introduction and Chapter Objectives

In *Chapter 2* the potential of floodplain riparian soils to remove a high percentage of both subsurface and surface borne NO_3-N and the ameliorating effect that this function imparts on the aquatic environment was established. The efficiency of these buffer systems was shown to be related to the extent to which the NO_3-N loaded water interacted with surface soils where these soils supported high denitrification potentials. While little research has focused specifically on the role of floodwater in these systems, it was suggested that the interaction of floodwater with the same surface floodplain soils might have significant implications for both the *in situ* floodplain soil NO_3-N concentration and the surface water NO_3-N budget at both local and reach scales.

The highly spatially and temporally dynamic nature of floods makes quantitative investigations into the effects of flood water on both *in situ* and stream-borne NO_3-N dynamics at the reach scale an inherently problematic undertaking using currently available methodologies based on field sampling (eg Maltby *et al.*, 1991; 1996; Brunet *et al.*, 1994). The results from such studies are often integrated over time and space to provide estimates of denitrification flux at the hectare (Hanson *et al.*, 1994) or catchment (Maltby *et al.*, 1991) scale. However, the spatially distributed floodplain hydrology-nitrate model developed in Chapters 3 and 4 provides the basis for such an investigation as it enables the passage of the flood wave and the resulting soil hydrological and NO_3-N processes to be modelled deterministically at a spatial and temporal resolution greater than that practically achievable through field survey.

The aim of this Chapter is to investigate the contention that floodplain inundation events represent periods of potentially high denitrification activity within the floodplain environment with

implications for both floodplain soil and surface water NO_3-N concentrations. The chapter also aims to assess the utility of the integrated approach to modelling floodplain hydrology and nitrate chemistry.

The research presented in this chapter addresses two issues relating to floodplain NO_3-N dynamics for which quantitative data, and the means of collecting such data, are currently lacking at the reach scale. Firstly, the research aims to investigate the effect that flood inundation has on floodplain NO_3-N dynamics and secondly, to assess the implication that the denitrification of NO_3-N supplied to the floodplain soil in infiltrating floodwater has on the floodwater NO_3-N budget. Both of these aspects are examined over a range of floodplain soils and initial soil moisture conditions.

Prior to conducting the simulations necessary for addressing the above objectives, the model template for the research is first identified along with the range of conditions over which the model is to be applied. Once this has been achieved, a simulation strategy is developed. The analysis is divided into two parts. The first of these considers the processes operating in the modelled floodplain environment through an examination of the results of the simulations. The second considers the magnitude of NO_3-N loss generated by the simulations run in the analysis and examines these in the context of published NO_3-N losses both in terms of the *in-situ* NO_3-N source and an event based floodwater NO_3-N budget. The chapter concludes with an assessment of the success of the integrated approach to modelling floodplain hydrology and nitrate chemistry.

7.2 Simulation of denitrification in the floodplain environment

In this Chapter the potential of floodplain soils to denitrify both flood borne and *in situ* NO_3-N during inundation events is assessed. In the absence of suitable validation data the aim remains effectively a sensitivity analysis rather than an attempt to verify actual losses for any one particular site. Indeed, the emphasis on reach choice and parameterisation has been towards the selection of soil types, initial conditions and a NO_3-N model parameterisation which provides a parameterisation which lies within a 'realistic' range rather than an attempt to represent conditions pertaining to one specific site. Thus, the conditions chosen for parameterisation in Chapters 4 and 5 represent generalisations of those encountered in the field, nevertheless, these have been selected from appropriate parameter ranges derived from the literature.

The specific aims of this section are:

- ***To determine the relative significance of floodwater infiltration derived and in situ NO_3-N as a source for denitrification during inundation events over a range of soil types and initial soil moisture conditions.***

- ***To determine the significance of changes in the in situ availability of NO_3-N upon total losses of NO_3-N from the floodplain system.***

- ***To determine the significance of the denitrification rate constant (k_1) upon total losses of NO_3-N from the floodplain system.***

- ***To determine the significance of varying the hydraulic conductivity upon total losses of NO_3-N from the floodplain system.***

- ***To assess the impact that the denitrification of NO_3-N supplied to the floodplain soil in infiltrating floodwater has on the floodwater NO_3-N budget.***

7.2.1 Choice of application reach, model parameterisation and simulations

(i) Selection of a reach template and flood event:

For this application the Culm 1 in 1 year event introduced in *Chapter 5* (5.3) is used. This event is suited to the application for a number of reasons: Firstly, the lower peak flood flows enable the flood progression and recession to be identified and this is especially important in terms of a fluctuating inundation extent which will be an important driving factor in the spatial and temporal distribution of floodplain denitrification (see Figure 5.6). Secondly, this event is well calibrated with the observed output discharge (see *Chapter 5*, section 5.3). Finally, it is the least computer intensive of the reach simulations used, which is a significant factor when longer simulation times can severely restrict the number of simulations possible.

(ii) Selection of soil types and initial soil moisture conditions:

Two soil types are investigated, the silty loam and clay soils which have been introduced in previous chapters (Chapters 5 (derivation of parameterisation data) and 6 (application in the floodplain environment). Again, these represent 'typical' soils developed in lowland alluvial floodplain sediments to which this research is applied. The initial soil moisture conditions chosen, 80% and 95% of the saturated totals, are chosen to represent a typical range of moisture conditions during autumn through to spring in Temperate regions. The derivation of the parameters to be used

in the model are (the soil characteristic curve, saturated hydraulic conductivity etc) are discussed fully in *Chapter 5* (5.4).

(iii) Simulations and model parameterisation for the analysis:

The simulated loss of NO_3-N will be dependant upon the four variables in Equation 4.31; the concentration of NO_3-N, the denitrification rate constant (k_1), the soil moisture content expressed through the dimensionless function f_w and time. As each simulation is run over an equal time period (15 hours) this variable can be ignored, the other three parameters are considered in the following analysis. The significance of each of these is considered in four series of simulations, referred to as 'A' ,'B ,'C' and 'D' which form the basis of the study and which shall now be discussed in turn:

(A) The first series of simulations comprises 12 runs parameterised to investigate the relative contribution of the two NO_3-N sources to total floodplain denitrification. Specifically, these are designed to consider: (i) The mass of NO_3-N denitrified when NO_3-N in infiltrating floodwater is the sole input to the system; for these runs NO_3-N concentration in floodwater is set at a constant $10mgl^{-1}$ for the duration of the event. (ii) The mass of NO_3-N denitrified when in-situ NO_3-N is the sole source of NO_3-N; for these runs an initial concentration of $66.67\mu gNO_3\text{-}Ng^{-1}$ is specified in the top soil layer at the beginning of each simulation. The *in situ* NO_3-N source represents that which is present in the soil at the time of the flood event and which can be derived from a number of sources including fertiliser additions, plant and microbial decay and subsequent mineralisation, atmospheric inputs (wet and dry) and previous inundation. All of these sources contribute to the residual fertility of the soil which is henceforth referred to as *in situ* NO_3-N. Although the magnitude of this source will vary considerably, the concentration is chosen to fall within the range typically encountered in managed soils (Trudgill *et al*, 1991; Rowell, 1994). (iii) The mass of NO_3-N denitrified when both sources of NO_3-N (floodwater and in situ) are available for denitrification; these simulations are initiated with concentrations of $10mgl^{-1}$ NO_3-N in floodwater and $66.67\mu gNO_3\text{-}Ng^{-1}$ in the top soil layer (The choice of the floodwater NO_3-N concentration is based on the discussion presented in *Chapter 4*).

Table 7.1 details the hydrological parameterisation adopted and Table 7.2 the NO_3-N model parameterisation for these simulations and identifies each with a simulation code (*Clay09 - Clay14* and *Sil09 - Sil14*). In addition, parameter s in the exponent of the soil water function (f_w) in Equation 4.32 is set at a value of 5 and remains at this value for all subsequent simulations.

To maintain consistency the same system used to identify simulations in *Chapter 6* shall be employed here. Each simulation is assigned a code in Table 7.1 (and in all tables thereafter), continuing numerically from those in *Chapter 6*, and thereafter when reference is made to a

simulation this code is cited together with an identification of the soil type (ie clay (Clay) or silty loam (Sil)) and its initial soil moisture content (ie 80 or 95% of the saturation value). Thus, simulation *Sil10* refers to an event run on the silty loam at 95% initial saturation and will be refereed to in the text as *Sil10* (substrate *Sil(95)*). All simulations in this Chapter are run using the Culm 1 in 1 year event thus no differentiation is required between events, as in *Chapter 6*.

(B) The second series of simulations comprises 4 runs parameterised to investigate the effect of the in-situ mass of NO_3-*N* on the total NO_3-*N* loss. The simulations are set-up in an identical manner to those in simulation series '**A**' except that the initial mass of NO_3-*N* in the top cell is set to 33.33μ gNO_3-*N*g^{-1} (half of that used in the previous investigation) . Tables 7.1 and 7.2 detail the parameterisation of these runs and identifies each with a code (*Clay15* - *Clay16* and *Sil15* - *Sil16*).

(C) The third series of simulations comprises 4 runs parameterised to investigate the effect of an increase in the denitrification rate constant on total NO_3-*N* loss. The simulations are set up in an identical manner to those in simulation series '**B**' except that the denitrification rate constant used is 0.0015hr^{-1} rather than 0.0001hr^{-1}. Tables 7.1 and 7.2 detail the parameterisation of these runs and identifies each with the following simulation codes; *Clay17* - *Clay18* and *Sil17* - *Sil18*.

(D) The forth and final series of simulations comprises eight runs parameterised to investigate the effect of variations in the saturated hydraulic conductivity on total NO_3-*N* loss through denitrification. The simulations are parameterised in an identical manner to those presented in simulation series 'C' but for each of the simulations the saturated hydraulic conductivity ($K_{(sat)}$) for each soil is both increased and decreased by one order of magnitude. Thus, for the Clay soil the $K_{(sat)}$ values used are $5.56x10^{-8}$ and $5.56x10^{-6}$ (mean is $5.56x10^{-7}$) and for the silty loam the values used are $1.25x10^{-7}$ and $1.25x10^{-5}$ (mean is $1.25x10^{-6}$). Tables 7.1 and 7.2 detail the parameterisation of these runs and identifies each with the following codes; *Clay19* - 22 and *Sil19* - 22.

7.2.2 Analysis of the results

The model simulations presented in Tables 7.1 and 7.2 were run to determine model response over the range of conditions specified. The results are now analysed in terms of (i) the hydrological and NO_3-*N* processes operating during the passage of the flood wave, (ii) the magnitude of the NO_3-*N* loss in the context of published losses from similar systems and (iii) a surface water NO_3-*N* budget.

7.2.2.1 The simulated contribution of floodborne and in situ NO_3-*N* to floodplain denitrification

The first series of simulations (*Clay09-Clay14* and *Sil09-Sil14*) identified under '**A**' in section 7.2.1, allow an investigation of the relative importance of the two sources of NO_3-*N* considered in terms of

their contribution to total loss of NO_3-N from the floodplain during a flood event. The results of this series of simulations are presented in Table 7.3 and Figures 7.1 to 7.5.

Simulation code	Simulation series	soil type	simulated soil depth (m)	simulated cell depth (m)	initial soil moisture content (%)	K(sat)
Clay09	A	Clay	0.6	0.1	80	$5.56x10^{-7}$
Clay10	A	Clay	0.6	0.1	95	$5.56x10^{-7}$
Sil09	A	silty loam	0.6	0.1	80	$1.25x10^{-6}$
Sil10	A	silty loam	0.6	0.1	95	$1.25x10^{-6}$
Clay11	A	Clay	0.6	0.1	80	$5.56x10^{-7}$
Clay12	A	Clay	0.6	0.1	95	$5.56x10^{-7}$
Sil11	A	silty loam	0.6	0.1	80	$1.25x10^{-6}$
Sil12	A	silty loam	0.6	0.1	95	$1.25x10^{-6}$
Clay13	A	Clay	0.6	0.1	80	$5.56x10^{-7}$
Clay14	A	Clay	0.6	0.1	95	$5.56x10^{-7}$
Sil13	A	silty loam	0.6	0.1	80	$1.25x10^{-6}$
Sil14	A	silty loam	0.6	0.1	95	$1.25x10^{-6}$
Clay15	B	Clay	0.6	0.1	80	$5.56x10^{-7}$
Clay16	B	Clay	0.6	0.1	95	$5.56x10^{-7}$
Sil15	B	silty loam	0.6	0.1	80	$1.25x10^{-6}$
Sil16	B	silty loam	0.6	0.1	95	$1.25x10^{-6}$
Clay17	C	Clay	0.6	0.1	80	$5.56x10^{-7}$
Clay18	C	Clay	0.6	0.1	95	$5.56x10^{-7}$
Sil17	C	silty loam	0.6	0.1	80	$1.25x10^{-6}$
Sil18	C	silty loam	0.6	0.1	95	$1.25x10^{-6}$
Clay19	D	Clay	0.6	0.1	80	$5.56x10^{-8}$
Clay20	D	Clay	0.6	0.1	80	$5.56x10^{-6}$
Clay21	D	Clay	0.6	0.1	95	$5.56x10^{-8}$
Clay22	D	Clay	0.6	0.1	95	$5.56x10^{-6}$
Sil19	D	silty loam	0.6	0.1	80	$1.25x10^{-7}$
Sil20	D	silty loam	0.6	0.1	80	$1.25x10^{-5}$
Sil21	D	silty loam	0.6	0.1	95	$1.25x10^{-7}$
Sil22	D	silty loam	0.6	0.1	95	$1.25x10^{-5}$

Table 7.1 Hydrological model parameterisation for each simulation in the sensitivity analysis.

Simulation code	Simulation series	NO_3-N condition	k_1 (denitrification rate constant)
Clay09	A	10mgl^{-1} in floodwater	0.0001hr^{-1}
Clay10	A	10mgl^{-1} in floodwater	0.0001hr^{-1}
Sil09	A	10mgl^{-1} in floodwater	0.0001hr^{-1}
Sil10	A	10mgl^{-1} in floodwater	0.0001hr^{-1}
Clay11	A	66.67μgNO_3-Ng^{-1} in top soil layer (10cm)	0.0001hr^{-1}
Clay12	A	66.67μgNO_3-Ng^{-1} in top soil layer (10cm)	0.0001hr^{-1}
Sil11	A	66.67μgNO_3-Ng^{-1} in top soil layer (10cm)	0.0001hr^{-1}
Sil12	A	66.67μgNO_3-Ng^{-1} in top soil layer (10cm)	0.0001hr^{-1}
Clay13	A	10mgl^{-1} in floodwater, 66.67μgNO_3-Ng^{-1} in top soil layer (10cm)	0.0001hr^{-1}
Clay14	A	10mgl^{-1} in floodwater, 66.67μgNO_3-Ng^{-1} in top soil layer (10cm)	0.0001hr^{-1}
Sil13	A	10mgl^{-1} in floodwater, 66.67μgNO_3-Ng^{-1} in top soil layer (10cm)	0.0001hr^{-1}
Sil14	A	10mgl^{-1} in floodwater, 66.67μgNO_3-Ng^{-1} in top soil layer (10cm)	0.0001hr^{-1}
Clay15	B	10mgl^{-1} in floodwater, 33.33μgNO_3-Ng^{-1} in top soil layer (10cm)	0.0001hr^{-1}
Clay16	B	10mgl^{-1} in floodwater, 33.33μgNO_3-Ng^{-1} in top soil layer (10cm)	0.0001hr^{-1}
Sil15	B	10mgl^{-1} in floodwater, 33.33μgNO_3-Ng^{-1} in top soil layer (10cm)	0.0001hr^{-1}
Sil16	B	10mgl^{-1} in floodwater, 33.33μgNO_3-Ng^{-1} in top soil layer (10cm)	0.0001hr^{-1}
Clay17	C	10mgl^{-1} in floodwater, 33.33μgNO_3-Ng^{-1} in top soil layer (10cm)	0.0015hr^{-1}
Clay18	C	10mgl^{-1} in floodwater, 33.33μgNO_3-Ng^{-1} in top soil layer (10cm)	0.0015hr^{-1}
Sil17	C	10mgl^{-1} in floodwater, 33.33μgNO_3-Ng^{-1} in top soil layer (10cm)	0.0015hr^{-1}
Sil18	C	10mgl^{-1} in floodwater, 33.33μgNO_3-Ng^{-1} in top soil layer (10cm)	0.0015hr^{-1}
Clay19	D	10mgl^{-1} in floodwater, 33.33μgNO_3-Ng^{-1} in top soil layer (10cm)	0.0015hr^{-1}
Clay20	D	10mgl^{-1} in floodwater, 33.33μgNO_3-Ng^{-1} in top soil layer (10cm)	0.0015hr^{-1}
Clay21	D	10mgl^{-1} in floodwater, 33.33μgNO_3-Ng^{-1} in top soil layer (10cm)	0.0015hr^{-1}
Clay22	D	10mgl^{-1} in floodwater, 33.33μgNO_3-Ng^{-1} in top soil layer (10cm)	0.0015hr^{-1}
Sil19	D	10mgl^{-1} in floodwater, 33.33μgNO_3-Ng^{-1} in top soil layer (10cm)	0.0015hr^{-1}
Sil20	D	10mgl^{-1} in floodwater, 33.33μgNO_3-Ng^{-1} in top soil layer (10cm)	0.0015hr^{-1}
Sil21	D	10mgl^{-1} in floodwater, 33.33μgNO_3-Ng^{-1} in top soil layer (10cm)	0.0015hr^{-1}
Sil22	D	10mgl^{-1} in floodwater, 33.33μgNO_3-Ng^{-1} in top soil layer (10cm)	0.0015hr^{-1}

Table 7.2 Nitrate model parameterisation for each simulation run in analysis. For each simulation information is given regarding the series to which that simulation belongs, the NO_3-N concentration of the floodwater, the mass of NO_3-N in the top soil layer and the denitrification rate constant used in Equation 4.31. The concentration of NO_3-N in μgNO_3-N g^{-1} is calculated by assuming a bulk density for the soil of 1.5.

Additional loose-leaf copies of both tables 7.1 and 7.2 are provided in the back cover of the thesis for reference throughout this chapter.

Simulation code	Total NO_3-N input in floodwater (g) *	Total NO_3-N in-situ (g) $^+$	Total available NO_3-N (g)	Total NO_3-N loss (g) *	Loss as a % of total available NO_3-N
Clay09	1535097.7	-	1535097.7	711.1	0.046
Clay10	891139.2	-	891139.2	424.0	0.048
Sil09	2247145.2	-	2247145.2	558.7	0.025
Sil10	1805267.5	-	1805267.5	472.6	0.026
Clay11	-	35129785.7	35129785.7	15890.1	0.045
Clay12	-	35129785.7	35129785.7	25382.3	0.072
Sil11	-	35129785.7	35129785.7	9135.8	0.026
Sil12	-	35129785.7	35129785.7	11647.2	0.033
Clay13	1535097.7	35129785.7	36664883.4	16601.2	0.045
Clay14	891139.2	35129785.7	36020924.9	25806.3	0.072
Sil13	2247145.2	35129785.7	37376930.9	9694.6	0.026
Sil14	1805267.5	35129785.7	36935053.2	12119.8	0.033

Table 7.3 Results of the simulations from series 'A'. (* = values integrated over the course of the simulation, $^+$ = mass present at the beginning of the simulation).

(i) Denitrification of the infiltrating floodwater NO_3-N source: When reference is made to the denitrification of the floodwater NO_3-N source this refers specifically to that NO_3-N in floodwater which infiltrates into the soil.

Prior to consideration of the denitrification of the floodwater NO_3-N source, this source itself will first be examined in terms of magnitude and availability. Total NO_3-N input to the floodplain for simulations *Sil09* (substrate *Sil(80)*), *Sil10* (substrate *Sil(95)*), *Clay09* (substrate *Clay(80)*) and *Clay10* (substrate *Clay(95)*) are presented in Table 7.3 as total inputs and in Figure 7.1(a) as cumulative input over the duration of the simulation. In terms of total NO_3-N input to the floodplain soil the pattern observed, beginning with the greatest input, is ***Sil09>Sil10>Clay09>Clay10*** which conforms to the expected pattern where soils with a higher $K_{(sat)}$ and a lower initial soil moisture content will receive the greatest infiltrated volume and associated NO_3-N mass. Indeed, in terms of infiltration this was found to be true in *Chapter 6* (see section 6.3). However, Figure 7.1(a) reveals a pattern of NO_3-N input in which the curves depicting NO_3-N input for simulations *Sil10* (substrate

(a)

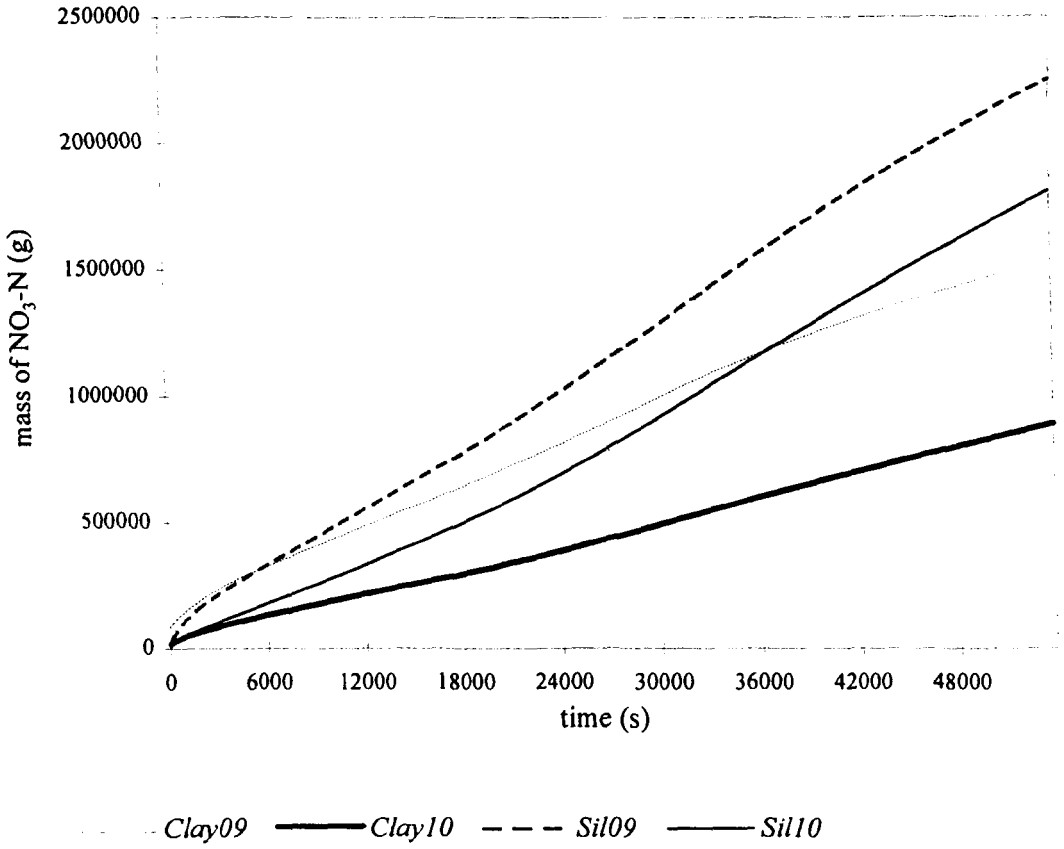

(b)

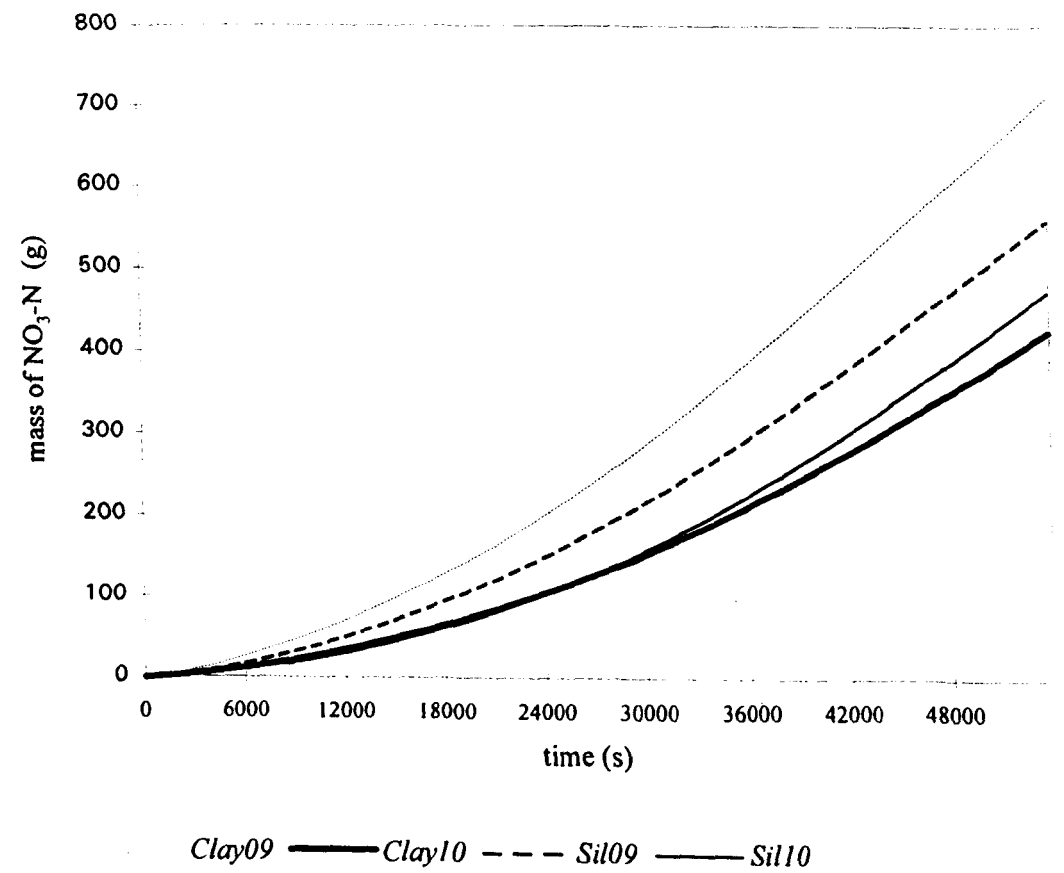

Figure 7.1 (a) *NO_3-N* input derived from infiltrating floodwater, (b) denitrification of floodwater derived *NO_3-N*.

Sil(95)) and *Clay09* (substrate *Clay(80)*) transect suggesting that the mass of NO_3-N input at any one time during the simulation is rather more complex than the final (cumulative) values suggest. This pattern can be explained in terms of the interaction between the soil type, ($K_{(sat)}$), and the soil moisture content of the soil: Initially the lower soil moisture content associated with the clay soil (80%) results in a hydraulic potential across the surface boundary which is greater than that across the surface boundary of the silty loam resulting in a greater flux of both water and NO_3-N across the soil surface of the clay and into cell 1. At this point, despite the higher $K_{(sat)}$ of the silty loam, this soil supports a lower flux of both water and NO_3-N across its surface boundary. As the soil moisture content of the clay increases the difference in the hydraulic potentials between the two soils decreases and the difference in $K_{(sat)}$ becomes dominant in determining the flux of NO_3-N across the surface boundary. At this point in the simulation the instantaneous input of NO_3-N into the silty loam would exceed that of the clay. Where the cumulative input is measured, as is the case depicted in Figure 7.1(a) this effect is delayed until the total input to the silty loam exceeds that input to the clay.

The time at which the two curves cross is further complicated by the spatially and temporally dynamic nature of the flood event. The period for which the higher hydraulic potential across the surface boundary dominates this flux will depend upon the nature of the flood event and is likely to be the dominant force during the rising limb of the flood hydrograph when water is spilling on to previously non-inundated ('dry') areas. Following the saturation of inundated soils and a slow down and the ultimate cessation in the inundation of previously 'dry' areas, $K_{(sat)}$ will become the dominant control over the flux across the surface and the flux of NO_3-N into the silty loam will then exceed that into the clay. The point at which this occurs will depend upon the nature of the inundation event. A storm for which floodwater remains on the floodplain surface for only a short period may result in NO_3-N losses from the clay exceeding those from the silty loam while the reverse might be expected for longer period events where water remains on the surface for longer thus reducing the relative significance of initial soil moisture content.

The results pertaining to the loss floodwater derived NO_3-N are now considered. The results are presented in Table 7.3 and Figure 7.1(b). The greatest total loss of infiltrated floodwater NO_3-N is generated by simulation *Clay09* (substrate *Clay(80)*) and totals 711.1g. The smallest loss, 424.0g, is generated by simulation *Clay10* (substrate *Clay(95)*).

An initial look at the results suggests that these are anomalous as the magnitude of NO_3-N received by each soil does not correspond to the magnitude in which it is subsequently lost. For example; (i) although the greatest loss is reported for simulation *Clay09* (substrate *Clay(80)*), the total input of NO_3-N to this system is in fact lower than that for simulations *Sil09* (substrate *Sil(80)*) and

simulation *Sil10* (substrate *Sil(95)*) (see Figure 7.1(a)), (ii) the loss generated by simulation *Sil09* (substrate *Sil(80)*) is second to that of simulation *Clay09* (substrate *Clay(80)*) yet NO_3-*N* input to the former exceeds that of the later, and (iii) Simulation *Sil10* (substrate *Sil(95)*) generates the third greatest loss while NO_3-*N* input is the second greatest while simulation *Clay10* (substrate *Clay(95)*) receives the smallest input and generates the smallest loss. In the same way that NO_3-*N* input was explained, these results can be explained in terms of the interaction between the initial soil moisture content of the soil the $K_{(sat)}$ of the soil and spatially and temporally dynamic nature of the flood event.

NO_3-*N* loss by denitrification is determined by the availability of NO_3-*N* and the soil moisture content acting through Equation 4.31. Taking the example of simulations *Sil09* (substrate *Sil(80)*) and *Clay09* (substrate *Clay(80)*) first, the results are explained in terms of the factors listed above. The change in soil moisture content for the top soil cell and the cumulative denitrification resulting from this cell are plotted in Figure 7.2(a) and 7.2(b) respectively for an equivalent floodplain node receiving a constant supply of floodwater with a concentration of $10mgl^{-1}$ NO_3-*N*. The increase in soil moisture of cell 1 in the clay soil occurs at a greater rate than that of the silty loam which has important implications for the rate of denitrification, where soil moisture content determines the value of the soil moisture function (f_w), and importantly, this occurs over a very sensitive range of the f_w curve (see Figure 4.2) where small changes in soil moisture result in large changes in f_w and correspondingly large changes in the rate of denitrification. The effect on the cumulative loss of NO_3-*N* through denitrification is evident in Figure 7.2(b) where the loss of NO_3-*N* is greater in the clay despite the lower availability of NO_3-*N* (see Figure 7.1(a)). Figure 7.3 illustrates what happens to the cumulative NO_3-*N* loss for an equivalent system run over 15 hours, a time base equivalent to that of the Culm simulations used in this Chapter. Once the soil moisture content of cell 1 in the silty loam reaches saturation, denitrification loss from this soil exceeds that of the clay (due to the greater availability of NO_3-*N* in the silty loam (see Figure 7.1(a)) and the cumulative loss from the silty loam exceeds that from the clay. However, this result does not conform to that for simulations *Sil09* (substrate *Sil(80)*) and *Clay09* (substrate *Clay(80)*) in which the total NO_3-*N* loss from the later exceeds that of the former despite a lower NO_3-*N* input. The results presented in Figures 7.2 and 7.3 represent a single node experiencing continual inundation and are therefore not representative of the dynamic situation resulting from a the flood event acting over the entire floodplain surface. It is these mechanisms acting in combination with the dynamic nature of the flood event can be used to explain the results obtained for simulations *Sil09* and *Clay09*. Where floodwater spills on to the clay soil the soil moisture content of cell 1 increases rapidly as does the denitrification rate. This situation is repeated wherever water advances on to previously 'dry' areas. In the case of the silty loam the initial rise in soil moisture content is slower as is the associated rise in denitrification rate. The spatially and temporally dynamic nature of the flood event means that

much of the floodplain is not inundated for periods long enough to result in high rates of denitrification in the silty loam soil and, furthermore, that once the flood is receding the silty loam will drain more rapidly resulting in reduced NO_3-N availability, reduced soil moisture contents and, once more, reduced denitrification rates. Figure 7.3 illustrates the situation resulting from a fully inundated domain over 15 hours. The dynamic nature of the flood event simulated which gives rise to a dynamic floodplain subsurface hydrology and NO_3-N supply means that despite receiving a greater NO_3-N loading, the cumulative loss of NO_3-N resulting from simulation *Sil09* is lower than that from simulation *Clay09*.

A similar pattern is observed for simulations *Sil10* (substrate *Sil(95)*) and *Clay10* (substrate *Clay(95)*). However, due to the higher initial soil moisture contents of these soils the effects are less pronounced. Although the silty loam initially responds less rapidly than the clay both to the wetting-up of cell 1 (see Figure 7.4(a)) and NO_3-N loss (see Figure 7.4(b)), these effects are much reduced when compared to those for simulation *Sil09* (substrate *Sil(80)*). At the same time the initial soil moisture content of 95% means that although this corresponds to a sensitive part of the soil moisture function curve, at 95% soil moisture saturation a relatively high rate of denitrification is occurring. The more rapid response of the silty loam at 95% saturation to changes in soil moisture content coupled with the higher input of NO_3-N derived from the floodwater source (see Figure 7.1(a)) results in a cumulative loss of NO_3-N through denitrification for simulation *Sil10* exceeding that of simulation *Clay10*. However, as was the case for the two simulations beginning at 80% initial saturation, the cumulative denitrification for the clay (*Clay10*) initially exceeds that of the silty loam (*Sil10*) (see Figure 7.1(b)).

(ii) Denitrification of in-situ NO_3-N: The discussion now considers the denitrification of the in-situ NO_3-N source, the results for which are presented in Table 7.1 and Figure 7.5(a). Presented in decreasing magnitude of NO_3-N loss, the simulations follow the sequence: *Clay12* (substrate *Clay(95)*) > *Clay11* (substrate *Clay(80)*) > *Sil12* (substrate *Sil(95)*) > *Sil11* (substrate *Sil(80)*). Figure 7.5(a) illustrates that the curves depicting cumulative NO_3-N loss for simulations *Clay11* and *Sil12* transect during the simulation following which the loss from simulation *Clay11* exceeds that from *Sil12*.

In this case the results can be explained in terms of the interaction between initial soil moisture content and the residence time of NO_3-N within the microbially active upper soil layer and the spatially and temporally dynamic nature of the flood event.

(a)

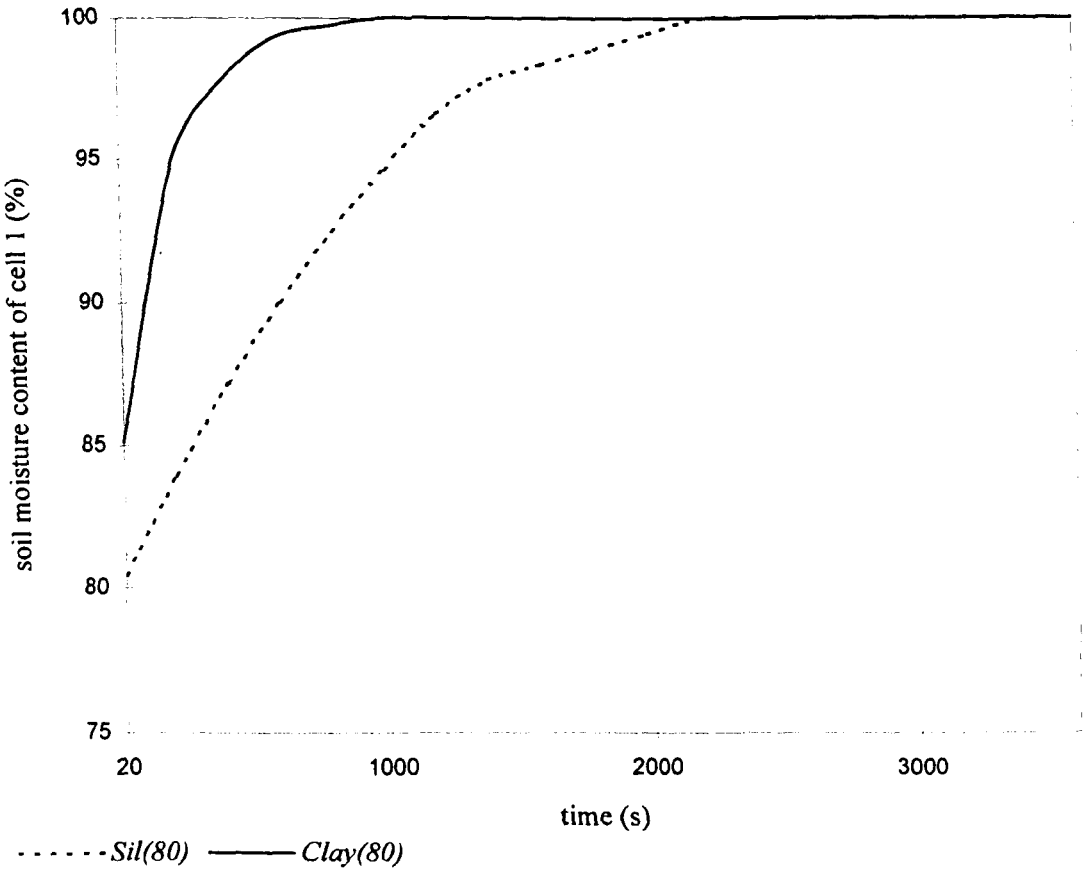

(b)

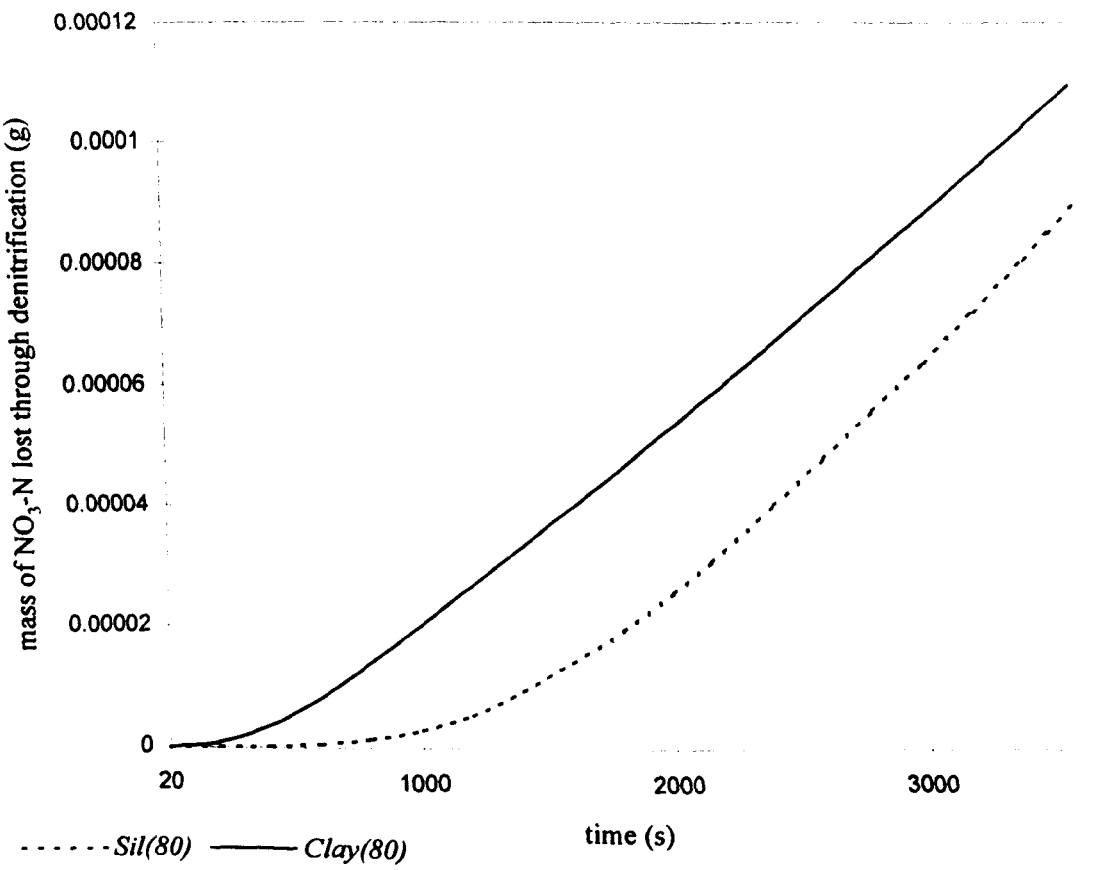

Figure 7.2 Illustration of (a) the change in soil moisture content of the top soil cell at an inundated node over one hour for a silty loam substrate at 80% initial saturation and a clay substrate at 80% initial saturation (b) the cumulative denitrification resulting from these two simulations.

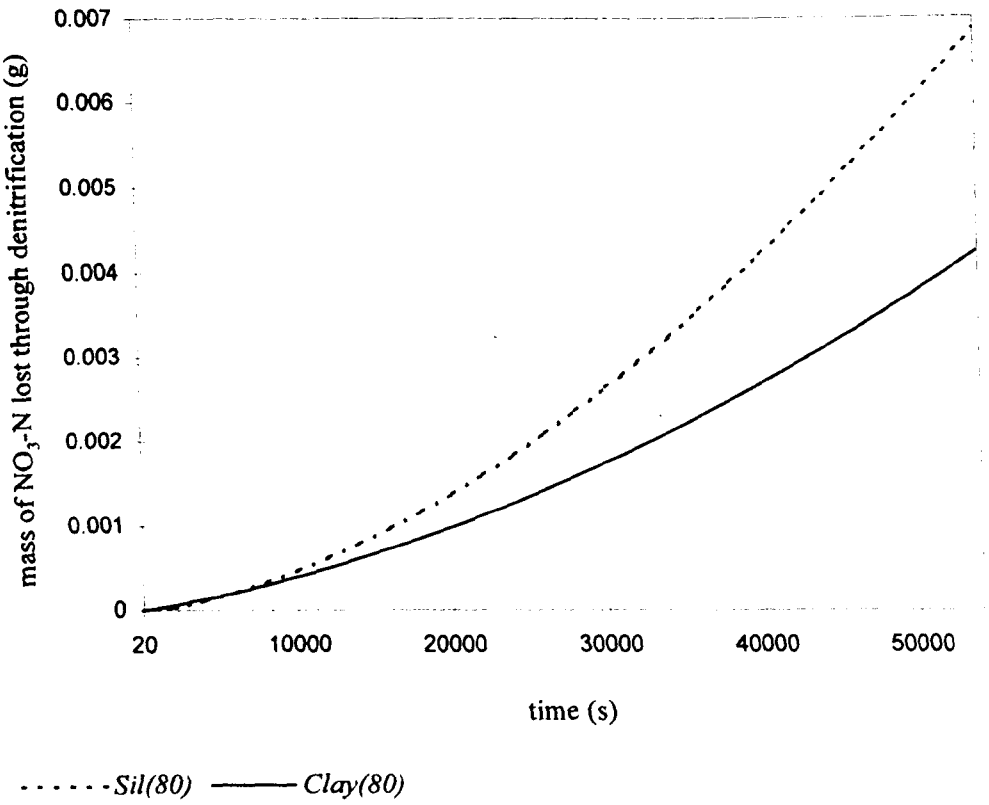

Figure 7.3 Illustration of the cumulative loss of NO_3-N through denitrification at single inundated nodes for a silty loam substrate at 80% initial saturation and a clay substrate at 80% initial saturation run over a 15 hour period.

It is evident from Figure 7.5(a) that initially the dominant control on denitrification activity is initial soil moisture content. NO_3-N losses are initially greater in the two soils with 95% initial saturation and prevails in these soils despite the shorter residence times associated with higher soil moisture contents. However, the relative dominance of soil moisture content and $K_{(sat)}$ in determining loss of NO_3-N through denitrification changes through time and residence time increasingly becomes the dominant process in determining NO_3-N loss. This is exemplified by the curves depicting NO_3-N loss for simulations *Clay11* (substrate *Clay(80)*) and *Sil12* (substrate *Sil(95)*) in Figure 7.5(a). Initially NO_3-N loss through denitrification is greater in the silty loam and results from the greater initial soil moisture content. This initially elevated soil moisture content also results in a higher rate of NO_3-N leaching from the top soil layer of the silty loam which is also enhanced by the higher $K_{(sat)}$. Thus, through the combined action of enhanced denitrification and enhanced leaching NO_3-N is depleted in the top layer of the silty loam at a greater rate than the clay soil. Conversely, NO_3-N is depleted at a reduced rate from the upper soil layer of the clay due to the effects of a lower initial denitrification rate and lower hydraulic conductivity resulting from the combined effects of a lower soil moisture content and a lower $K_{(sat)}$. As the soil moisture content in the top cell of the clay

increases so does the associated denitrification rate (see Equations 3.31 and 3.32). This higher potential for denitrification acts on a higher concentration of NO_3-N in the clay (resulting from

(a)

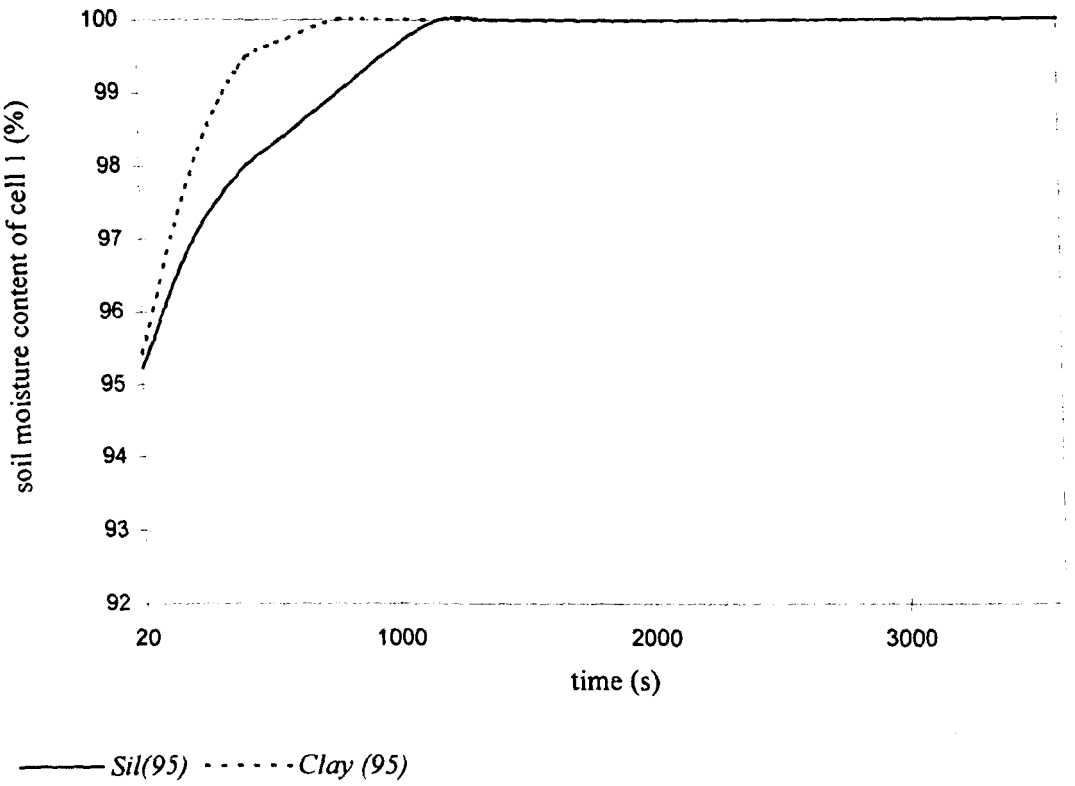

(b)

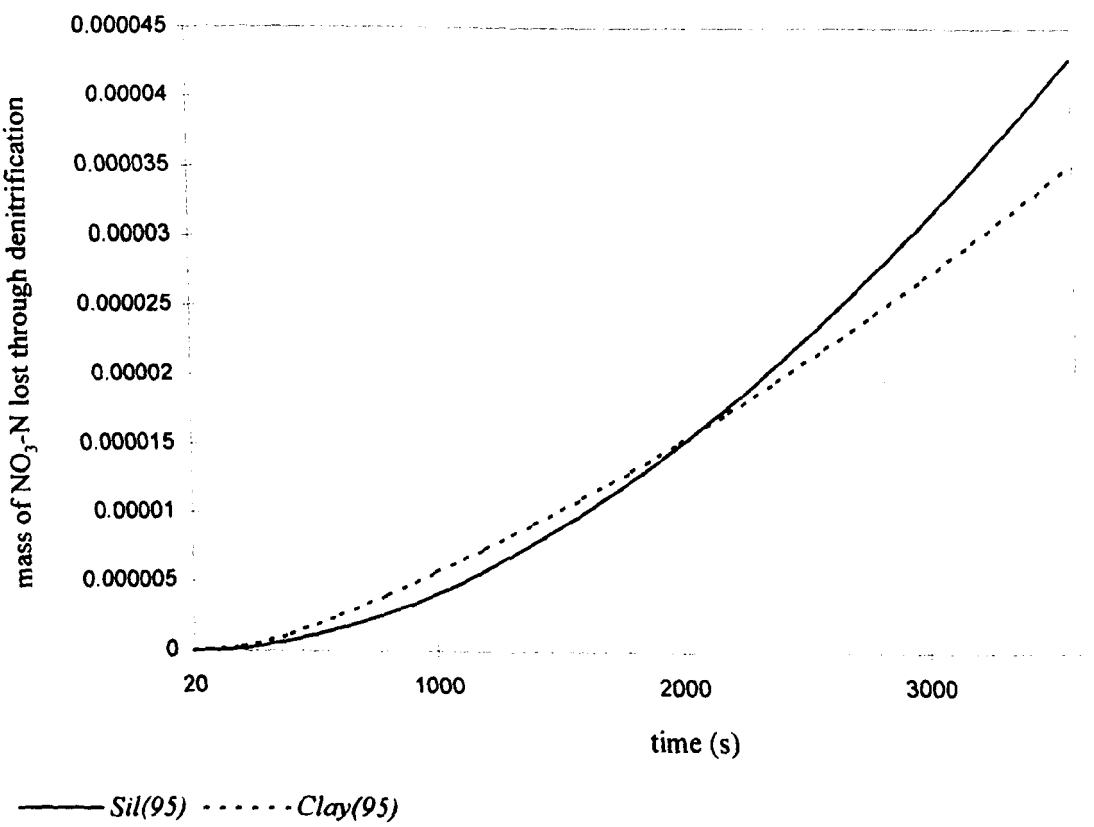

Figure 7.4 Illustration of (a) the change in soil moisture content of the top soil cell at an inundated node over one hour for a silty loam substrate at 95% initial saturation and a clay substrate at 95% initial saturation (b) the cumulative denitrification resulting from these two simulations.

previously lower denitrification rates and comparatively less leaching loss compared to the silty loam) and results in a higher rate of denitrification when compared to the silty loam. This is evident in Figure 7.5(a) where the curves depicting cumulative NO_3-N loss for simulations *Sil12* and *Clay11* cross.

(iii) Denitrification of combined floodwater and in-situ NO_3-N sources: The sequence of losses for this set of simulations (*Clay13*-14 and *Sil13*-14) follows that of the previous set (simulations *Clay11*-12 and *Sil11*-12) and the total losses reported represent the combined floodwater and *in-situ* losses. Total losses are presented in Table 7.3. All subsequent simulations will be run with both a floodwater NO_3-N and an in situ NO_3-N source as this most closely approximates reality.

Both soil water content and the residence time of NO_3-N within the microbially active (denitrifying) environment are widely implicated as major factors in determining the rate of denitrification. Given the importance attached to these two parameters these results are not unexpected and are indeed consistent with results reported by other authors both through observation in the field (Cooper, 1990; Schabel and Stout, 1994) and through modelling studies (Philips, 1989a, b; Chesheir *et al.*, 1987)).

When considering the denitrification of NO_3-N in both surface and subsurface flows saturated hydraulic conductivity assumes a potentially contradictory role in determining NO_3-N loss: elevated permeability increases the total dissolved NO_3-N input to the floodplain buffer by supporting higher infiltration rates but offsets this potential advantage by promoting increased subsurface flow rates, reducing residence time and the opportunity for soil microbes and substrate to interact and, as a direct consequence, lowering NO_3-N attenuation. Philips (1989(b)) demonstrates the interaction between NO_3-N input through infiltration and residence time in a detention-time model developed to evaluate the nonpoint source pollution control effectiveness of riparian buffer zones. Buffer zone effectiveness is based on the detention time of both surface and subsurface flow compared to a reference buffer of known effectiveness (as a reference the author determined the width of buffer necessary to remove 90% of the incoming NO_3-N load) which assumes a first order rate constant for denitrification. With respect to surface-borne pollutants the model illustrates that increasing infiltration in the buffer zone will increase the effectiveness of both dissolved and adsorbed pollution control. Although saturated hydraulic conductivity was found to be a critical factor in deriving the detention model, its ultimate contribution to model output was found to be minor due to conflicting processes operating. High conductivity tended to enhance buffer effectiveness through increasing surface water infiltration but higher conductivity also acted to reduce buffer effectiveness by supporting rapid throughflow in the saturated zone. In terms of a *net* effect, Phillips found that

for his simulations higher saturated hydraulic conductivity infers a slightly positive effect on buffer effectiveness. Total infiltration and associated input of NO_3-N to the Culm site increase with increasing saturated hydraulic conductivity (Figure 7.1(a)), however, total loss of NO_3-N through denitrification of this source is influenced by the interaction of the three controlling factors; initial soil moisture content (which determines initial denitrification rates (see equation 4.32) and residence time), the $K_{(sat)}$ of the soil (which will determine residence time) and the character of the flood event.. Thus, while the total input of NO_3-N in infiltrating floodwater is positively correlated with $K_{(sat)}$, the total loss of floodwater derived NO_3-N through denitrification is found to be the product of the initial soil moisture content, $K_{(sat)}$ and the spatially and temporally nature of the flood event.

Where the denitrification of in situ NO_3-N is considered, the greatest losses are associated with soils that provide the most favourable soil moisture conditions for denitrification (ie 95% saturation rather than 80% saturation) and those which lead to the greatest residence time of NO_3-N within the micobially active top soil layer (ie Clay rather than the silty loam).

From a consideration of the results presented in Table 7.3 in terms of the relative magnitude *of* NO_3-N loss from the two sources it is evident that the overall pattern is dominated by the in-situ NO_3-N source and not by floodwater derived NO_3-N input. These results illustrate that while infiltration increases the soil moisture content of the top soil cell which is significant in providing the conditions required for denitrification (of both the infiltration derived and *in situ* sources), denitrification resulting from infiltration derived NO_3-N represents only a small fraction of the total NO_3-N loss. This is a direct consequence of the relative magnitude of the two sources. For example, the floodwater NO_3-N input in simulation *Clay09* (substrate Clay(80)) is 1535.097Kg while the *in situ* source is 35129.786Kg (the *in situ* source is 22.8 times greater than the cumulative total derived from infiltration). The corresponding losses associated with the two sources are 0.711Kg and 15.89 Kg respectively, a loss from the *in situ* source which is 22.3 times greater than that from the infiltrating floodwater source.

The results from this series of simulations suggests that the overall pattern of NO_3-N loss through denitrification is dominated by the *in situ* NO_3-N source. However, floodwater imparts a significant effect through its effect upon soil moisture content. These observations and comments are drawn from a single set of parameterisation data thought to represent 'typical' parameter values but therefore makes no allowance for parameter variability. Parameter variability is addressed in the following sections.

(a)

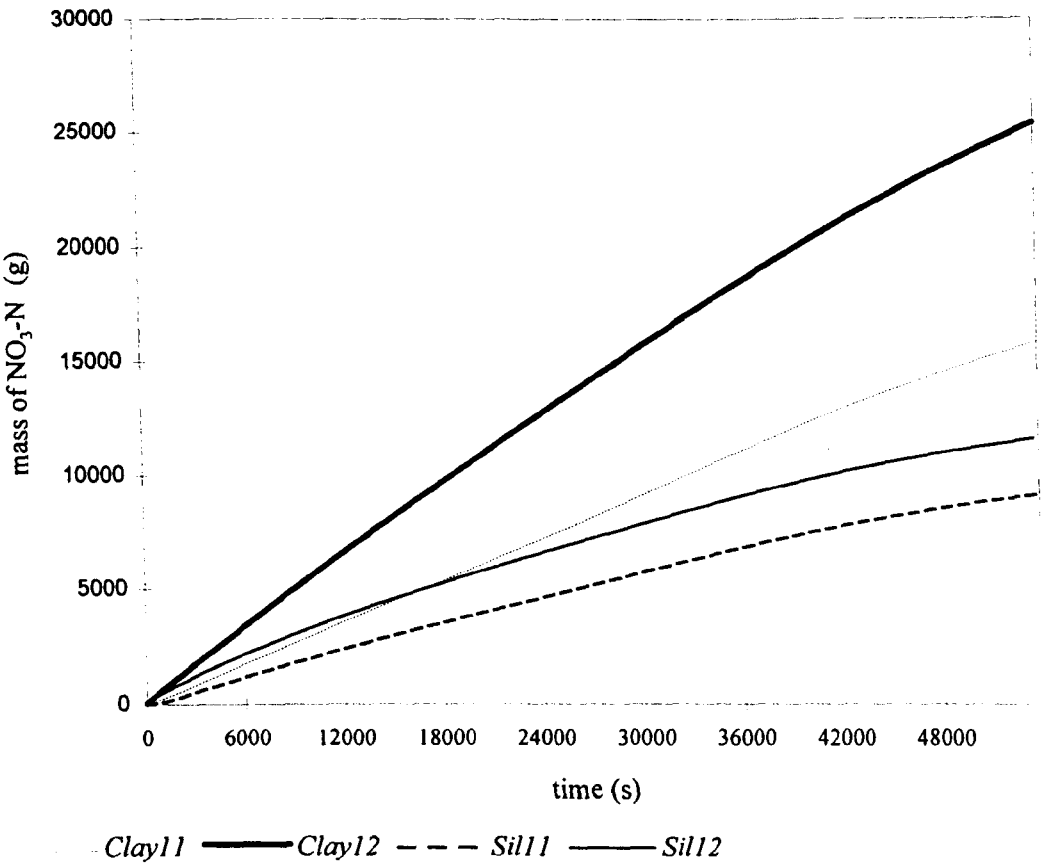

(b)

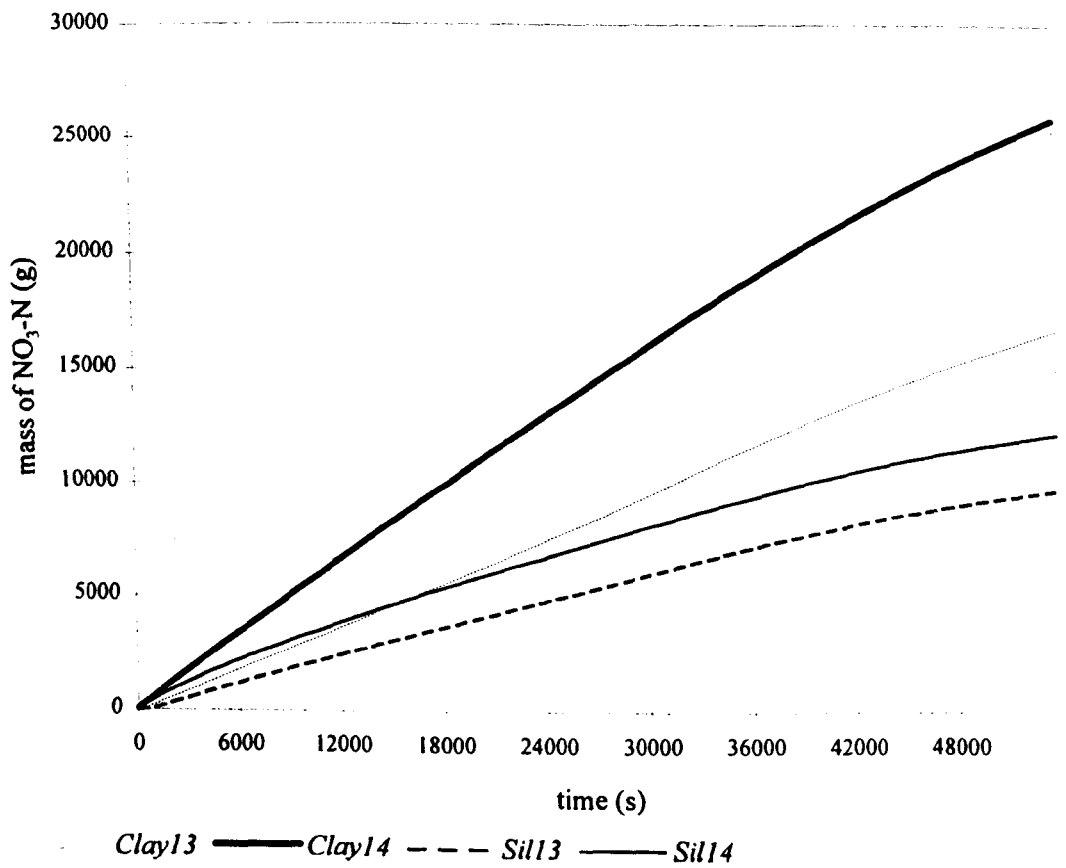

Figure 7.5 (a) Denitrification of in-situ NO_3-N (no input from floodwater), (b) denitrification of the *in situ* and floodwater NO_3-N sources.

7.2.3.2 The sensitivity of the model to in-situ NO_3-N concentration

The second series of simulations (*Clay15*, *Clay16*, *Sil15* and *Sil16*) identified under '**B**' in Tables 7.1 and 7.2 were set up to investigate the effect of the in situ NO_3-N concentration on total denitrification over the range of soil conditions investigated in section 7.2.2.1 and are parameterised in an identical manner except that the in situ NO_3-N concentration is 33.33$\mu g NO_3$-$N g^{-1}$ soil (see Table 7.2). The results illustrate that a halving of the in situ NO_3-N concentration results in a halving of the denitrification loss for all simulations. Halving the initial substrate mass while maintaining the same reaction rate (k_1) is expected to result in a halving of the total NO_3-N loss. The results presented in Table 7.4 illustrate this after account has been taken of the floodwater derived NO_3-N. This has implications for model use where a single model run for a given set of environmental conditions can be used to predict losses for different initial in situ NO_3-N concentrations without the need for further runs.

Simulation code	Total available NO_3-N (g)$^+$	Total NO_3-N loss (g)	Loss as a percentage of total available NO_3-N
Clay15	19099990.6	8656.2	0.045
Clay16	18456032.1	13115.2	0.071
Sil15	19812038.1	5126.7	0.026
Sil16	19370160.4	6296.2	0.033

Table 7.4 Table of results relating to the effect of in situ NO_3-N concentration on denitrification loss (+ = sum of in-situ NO_3-N and total floodwater derived NO_3-N input integrated over the simulation).

7.2.2.3 The sensitivity of the model to the denitrification rate constant.

The third series of simulations (*Clay17*-19, *Sil17*-19) identified under '**C**' in section 7.2.1 enable an investigation into the effect of the denitrification rate constant on total NO_3-N loss over the range of soil conditions already investigated above. The simulations are parameterised in an identical manner to those used in series '**B**' except that the denitrification rate constant employed is 0.0015 rather than 0.0001. The results of the simulations are presented in Table 7.5.

The results illustrate the effect of changes in the denitrification rate constant on the total NO_3-N loss from the floodplain. The results show that there is no simple relationship between the mass of NO_3-N lost and the value of the rate constant (as was the case for initial NO_3-N mass). The rate constant used in this series is 0.0015, which is 15 times larger than in the previous series yet the loss of NO_3-

N in all simulations is less than 15 times the loss from series '**B**'. Dividing each value for total loss in Table 7.5 by 15 produces values which are consistently slightly lower than the output for the comparative simulations presented in Table 7.4. The explanation lies in understanding the dynamic state of these simulations where total NO_3-*N* loss is a product of Equation 4.31 (determined by k_1 and the mass of NO_3-*N*) and the loss of NO_3-*N* from the microbially active cell 1 through infiltration.

Simulation code	Total available NO_3-*N* (g)$^+$	Total NO_3-*N* loss (g)	Loss as a percentage of total available NO_3-*N*
Clay17	19099990.6	129151.7	0.68
Clay18	18456032.1	195573.4	1.06
Sil17	19812038.1	76684.6	0.39
Sil18	19370160.4	94939.7	0.49

Table 7.5 Table of results showing the effect of denitrification rate constant on NO_3-*N* loss. ($^+$ = sum of in-situ NO_3-*N* and total NO_3-*N* input in floodwater integrated over the simulation).

7.2.2.4 Sensitivity of the model to variations in saturated hydraulic conductivity

The forth series of simulations (*Clay19*-22 and *Sil19*-22)) identified as '**D**' in section 7.2.1 investigate the effect of variations in hydraulic conductivity on nitrate loss from the floodplain. The importance of variability in this parameter has already been demonstrated with regard to its control over infiltration rate and it is thus expected to be influential in controlling both the input of NO_3-*N* into floodplain soils and the residence time of the finite *in situ* NO_3-*N* source. The simulations used are set up in an identical way to those used in series '**C**' but for each simulation the value of $K_{(sat)}$ is varied by plus and minus one order of magnitude. The results of the simulations are presented in Table 7.6.

The results for the Silty loam soil at 80% saturation and the Clay soil at 95% saturation only are analysed further in this section. These two soils are chosen as they have previously been shown to result in the minimum and maximum NO_3-*N* losses respectively from the floodplain (see Figure 7.5(b)) and thus represent the two extremes in the model parameterisation. The cumulative NO_3-*N* input to both soils is illustrated in Figure 7.6 for simulations *Sil19, Sil20, Clay21* and *Clay22* and for simulations *Sil09* and *Clay10* which represent the two controls (mean $K_{(sat)}$ values). The cumulative NO_3-*N* loss through denitrification is illustrated in Figure 7.7 for the same simulations (*Sil19, Sil20, Clay21* and *Clay22*) and the controls are *Sil17* and *Clay18.*

(a)

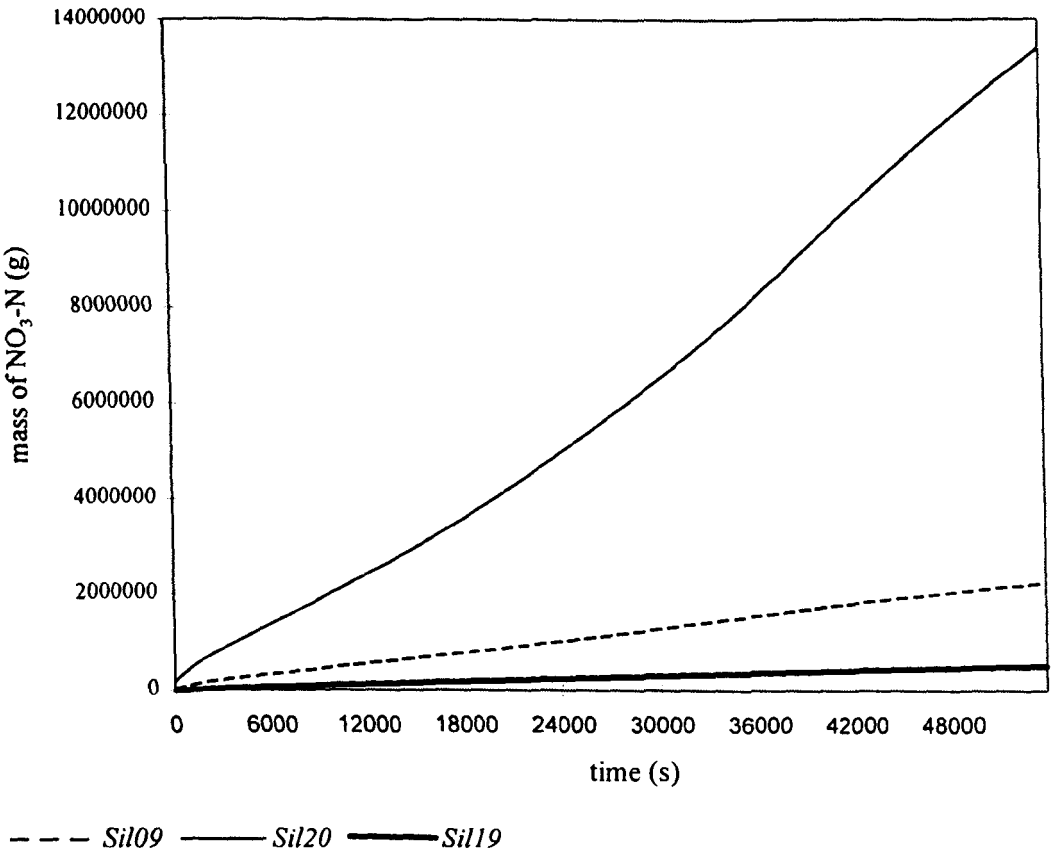

(b)

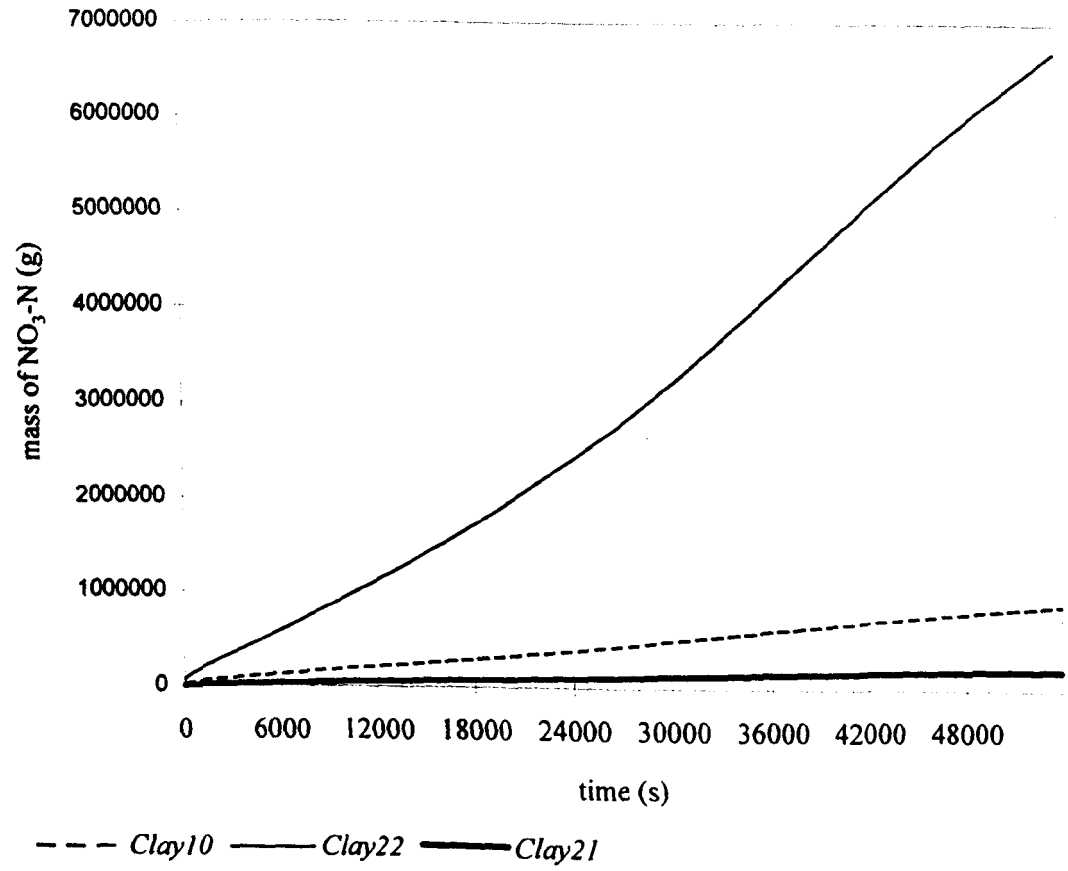

Figure 7.6 Illustration of the total NO3-N input in infiltrating floodwater for simulations (a) Sil09, Sil19 and Sil20 and (b) Clay10, Clay21 and Clay22.

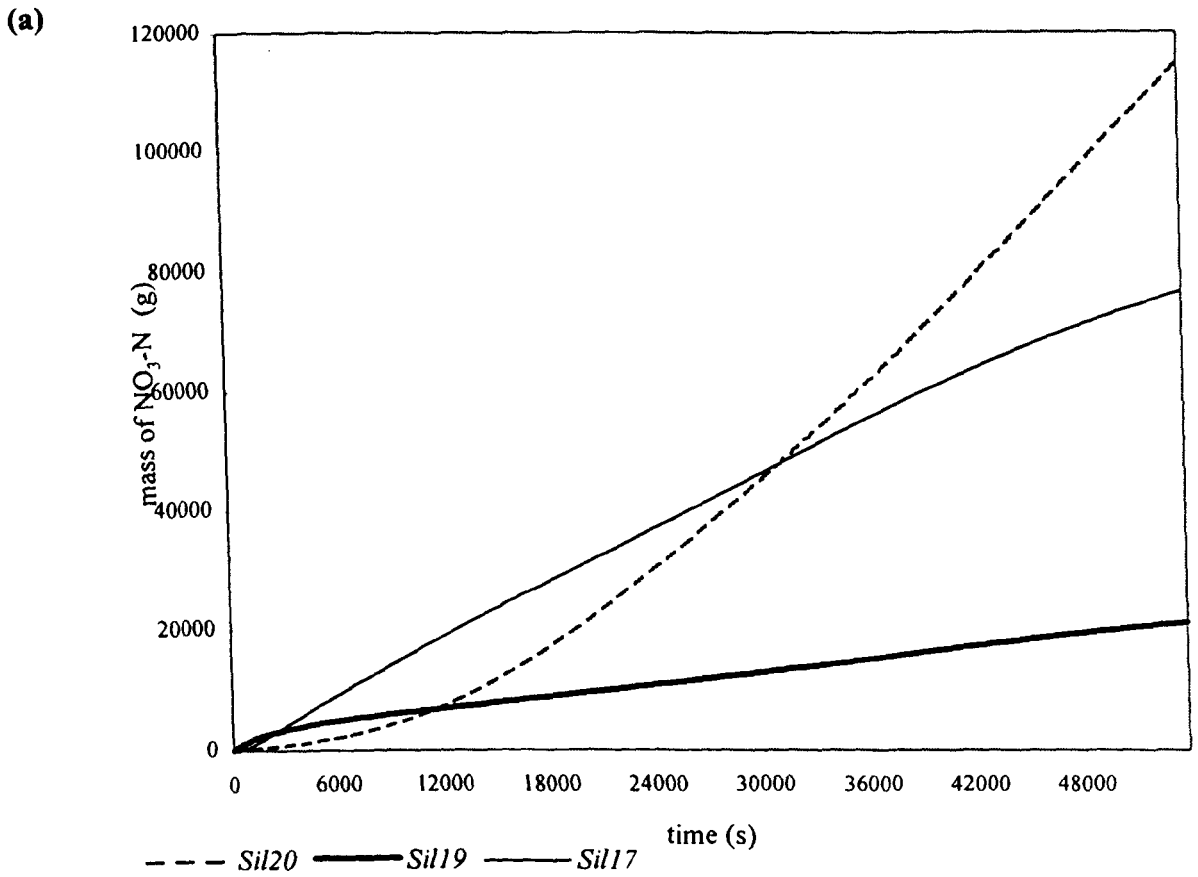

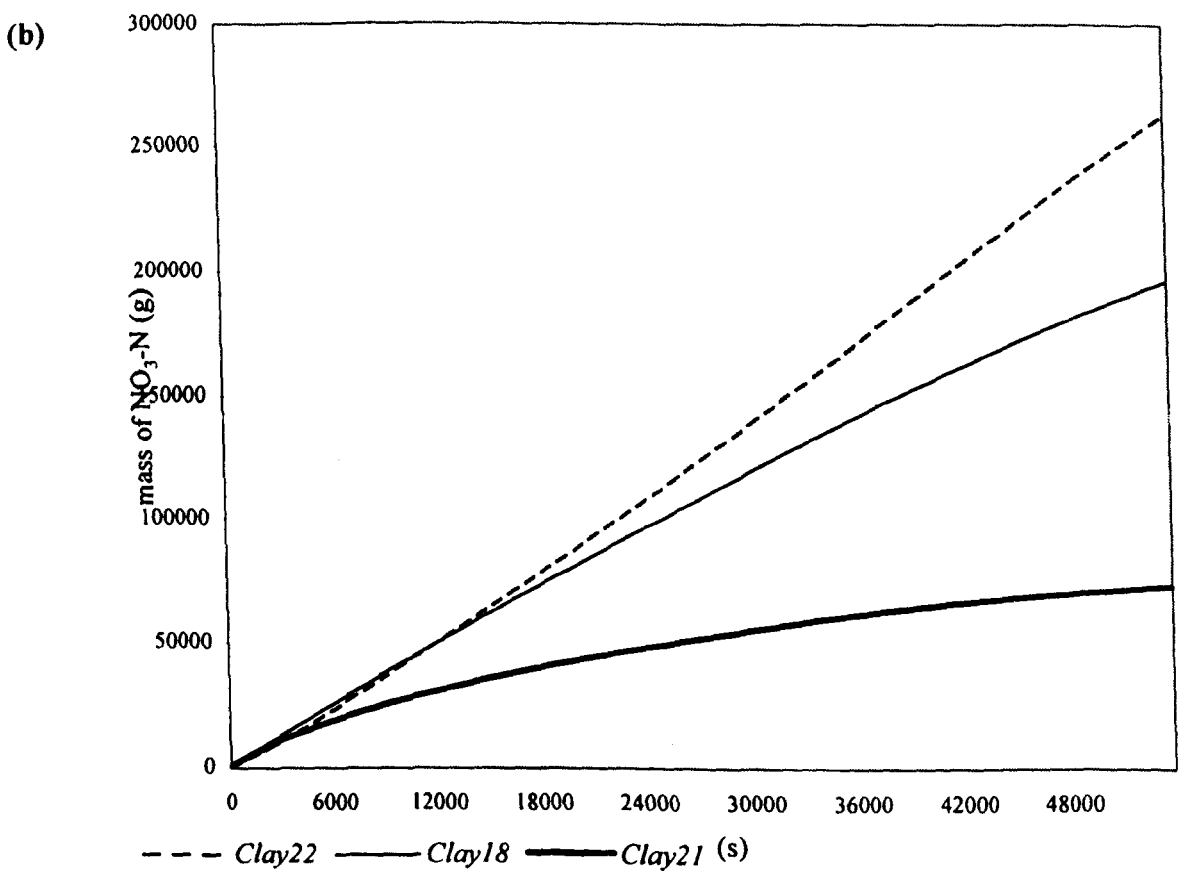

Figure 7.7 Illustration of the total NO3-N loss through denitrification for simulations (a) Sil17, Sil19 and Sil20 and (b) Clay18, Clay21 and Clay22.

Simulation code	Saturated hydraulic conductivity (K_{sat})	Total available NO_3-N (g) $^+$	Total NO_3-N loss (g)	Loss as a percentage of total available NO_3-N
Clay19	$5.56x10^{-8}$	24792244.0	36810.7	0.15
Clay20	$5.56x10^{-6}$	18094067.1	177573.1	0.98
Clay21	$5.56x10^{-8}$	24271285.1	73382.3	0.30
Clay22	$5.56x10^{-6}$	17768732.0	262501.9	1.48
Sil19	$1.25x10^{-7}$	30957531.2	21116.4	0.07
Sil20	$1.25x10^{-5}$	18079105.4	114810.1	0.64
Sil21	$1.25x10^{-7}$	30752847.4	23516.2	0.08
Sil22	$1.25x10^{-5}$	17826398.2	181069.9	1.02

Table 7.6 Table of results showing the effect of saturated soil hydraulic conductivity on NO_3-N loss.

These results demonstrate a significant impact on both the total input of NO_3-N to the floodplain soil and the pattern of subsequent NO_3-N loss through denitrification. These results can be explained in terms of the interaction between residence time, initial soil moisture content and NO_3-N supply. Considering the silty loam soil first, the observed pattern can be explained as follows: Initially the rate of NO_3-N loss through denitrification is greatest for the silty loam soil with lowest saturated hydraulic conductivity (simulation *Sil19*) with the lowest loss corresponding to the silty loam with the highest $K_{(sat)}$ (simulation *Sil20*). This initial pattern can be explained in terms of the different NO_3-N residence times for the soils where the soil with the highest $K_{(sat)}$ allows rapid leaching of NO_3-N from the top cell which in turn limits the availability of NO_3-N for denitrification and thus total denitrification. Conversely, the soil with the lowest $K_{(sat)}$ has the longest residence time which supports a lower rate NO_3-N leaching and consequently the greatest NO_3-N loss through denitrification. Initially, the in situ NO_3-N concentration dominates in determining the magnitude of the denitrification loss (this has been demonstrated before - see section 7.2.2.1) and thus the input of NO_3-N in infiltrating floodwater is not significant during this initial phase of the simulation.

However, with time the relative importance of two effects, residence time and the supply of NO_3-N in infiltrating floodwater, alter such that the supply of NO_3-N dominates in determining denitrification losses. This can be seen in the progression of the curve for simulation *Sil20* which begins with the lowest NO_3-N loss through denitrification but this then increases to exceed that of simulations *Sil19* and *Sil17*. The same pattern is observed for the simulations run on the clay

substrate but the effects are less pronounced. This can be explained through the lower $K_{(sat)}$ values associated with this soil which dampens the effects observed for the silty loam.

The results from section 7.2.2.1 illustrate that the pattern of NO_3-N loss through denitrification is dominated by the in situ NO_3-N source. The results from this section suggest that where variability in $K_{(sat)}$ is considered, this is not necessarily the case. The results illustrate that increasing $K_{(sat)}$ both diminishes the influence of the in situ NO_3-N source through increasing the rate at which this finite supply is leached from the microbially active top soil layer and at the same time increases the magnitude and relative significance of the floodwater derived NO_3-N source. Thus, in these simulations where $K_{(sat)}$ is increased the overall pattern of NO_3-N loss through denitrification changes to become dominated by the floodwater derived NO_3-N source which represents a reversal of the findings presented in section 7.2.2.1. These results illustrate the potential significance of variations in $K_{(sat)}$ on model predictions.

7.2.3.4 Culm floodplain NO_3-N losses in the context of reported floodplain losses

The discussion above concentrates on an explanation of the results in terms of the processes operating in the floodplain environment. The following discussion considers the magnitude of the results of simulations *Clay13-Clay22* and *Sil13*-22 in the context of published data on denitrification rates (simulations *Clay09-Clay12* and *Sil09-Sil12* are not considered as they neglect the effects of in situ and floodwater NO_3-N). The rate of NO_3-N loss associated with each simulation is presented in Table 7.8 both as a loss per hectare (KgN $ha^{-1}d^{-1}$) and a loss per gram of soil (μgN $g^{-1}d^{-1}$) for direct comparison with the denitrification rate data presented in *Chapter 4* (Table 4.3).

The simulated losses of NO_3-N for the Culm represent an integrated loss resulting from a potential floodplain soil volume of 351297.86 m^3 which is derived by multiplying the modelled floodplain surface area of 3512978.6 m^2 by the assumed microbially active layer which extends to a depth of 0.1m below the floodplain surface. Losses expressed per gram of soil are calculated for the same soil volume by assuming a soil bulk density of 1.5g cm^3 (which is considered a reasonable estimate for alluvial soils - Brady, 1990) resulting in a total mass of 5.2694679×10^{11}g .

Measured denitrification rates for riparian and agricultural (non-riparian) soils are presented in Table 4.3 along with DNP data. The range of denitrification rates encompassed by each of these different 'systems' is presented in Table 7.8 for comparative purposes in the following discussion.

Measured denitrification rates for the riparian soils presented in Table 7.8 range from 0.014 (Hanson *et al.*, 1994) to 81.12 KgN ha^{-1} d^{-1} (Cooper, 1990) which compares to a range of 0.0233 to 1.196 KgN ha^{-1} d^{-1} for the Culm simulations. The lowest rate is associated with simulation *Sil15*

(substrate *Sil(80)*, 10mgl^{-1} in floodwater, 33.33µg NO_3-N g^{-1} , k_1 = 0.0001) and compares to the lowest rates measured by Hanson *et al.* (1994) for a moderately well drained soil receiving low NO_3-N loading in groundwater (see Table 4.3). In the same study denitrification rates reached a maximum of approximately 0.11 KgN ha^{-1} d^{-1} in poorly drained soils located in the valley bottom supporting both higher soil moisture contents and higher available carbon contents. Estimates of annual losses ranging from 30 to 40 KgN ha^{-1} y^{-1} have consistently been reported in the literature for natural forested buffer systems in the USA (Hanson *et al.* (1994), Lowrance *et al.*, 1984) and are consistent with the lowest rates reported for the Culm simulations (see Table 7.7).

Simulation code	simulation series	Total loss of NO_3-N /15hrs (g)	Loss per hectare (KgNha^{-1}d^{-1})	Loss per hectare (KgNha^{-1}y^{-1})	Loss per gram of soil (µgNg^{-1}d^{-1})
Clay13	A	16601.2	0.0756	27.59	0.0504
Clay14	A	25806.3	0.1175	42.88	0.0784
Sil13	A	9694.6	0.0442	16.13	0.0294
Sil14	A	12119.8	0.0552	20.15	0.0368
Clay15	B	8656.2	0.0394	14.38	0.0263
Clay16	B	13115.2	0.0597	21.79	0.0398
Sil15	B	5126.7	0.0233	8.50	0.0156
Sil16	B	6296.2	0.0287	10.48	0.0191
Clay17	C	129151.7	0.5882	214.69	0.3922
Clay18	C	195573.4	0.8908	325.14	0.5938
Sil17	C	76684.6	0.3493	127.49	0.2328
Sil18	C	94939.7	0.4324	157.82	0.2883
Clay19	D	36810.7	0.1677	61.21	0.1118
Clay20	D	177573.1	0.8088	295.2	0.5392
Clay21	D	73382.3	0.3342	121.98	0.2228
Clay22	D	262501.9	1.1956	436.39	0.7971
Sil19	D	21116.4	0.0962	35.11	0.0641
Sil20	D	114810.1	0.5229	190.86	0.0349
Sil21	D	23516.2	0.1071	39.09	0.0714
Sil22	D	181069.9	0.8247	301.0	0.5498

Table 7.7 Rates of NO_3-N loss for the Culm simulations expressed as totals for each simulation and equivalent daily losses per hectare and per gram of soil.

Ecosystem type	minimum denitrification rate (KgN ha^{-1} d^{-1})	maximum denitrification rate (KgN ha^{-1} d^{-1})
Riparian soils	0.014 (Hanson et al, 1994)	81.12 (Cooper, 1990)
Agricultural (non-riparian) soils	0.069 (Barraclough et al, 1992)	>2 (Eggington and Smith, 1986)
DNP	0.014 (Cooper et al, 1990)	174.9 (Bijay-Singh et al, 1988)
Culm	0.023	1.196

Table 7.8 Range of denitrification rates reported for riparian soils, agricultural (non-riparian) soils, denitrification potentials and the Culm simulations.

There are obvious problems in comparing annual averages reported by authors such as Hanson *et al.* (1994) with the short time event based Culm simulations which are integrated over considerably shorter time base (15 hours). Perhaps the most significant problem is that while the Culm simulations represent potentially high denitrification flux periods such events are subsumed within the average values presented by Hanson *et al.* (1994) and other annually reported losses. It might reasonably be expected, therefore, that the equivalent daily losses reported for natural forested buffer systems in the USA will be less than, or at least at the lower end of the range for, those found for the Culm simulations. Denitrification rates in floodplain riparian soils have also been reported over considerable shorter time periods, including hourly (Cooper, 1990), daily (Schipper *et al.*, 1993; Gale *et al.*, 1993) and monthly (Haycock and Burt, 1993; Maltby *et al.*, 1996). Such data are potentially of greater use for comparison with the results of the Culm simulations as they are indicative of shorter term environmental factors.

Schipper *et al.* (1993) and Haycock and Burt, 1993) both reported measured rates of denitrification which exceed the maximum rates for the Culm simulations by an order of magnitude. Schipper *et al.* (1993) measured very high denitrification rates in the top 30cm of an organic riparian soil in New Zealand (11.2 KgN ha^{-1} d^{-1}). However, despite the fact that denitrification rates associated with the soils of this study are likely to be high, supported by average organic matter contents of 26% and high soil moisture contents, the reported rates are probably over estimates of actual denitrification rates as they were derived from soil slurries which were made anaerobic with argon gas (in effect, therefore, they represent estimates of DNP). For a floodplain section of the River Leach, UK, Haycock and Burt (1993) inferred a maximum monthly mean denitrification rate for February 1990 of 740mg NO_3-N m^{-2} d^{-2} which equates to a daily loss per hectare of 7.4 Kg. Again,

this represents a maximum loss which exceeds the maximum losses from the Culm simulations by an order of magnitude.

The highest rates of denitrification presented in Table 4.3 were reported by Cooper (1990) for riparian soils of a small headwater stream in New Zealand. Rates equivalent to 81.12 KgN ha^{-1} d^{-1} were recorded for anoxic soils with high microbially available carbon contents and a high enzymatic capacity to denitrify. However, high rates such as those reported above were limited spatially to the interface with the organic soil and where denitrification rates were calculated on a catchment-wide basis the mean areal rates of denitrification fell to between 0.3 and 2.1 mg m^{-2} h^{-1} (which equates to losses of 0.072 KgN ha^{-1} d^{-1} / 26.28 KgN $ha^{-1}y^{-1}$ and 0.504KgN ha^{-1} d^{-1} / 183.96 KgN ha^{-1} y^{-1}, assuming a microbially active layer of 10cm in depth and a bulk density of 1.5g cm^3) which fall within the range generated by the Culm simulations. Little or no NO_3-N penetrated beyond the first 5m into the organic soil, accordingly the reduction in arealy integrated denitrification rates was attributed to NO_3-N limitations.

Other authors have recorded rates of denitrification which match those reported for the Culm simulations. In a study into the denitrification capacity of riparian soils associated with the River Torridge in NW Devon, UK, Maltby *et al.* (1996) reported (mean monthly) denitrification rates of between 0.026 and 0.67 Kg ha^{-1} d^{-1} which falls within the range reported for the Culm simulations.

However, there are a number of significant problems in comparing the results obtained from the Culm simulations with those reported for equivalent ecosystems in the literature. Firstly, rates of denitrification reported in the literature derive from point samples for which denitrification rates are taken and then extrapolated to provide daily, monthly or annual losses. For example, Hanson *et al.* (1994) estimate daily and annual denitrification losses (in KgN ha^{-1}) for each soil type in their study based on the results of 5 to 6 soil cores (15cm depth by 2cm diameter) taken at weekly or biweekly intervals during the spring and autumn and monthly intervals during the summer for a total of fifteen sampling dates between March 1991 and March 1992. In contrast, the rates generated by the Culm simulations derive from dynamic conditions which are spatially and temporally variable and from which an integrated loss is calculated for the entire floodplain area which includes areas which attain high rates of denitrification as well as those in which denitrification occurs at the background rate. Secondly, the available concentration of NO_3-N is often found to be the limiting factor in denitrification rates in riparian soils (Cooper, 1990) while at the same time it is critical in determining the rate of NO_3-N loss in the Culm simulations (see Equation 4.31). Differences in the availability of NO_3-N will greatly influence the rates of loss from different soils.

However, it is the very nature of the research in which the spatial and temporally integrated nature of floodplain NO_3-N dynamics is studied that presents the problems identified above while at the same time highlight the potential problems in validating such a model. However, what the discussion does provide is an indication of how the results of the Culm simulations, presented as daily rates of NO_3-N loss, compare to those reported in the literature for other riparian systems. This comparison suggests that the results of the Culm simulations are broadly consistent with those reported in the literature for riparian soils. Those cases in which rates are found to be higher (eg Cooper et al, 1990; Haycock and Burt, 1993) relate to maximum rates which are subsumed in the spatial and temporal integration of NO_3-N loss and rates calculated for the Culm simulations.

7.2.3 Developing an event based surface water NO_3-N budget

The results from the first four simulations undertaken in this analysis (*Sil09*, *Sil10*, *Clay09* and *Clay10*) provide data pertaining to the potential of the floodplain NO_3-N sink in terms of its effect upon the surface water NO_3-N budget. These data are presented in Table 7.9 in terms of their effects upon the surface water budget for two scenarios where: (i) only that NO_3-N which is denitrified is considered in the NO_3-N river budget (this assumes that all other NO_3-N entering the floodplain soil system re-enters the surface water system at some later point in space and time and (ii) all NO_3-N entering the floodplain soil through infiltration is subsequently 'attenuated' and does not re-enter the river system (surface water). As the passage of water back into the surface water system is not considered the NO_3-N filtering capacity of the floodplain cannot be considered in terms of its implications for surface water quality (ie changes in the concentration of NO_3-N in surface water) and such effects can only be implied. However, losses can be considered in terms of a flood water NO_3-N budget.

Simulation code	Total flood volume (input) (m^3)	Total NO_3-N input to domain (g)	Total NO_3-N infiltrated (g)	Total NO_3-N denitrified (g)	*Considering denitrified NO_3-N only:* Total loss as (%)	*Considering infiltrated NO_3-N:* Total loss as (%)
Clay09	2205579.8	22055797.5	1535097.7	711.1	0.0032	6.96
Clay10	2205579.8	22055797.5	891139.2	424.0	0.0019	4.04
Sil09	2205579.8	22055797.5	2247145.2	558.7	0.0025	10.19
Sil10	2205579.8	22055797.5	1805267.5	472.6	0.0021	8.19

Table 7.9 Table of results showing NO_3-N losses in terms of (a) NO_3-N denitrified and (b) total NO_3-N infiltrated to the floodplain.

The quality of surface water is determined by the quality of the various water sources from which it is derived. These include the groundwater source, surface runoff and direct inputs through precipitation and non-point pollution sources. Within the channel water quality can be further influenced through the metabolic processes of within channel aquatic plants and through denitrification occurring at the water-sediment interface (Van Kissel, 1977) where the flow of water is slow enough not to aerate the thin layer of anaerobic sediment. During flooding, water quality will be further influenced through the interaction of floodwater with the subsurface soil environment following infiltration (Maltby *et al.*, 1991;1996; Brunet *et al.*, 1994). The potential improvement that riparian soils infer upon the quality of both subsurface and surface water moving laterally towards the channel and the subsequent within channel processing of NO_3-N have been widely implicated in improvements in catchment surface water quality and have been discussed in *Chapter 4*. In contrast very little has been done to quantify the potential surface water quality improvements derived through the interaction of NO_3-N loaded floodwater with floodplain soils at scales above that of the field (Maltby et al, 1991). Yet, if the floodplain can remove NO_3-N from inundating floodwater then the potential for water quality improvement exists. This is considered now with reference to simulations *Clay09*, *Clay10*, *Sil09* and *Sil10* in terms of a floodwater NO_3-N budget.

The results presented in Table 7.3 from simulations *Clay09*, *Clay10*, *Sil09* and *Sil10* demonstrate that the floodplain acts as a sink for flood borne NO_3-N which is denitrified after entering the floodplain soil. The floodplain also provides a potential sink for a considerably greater mass of NO_3-N which enters the soil as a dissolved load with infiltrating floodwater, however, as this is not denitrified immediately it is available to re-enter the surface water system through subsurface flows or to be denitrified later. These losses can be considered in terms of a surface water NO_3-N budget which considers the loss of NO_3-N in terms of the total NO_3-N input in the flood hydrograph.

The results presented in Table 7.9 illustrate that for all of the simulations while the total NO_3-N input in infiltrating floodwater is considerable the denitrification of this source is small and as such an insignificant effect is inferred upon the surface water NO_3-N budget. The maximum loss of floodwater NO_3-N, generated by simulation *Sil09* (substrate *Sil(80)*), represents 0.0032% of total NO_3-N entering the reach (22055.7975 Kg) calculated as a percentage of the total NO_3-N entering the reach during the flood hydrograph. NO_3-N denitrified cannot re-enter the surface water system. However, if it is now assumed that all of the NO_3-N entering the soil system is subsequently denitrified (or at least stored) within the floodplain soil and does not therefore re-enter the surface water system then the magnitude of loss becomes significant. Losses now range from 10.19% of the total NO_3-N input to the system for simulation *Sil09* (substrate *Sil(80)*) to 4.04% for simulation *Clay10* (substrate *Clay(95)*).

Reductions in the mass of NO_3-N in surface waters during flood events will derive from the metabolic utilisation of NO_3-N by aquatic plants, denitrification at the water-sediment interface and denitrification following the infiltration of NO_3-N loaded floodwater into floodplain soils. The results suggests that while the total input of NO_3-N into the floodplain soils is high, denitrification accounts for the loss of only a small fraction of this and consequently has an insignificant effect upon the NO_3-N budget of the river. However, this effect will be considerably greater if the total input of NO_3-N to floodplain soils is considered in the floodwater NO_3-N budget. This suggests that where the management of floodplains is directed towards increasing the attenuation of NO_3-N within the floodplain soil this could have a potentially profound impact on the ability of the floodplain to regulate storm water NO_3-N loads. In upland regions considerable water quality improvements can derive from the nutrient filtering effects of riparian buffers through which water passes on route to the channel. The relative effects of buffering lateral flows on surface water are substantially reduced in lowland floodplain environments during flood events which implies that any buffering of NO_3-N entering the floodplain environment brought about through the interaction of floodwater NO_3-N with floodplain soils is of particular significance. Through maximising the attenuation of floodwater NO_3-N before it passes back into the surface water system, or indeed groundwater or aquifer systems, significant reductions in NO_3-N may therefore be achieved.

7.3 Discussion and Conclusions

The utility of the integrated floodplain hydrology-nitrate model has been assessed through its application to the five specific aims outlined at the beginning of this chapter.

The results have illustrated that the relative importance of the floodwater derived and in situ NO_3-N sources is related to the $K_{(sat)}$ of the soil where an increasing $K_{(sat)}$ increases the relative significance of the floodwater NO_3-N source through increased NO_3-N input to the soil environment. Indeed, changes in $K_{(sat)}$ have been shown to result in a profound effect upon the relative significance of the two potential sources of NO_3-N for denitrification investigated. Changes in the mass of in situ NO_3-N and changes in the denitrification rate constant have predictable results upon the loss of NO_3-N through denitrification.

Model predicted NO_3-N loss depends upon the parameterisation chosen for each simulation. However, a comparison of the simulation results covering the range of parameter values employed with those reported for similar ecosystems in the literature suggests that the model predictions are consistent with those reported for a wide range of similar riparian environments.

The point was made in *Chapter 6* that it is not possible to examine the potential variability in all model parameters consistent with a full sensitivity analysis. As was the case for *Chapter 6*, the simulations run in this chapter have concentrated on a relatively narrow parameter range. Nevertheless, from the results obtained, which demonstrate the direction and magnitude of the interacting processes, it is possible to speculate about the impact of inundation in different environments. For example, the results from section 7.2.2.4 illustrate the importance of $K_{(sat)}$ on model prediction and illustrate that higher values of this parameter can lead to an increase in the importance of floodwater derived NO_3-N in the total loss of NO_3-N from floodplain soils. Where increased NO_3-N input is coupled with an increase in the potential of the soil to denitrify (represented in the model through an increase in the denitrification rate constant) then the potential for the floodplain to act as a significant sink for flood-borne NO_3-N increases. This is suggested by the results of section 7.2.2.4 which are illustrated in Figure 7.6 and 7.7. Indeed, the model offers the potential for developing scenario testing in which parameters relating to the hydraulic, hydrological and chemical (nitrogen) nature of the floodplain under investigation are varied over a specified range to determine model response (in this case denitrification loss). The results of such analyses could then be used to determine the NO_3-N management potential of floodplain riparian sites. The potential for model application need not stop at investigations of NO_3-N as the transport and decay of other chemical species could be included within the existing model structure. The model is currently being applied to model the spatial variability of floodplain soil contamination during flooding in an attempt to improve flood chemical mass balance estimates (see Stewart *et al.* (*in press*))

Although the results obtained derive from a narrow range of parameter values they adequately serve to demonstrate the utility of the model both in terms of the original concept (developing an integrated approach to modelling floodplain hydrology and NO_3-N chemistry) and in terms of the need for a spatially distributed approach to modelling floodplain NO_3-N dynamics.

Chapter eight

Conclusions and Recommendations

8.1 Introduction

The aim of this thesis has been to present a novel conceptual approach to modelling floodplain hydrology which addresses the fundamental need to consider the interaction between surface and subsurface flows in the floodplain environment.

A deterministic approach is adopted which combines the high spatial resolution of surface flow processes afforded by a state-of-the-art finite element hydraulic model with a 1D finite difference approximation of subsurface flow. The utility of this integrated approach is addressed through application of the model to assess the impact of infiltration on hydraulic model prediction and the impact of flood events on NO_3-N dynamics within the floodplain environment.

In *Chapter 1* the development of an integrated floodplain hydrology model was identified as a prerequisite to the accurate representation of fluvial, hydrological, chemical, sedimentological and geomorphological processes operating on the floodplain. This argument is developed in *Chapter 2* through the examples of floodplain flow prediction using numerical models and the impact of flood water on floodplain nutrient loading and the buffering capacity of floodplain soils.

Chapter 3 describes the development of the coupled physically-based floodplain hydrology model which is to provide the basis of the investigation into the stated need for an integrated approach to modelling floodplain hydrology. The model couples the 2D spatial resolution of surface flow afforded by a 2D finite element model with a 1D finite-difference representation of subsurface hydrology.

In *Chapter 4* those factors which are influential in determining the concentration of the NO_3-N ion in temperate floodplain ecosystems during the winter months are identified and incorporated within the coupled floodplain hydrology model. By incorporating the nitrate model within the structure of the coupled floodplain hydrology model it (the transport of the NO_3-N ion) is afforded the same level of spatial representation as the subsurface hydrology.

Chapters 5, 6 and 7 are concerned with the application of the coupled floodplain hydrology-nitrate model. *Chapter 5* provides the range of conditions over which the model is to be applied, including the reach, flood events and the range of soil and NO_3-N conditions. In *Chapter 6* the impact of relaxing the surface boundary of TELEMAC2D on flood flow prediction is assessed. In Chapter 7 the potential of the integrated approach to modelling floodplain hydrology is investigated in terms of its applicability to the investigation of flood driven NO_3-N dynamics in the floodplain environment.

This chapter now considers the extent to which the research objectives have been accomplished and ends with recommendations for further research needs which have become apparent during this thesis.

8.2 Realisation of the thesis aims

Four specific research objectives are listed in Chapter 2. It is the intention of this section to consider the extent to which objectives (2) and (4) have been met through the application of the integrated floodplain hydrology-nitrate model developed according to objectives (1) and (3). Objectives (2) and (4) were respectively:

- *to determine the impact of infiltration on hydraulic model flow prediction*

- *to examine the contention that flood events represent high denitrification flux periods in floodplain soils in terms of (i) the loss of in situ soil NO_3-N and (ii) the input and subsequent loss of infiltrating floodwater NO_3-N.*

8.2.1 Impact of infiltration on flow prediction

The importance attached to the accurate prediction of the spatial distribution and character of flood flow was established in *Chapter 1* while in *Chapter 2* it was demonstrated that 2D finite element hydraulic models which currently provide the best spatially distributed representation of floodplain flows are potentially compromised through a failure to account for infiltration. The results of

Chapter 6 illustrate that infiltration can have a potentially significant impact upon the distributed nature of flood flow over the surface (for example see Figures 6.5 and 6.7 which illustrate the impact of infiltration on simulated mean surface water depth and on inundation extent respectively) which impacts on the simulated output hydrograph characteristics measured at the downstream boundary (for example see Figure 6.1 which illustrates the impact of infiltration on the predicted output hydrograph). The magnitude of the effect is found to be related to both the propensity of the floodplain soil to infiltrate and to the characteristics of the flood event. Total losses are consistently greater for the silty loam soil (mean $K_{(sat)}$ of 1.25×10^{-6}) compared to the clay soil (mean $K_{(sat)}$ of 5.56×10^{-7}) and for soils at 80% initial soil moisture compared to those at 95%. The effect of flood character on volumetric infiltration loss can be seen in terms of the total reduction in simulated discharge volume which is greater for the 1 in 5 year event for all comparative runs, however, the relative loss, expressed in terms of the respective control runs, is consistently greater for the 1 in 1 year event.

The spatially distributed approach has highlighted the changing controls over process domination within the floodplain. This is illustrated throughout the simulations in *Chapter 6* through the change in the relative importance of initial soil moisture and $K_{(sat)}$ in determining the rate of infiltration during the simulations. The result of this is illustrated, for example, in Figure 6.1 (the simulated output hydrographs) and Figure 6.5 (the mean difference in water depth between the simulations incorporating a relaxed surface boundary and their respective controls).

The impact of infiltration on the flood hydrograph characteristics is demonstrated in Table 8.1 which summarises the greatest effects resulting from the simulations run in *Chapter 6* where mean $K_{(sat)}$ values are employed.

Flood hydrograph characteristic	Simulation code	Magnitude of effect (%)
Total discharge volume (m^3)	*Sil01*	-11.0
Time to peak discharge (s)	*Sil03*	+0.53
Peak discharge (m^3s^{-1})	*Sil01 & Sil02*	-6.77

Table 8.1 Summary of the maximum impact on infiltration resulting from the simulations run in *Chapter 6* where 'mean' $K_{(sat)}$ values are used.

These results illustrate that a potentially significant process is not considered in current 2D representations of floodplain surface flow. However, the potential magnitude of the error on the

observed outflow hydrograph is significant (see section 5.2.2.1) making a quantitative comparison with the observed data difficult. Nevertheless, the results illustrate that infiltration has a potentially significant impact on model prediction and that this can be quantified with reference to the control simulations. The discussion returns to consider the issues of calibration and validation data later.

The impact of infiltration on model prediction suggests that it has implications for the fluvially driven processes operating on the floodplain including sedimentology and floodplain chemical processes. The impact of infiltration on flow velocities, for example, will have important implications for sediment transport where velocities are reduced below threshold particle settling values. Thus the impact of infiltration has implications relating to both the type of sediment deposited and the total area of deposition.

In terms of addressing objective (2), the research has demonstrated that infiltration can significantly impact on the prediction of flood flow using 2D finite element hydraulic models.

8.2.2 An integrated approach to modelling floodplain NO_3-N dynamics

Perhaps the most important point to highlight here is that prior to the development of the model such a spatially distributed approach to modelling fluvially driven *NO_3-N* process dynamics was not available. A simplistic approach was adopted for modelling both *NO_3-N* transport and denitrification and the model takes no account of diffusive and dispersive processes in *NO_3-N* transport but instead assumes complete solute mixing within each cell prior to the subsequent time step. The representation of denitrification through a simple rate equation takes no account of carbon availability, temperature or pH while other processes of the N-cycle which impact on the concentration of *NO_3-N* were not included (for example, nitrification and immobilisation).

Mathematical models will always represent simplifications of the systems and processes they purport to describe while the results of the deterministic model developed and applied here are further limited through an inability to account for parameter variability. However, the research in *Chapter 7* has shown the use of a spatially distributed modelling approach to be indispensable in modelling flood water *NO_3-N* dynamics. Significantly, the model is able to discern internal process interaction, for example, with regard to the denitrification of the infiltrating floodwater *NO_3-N* source (see Figure 7.1(b)) while the magnitude of *NO_3-N* loss is found to fall within the range reported for riparian soils (see Table 7.8). However, as the variability in denitrification rates measured in the field is often considerable (see Table 4.3) a failing in the model developed, and one which is common to all deterministic approaches, is an inability to account for such variation. This is true as much for the representation of hydrological processes as for *NO_3-N* processes and is

considered in the following section.

In terms of addressing objective (4), the research has demonstrated the utility of the hydrologically and chemically integrated approach for investigating flood mediated floodplain NO_3-N dynamics.

8.3 Future research directions

Through addressing the need to consider the floodplain as an integrated hydrological system the research presented in this thesis has highlighted a number of opportunities and requirements for further research. The following section considers:

- the representation of parameter variability
- the need for further increases in process representation
- the pressing requirement for both calibration and validation data for this class of model

8.3.1 The representation of parameter variability

The deterministic modelling approach adopted limits any analysis into the effects of parameter variability on model prediction to a simple sensitivity analysis in which the effect of varying individual parameter values on model output can be determined. This has been done, for example, with respect to variability in $K_{(sat)}$, the in situ concentration of NO_3-N and the denitrification rate constant (k_1). This approach has provided an insight into the sensitivity of the model to variations in the magnitude of individual parameter and has demonstrated significant variability in model response within the ranges tested. For example, a reduction in simulated peak hydrograph discharge ranging from -1.48 to -30.5 resulted from a range of $K_{(sat)}$ values of two orders of magnitude (see Table 6.3, simulations *Clay05* and *Clay06*). Model output has been shown, therefore, to incorporate a large degree of uncertainty due to the inability to account for known variability in the model parameterisation used. To overcome this a future development might be to incorporate a stochastic method to account for this variability in model parameterisation and to establish the uncertainty in model prediction. This applies to the parameterisation of the floodplain hydraulic, hydrology and nitrate model components.

8.3.2 Improving process representation

A major model assumption made in this research has been the representation of infiltration as a 1D process. It is argued in *Chapter 3* that such an approximation is appropriate where the floodplain

comprises shallow lateral and downstream gradients and the soil is texturally homogeneous. Under these circumstances vertical flows are expected to dominate following inundation during the relatively short event based simulations that hydraulic models are typically applied to. Such a representation is also adequate for this initial investigation into the interaction between surface and subsurface flows in the floodplain environment.

However, where the influence of hillslope hydrology (both surface and subsurface) is significant and the floodplain soil is texturally heterogeneous (for example including former channel deposits (Haycock and Burt, 1993)) then a different approach is required which considers the impact of both surface and subsurface lateral flow on floodplain hydrology. Where these lateral processes can be shown to be significant then a 2- or 3D representation of the hillslope-floodplain-channel continuum is suggested. Recent research into the effects of hillslope inputs on the hydraulic characteristics of floodplain flow by Charlton (1995) and Bates *et al.* (1996) have demonstrated that these can impact significantly on surface flow. Where it can be demonstrated that subsurface flow originating on, or within, the hillslope has a significant effect upon subsurface floodplain hydrology over the simulation time period then there is an argument for increasing process representation to include this. This is true also for the supply of NO_3-N. In *Chapter 2* the importance of the hillslope in transferring NO_3-N to the floodplain was established. Where hillslope hydrology imparts a significant impact on floodplain hydrology floodplain chemistry may be similarly affected.

8.3.3 Model calibration and validation

The research has highlighted the lack of both calibration and validation data available for this class of model. Currently calibration of 2D finite element hydraulic models is achieved through a matching of the timing of the observed and simulated hydrographs. This was the method used to obtain the calibrated simulations used in this thesis. However, due to the inherent inaccuracy associated with the determination of the observed output hydrograph at Rewe (see sections 5.2.2.1 and 5.3.3.3) it has already been shown that a quantitative assessment of the impact on the simulated output hydrograph cannot be undertaken with reference to the observed output hydrograph. However, the output hydrograph represents only a small fraction of the data potentially available for calibration which also includes inundation extent and stage and velocity data at selected nodes or internal domain cross-sections. Spatially distributed hydraulic models which represent floodplain flow processes over the entire domain require calibration and validation data which is currently not readily available. There is thus a need for the provision of such data as calibration and validation necessarily moves from a reliance on the observed output hydrograph.

8.4 Conclusion

This thesis set out to explore the need for a new conceptual approach to modelling the integrated nature of floodplain hydrology. A deterministic approach was adopted which, despite being unable to account for the inherent and often considerable parameter variability encountered in the floodplain environment, has demonstrated the utility of such an approach through the successful determination of the broad direction and magnitude of both the hydrological and chemical process investigated. The research conducted has considered only a small part of a much larger research question for which some of the work still outstanding has been identified in this final chapter.

It was suggested in *Chapter 1* that underlying the accurate representation of floodplain fluvial, hydrological, chemical, sedimentological and geomorphological processes is the provision of a suitable floodplain hydrology model capable of representing the interaction between surface hydraulics and subsurface hydrology at a spatial and temporal resolution appropriate to the highly spatially distributed nature of these processes. This thesis has developed such a modelling platform and has demonstrated, for the first time, the utility of such an approach with reference to two areas of contemporary research interest in the floodplain, it remains now for this model, or the ideas explored through the novel approach adopted, to be applied further. Such work is already underway to determine the potential of the model in assessing the spatial variability in floodplain soil contamination during flooding to improve the determination of reach scale mass balance estimates. These ideas are discussed fully by Stewart *et al.* (*in press*).

Abbott, M.B., Bathurst, J.C., Chunge, J.A., O'Connell, P.E. and Rasmussen, J. (1986) An introduction to the European Hydrological System - System Hydrologique Europeen, 'SHE', 2: Structure of a physically-based, distributed modelling system. *Journal of Hydrology*, **87**, 61-77.

Addiscott, T.M., Bailey, N.J., Bland, G.J. and Whitmore, A.P. (1991) Simulation of nitrogen in soil and winter-wheat crops - a management model that makes the best use of limited information. *Fertiliser Research*, **27**, 305-312.

Ambus, P. and Christensen, S. (1993) Denitrification variability and control in a riparian fen irrigated with drainage water. *Soil Biology and Biochemistry*, **25**, 915-923.

Anderson, M.G. and Burt, T.P. (1978) The role of topography in controlling throughflow generation. *Earth Surface Processes and Landforms*, **3**, 331-334.

Anderson, M.G. and Bates, P.D. (1994) Evaluating data constraints on two dimensional finite element models of floodplain flow. *Catena*, **22**, 1-15.

Anderson, M.G. and Howes, S. (1985) Development and application of a combined soil water-slope stability model. *Quaterly Journal of Engineering Geology*, **18**, 225-236.

Arah, J.R.M. (1990) Modelling spatial and temporal variability of denitrifcation. *Biology and Fertility of Soils*, **9**, 71-77.

Arah, J.R.M and Smith, K.A. (1989) Steady-state denitrification in aggregated soils: a mathematical model. *Journal of Soil Science*, **40**, 139-149.

Armstrong, A.C. and Burt, T.P. (1993) Nitrate losses from agricultural land. In: T.P. Burt, A.L. Heathwaite ans S.T. Trudgill (eds), *Nitrate; Processes, Patterns and Management*, John Wiley and Sons, Chichester, 239-267.

Atteia, O. (1994) Major and trace elements in precipitation on western Switzerland. *Atmospheric Environment*, **28**, 3617-3624.

Baird, L., Gee, D.M. and Anderson, M.G. (1992) Unguaged catchment modelling. II. Utilization of hydraulic models for validation. *Catena*, **19**, 33-42.

Barraclough, D. (1989) A usable mechanistic model of nitrate leaching. 1. The model. *Journal of Soil Science*, **40**, 543-554.

Barraclough, D., Jarvis, S.C., Davies, G.P., and Williams, J. (1992) The relationship between fertiliser nitrigen application and nitrate leaching from grazed grassland, *Soil Use and Management*, **8**, 51-56.

Bates, P.D., Anderson, M.G., Baird, L., Walling, D.E. and Simm, D. (1992) Modelling floodplain flows using a two-dimensional finite element model. *Earth Surface Processes and Landforms*, **17**, 575-588.

Bates, P.D., Anderson, M.G., and Hervouet, J-M. (1995) Initial comparison of two 2D finite element codes for river flood simulation. *Proceedings of the Institute of Civil Engineers: Water, Maritime and Energy* (*in press*).

Bates, P.D., Anderson, M.G. and Hervouet, J-M. (1994) Computation of a flood event using a 2D finite element model and its comparison to field data. In: P. Molinaro and L. Natale (eds), *Modelling flood propagation over initially dry areas*, American Society of Civil Engineers, New York, 243-256.

Bates, P.D., Anderson, M.G., Price, D.A., Hardy, R.J. and Smith, C.N. (1996). Analysis and development of models for floodplain flows. In: M.G. Anderson, D.E. Walling and P.D. Bates (eds), *Floodplain Processes*, John Wiley and Sons, Chichester, 215-254.

Bathurst, J.C. (1986) Physically-based distributed modelling of an upland catchment using the Systeme Hydrologique Europeen. *Journal of Hydrology*, **87**, 79-102.

Bijay-Singh, Ryden, J.C. and Whitehead, D.C. (1988) Some relationships between denitrifcation potential and fractions of organic carbon in air-dried and field-moist soils. *Soil Biology and Biochemistry*, **20**, 737-741.

Bijay-Singh, Ryden, J.C. and Whitehead, D.C. (1989) Denitrification potential and actual rates of denitrification in soils under long-term grassland and arable cropping. *Soil Biology and Biochemistry*, **21**, 897-901.

Black, P.E. (1970) runoff from watershed models. *Water Resourses Research*, **6**, 465-477.

Bollag, J.M., Drzymala, S., and Kardos, L.T. (1973) Biological versus chemical nitrite decomposition in soil. *Soil Science*, **116**, 44-50.

Brady, N.C. (1990). *The nature and properties of soils*. MacMillan, pp621.

Brooks, A.N. and Hughes, T.J.R. (1982) Streamline Upwind/Petrov-Galerkin formulations for convection dominated flows with particular emphasis on the incompressible Navier-Stokes equations. *Computer Methods in Applied Mechanics and Engineering*, **32**, 199-259.

Brooks, R.H. and Corey, A.T. (1966) Properties of porous media affecting fluid flow. *J. Irrig. Drain. Div., American Society of Civil Engineering*, **92**, 61-88.

Brooks, S.M. (1991) Modelling the role of mass movement in slope development: the interaction between pedogenesis and hillslope hydrology. Unpublished Ph.D. thesis, University of Cambridge.

Brooks, S.M., Richards, K.S. and Anderson, M.G. (1993) Shallow failure mechanisms during the Holocene: Utilisation of a coupled slope hydrology-slope stability model. In D.S.G. Thomas and R.J. Allison (Eds) *Landscape Sensitivity*, John Wiley and Sons, Chichester.

Brunet, R.C., Pinay, G., Gazelle, F. and Roques, L. (1994) Role of the floodplain and riparian zone in suspended matter and nitrogen retention in the Adour River, South-West France. *Regulated Rivers*, **9**, 55-63.

Bulla, L.A., C.M. Gilmour and W.B.Bollen. (1970) Non-biological reduction of nitrite in soil. *Nature*, **225**, 664.

Buresh, R.J. and Patrick, W.H. Jr. (1978) Nitrate reduction to ammonium in anarobic soil. *Soil Science Society of America Journal*, **42**, 913-918

Burns, I.G. (1974) A model for predicting the redistribution of salts applied to fallow soils after excess rainfall or evaporation. *Journal of Soil Science*, **25**, 165-178

Burns, I.G. and Collier, G.F. (1980) A simulation model for the leaching of borate in soils and pulverised fuel ash. *J. Sci. Food Agric*, **31**, 743-749.

Burris, I.G. (1980) The global nitrogen budget - science or seance? In: Newton, W.E. and Orme-Johnson, W.H. (eds), *Nitrogen Fixation, Volume 1*, University Park Press, Baltimore, 7-16.

Burt, T.P. and Haycock, N.E. (1996) Linking hillslopes to floodplains. Analysis and development of models for floodplain flows. In: M.G. Anderson, D.E. Walling and P.D. Bates (eds), *Floodplain Processes*, John Wiley and Sons, Chichester, 461-492.

Calvar, A. and Wood, L.W. (1995) The Institute of Hydrology Distributed Model. In: V.P. Singh (ed) *Computer models of watershed hydrology*, Water Resources Publications, 595-626.

Carsel, R.F. and Parrish, R.S. (1988). Developing joint probability distributions of soil water retention characteristics. *Water Resourses Research*, **24**, 755-769.

Charlton, R.M. (1995) An investigation into the effect of lateral hillslope inputs on floodplain hydraulic model predictions. Unpublished Ph.D. thesis, University of Bristol.

Chery, D.L.Jr. (1966) Design and tests of a physical watershed model. *Journal of Hydrology*, **4**, 224-235.

Chescheir, G.M., Gilliam, J.W., Scaggs, R.W., and Broadhead, R.G. and Lea, R. (1987) The hydrology and pollutant removal effectiveness of wetland buffer areas receiving pumped agricultural drainage water. Univ. of N.C., Water Resourses Research Institute Report 231, Raleigh, N.C., 170pp.

Chow, V.T. (1959) *Open Channel Hydraulics*, McGraw-Hill, London, pp 680.

Chung, T.J. (1978) *Finite Element Analysis in Fluid Dynamics*. McGraw-Hill, London, pp 378.

Clayden, B. (1971) *Soils of the Exeter district. Memoirs of the Soil Survey of Great Britain England and Wales*, Harpenden, pp 254.

Colbourn, P. (1992) Denitrification and N_2O production in pasture soil - the influence of nitrigen supply and moisture. *Agricultural ecosystems and Environments*, **39**, 267-278.

Collison, A. (1993) assessing the influence of vegetation on slope stability in the Tropics. Unpublished Ph.D. thesis, University of Bristol.

Cooper, A.B. (1990) Nitrate depletion in the riparian zone and stream channel of a small headwater catchment. *Hydrobiologia*, **202**, 13-26

Cooper, A.J. (1996) TELEMAC2D (version 3.0) validation document. EDF Report, HE-43/96/006/A.

Corwin, D.L., Waggoner, B.L. and Rhoades, J.D. (1991) A functional model of solute transport that accounts for bypass. *Journal of Environmental Quality*, **20**, 647-658.

Craswell, E.T. (1978) Some factors influencing denitrification and nitrogen immobilisation in a clay soil. *Soil Biology and Biochemistry*, **10**, 241-245. (check this date)

D'Alpoas, L., Defina, A., and Matticchio, B. (1994) 2D finite element modelling of flooding due to river bank collapse. In: P. Molinaro and L. Natale (eds), *Modelling flood propagation over initially dry areas*, American Society of Civil Engineers, New York, 60-71.

Davie, T.J.A. (1992) Modelling the effects of vegetation change on sttormflow hydrology. Unpublished PhD thesis. University of Bristol.

Defina, A., D'Alpaos, L. and Matticchio, B. (1994) A new set of equations for very shallow water and partially dey areas suitable to 2D numsrical models. In: P. Molinaro and L. Natale (eds), *Modelling flood propagation over initially dry areas*, American Society of Civil Engineers, New York, 72-81.

Denmead, O.T., Frency, J.R., and Simpson, J.R. (1976) A closed ammonia cycle within a plant canopy. *Soil Boichemistry*, **8**, 161-164

Dorland, S. and E.G. Beauchamp. (1991) Denitrification and ammonification at low soil temperatures. *Canadian Journal of Soil Science*, **71**, 293-303.

Duffy, J., Chung, C., Boast, C. and Franklin, M. (1975) A simulation model of biophysiochemical transformations of nitrigen in tile0drained corn belt soil. *Journal of Environmental Quality*, **4**, 477-486.

Egginton, G.M. and Smith, K.A. (1986) Nitrous oxide emission from a grassland soil fertilised with slurry and calcium nitrate. *Journal of Soil Science*, **37**, 59-67.

Findlay, D.C., Colborne, G.J.N., Cope, D.W., Harrod, T.R., Hogan, D.V. and Stains, S.J. (1984) *Soils and their use in South West England.* Soil Survey of England and Wales, Bulletin No. 14., Harpenden, pp 419.

Firestone, M.K. (1982) Biological denitrification. In: F.J. Stevenson (ed*), Nitrogen in Agricultural soils*. American Society of Agronomy, Madison, Wisconsin, 289-318.

Foster, I.D.L. and Walling, D.E. (1978) The effects of the 1976 drought and autumn rainfall on stream solute levels. *Earth Surface Processes*, **3**, 393-406.

Gale, P.M., Devai, I., Reddy, K.R. and Graetz, D.A. (1993) Denitrifcation potential od soils from constructed and natural wetlands. *Ecological Engineering*, **2**, 119-130.

Garwood, E.A., Ryden, J.C. and Tyson, K.C. (1986) Nitrogen losses from drained grassland. British Grassland Occasional Symposium No. 20, Hurley, pp70-74.

Gee, M.D., Anderson. M.G., and Baird, L. (1990) Large-scale floodplain modelling. *Earth surface processes and landforms*, **15**, 513-523.

Goulding, K.W.T., Webster, C.P., Rowlson, D.S. and Poulton, P.R. (1993) Denitrification losses of nitrigen fertiliser applied to winter wheat following ley and arable rotations as established by acetylene inhibition and ^{15}N balance. *Journal of Soil Science*, **44**, 63-72.

Green, I.R.A. and Stephenson, D. (1986) Criteria for comparison of single event models. *Hyrological Sciences Journal*, **3**, 395-411.

Groffman, P.M., Axelrod, E.A., Lemunyon, J.L., and Sullivan, W.M. (1991) Denitrification in grass and forest vegetated filter strips. *Journal of Environmental Quality*, **20**, 671-674.

Groffman, P.M., Gold, J.J. and Simmons, R.C. (1992) Nitrate dynamics in riparian forests: microbial studies. *Journal of Environmental Quality*, **21**, 666-671.

Groffman, P.M. and Tiedje, J.M. (1991) Denitrification in northern temperate forest soils I. Spatial and temporal patterns at the landscape and seasonal scales. *Soil Biology and Biochemistry*, **21**, 613-620.

Gupta, S.C. and Larson, W.E. (1979) Estimating soil water retention characteristics from particle size distribution, organic matter percent and bulk density. *Water Resourses Research*, **15**, 1633-1635.

Hanson, G.C., Groffman, P.M. and Gold, A.J. (1994) Denitrification in riparian wetlands receiving high and low groundwater nitrate inputs. *Journal of Environmental Quality*, **23**, 917-922.

Havelka, U.D., Boyle, M.G., and Hardy, R.W.F. (1982) Biological nitrogen fixation. In: Stevenson, F.J. (ed), *Nitrogen in agricultural soils*. American Society of Agronomy, Madison, Wisconsin, 365-413.

Havno, K., Madsen, M.N. and Dorge, J. (1995) MIKE 11 - A generalised river modelling package. In: V.P. Singh (Ed) *Computer models of watershed hydrology*, Water Resources Publications, 733-782.

Haycock, N.E. and Burt, T.P. (1993) Role of floodplain sediments in rducing the nitrate concentration of subsurface run-off: a case study in the cotswolds, UK. *Hydrological Processes*, **7**, 287-295.

Haycock, N.E. and Pinay, G. (1993) Groundwater nitrate dynamics in grass and poplar vegetated riparian buffer strips during the winter. *Journal of Environmental Quality*, **22**, 273-278.

Haynes, R.J. (1986) *Mineral Nitrogen in the plant-soil system*, Academic Press, pp 483.

Hendrix, J.M.H. (1990) Determination of hydraulic soil properties. In: Anderson, M.G. and Burt, T.P. (eds), *Process studies in Hillslope Hydrology*, John Wiley and Sons, Chichester, 43-92.

Herschy, R.W. (1978) Accuracy. In: R.W. Herschy (ed), *Hydrometry: Principles and Practices*, John Wiley and Sons, 353-397.

Hervouet, J-M. and Janin, J-M. (1994) Finite element algorithms for modelling flood propagation. In: P. Molinaro and L. Natale (eds), *Modelling flood propagation over initially dry areas*, American Society of Civil Engineers, New York, 102-113.

Hervouet, J-M. and Van Haren, L. (1996) Recent advances in numerical methods for fluid flows. In: M.G. Anderson, D.E. Walling and P.D. Bates (eds), *Floodplain Processes*, John Wiley and Sons, Chichester, 183-214.

Hill, A.R., and Sanmugadas, K. (1985) Denitrification rates in relation to stream sediment characteristics. *Water Resourses*, **19**, 1579-1586.

Hill, A.R. (1991a) Groundwater cation concentrations in the riparian zone of a forested headwater stream. *Hydrological Processes*, **4**, 121-130.

Hill, A.R. (1991b) Groundwater flow paths in relation to nitrogen chemistry in the near-stream zone. *Hydrobiologia*, **206**, 39-52.

Hillel, D. (1971) Soil and Water. Physical principles and processes. Academic Press, New York, pp 288.

Hillel, D. (1980) Fundamentals of soil physics. Academic Press, New York, pp 413.

Howard-Williams, C. (1985) Cycling and retention of nitrogen and phosphorus in wetlands: a theoretical and applied perspective. *Freshwater Biology*, **15**, 391-431.

Howard-Williams, C. and Downes, M.T. (1993) Nitrogen cycling in wetlands. In: T.P. Burt, A.L. Heathwaite and S.T. Trudgill (eds), *Nitrate: Processes, Patterns and Management*, John Wiley and Sons, Chichester, 141-167.

Imamoto, H. and Ishigaki, T. (1987) "Three dimensional structure of turbulence in an open channel flow near the corner". In J.A. Cunge and P. Ackers (eds) "*Topics in hydraulic modelling*" Proccedings of technical session B, XXII Congress, International Association for Hydraulic Research, 162-163.

Jacobs, T.C. and Gilliam, J.W. (1985) Riparian losses of nitrate from agricultural drainage waters. *Journal of Environmental Quality*, **14**, 472-478.

Jacobson, S.N. and M. Alexander. (1980) Nitrate loss from soil in relation to temperature, carbon source and denitrifier populations. *Soil Biology and Biochemistry*, **12**, 501-505.

Jansson, P-E., Borg, G.C., Lundin, L-C. and Linden, B. (1991) Simulation of soil nitrogen storage and leaching, applications to different Swidish agricultural systems. National Swedish Environmental Protection Board, Report 3356, pp63.

Jaynes, D. B. (1990) Soil water hysteresis: models and implications. In: Anderson, M.G., and Burt, T.P. (eds), *Process studies in Hillslope Hydrology*, John Wiley and Sons, Chichester, 93-126.

Johnes, P.J. and Burt, T.P. (1993) Nitrate in Surface Water. In T.P. Burt, A.L. Heathwaite and S.T. Trudgill (eds), *Nitrate: Processes, Patterns and Management*. John Wiley and Sons, Chichester, 269-317.

Jordan, T.E., Correll, D.L. and Weller, D.E. (1993) Nutrient interception by a riparian forest receiving inputs from adjacent cropland. *Journal of Environmental Quality*, **22**, 467-473.

Jury, W.A. and Nielsen, D.R. (1989) Nitrate transport and leaching mechanisms. In: R.F. Follett (ed), *Developments in Agricultural and Managed Forest Ecology 21. Nitrogen management and ground water protection*. Elsevier.

Jury, W.A., Gardener, W.R. and Gardener, W.W. (1991) Soil Physics. John Wiley and Sons, pp 328.

Kawahara, M. and Umetsu, T. (1986) Finite element method for moving boundary problems in river flows. *International Journal of Numerical Methods in Fluids*, **6**, 365-386.

Kachroo, R.K. (1991) River flow forcasting. Part 1. A discussion of the principles. *Journal of Hydrology*, **133**, 1-15.

Kaluarachchi, J.J and Parker, J.C. (1988) Finite element model of nitrogen species transformation and transport in the unsaturated zone. *Journal of Hydrology*, **103**, 249-274.

King, I.P. and Norton, W.R. (1978) Recent applications of RMA's finite element models for two dimensional hydrodynamics and water quality. In: C.A. Brebbia, W.G. Gray and G.F. Pinder (eds), *Proceedings of the Second International Conference on Finite Elements in Water Resources*, Pentech Press, London, 81-99.

King, I.P. and Roig, L.C. (1988) 2D finite element model for floodplains and tidal flats. In: K. Kiki and M. Kawahara (eds) Computational methods in flow analysis, Proceedings of an International Conference on Computational Methods in Flow Analysis, Okayama, Japan, 711-718.

Kirkby, M.J. (1969) Infiltration, Throughflow, and Overland Flow. In R.J. Chorley (ed), Water, Earth and Man, Methuen, 215-227.

Knight, D.W. and Shiono, K. (1996) River Channel and Floodplain Hydraulics. In: M.G. Anderson, D.E. Walling and P.D. Bates (eds), *Floodplain Processes*, John Wiley and Sons, Chichester, 139-181.

Kuehnet, A. and Faeh, R. (1983) Application of a mathematical model to design measures for flood protection. (Eds. Stephens, H.S. and Stapleton, C.A.) Int. Conf. on the hydraulic aspects of floods and flood control (13-15 Sept.) 1983, London.

Leclerc, M., Bellemare, J-F., Dumas, G. and Dhatt, G. (1990) A finite element model of estuarine and river flows. *Advances in Water Resources*, **13**, 158-168.

Linn, D.M. and Doran, J.W. (1985) Effect of water-filled pore space on carbon dioxide and nitrous oxide production in tilled and non-tilled soils. *Soil Science Society of America Journal*, **48**, 1267-1272.

Lowrance, R. (1992) Groundwater nitrate and denitrification in a coastal plain riparian forest. *Journal of Environmental Quality*, **21**, 401-405.

Lloyd, D. M. (1990) Modelling the hydrology and stability of tropical cut slopes. Unpublished Ph.D. thesis, University of Bristol.

Lynch, D.R. and Grey, W.G. (1978) Finite element simulation of shallow water problems with moving boundaries. *Finite elements in Water Resourses*, Proceedings of the Second International Conference on F.E. in Water Resourses, Pentech Press, London.

Magg, M and Lind, A, M. (1992) Influence of airfilled porosity on denitrifcation in a sandy loam soil. Paper presented at the 7th nitrogen workshop, Edinburgh.

Maltby, E., Hogan, D.V., Immirzi, C.P. and Oliver, G.A. (1991) Nutrient dynamics and functional assessment of European wetlands, Report to EC DG XII, Weland Ecosystems Research Group, Report 9, Department of Geography, University of Exeter, UK.

Maltby, E., Hogan, D.V. and McInnes, R.J. (1996) Functional analysis of European wetland ecosystems - Phase I: The function of river marginal wetland ecosystems. Final report to EC DG XII, Ecosystams research report 18.

Marriot, S.B. (1996) Analysis and modelling of overbank deposits. In: M.G. Anderson, D.E. Walling and P.D. Bates (eds), *Floodplain Processes*, John Wiley and Sons, Chichester, 63-93.

Marron, D.C. (1989) The transport of mine tailings as suspended sediment in the Belle. *IAHS Publication*, **184**, 19-26.

Marron, D.C. (1992) Floodplain storage of mine tailings in the Belle Fourche river system: a sediment budget approach. *Earth surface processes and landforms*, **17**, 675-685.

Martin, L.A. and Myers, W.R.C. (1991) Measurement of overbank flow in compound river channels. *Proceedings of the Institute of Civil Engineers*, **91**, 645-659.

McColl, R.H. (1978) Chemical runoff from pasture: the influence of fertilizer and riparian zones. *New Zealand Journal of Marine and Freshwater Research*, **12**, 371-380.

Millington, R.J. and Quirk, J.P. (1959) Permeability of porous media. *Nature*, **183**, 387-388.

Misra, C., Nirlsen, D.R. and Biggar, J.W. (1974a) Nitrogen transformations in soil during leaching: II. Steady state nitrification and nitrate reduction. *Soil Science Society of America Proceedings*, **38**, 294-299.

Misra, C., Nirlsen, D.R. and Biggar, J.W. (1974b). Nitrogen transformations in soil during leaching: III. Nitrate reduction in soil columns. *Soil Science Society of America Proceedings*, **38**, 300-304.

P. Molinaro and L. Natale (1994) *Modelling flood propagation over initially dry areas*, American Society of Civil Engineers, New York, pp373.

Mulholland, P.J., Yarbro, L.A., Sniffen, R.P. and Kuenzler, E.J. (1981) Effects of floods on nutrient and metal concentrations in a coastal plain stream. *Water Resources Research*, **17**, 758-764.

Myrold, D.D., and J.M. Tiedje. (1985) Establishment of denitrification capacity in soil: effects of carbon, nitrate and moisture. *Soil Biology and Biochemistry*, **17**, 819-822.

McCuen, R.H. (1973) The role of sensitivity analysis in hydrologic modelling. *Journal of Hydrology*, **18**, 37-53.

Nash, J.E. and Sutcliffe, J.V. (1970) River flow forcasting through conceptual models part 1 - a discussion of principles. *Journal of Hydrology*, **10**, 282-290.

Norton, W.R., King, I.P. and Orlob, G.T. (1973) A finite element model for Lower Granite reservoir. Water Resources Engineers, California.

Nelson, D.W. (1982) Gaseous losses other than through denitrification. In: Stevenson, F.J. (ed), *Nitrogen in agricultural soils*. American Society of Agronomy, Madison, Wisconsin, 327-358.

Nommik, H. (1956) Investigations on denitrification in soil. *Acta Agriculturoe Scandinavica*, **6**, 195-228.

Obenhuber, D.C. and Lowrance, R. (1991) Reduction of nitrate in aquifer microcosms by carbon additions. *Journal of Environmental Quality*, **20**, 255-258.

Oenema, O and Velthof, G. (1992) Soil depth profiles of potential denitrifcation rates. Paper presented at the 7th nitrogen workshop, Edinburgh.

Parkin, T.B. and Meisinger, J.J. (1989) Denitrification below the crop rooting zone as affected by surface tillage. *Journal of Environmental Quality*, **20**, 255-258.

Paul, A.E., and Clark, F.E. (1989) *Soil microbiology and biochemistry*. Academic Press, pp 273.

Peterjohn, W.T. and Correll, D.L. (1984) Nutrient dynamics in an agricultural watershed - observations on the role of a riparian forest. *Ecology*, **65**, 1466-1475.

Philip, J.R. (1983) Infiltration in one, two and three dimensions. *Advances in Infiltration, Proceedings of the National Conference on Advances in Infiltration*. American Society of Agricultural Engineers, 1-13.

Phillips, J.D. (1989a) Nonpoint source pollution control effectiveness of riparian forests along a coastal plain river. *Journal of Hydrology*, **110**, 221-237.

Phillips, J.D. (1989b) An evaluation of the factors determening the effectiveness of water quality buffer zones. *Journal of Hydrology*, **107**, 133-145.

Pinder, G.F. and Grey, W.G. (1977) *Finite element simulation in surface and subsurface hydrology*. Academic Press.

Ponnamperuma, F.N. (1972) The chemistry of submerged soils. In: N.C. Brady (ed), *Advances in Agronomy, Volume 24*, Academic, New York, 29-96.

Powlson, D.S., P.G. Saffigna. and M. Kragt-Cattair. (1988) Denitrification at suboptimal temperatures in soils from different climatic zones. *Soil Biology and Biochemistry*, **20**, 719-723.

Price, D.A., Stewart, M.D., Bates, P.D., Anderson, M.G. and Burt, T.P. (1997) Modelling floodplain hydraulic and nitrate processes using a coupled floodplain-hydrology model. In Haycock, N.E., Burt, T.P., Goulding, K.W.T. and Pinay, G. (Eds). Buffer Zones: Their processes and potential in water protection. Proceedings of the International Conference on buffer zones, September 1996.

Reddy. K.R., P.S.C. Rao. and R.E. Jessup. (1982) The effect of carbon mineralization on denitrification kinetics in mineral and organic soils. *Soil Science Society of America Journal*, **46**, 62-68.

Reddy,K.R., Patrick, W.H. Jr., and Lindan, C.W. (1989) Nitrification-denitrification at the plant root sediment interface in wetlands. *Limnol. Ocenaogr*, **34**, 1004-1013.

Refsgaard, J.C., and Havnoe, K. (1983) A mathematical modelling system for flood forcasting. Int. Conf. on the hydraulic aspects of floods and flood control (13-15 Sept. 1983), London.

Refsgaard, J.C. and Storm, B. (1995) MIKE SHE. In: V.P. Singh (Ed) *Computer models of watershed hydrology*, Water Resources Publications, 809-846.

Rolston, D.E., Rao, P.S.C., Davidson, J.M. and Jessup, R.E. (1984) Simulation of denitrification losses of nitrate fertilizer applied to uncropped, cropped, and manure-ammended field plots. *Soil Science*, **137**, 270-279.

Ross, S. (1989) *Soil processes. A systematic approach.* Routledge, London and New York, pp 444.

Rowell, D.L. (1994) Soil Science. Methods and Applications. Longman, pp350.

Sabey, B.R. (1969) Influence of soil moisture tension on nitrate accumulation in soils. *Soil Science Society of America Proceedings*, **33**, 263-266.

Schiono, K. and Knight, D.W. (1991) Turbulent open channel flows with variable depth across the channel. *Journal of Fluid Mechanics*, **222**, 617-646.

Schlosser, I.J. and Karr, I.R. (1981) Water quality in agricultural watersheds: impact of riparian vegetation during base flow. *Water Resourses Bulletin*, **17**, 233-240.

Schnabel, R.R. and Stout, W.L. (1994) Denitrification loss from two Pennsylvania floodplain soils. *Journal of Environmental Quality*, **23**, 344-348.

Schipper, L.A., Cooper, A.B., Harfoot, C.G. and Dyck, W.J. (1993) Regulators of denitrification in an organic riparian soil. *Soil Biology and Biochemistry*, **25**, 925-933.

Selim, H.M., and Iskandar, I.K. (1981a) Modelling nitrogen transport and transformations in soils: Theoretical considerations. *Soil Science*, **131**, 233-241.

Selim, H.M., and Iskandar, I.K. (1981b) Modelling nitrogen transport and transformations in soils: Validation. *Soil Science*, **131**, 303-312.

Sellin, R.H.J. (1964) A laboratory investigation into the interaction between the flow in the channel of a river and that over its floodplain. *La Houille Blanche*, No. 7, 793-801.

Sextone, A.J., Revsbech, N.P., Parkin, T.B. and Tiedje, J.M. (1985) Direct measuremrnt of oxygen profiles and denitrification rates in soil aggregate. *Soil Science Society of America Journal*, **49**, 645-651.

Sextone, A.J, Parkin, T.B. and Tiedje, J.M. (1988) Denitrification response to soil wetting in aggregated and unaggregated soil. *Soil Biology and Biochemistry*, **20**, 767-769.

Simmons, R.C., Gold, A.J., and Groffman, P.M. (1992) Nitrate dynamics in Riparian Forests: Groundwater studies. *Journal of Environmental Quality*, **21**, 659-665

Singh, B.R. and Kanehiro, Y. (1969) Adsorption of nitrate in amorphous and kaolinitic Hawaiian soils. Soil Science Society of America Proceedings, 33, 681-683.

Smid, A.E., and E.G. Beauchamp. (1976) Effects of temperature and organic matter on denitrification in soil. *Canadian Journal of Soil Science*, **56**, 385-391.

Stanford, G., Vander Pol, R.A., and Dzienia, S. (1975a) Denitrification rates in relation to total and extractable soil carbon. *Soil Science Society of America Proceedings*, **39**, 284-289.

Stanford, G., Dzienia. S. and Vander Pol, R.A. (1975b) Effect of temperature on denitrification rate in soils. *Soil Science Society of America Proceedings*, **39**, 867-870.

Steinbeck, J. (1993) The grapes of wrath. Mandarin.

Stevenson, F.J. (1982) *Nitrogen in agricultural soils*, No 22 in the series Agronomy, American Society of Agronomy, CSSA, Soil Science Society of America, Madison, Wisconsin.

Stewart, M. D., Bates, P.D., Price, D.A. and Burt, T.P. Modelling the spatial variability in floodplain soil contamination during flood events to improve chemical mass balance estimates. *Hydrological Processes*, (*in press*).

Tiedje, J.M., Sextone, A.J., Parkin, T.B., Revsbech, N.P. and Shelton, D.R. (1984) Anaerobic processes in soils. *Plant and Soil*, **76**, 197-212.

Topp, G.C. (1969) Soil water hysteresis measured in a sandy loam and compared with the hysteresis domain model. *Soil Science Society of America Proceedings*, **33**, 645-651.

Topp, G.C. and Miller, E.E. (1966) Hysteresis moisture characteristics and hydraulic conductivities for glass-bead media. *Soil Science Society of America Proceedings*, **39**, 156-162.

Triska, F.J., Kennedy, V.C., Avanzino, R.J., Zellweger, G.W. and Bencala, K.E. (1989) Retention and transport of nutrients in a third-order stream in Northwestern California:hyporheic processes. *Ecology*, **70**, 1893-1905.

Trudgill, S.T., Burt, T.P., Heathwaite, A.L. and Arkell, B.P. (1991) Soil nitrate sources and nitrate leaching losses, Slapton, South Devon. *Soil Use and Management*, **7**, 200-206.

Turner, M.J., Clough, R.W., Martin, H.C., and Topp, L.P. (1956) Stiffness and deflection analysis of complex structures. *Journal of Aeronautical Science*, **23**, 805-823.

Van Cleemput. O., and L. Baert. (1984) Nitrite: a key compound in N loss processes under acid conditions? *Plant and Soil*, **76**, 233-241.

Van Genuchten, M. Th. (1980) A closed-form equation for predicting the hydraulic properties of unsaturated soils. *Soil Science Society of America Journal*, **44**, 892-898.

Vinten, A.J.A. and Smith, K.A. (1993) Nitrogen Cycling in Agricultural Soils. In T.P. Burt, A.L. Heathwaite and S.T. Trudgill (eds), *Nitrate: Processes, Patterns and Management*. John Wiley and Sons, 39-73.

Walling, D.E. and Foster, I.D.L. (1975) Variations in the natural chemical concemtration of river water during flood flows, and the lag effect: some further comments. *Journal of Hydrology*, **26**, 237-244.

Walling, D.E. and Webb, B.W. (1985) Solutes in River Systems. In (ed) S.T. Trudgill, *Solute Processes*, Wiley, pp509.

Walling, D.E. and Peart, M.R. (1986) Fingerprinting sediment sources: the example of a drainage basin in Devon, UK. In (ed.) Hadley, R.F. Drainage basin sediment delivery. *IAHS Publication*, 159,

Walling, D.E., Quine, T.A. and He, Q. (1992) Investigating contemporary rates of floodplain sedimentation. In: P.A. Carling and G.E. Petts (eds), *Lowland Floodplain Rivers: A Geomorpological Perspective*, John Wiley and Sons, Chichester, 165-184

Webb, B.W. and Walling, D.E. (1985) Nitrate behaviour in streamflow from a grassland catchment in Devon, UK. *Water Research*, **19**, 1005-16.

Whelan, M.J. (1993) Numerical modelling of small catchment nitrogen dynamics with particular reference to the Slapton Wood catchment, South Devon. Unpublished PhD Thesis, University of Leeds, UK.

Williams, J.R. and Hann, R.W. (1972) HYMO, a problem-orientated computer language for building hydrologic models. *Water Resources Research*, **8**, 79-68.

Wosten, J.H.M. and Van Genuchten, M. Th. (1988) Using texture and other soil properties to predict the unsaturated soil hydraulic functions. *Soil Science Society of America Journal*, **52**, 1762-1770.

Appendix One

Mass balance results for all simulations run in Chapters 6 and 7.

	TELEMAC2D mass balance					Soil moisture mass balance
Simulation code	Initial surface water volume	Final surface water volume	volume that entered the domain	volume added by the source term	total volume lost	Soil moisture mass balance
Control01	724246.0	1348993.0	348439.8	0.0	-276306.8	-3.79×10^{-12}
Control02	1304311.0	757971.9	-1439395.0	0.0	-893055.7	-6.1×10^{-12}
Clay01	724246.0	1324015.0	497221.7	-153509.8	-256057.2	-2.3×10^{-12}
Clay02	724246.0	1328413.0	428373.9	-89113.9	-264907.0	-1.1×10^{-11}
Clay03	1304311.0	745558.3	-1149648.0	-271913.2	-862809.0	4.46×10^{-13}
Clay04	1304311.0	745588.7	-1232457.0	-199407.1	-873141.8	-1.6×10^{-11}
Sil01	724246.0	1300653.0	553267.2	-224714.5	-247854.0	-1.1×10^{-11}
Sil02	724246.0	1302983.0	504728.0	-179216.3	-253225.7	-4.2×10^{-12}
Sil03	1304311.0	730022.8	-943483.8	-474059.0	-843254.6	-1.8×10^{-4}
Sil04	1304311.0	730061.3	-1005831.0	-419621.6	-851202.8	-3.1×10^{-4}
Clay05	724246.0	1165270.0	975451.0	-722735.1	-188306.9	-1.3×10^{-5}
Clay06	724246.0	1341323.0	400584.5	-52917.4	-269410.2	-2.1×10^{-11}
Clay07	724246.0	951265.2	1411288.0	-1318795.0	-134526.6	-1.3×10^{-5}
Clay08	724246.0	1345308.0	367756.0	-20383.9	-273689.4	-6.8×10^{-13}
Sil05	724246.0	951005.1	1431950.0	-1339264.0	-134072.5	-3.16×10^{-3}
Sil06	724246.0	1339066.0	396904.6	-51421.3	-269336.6	-1.7×10^{-13}
Sil07	724246.0	951265.2	1411288.0	-1318795.0	-134526.6	-2.8×10^{-3}
Sil08	724246.0	1343187.0	372060.9	-26150.5	-273030.9	-7.4×10^{-13}

	TELEMAC2D mass balance					Soil moisture mass balance	
Simulation code	**Initial surface water volume**	**Final surface water volume**	**Volume that entered the domain**	**volume added by the source term**	**total volume lost**	**Soil moisture mass balance**	**Nitrate mass balance**
Clay09	724246.0	1324015.0	497221.7	-153509.8	-256057.2	-2.3x10-12	$-2.6x10^{-7}$
Clay10	724246.0	1326413.0	428373.9	-89113.9	-264907.0	-1.1x10-11	$4.7x10^{-7}$
Sil09	724246.0	1300653.0	553267.2	-224714.5	-247854.0	-1.1x10-11	$-1.6x10^{-6}$
Sil10	724246.0	1302847.0	506134.2	-180526.7	-252993.2	-3.9x10-12	$-8.3x10^{-7}$
Clay11	724246.0	1324015.0	497221.7	-153509.0	-256057.2	-2.3x10-12	$1.7x10^{-7}$
Clay12	724246.0	1328413.0	428373.9	-89113.9	-264907.0	-1.1x10-11	$2.7x10^{-6}$
Sil11	724246.0	1300653.0	553267.2	-224714.5	-247854.0	-1.1x10-11	$-5.5x10^{-6}$
Sil12	724246.0	1302847.0	506134.2	-180526.7	-252993.2	-3.9x10-12	$-9.3x10^{-6}$
Clay13	724246.0	1324015.0	497221.7	-153509.8	-256057.2	-2.3x10-12	$-2.8x10^{-6}$
Clay14	724246.0	1328413.0	428373.9	-89113.9	-264907.0	-1.1x10-11	$-1.8x10^{-6}$
Sil13	724246.0	1300653.0	553267.2	-224714.5	-247854.0	-1.1x10-11	$-2.9x10^{-6}$
Sil14	724246.0	1302847.0	506134.2	180526.7	-252993.2	-3.9x10-12	$-7.1x10^{-7}$
Clay15	724246.0	1324015.0	497221.7	-153509.8	-256057.2	-2.3x10-12	-2.8x10-6
Clay16	724246.0	1328413.0	428373.9	-89113.9	-264907.0	-1.1x10-11	-3.0x10-6
Sil15	724246.0	1300653.0	553267.2	-224714.5	-247854.0	-1.1x10-11	-3.8x10-6
Sil16	724246.0	1302847.0	506134.2	-180526.7	-252993.2	-3.9x10-12	-3.4x10-6

	TELEMAC2D mass balance					Soil moisture mass balance	
Simulation code	**Initial surface water volume**	**Final surface water volume**	**Volume that entered the domain**	**volume added by the source term**	**total volume lost**	**Soil moisture mass balance**	**Nitrate mass balance**
Clay17	724246.0	1324015.0	497221.7	-153509.8	-256057.2	$-2.3X10^{-12}$	-2.9x10-6
Clay18	724246.0	1328413.0	428373.9	-89113.9	-264907.0	$-1.1x10^{-11}$	-3.0x10-6
Sil17	724246.0	1300653.0	553267.2	-224714.5	-247854.0	$-1.1x10^{-11}$	-3.6x10-6
Sil18	724246.0	1302983.0	504728.0	-179216.3	-253225.7	$-4.2x10^{-12}$	-3.2x10-6
Clay19	724246.0	1165270.0	975451.0	-722735.1	-188306.9	$-1.3x10^{-5}$	-4.2x10-6
Clay20	724246.0	1341323.0	400584.5	-52917.4	-269410.2	$-2.1x10^{-11}$	-1.5x10-8
Sil21	724246.0	951265.2	1411288.0	-1318795.0	-134526.6	$-1.3x10^{-5}$	-3.3x10-6
Sil22	724246.0	1345308.0	367756.0	-20383.9	-273689.4	$-6.8x10^{-13}$	-8.6x10-6
Clay19	724246.0	951005.1	1431950.0	-1339264.0	-134072.5	$-3.16x10^{-5}$	-2.1x10-6
Clay20	724246.0	1339066.0	396904.6	-51421.3	-269336.6	$-1.7x10^{-13}$	-1.2x10-6
Sil21	724246.0	951265.2	1411288.0	-1318795.0	-134526.6	$-2.8x10^{-5}$	-1.7x10-6
Sil22	724246.0	1343187.0	372060.9	-26150.5	-273030.9	$-7.4x10^{-13}$	-4.2x10-6

UNIVERSITY OF BRISTOL LIBRARY